https://doi.org/10.15388/vu.thesis.420
https://orcid.org/0000-0002-3333-2242

VILNIUS UNIVERSITY
CENTER FOR PHYSICAL SCIENCES AND TECHNOLOGY

Edvinas Radiunas

Incoherent NIR photon conversion to the visible region in rubrene compounds

DOCTORAL DISSERTATION

Natural Sciences,
Physics (N 002)

VILNIUS 2022

The dissertation was prepared between 2018 and 2022 at the Institute of Photonics and Nanotechnology, Vilnius University. The research was supported by Research Council of Lithuania (doctoral scholarships for academic achievements, No.: PDAP-19-39, PDAP-21-3). The research was also partially funded by the European Social Fund Project No. 09.3.3-LMT-K-712-01-0084.

Academic supervisor – Dr. Karolis Kazlauskas (Vilnius University, Natural Sciences, Physics – N 002)

This doctoral dissertation will be defended in a public/closed meeting of the Dissertation Defence Panel:

Chairman – Prof. Dr. Mikas Vengris (Vilnius University, Natural Sciences, Physics – N 002).
Members:
Prof. Habil. Dr. Vidmantas Gulbinas (Center for Physical Sciences and Technology, Natural Sciences, Physics – N 002),
Dr. Tadas Malinauskas (Kaunas University of Technology, Natural Sciences, Chemistry – N 003),
Prof. Habil. Dr. Gediminas Niaura (Center for Physical Sciences and Technology, Natural Sciences, Physics – N 002),
Prof. Dr. Yoan C. Simon (The University of Southern Mississippi, Natural Sciences, Chemistry – N 003).

The dissertation shall be defended at a public/closed meeting of the Dissertation Defence Panel at 4 PM on December 6, 2022 in conference room A101 of the National Center for Physical Sciences and Technology.
Address: Saulėtekio av. 3, Vilnius 10257, Lithuania
Tel. +3702649211; email: office@ftmc.lt.

The text of this dissertation can be accessed at the Vilnius University Library, as well as on the website of Vilnius University:
www.vu.lt/lt/naujienos/ivykiu-kalendorius

https://doi.org/10.15388/vu.thesis.420
https://orcid.org/0000-0002-3333-2242

VILNIAUS UNIVERSITETAS
FIZINIŲ IR TECHNOLOGIJOS MOKSLŲ CENTRAS

Edvinas Radiunas

Nekoherentinė NIR fotonų konversija į regimąją sritį rubreno junginiuose

DAKTARO DISERTACIJA

Gamtos mokslai,
Fizika (N 002)

VILNIUS 2022

Disertacija rengta 2018–2022 metais Vilniaus Universiteto Fotonikos ir nanotechnologijų institute. Mokslinius tyrimus rėmė Lietuvos mokslo taryba (paramos už studijų rezultatus registracijų Nr.: PDAP-19-39, PDAP-21-3). Eksperimentinė veikla iš dalies finansuota Europos socialinio fondo lėšomis, pagal dotacijos sutartį su Lietuvos mokslo taryba, sutarties Nr. 09.3.3-LMT-K-712-01-0084.

Mokslinis vadovas – dr. Karolis Kazlauskas (Vilniaus universitetas, gamtos mokslai, fizika - N 002)

Gynimo taryba:
Pirmininkas – prof. dr. Mikas Vengris (Vilniaus universitetas, gamtos mokslai, fizika - N 002).
Nariai:
Prof. habil. dr. Vidmantas Gulbinas (Fizinių ir technologijos mokslų centras, gamtos mokslai, fizika - N 002),
Dr. Tadas Malinauskas (Kauno technologijos universitetas, gamtos mokslai, chemija, N 003),
Prof. habil. dr. Gediminas Niaura (Fizinių ir technologijos mokslų centras, gamtos mokslai, fizika - N 002),
Prof. Dr. Yoan C. Simon (Pietų Misisipės universitetas, gamtos mokslai, chemija - N 004).

Disertacija ginama viešame Gynimo tarybos posėdyje 2022 m. gruodžio mėn. 6 d. 16 val. Nacionalinio fizinių ir technologijos mokslų centro posėdžių salėje A101.
Adresas: Saulėtekio al. 3, Vilnius 10257, Lietuva.
Tel. Nr. +3702649211, el. pastas: office@ftmc.lt.

Disertaciją galima peržiūrėti Vilniaus universiteto bibliotekoje ir VU interneto svetainėje adresu:

ACKNOWLEDGEMENTS

The four-year journey of writing this thesis was full of memorable moments. Many people were responsible for these memories. Here, I would like to express my gratitude to colleagues, friends and family for the support and love they gave me.

To begin with, I sincerely appreciate having Dr. Karolis Kazlauskas as my supervisor. Over the years his mentorship was invaluable to me. He not only showed me the intricate details of scientific writing but also proved that it is possible to kayak 4 kilometers in one hour and still return to the conference in time, without missing any presentations. I'm grateful for the long scientific discussion and the late-day meetings over a cup of tea, which often led to interesting observations. Karolis showed confidence in me and provided me with sufficient autonomy and freedom to think and express my thoughts.

I would also like to thank Dr. Steponas Raišys, who is not only a father of two beautiful kids but also, Lithuania's father of Upconversion. I was lucky to cooperate with Steponas and share with him the daily discussions on various interesting (and sometimes wild) topics of physics. Steponas always provided a healthy sense of realism in chaotic situations.

A big thanks to the current and past members of the organic optoelectronics group. I don't know why, but perhaps, this place attracts a certain kind of individuals, burning with interesting ideas. I would like to thank Regimantas for many interesting perspectives on the properties of organic molecules. Thanks to Rokas for setting an example on how to compose a compact and a well-written thesis, the engineering and programming tips and to the friendly occasions shared with the collection of Rokas science inspiring home brew. I would like to thank Dovydas for sharing the PhD journey and the experience of teaching and growing the young generation of physics students. I thank Paulius for pushing the standards of our research group and the endless discussions on the value of science. I thank Gediminas for showing that it is possible not to overthink and deliver a concise and smile provoking argument. I thank Justina for setting an example on how to step outside the norm and collaborate, lead, and deliver interesting research. I would like to thank my younger students and now competent colleagues Lukas, Justas and Manvydas. Your curiosity and quick learning constantly pushed me out of my comfort zone.

I would like to thank the constant visitors of cabinet B211 (aka the coffee room). In particular, the active members: Augustas, Dovydas, Justina, Kamilė, Tomas, Steponas, Ramūnas, Saulius, Tadas, Arūnas. Also, the temporal reservists: Akvilė, Jonas, Paulius, Džiugas, Eglė and Lukas. This place was a

constant inspiration throughout the dissertation. I will always remember the smell of coffee in the room, mixed with a passion for physics and spiced with sophisticated humour. There is probably no other place where you can laugh so hard, and learn so much, in such a short time.

Special thanks to my dear friends Karolis, Laurynas, Ieva, Beata, Marija, Kasparas, Arminas, Edgaras and others that genuinely showed interest in my work. By continuously asking for updates, perhaps without even knowing, you encouraged me to step up and go further.

I’m very grateful for the support from my mother Vale and father Ryšard who always showed love and inspired me to excel.

Finally, I am most grateful to my beloved soulmate Gerta for her immeasurable patience and emotional support. Her genuine interest in my personality and my work fuelled every step.

CONTENTS

LIST OF ABBREVIATIONS

PV – photovoltaic
SQ - Shockley−Queisser
SF – singlet fission
UC – Upconversion
TTA – triplet-triplet annihilation
TTA-UC – triplet-triplet annihilation-based photon upconversion
NIR – near infrared
Vis - visible
NIR-to-Vis – near infrared to visible
ISC – intersystem crossing
TET – triplet energy transfer
TPA – two photon absorption
SHG – second harmonic generation
Rub – Rubrene
PdPc – pallladium-phtalocyanine
PtPc – platinum-phtalocyanine
tBRub – *tert*-butyl-rubrene
FL – fluorescence
MPc – metallo-phthalocyanine
TADF – thermally activated delayed fluorescence
PbS – lead sulfide
CdSe - cadmium selenide
HOMO - highest occupied molecular orbital
LUMO - lowest unoccupied molecular orbital
PbSe – lead selenide
DBP – tetraphenyldibenzoperiflanthene
PS – polystryrene
PVA – polyvinylalcohol
PDI – perylenediimide
NC – nanocrystals
QD – quantum dots
TXP – texaphyrin
DFT – density-functional theory
TDDFT - time-dependent density-functional theory
QY – quantum yield
FRET - Förster resonance energy transfer
CCD charge-coupled device
STA - singlet-triplet annihilation

1. INTRODUCTION

It seems that there is a never-ending race between technological progress and constantly increasing energy demand. As a result, novel technologies aim to be cheaper, more efficient, more potent yet less adverse to the environment. Some technologies ultimately reach maturity and further progress requires smart innovations. A case can be made for photovoltaic (PV) cells. Regardless of the active material utilized in the PV, either conservative crystalline silicon or enthusiastic and promising perovskite, the single junction PVs are bounded by Shockley−Queisser (SQ) limit for solar conversion efficiency. This limit is quantified to be ~30% for PV with a band gap of 1.1 eV.[1,2] Evidently, the single junction PV design has apparent flaws: the high-energy photons lose part of their energy by thermalization, while the sub-bandgap photons lack the energy to be absorbed, thus tend to be unnoticed by the PV. The described SQ limit seems to be clear, however, attracts curiosity from the scientific perspective. As for every ingenious scientist the set limits are a mere puzzle, not an obstacle. Therefore, several solutions are suggested to overcome the SQ limit: i) use multiple junctions and cover a wider part of the spectrum or ii) utilize spectral conversion to be more suitable for the single PV cell. As the first approach is expensive, and for the time being technologically rather complicated, it will not be discussed further. The second approach, related to spectral conversion, is well suited to be utilized together with organic semiconductors. The PV problem with high-energy photons can be mitigated through singlet fission (SF) where excitation created in the organic film is split into two lower-energy excitons and transferred to the PV cell, thus omitting thermalization effects. Likewise, sub-bandgap photons can also be utilized through photon upconversion (UC), where two low-energy excitations in organic film can combine to produce higher-energy photons, which subsequently can be employed by the PV cell. Indeed, this dissertation is devoted to exploring the process of TTA mediated photon upconversion (TTA-UC) occurring in organic media and specifically targeting the conversion of light from near infrared to visible (NIR-to-Vis) spectral range.

In fact, the utility of UC is not limited to PVs.[1,3] The increasing demand for organic systems capable of incoherent NIR-to-Vis UC is also stimulated by a growing variety of other applications such as 3D printing,[4] photocatalysis,[5,6] bioimaging,[7] stress sensing,[8] night vision,[9] memory devices,[10] targeted drug delivery[11] and many more[12]. The surge of interest for NIR-to-Vis UC is highly motivated by applications in biomedicine related to the superior penetration of NIR light through the biological tissue.[5] In these typically bicomponent systems, composed of sensitizer and emitter species, the long-lived triplet-states of emitters are utilized to the energy and produce delayed UC emission from the singlet state that is blue-shifted compared to the absorbed light. The higher energy UC emission from an emitter emerges through a process called triplet-triplet annihilation (TTA) sometimes also referred to as triplet fusion. In the TTA-UC process sensitizer species serve as light absorbers, which subsequently generate triplets via intersystem crossing (ISC) and transfer triplet energy (TET) to the emitter. Importantly, in contrast to two-photon absorption (TPA) which requires high excitation densities (~GW/cm^2), or second-harmonic generation (SHG) that requires a coherent light source, the TTA-UC can operate at incoherent low energy excitation readily available from the sunlight (~mW/cm^2).[1,3] Low power UC can also be obtained from rare-earth elements such as lanthanoids. However, these phosphors use the same electronic manifold to absorb, store and re-emit photons, thus exhibit low absorptivity.[1]

Currently, the NIR-to-Vis TTA-UC suffers from low efficiency, particularly in the solid-state, which in turn hinders practical applications. While a great number of efficient UC systems with a quantum yield (Φ_{UC}) of up to ~30% was demonstrated in the Vis-to-Vis spectral region,[13–18] only several molecular systems were shown to produce NIR-to-Vis UC with Φ_{UC} above 4%[19–21]. It seems that finding proper materials capable of operating with high UC efficiencies under NIR excitation is a big challenge.

For optimal UC performance, it is important to utilize a proper emitter with the triplet state sufficiently low in energy to accept triplet excitons from a NIR sensitizer. The best-performing NIR-to-Vis UC systems demonstrated so far, both in solution and solid state, rely on the rubrene (Rub) emitter.[14] From the multiple UC studies it is evident that Rub is the most popular choice amongst the emitters in the NIR-to-Vis range. Moreover, the Rub is almost exclusively used in the solid-state UC systems. However, there are challenging unresolved issues related to Rub. The highest UC efficiencies achieved so far are substandard for practical applications and require systematic studies and fundamental understanding to be improved.

1.1. Aim and novelty

The aim of this dissertation is to investigate UC systems based on the benchmark emitter rubrene both in solution and solid-state and identify the limiting factors hindering the UC performance. The in-depth study presented here is anticipated to uncover novel approaches capable of enhancing the efficiency of NIR-to-Vis TTA-UC. It is evident from the literature that the limiting factors are not well understood and lack clear consensus or definitive explanations. This knowledge would provide a solid foundation for improved NIR-to-Vis TTA-based UC systems applicable in many desirable practical applications such as photovoltaics, medical diagnostics etc. The following tasks were formulated to achieve this aim:

1) Utilize different combinations of sensitizer (PtPc/PdPc) and emitter (Rub/tBRub) pairs as well as carry out delicate optimization steps towards best UC efficiency in solution.
2) Produce and fully characterize a series of Rub and tBRub based UC films by determining FL and UC quantum yields, the optimal doping concentration in the polymer matrix, UC thresholds, triplet, and UC lifetimes.
3) Reveal the impact of bulky side moieties on the TTA-UC performance of Rub-based UC solutions and solid films.
4) Assess how different Rub deposition techniques influence Rub PL properties and UC performance.
5) Quantify exciton diffusion properties in amorphous-like Rub-based UC films utilizing bulk-quenching technique coupled with time-resolved PL.

1.2. Statements to be defended

I A key factor limiting upconversion efficiency in metallophthalocyanine sensitized NIR-to-Vis UC system based on rubrene emitter is it’s low statistical probability (f) to obtain a singlet state from two triplets via TTA.

II Modifying rubrene with *t*-butyl groups suppresses the aggregation induced quenching effects mainly due to singlet fission and enables to achieve higher UC efficiency.

III Although peripheral- and core-linking of rubrene emitters by the bulky side-moieties reduce singlet fission and enhance FL quantum yield, the former linking pattern is superior as it does not impede TTA.

IV Emissive properties of rubrene films are sensitive to rubrene deposition mode, and thus can be tuned to deliver the features (highest FL quantum yield and longest FL lifetime) most resembling those of amorphous rubrene film desirable for improved UC performance.

V TTA-UC performance of disordered rubrene films is limited by the modest maximal triplet diffusion length resulting from the short maximum triplet lifetime inherent to this emitter.

1.3. Layout of the dissertation

This dissertation is presented as a collection of articles. Essentially, a summary of five publications is composed that complements as well as highlights the key findings of the papers **PI**-**PV**. The papers are presented in chronological order based on their publication date. This constitutes the core of the dissertation that is enriched by the supplementary information.

The introductory part of the dissertation lays out the basic concepts of TTA mediated photon upconversion (TTA-UC). The chapter briefly touches the main ideas that help to grasp and follow the argumentations laid out in the thesis. It is written with an aim to be useful for topic newcomers as well as to serve as a recap for those who are well familiar with TTA-UC. Thus, the introductory part covers the sensitizers used in TTA-UC, emphasizing the metallophthalocyanines. The reader can also find details on triplet energy transfer and TTA process, details on TTA statistical probability and a summary of novel NIR TTA-UC systems, highlighting the influence of rubrene.

The experimental details section is full of recipes on the characterization of TTA-UC. Namely, the procedures are laid out on how to determine the UC quantum yield using comparative or absolute methods. Additionally, the reader can find information on the UC intensity dependence *vs.* excitation power followed by a description of the UC threshold. Finally, the section provides the description of the time-evolution of the UC intensity and what parameters can be extracted based on this information.

Next, the core of the dissertation is presented. It starts with chapter 4 where **PI** is reviewed. The later publication covers UC system in solution based on Rub and tBRub emitters. By carrying out delicate optimization steps toward higher UC efficiency we outline the main losses that are limiting the UC performance. The following chapter 5 discusses the findings of **PII**, where we characterize and optimize solid-state Rub- and tBRub-based UC system. Then, the chapter 6 complements **PIII**, where we introduce novel modified Rub emitters and observe the changes to UC performance these modifications induce. The **PIV** is reviewed in the chapter 7, where we test various Rub deposition techniques trying to determine which one is the most suitable to achieve maximal UC efficiency in the solid-state. The final publication **PV** is reviewed in the chapter 8. Here, we study the set of Rub-based UC films intentionally doped with singlet and triplet quenchers aiming to determine both singlet and triplet diffusion parameters in these disordered films. The end of the dissertation is summarized by laying out the conclusions.

1.4. Contribution of the author

Most of the experimental data presented in the dissertation is obtained by the author. This includes the sample preparation, spectroscopic and microscopic characterization, relevant calculations, and data processing. The author was heavily involved in the manuscript preparation process related to all five publications that are the foundation of this dissertation. Namely, the author participated in the initial conceptualization, took part in all the discussions, carried out the writing of the initial drafts and contributed to the reviewing process.

However, the substantial work can only be done with a great and proficient team. The synthesis of novel compounds was carried out by the organic chemist group lead by prof. Edvinas Orentas in the department of organic chemistry (Vilnius University). The materials were purified using sublimation technique by dr. Gediminas Kreiza. The excited state absorption measurements were performed by dr. Paulius Baronas. The thermal vacuum deposition of the Rub films was done by dr. Dovydas Banevičius. The exciton diffusion evaluation was performed by Manvydas Dapkevičius and dr. Steponas Raišys. Lukas Naimovičius assisted in the UC characterization experiments. The author acknowledges the help and contribution made by the colleagues and feels very grateful for the opportunity to work with the team.

1.5. Publications and conferences

On the dissertation topic

PI **E. Radiunas**, S. Raišys, S. Juršėnas, A. Jozeliūnaitė, T. Javorskis, U. Šinkevičiūtė, E. Orentas, K. Kazlauskas. Understanding the Limitations of NIR-to-Visible Photon Upconversion in Phthalocyanine-Sensitized Rubrene Systems. *J. Mater. Chem. C* 8(16), 5525–5534, **2019**. https://doi.org/10.1039/C9TC06031F.

PII **E. Radiunas**, M. Dapkevičius, S. Raišys, S. Juršėnas, A. Jozeliūnaitė, T. Javorskis, U. Šinkevičiūtė, E. Orentas, K. Kazlauskas. Impact of T-Butyl Substitution in a Rubrene Emitter for Solid State NIR-to-Visible Photon Upconversion. *Phys. Chem. Chem. Phys.* 22(14), 7392–7403, **2020**. https://doi.org/10.1039/D0CP00144A.

PIII **E. Radiunas**, M. Dapkevičius, L. Naimovičius, P. Baronas, S. Raišys, S. Juršėnas, A. Jozeliūnaitė, T. Javorskis, U. Šinkevičiūtė, E. Orentas, K. Kazlauskas. NIR-to-Vis Photon Upconversion in Rubrenes with Increasing Structural Complexity. *J. Mater. Chem. C* 9(12), 4359–4366, **2021**. https://doi.org/10.1039/D1TC00296A.

PIV **E. Radiunas**, L. Naimovičius, S. Raišys, A. Jozeliūnaitė, E. Orentas, K. Kazlauskas. Efficient NIR-to-Vis Photon Upconversion in Binary Rubrene Films Deposited by Simplified Thermal Evaporation. *J. Mater. Chem. C* **2022**. https://doi.org/10.1039/D1TC05332A.

PV **E. Radiunas**, M. Dapkevičius, S. Raišys, K. Kazlauskas. Triplet and singlet exciton diffusion in disordered rubrene films: implications for photon upconversion. *Phys. Chem. Chem. Phys. Accepted manuscript*, https://doi.org/10.1039/D2CP02798D.

Other publications

1. I. Reklaitis, **E. Radiunas**, T. Malinauskas, S. Stanionytė, G. Juška, R. Ritasalo, T. Pilvi, S. Taeger, M. Strassburg, R. Tomašiūnas. A Comparative Study on Atomic Layer Deposited Oxide Film Morphology and Their Electrical Breakdown. *Surf. Coat. Technol.* 399, 126123, **2020**. https://doi.org/10.1016/j.surfcoat.2020.126123
2. M. Kolenda, D. Kezys, I. Reklaitis, **E. Radiunas**, R. Ritasalo, A. Kadys, T. Grinys, T. Malinauskas, S. Stanionytė, M. Skapas, R. Petruškevičius, R. Tomašiūnas. Development of Polarity Inversion in a GaN Waveguide Structure for Modal Phase Matching. *J. Mater. Sci.* 55(26), 12008–12021, **2020**. https://doi.org/10.1007/s10853-020-04831-z
3. K. Badokas, A. Kadys, J. Mickevičius, I. Ignatjev, M. Skapas, S. Stanionytė, **E. Radiunas**, G. Juška, T. Malinauskas. Remote Epitaxy of GaN via Graphene on GaN/Sapphire Templates. *J. Phys. D: Appl. Phys.* 54(20), 205103, **2021**. https://doi.org/10.1088/1361-6463/abe500
4. P. Baronas, G. Kreiza, L. Naimovičius, **E. Radiunas**, K. Kazlauskas, E. Orentas and S. Juršėnas, Sweet Spot of Intermolecular Coupling in Crystalline Rubrene: Intermolecular Separation to Minimize Singlet Fission and Retain Triplet–Triplet Annihilation, *J. Phys. Chem. C*, 126, 15327–15335, **2022.** https://doi.org/10.1021/acs.jpcc.2c04572
5. M. Kolenda, A. Kadys, T. Malinauskas, **E. Radiunas**, R. Ritasalo and R. Tomašiūnas, The importance of nucleation layer for the GaN N-face purity on the annealed Al2O3 layers deposited by atomic layer deposition, *Mater. Sci. Eng. B*, 284, 115850. **2022.** https://doi.org/10.1016/j.mseb.2022.115850

Conference presentations

C1 **E. Radiunas**, S. Raišys, S. Juršėnas, A. Jozeliūnaitė, T. Javorskis, U. Šinkevičiūtė, E. Orentas, K. Kazlauskas. Phthalocyanine-Sensitized Rubrene Films for IR-to-Visible Up Conversion, Open Readings, **2019**, Vilnius, Lithuania.

C2 **E. Radiunas**, S. Raišys, S. Juršėnas, A. Jozeliūnaitė, T. Javorskis, U. Šinkevičiūtė, E. Orentas, K. Kazlauskas. Infrared-to-visible upconversion in solution-processed rubrene-doped polymer films sensitized with phthalocyanines, 14th International Symposium on Functional π-Electron Systems, **2019**, Berlin, Germany.

C3 **E. Radiunas**, S. Raišys, S. Juršėnas, A. Jozeliūnaitė, T. Javorskis, U. Šinkevičiūtė, E. Orentas, K. Kazlauskas. Triplet-Fusion Mediated NIR-to-Orange Upconversion in Phthalocyanine Sensitized Rubrene Films, 13th International Conference on Optical Probes of Organic and Hybrid Optoelectronic Materials and Applications **2019**, Vilnius, Lithuania.

C4 **E. Radiunas**, S. Raišys, S. Juršėnas, A. Jozeliūnaitė, T. Javorskis, U. Šinkevičiūtė, E. Orentas, K. Kazlauskas. Determining NIR-to-Visible Light Upconversion Yield in Novel Phthalocyanine-Sensitized Rubrene Emitters, 24th International Krutyn Summer School, **2019**, Krutyn, Poland.

C5 **E. Radiunas**, L. Naimovičius, S. Raišys, S. Juršėnas, E. Orentas, K. Kazlauskas. Technology to Produce Efficient NIR-to-Vis Photon Upconversion in Rubrene films, 44th National Lithuanian Physics Conference – LNFK 44, 2021, Vilnius, Lithuania.

C6 **E. Radiunas**, L. Naimovičius, S. Raišys, S. Juršėnas, E. Orentas, K. Kazlauskas.Technology to Optimize Rubrene for Solid-State NIR-to-Vis Upconversion, SPIE Photonics Europe, **2022**, Strasbourg, France.

Participation in scientific project

- Triplet state engineering in organic optoelectronic compounds (Global Grant, The Research Council of Lithuania, **2018-2022**)

2. INTRODUCTION TO INCOHERENT NIR-TO-VIS PHOTON UPCONVERSION MEDIATED BY TTA

The current chapter focuses on the introduction to the basic concepts of TTA-based photon upconversion (TTA-UC) operating in the NIR region ($\lambda > 700$ nm) and producing visible emission. A brief overview of this rapidly developing field is provided by focusing on the main achievements, the current developments, and still unresolved problems.

2.1. TTA mediated photon upconversion

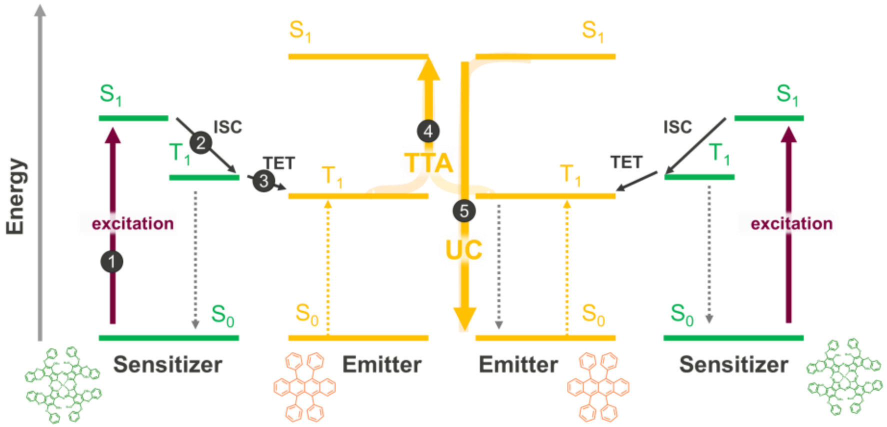

Fig. 2.1 The TTA-based upconversion (UC) energy scheme using a sensitizer and an emitter. The main energy transfer steps are indicated: (**1**) low energy photon absorption; (**2**) the intersystem crossing (ISC); (**3**) the triplet energy transfer (TET); (**4**) the triplet-triplet annihilation (TTA); (**5**) higher energy UC emission. S and T indicate singlet or triplet states, correspondingly, where subscript indicate either ground (0) or excited (1) state.

The photon upconversion (UC) from lower to higher energies utilizing organic semiconductors can be realized in bicomponent systems, composed of sensitizer and emitter species. The long-lived emitter triplet states are utilized to produce delayed UC emission from singlet state that is blue-shifted as compared to the absorbed light. Schematically, the main energy conversion steps are illustrated in the Fig. 2.1. Firstly, the sensitizer species serve as light absorbers and generate triplets via intersystem crossing (ISC). Afterwards, the triplet excitons undergo triplet energy transfer (TET) to an emitter species. Finally, the higher energy UC emission from an emitter emerges through triplet-triplet annihilation (TTA). To make this overall process efficient, each energy transfer step needs to be optimized, providing minimal energy losses. Next, we will discuss the sensitizer part of the TTA-UC scheme.

2.2. NIR sensitizers based on metallophthalocyanines

A crucial part of the TTA-UC scheme is the generation of the triplet states. A fragment that converts excitation to triplet states later supplied to an emitter is called a sensitizer. An ideal sensitizer should fulfil these properties: i) exhibit high absorption in the region of interest; ii) convert absorbed photons to triplet excitons with high yield and low energy loss; iii) display long triplet lifetime (ideally infinite); iv) have negligible absorption in the UC region. Unsurprisingly, finding a suitable sensitizer satisfying all the listed requirements is challenging. Also, the NIR region is well-known for its poor library of worthy sensitizers.[22,23] However, standing out of the group, the phthalocyanine-based molecules meet the majority of the set criteria.

Phthalocyanines (Pc) are widely known materials exhibiting high thermal and chemical stability.[24] Although many Pc derivatives exhibit rigid and planar structure the chemist can functionalize these compounds to meet specific applications. For instance, in the centre of the macrocycle, two hydrogen atoms can be replaced by more than 70 metals, whereas at the periphery, various substituents can be attached.[24] The function of the metal in the centre of the Pc is to shorten the singlet state lifetime by facilitating the intersystem crossing (ISC) to the triplet state by means of heavy-metal atom effect.[25] The rate of ISC (k_{isc}) is proportional to the atomic mass of the incorporated metal. The sensitizer should exhibit rapid ISC to outcompete any other existing deactivation pathways. This leads to an effective population of triplet states with high triplet yield (Φ_{ISC}). For this purpose, in the **PI** (to be introduced bellow) the heavy metal palladium (Pd) or its congener platinum (Pt) are incorporated into Pc core. Additionally, we modified metallophthalocyanines (MPc) with phenoxy and butoxy groups in the periphery, specifically to increase solubility and accordingly to reduce molecular aggregation (see Fig. 2.2).

As alternatives to MPc, typical sensitizers utilized in TTA-UC scheme are TADF molecules[26,27], perovskites[28] or inorganic nanocrystals like PbS[29,30] or CdSe[31]. However, in this vast array of sensitizers, the MPc have apparent advantages. For example, other sensitizers have broadband absorption spanning across the visible range inevitably overlapping with the emerging UC emission. However, the MPc have absorption spectrum that is split into short wavelength Soret band and long wavelength Q-band with a transparency window in between (see Fig. 4.1). By strategically positioning the UC emission either by picking or tunning the emitter, the reabsorption losses inflicted by the sensitizer are mitigated without directly compromising the UC efficiency. Moreover, the Q-band absorption itself is intense, exhibiting molar extinction coefficient $\varepsilon > 1 \times 10^5\ M^{-1} \cdot cm^{-1}$. This partly enables to use of relatively small amounts of MPc to generate high triplet concentrations required for efficient TTA.

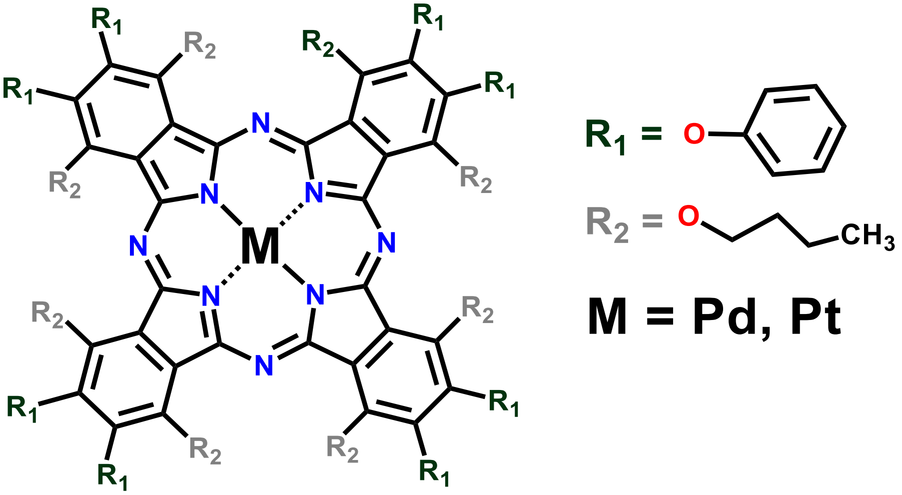

Fig. 2.2 Schematic structure of two metallophthalocyanines studied in this work and used as sensitizers for NIR-to-Vis upconversion. Both sensitizers have peripheral modifications: R_1 – phenoxy and R_2 – octabutoxy groups. M – central metal atom, either palladium or platinum.

However, the utilization of MPc can have notable disadvantages. Firstly, the difference between the first singlet and triplet excited states (S_1-T_1) is significant, resulting in comparatively high energy losses inflicted by ISC. These losses can be as high as ~ 0.6 eV automatically reducing the anti-Stokes shift that could be potentially obtained from the UC system. For example, using other sensitizers without these losses, such as osmium complexes which exhibit direct singlet-triplet (S-T) state absorption, the UC operates from NIR(700nm)-to-violet(450nm) resulting in 1.28 eV anti-Stokes shift.[32] The similar situation is for the perovskites or PbS nanocrystals where generated excitons do not undergo ISC. The second problem with MPc is related to the relatively short T_1 state lifetime (τ_T). The central heavy metal in MPc utilized to facilitate the rate of $S_1 \rightarrow T_1$ transition, also increases the rate of non-radiative $T_1 \rightarrow S_0$ transition. The latter reason, in combination with consequences of the energy gap law results in $\tau_T \sim 1\ \mu s$ range for MPc absorbing in the NIR region.

Although not ideal, the MPc used as sensitizers in the UC scheme demonstrate one of the highest UC quantum yields (see Table 2.3).

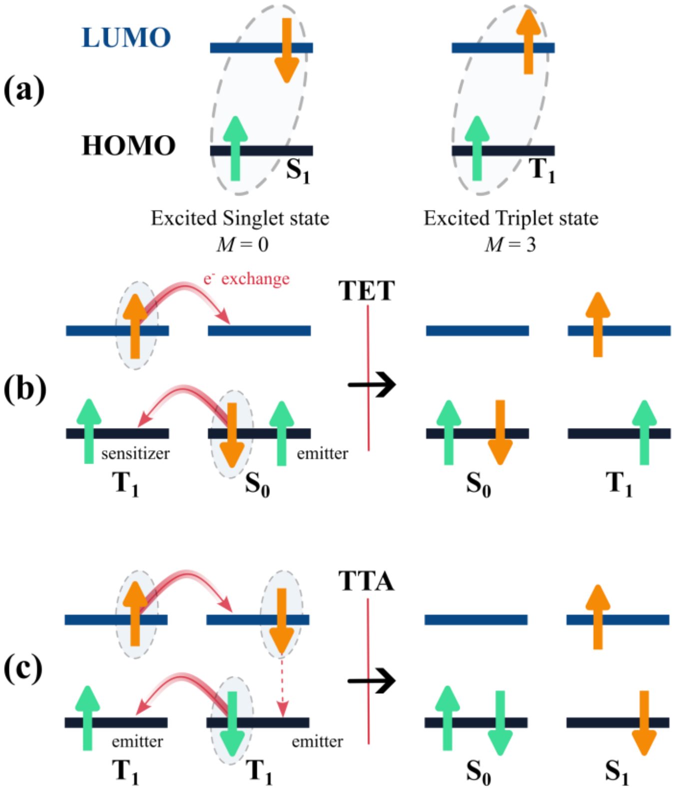

Fig. 2.3 (a) Simplified representation of the excited singlet (S_1) and the triplet (T_1) states. (b) The schematic representation of the triplet energy transfer process (TET); (c) displays triplet-triplet annihilation (TTA) between two emitters, leading to an excited singlet state.[22,33]

2.3. Triplet energy transfer and encounter of triplet states

As established earlier, the UC process is based on both singlet (S_1) and triplet (T_1) excited states. It is useful to remind ourselves of the basic properties of S_1 and T_1 to better understand the triplet energy transfer (TET) and triplet-triplet annihilation (TTA) in the UC. The visual representation of S_1 and T_1 are illustrated in Fig. 2.3a. S_1 state is composed of two spin (s) ½ particles with a total spin quantum number $S = 0$ (sum of all individual spins) and multiplicity $M = 2S+1 = 1$ (thus the name singlet). Notably, the S_1 is composed of one electron in the HOMO (*highest occupied molecular orbital*), and one in the LUMO (*lowest unoccupied molecular orbital*). It is considered that in this state all electrons are paired. It is useful to represent this state with two arrows, one pointing up and another down, indicating that these electrons have completely anti-parallel spins. Conversely, in a similar manner, the T_1 state is described by a total spin quantum number $S = 1$ and $M = 3$ (thus name triplet). This state is composed of two unpaired electrons one in HOMO, while other in LUMO, and they exhibit parallel spins, represented with arrows pointing in the same direction.

The process of TET is represented in the Fig. 2.3b. Under right conditions, the excited sensitizer in T_1 state can be quenched by the presence of the emitter in the ground state (S_0), resulting in the transfer of the excitation (Fig. 2.3b). The underlying mechanism is based on the Dexter type energy transfer involving electron exchange between the sensitizer and the emitter.[34] Namely, the excited electron of the sensitizer is swapped with the ground-state electron of the emitter. This non-radiative energy transfer becomes probable at short distances ($r < 1$nm), since it requires wavefunction overlap between donor and acceptor.[35] The rate of this process is exponentially dependent on the separation between molecules.

2.4. TTA and probability to obtain a singlet state

As for TET the TTA process also requires electron exchange (Fig. 2.3c). TTA can occur between two emitters in the T_1 state. Within their lifetime triplets can encounter each other and undergo TTA. By considering that singlet state is accessible ($S_1 \leq 2\times T_1$), TTA can lead to one exciton in the singlet state with double the energy, while other is quenched to the ground state. The process can be written as $T_1 + T_1 \rightarrow S_1 + S_0$. Experimentally, S_1 produced by TTA can be distinguished by registering emission of singlet spectra yet with triplet lifetime. This is commonly referred to as delayed fluorescence and typically occurs in the ~ µs range. Originating from TTA the delayed fluorescence has quadratic intensity dependence on pump fluence at low excitation power (discussed in detail in experimental section 3.6).

Another critical parameter having a direct impact on the overall efficiency of UC is the statistical probability factor f. The factor describes the probability for the triplet pair in an emitter to form one singlet via TTA. The encounter between two T_1 states does not necessarily lead to S_1 state. In fact, based on quantum statistics, the S_1 pathway is relatively improbable. The summary of the viable outcomes of TTA are depicted in Table 2.1. Namely, the encounter of $T_1 + T_1$ can result in 9 distinct arrangements (3×3 combinations) of electron spin multiplicities. There is one way to get a complex of singlet (S) multiplicity. However, there is 3 ways to yield a triplet (T), and 5 ways to

Table 2.1 Outcomes of encounter of the two excited triplet states.[25,36] *S* – spin quantum number, *M* – state multiplicity, S – singlet state, T – triplet state, Q - quintet state.

Prior to TTA	Encounter complex	*S*	*M*	Statistical weight	*After TTA
	^{1}(TT)	0	1 (S)	1/9	$S_1 + S_0$
$T_1 + T_1$	^{3}(TT)	1	2 (T)	3/9	$T_1 + S_0$
	^{5}(TT)	2	3 (Q)	5/9	$T_1 + T_1$

*Assuming 2 × T_1 is insufficient to form a quintet state, while T_2 is energetically accessible.

yield a quintet state (Q). Consequently, the encounter of two triplets will form a fluorescent S_1 state with a probability of $f = 1/9$ or 11.1%.[15,37,38] This theoretical limit strongly discourages to envision TTA-UC for many practical applications since it states that ideally, the UC yield (Φ_{UC}) can reach 5.5% (1 S_1 per 9 pairs of T_1 or $\Phi_{UC} = ½ \times f = ½ \times 1/9$). However, many reports proved this limit to be incorrect,[15,38] and suggest alternative interpretations explaining higher *f* values. The visual representation leading to different *f* values is shown in Fig. 2.4b-c. Since normally molecular Q states are energetically inaccessible, it is assumed that Q encounter complex dissociates back to T_1 having no effect to overall T_1 population (Fig. 2.4b). Although omitting Q states increases *f* to 25%, this value is far from ideal. The *f* limit can be pushed further by considering that ^{3}(TT) complex forms a T_2 state, which due to internal conversion, relaxes back to T_1 (Fig. 2.4c). After this, only one T_1 state is quenched. Now, from 4 encounter complexes, 1 will yield a S_1 quenching 2 triplets, while additional 3 triplets will be quenched from ^{3}(TT) yielding a probability per quenched triplet 1/(2 + 3) = 20% or $f = 40\%$ (per triplet pair).

Ideally, emitter could potentially have energy level alignment where $2 \times T_1 < T_2$, meaning inaccessible both Q and T_2 states. Subsequently, only ^{1}(TT) depletes the T_1 population as other complexes dissociate back to T_1. In this way $f = 100\%$ since each quenched triplet pair produces a singlet state (Fig. 2.4d). In summary, relative energy levels of the emitter excited states, both of S and T character, are important and heavily influence the outcomes of the TTA. Thus, the condition that $2T_1 > S_1$ for TTA emitter is important, yet not sufficient for high performance UC.

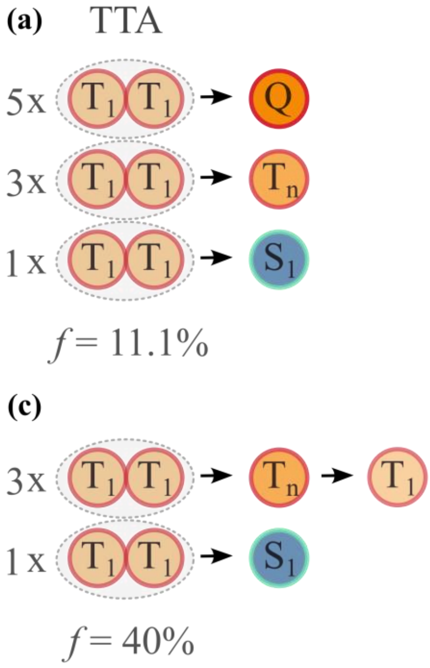

Fig. 2.4 Schematic representation of the TTA event leading to Q - quintet, T – triplet and S – singlet state. Here *f* is a statistical probability factor to obtain a singlet state from two triplets in different scenarios: (a) TTA event results according to spin statistics; (b) quintet states are energetically inacessible; (c) Q are inaccessible and only one T_1 state is quenched when T complex is formed; (d) both Q and T_n states are energetically inaccessible, thus all TTA events lead to S state.

It is challenging to determine the *f* parameter experimentally and most of the time it is done indirectly. Yet there are several studies reporting *f* of popular TTA emitters. Most notable are TTA emitters operating in the Vis-Vis UC, namely exhibiting blue light emission. For example, the most popular green-to-blue UC emitter DPA (diphenylanthracene) is extensively reported to exhibit *f* of ~40%[38–40]. The overall highest *f* of ~100% is reported by Monguzzi et al. using blue emitter perylene and deriving that in this molecule T_2 is inaccessible.[15] Moving to lower T_1 energies, the data on *f* becomes ambiguous. There is a limited number of studies on *f* for emitters suitable for the NIR-to-Vis UC. Almost exclusively the reports are on rubrene in solution. Moreover, the reports on rubrene *f* are scattered in range from 33%[37] to as high as ~ 66%[3,40,41]. However, in our work we emphasize that relatively high *f* is not supported by experimental Φ_{UC} measurements (see Table 2.2). Conversely to the DPA UC systems (*f* of ~ 40%), where Φ_{UC} is reported to be as high as ~ 25%[3,42], in the rubrene UC systems the $\Phi_{UC} < 8\%$ (see chapter below).

Hopefully, up to this point, the reader is convinced that *f* of TTA emitters is an important parameter, projecting a potential limit to Φ_{UC}. There is an apparent need and aspiration for qualitative reports on this parameter, especially for TTA emitters with low T_1 energies.

2.5. Modern NIR-to-Vis TTA-UC systems and the role of rubrene

There are an increasing number of reports attempting to design and characterize a NIR-to-Vis UC system. This is mainly motivated by various novel practical solutions projected to be solved by NIR-to-Vis UC. For example of high interest is operation in biological transparency window (650 - 950 nm) where light has a relatively high penetration depth.[43] In this region TTA-UC can be utilized for targeted drug delivery[11], or medical diagnostics[44,45]. In practice, it is important that the TTA-UC system exhibit high performance in terms of high Φ_{UC} at relatively low operating power, or threshold (I_{th}). The summary of the current TTA-based NIR (λ ~ 700nm) UC systems are depicted in Table 2.3. The first part of the table depicts the sensitizer and emitters pairs used in solutions. A clear distinction between molecular (PdPc, PtTPTNP, PdTNP) and inorganic (PbSe, PbS, CdS) sensitizers can be seen as typically the later operate at longer wavelengths (> 780 nm) and exhibit a superior anti-Stokes shift of up to 0.95 eV. However, most inorganic sensitizer-based systems suffer from high I_{th}. This is mainly related to low absorption at the region of interest as well as suboptimal triplet energy transfer from the sensitizer to the emitter. Although there are three outstanding studies in terms of highest Φ_{UC} (~5.6-7.0%) possessing Rub or perylene derivative (Py5) as emitters, the Φ_{UC} significantly lower compared to Vis-Vis UC systems. There are numerous demonstrations of green-to-blue UC showing Φ_{UC} of 25-38%[3,15,42]. Namely, the observed decrease of Φ_{UC} when pushing the excitation of UC systems from Vis to NIR is not well understood and requires more research.

The UC performance is further diminished in solid films (see the lower part of Table 2.3), where additional problems arise from aggregation-induced quenching effects in the emitter, that inhibit Φ_{FL}. As a result, most of the works report minuscule Φ_{UC}. The highest Φ_{UC} of ~2% is reported by the group of Kinoshita et. al. using osmium complex as a sensitizer and Rub nanoparticles doped with DBP exciton sink and dispersed in PVA matrix, composing a ternary UC system. Comparable result and the highest Φ_{UC}

Table 2.3 Demonstrated NIR-to-Vis UC systems based on TTA with main UC characteristics: ^{a} UC quantum yield (max. 50%), ^{b} UC threshold (the intersection of quadratic and linear dependence versus excitation power), ^{c} excitation wavelength, ^{d} wavelength of the UC emission, ^{b} anti-Stokes shift energy.

UC in solutions							
Sensitizer	Emitter	$^a\Phi_{UC}$ (%)	$^bI_{th}$ (W/cm^2)	$^c\lambda_{exc}$ (nm)	$^d\lambda_{UC}$ (nm)	$^e\Delta E_{UC}$ (eV)	Ref.
PbSe NC	Rub	0.01	60	980	560	0.95	46
PbS/CPT NC	Rub	0.85	-	808	560	0.68	47
PbSe/CPT NC	Rub	1.05	-	808	560	0.68	47
PbS/CdS/5-CT NC	Rub	4.20	0.03	808	560	0.68	48
PbS-ZnS NC	Rub	0.14	-	983	560	0.95	49
PbS/5-CT NC	Rub	5.90	53.4	781	560	0.63	19
PbS NC	TES-ADT	0.15	33	785	610	0.45	50
$PdPc(OBu)_8$	TIPS-Tc	0.20	44.5	730	540	0.60	51
$PdPc(OBu)_8$	TIPS-Tc dimer	0.26	4.3	730	540	0.60	51
PtTPTNP	Rub	3.30	-	690	560	0.42	52
PtTPTNP	PDI	3.00	-	690	550	0.46	52
PdTNP	Py5	7.05	0.05	720	570	0.45	20
PdTNP	Py4	3.20	0.05	720	560	0.49	20
TXP	Rub	1.54	2	750	560	0.56	22
$Os(peptpy)_2{}^{2+}$	TTBP	2.95	0.66	724	462	0.97	45
PdPc	**Rub**	**5.60**	**1.9**	**730**	**560**	**0.52**	**PI**
PdPc	**tBRub**	**1.30**	**3.6**	**730**	**560**	**0.52**	**PI**
UC in films							
PbS NC	Rub/DBP 0.5%	0.36	1.1	980	610	0.77	53
PbS NC	Rub/DBP 0.5%	0.29	12	850	610	0.57	54
PbS NC	Rub/DBP 0.5%	3.5*	-	808	610	0.50	55
Perovskite MAFAPBI3	Rub/DBP 1%	0.22	0.06	785	610	0.45	56
Os(atpy)(tbbpy)Cl+	Rub	0.22	10	730	560	0.52	57
Os(atpy)(tbbpy)Cl+	Rub/DBP 0.5% nps in PVA	2.05	10	730	610	0.33	57
PdTPTAP	Rub nps	0.25	0.1	785	570	0.60	58
MAFAPbI	Rub/DBP 1%	0.15	0.5	785	610	0.45	59
PbS NCs	Rub/DBP 1%	0.05	0.01	980	610	0.77	30
PbS QD	TES-ADT	0.21	2.5	975	660	0.61	60
PdPc	**Rub/DBP 0.5%/PS**	**0.07**	**2.1**	**730**	**610**	**0.33**	**PII**
PdPc	**tBRub/DBP 0.5%/PS**	**0.30**	**2.4**	**730**	**610**	**0.33**	**PII**
PdPc	**Rub/PS**	**1.20**	**1.4**	**730**	**560**	**0.52**	**PIV**

Rub – rubrene, DBP – tetraphenyldibenzoperiflanthene, PS – polystryrene, PVA – polyvinylalcohol, PdTNP - palladium tetraaryltetranaphthoporphyrin, TXP – texaphyrin, TIPS-Tc – triisopropylsilyl tetracene, PDI – perylenediimide, NC – nanocrystals, QD – quantum dots, nps – nanoparticles. *Value is normalized to Φ_{FL}.

overall, amongst binary UC systems, was achieved in **PIV**. This binary system composed of Rub emitter and PdPc sensitizer demonstrated Φ_{UC}~1.2%.

If we focus on the emitters part in Table 2.3 we can see that Rub is the dominant choice for most of the works. With only one exception, Rub is used almost in all NIR-to-Vis UC solid systems. This is mainly related to the lack of TTA emitters exhibiting low triplet energy suitable for NIR-to-Vis UC and still emissive in the solid-state.[61,62] By being the most popular choice, Rub and its modifications need further investigation to understand the limiting factors that inhibit UC performance. Additionally, as the field of NIR-to-Vis UC progresses, search for novel emitters could be of crucial importance.

3. EXPERIMENTAL DETAILS

3.1. Quantum chemical simulations

As complementary information to experimental measurements, each investigated molecule undergoes a quantum chemical simulation procedure. Namely, to determine excited state energies, molecule’s ground-state geometry optimization is required. This is done by setting up a force field MMFF94[63] developed by Merck (*Merc Molecular Force Field*) in the Avogadro software package[64] to initially guess the lowest energy conformer. Then a more complex and time-consuming geometry optimization is carried out by utilizing DFT. For this purpose, Orca software package is utilized.[65] Equilibrium geometry of the ground state was obtained at the B3LYP functional level with the 6-31G(d) basis set in a vacuum. Finally, time-dependent DFT (TDDFT) is employed to calculate vertical excitation energies S_1 and T_1.

3.2. Synthesis of the compounds

Most of the emitters and sensitizers used throughout the dissertation as well as in publications **PI-IV** are synthesized by the brilliant matter manipulators – the chemist group which is led by prof. Edvinas Orentas in the department of organic chemistry, Vilnius University. The details on the synthesis of palladium and platinum phthalocyanines (PdPc, and PtPc), together with modified tBRub can be found in the **PI** while the synthesis of structurally complex rubrenes peri-tBRub and core-tBRub can be found in **PIII**.

3.3. Sample preparation

All liquid and rigid samples presented in this work were prepared in the nitrogen-filled glovebox with O_2 and H_2O concentrations below 0.1 ppm. At first concentrated emitter and sensitizer solutions (10mg/mL) were prepared separately. The UC solutions were prepared by mixing emitters (Rub, tBRub, peri-tBRub, core-tBRub) and sensitizers (PdPc, PtPc) at appropriate ratios to result in the final concentrations (i.e., 18mM of emitter and 15μM of sensitizer). Prior to mixing each solution was stirred overnight at 50 °C. Quartz cells having inner dimensions of 10×10 mm with UC solutions were carefully sealed before removing from the glovebox for measurements. The sealing was essential to protect from triplet quenching by oxygen as well as to avoid photoinduced degradation of rubrene emitter through singlet oxygen induced formation of rubrene endoperoxide[66].

In the case of UC films, we prepared a stock solution (50 mg/mL) of dissolved polymer (polystyrene – PS), which was then used at appropriate ratios to produce a mixed solution of the emitter in PS indicated as wt%. Here wt% is defined as a weight percentage relative to the total weight content of the mixture. After mixing, the films were prepared by spin-coating at 4000 rpm for 1 min on 1-mm-thick 25x25 mm microscope glass slides. Low concentration PS films (< 1 wt%) were drop-casted to produce thicker films. Finally, before carrying out sample photophysical characterization at ambient conditions, we covered each prepared film with an additional microscope slide and encapsulated the film with 2-component epoxy resin.

3.4. Determination of upconversion quantum yield: the absolute method

In TTA-based upconversion, two triplet excitons recombine to form a one higher energy singlet state. This is usually achieved in molecular systems that undergo a cascade of energy transfer processes. The overall efficiency of upconversion quantum yield (Φ_{UC}) of the emitter-sensitizer system is described by the yields of intermediate energy transfer/conversion steps (see Fig. 3.1), namely, ISC, TET, TTA and FL quantum yields. Thus, Φ_{UC} can be expressed as[21,42,67,68]:

$$\Phi_{UC} = \frac{1}{2} f \Phi_{ISC} \Phi_{TET} \Phi_{TTA} \Phi_{FL} \tag{3.1}$$

here f is a statistical factor representing probability to obtain a singlet in an emitter from two emitter triplets via TTA. In principle, all intermediate processes can reach 100%, while the ½ multiplier determines that, ideally, Φ_{UC} can reach 50%. This is in accordance to standard IUPAC definition of quantum yield (QY)[21,42,67,69]:

$$\Phi_{UC} = \frac{\#\, of\ events}{\#\, absorbed\ photons} = \frac{\#\, UC\ photos}{\#\, absorbed\ photons} \tag{3.2}$$

Here I want to emphasize that in this dissertation and in the **PI-V**, all the Φ_{UC} values are reported based on this definition above. This is important since in the community there is some vagueness and uncertainty on how to report the Φ_{UC} values.[67] Some groups normalize UC yield to 100% or even additionally normalize the result to Φ_{FL}, which produces highly misleading results that are difficult to compare.

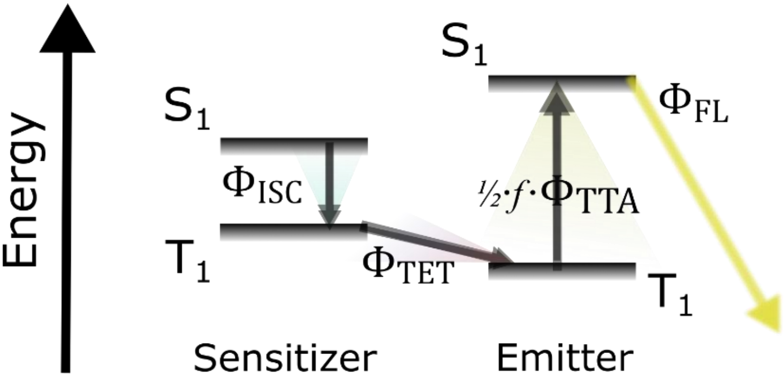

Fig. 3.1 Main energy transfer steps in the sensitizer and emitter based TTA-UC scheme with corresponding yields (Φ) indicated: ISC – intersystem-crossing; TET – triplet energy transfer; TTA - triplet-triplet annihilation; FL – fluorescence.

The measurement of Φ_{UC} is carried out by using an integrating sphere and executing a standard procedure described by Mello et. al.[70] Additionally, for samples exhibiting poor Φ_{UC} a dichroic mirror (notch filter) is used to observe both the UC emission and the excitation in the same spectra. However, for most efficient samples filter was unnecessary since UC samples absorbed (A) >95% of incident light allowing us to measure both NIR excitation (N_{exc}) and sample emission in the visible region (N_{UC}) during the same acquisition and calculate the Φ_{UC}:

$$\Phi_{\mathrm{UC}} = \frac{N_{UC}}{A \cdot N_{exc}} \qquad 3.3$$

Due to high concentrations of the emitter and the presence of the sensitizer, the UC spectrum in the integrated sphere is heavily reabsorbed (see Fig. 3.2). Namely, the right shoulder of the UC spectrum is inhibited by the self-absorption of the emitter, while the right shoulder (clearly visible at 640 nm and 700 in Fig. 3.1) is inhibited due to the presence of the sensitizer. The extent of this effect depends on the sample geometry and can be minimized or altogether diminished for small/thin samples. Thus, to obtain true maximal Φ_{UC} of the system under investigation, the reabsorption correction is executed, and UC spectra is reconstructed by fitting the tail of the UC spectra to match the unperturbed spectra of the sensitizer (see Fig. 3.2). The reconstructed UC spectra is then integrated in the visible region to yield the corrected value of N_{UC}.

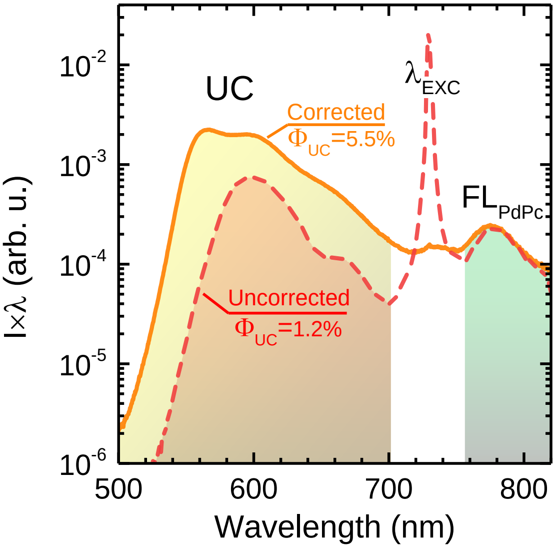

Fig. 3.2 The UC spectra of UC sample taken in the integrating sphere (red dashed line) and the same sample spectra measured outside the integrating sphere without the influence of reabsorption (orange line). The reabsorbed UC spectra can be reconstructed based on unaltered fluorescence of the sensitizer peaking at 774 nm yielding a true UC spectrum.

3.5. Determination of upconversion quantum yield: the inner reference method

One of the key parameters describing the performance of the UC system is Φ_{UC}. The correct evaluation of this parameter is crucial to i) on one hand compare different UC systems; ii) on the other adjust and optimize the existing system to get the best Φ_{UC}. Above mentioned absolute method using an integrating sphere has its drawbacks. Firstly, absolute method is time consuming. Before measurements, it requires time-consuming, delicate calibration. The same sample needs to be measured more than several times, at different configurations, while the final UC spectra needs to be additionally reabsorption corrected by using the unabsorbed spectra taken outside of the integrating sphere. Most importantly the absolute method losses its reliability for samples exhibiting low Φ_{UC} (< 0.05%) due to the difficulty to discern the UC signal from the background. Additionally, the absolute method is not suitable for samples exhibiting low absorption (e.g. A < 5%) since instrumental fluctuations or sample instability can heavily influence the final Φ_{UC}, and thus produce unreliable results.

Compared to the absolute method, the internal reference method for determining the Φ_{UC} is much more versatile, flexible, and adaptable. Usually, only one UC measurement is enough to determine the sample Φ_{UC}. Moreover, there are no strict minimum Φ_{UC} or absorption requirements. The method is viable as long as UC and the reference signal can be separated from the background. The inner-reference method is essentially very similar to Φ_{FL} determination by using comparative (relative) method[69] described by:

$$\Phi_{\mathrm{FL}} = \Phi_R \frac{I}{I_R} \frac{OD_R}{OD} \frac{n^2}{n_R^2} \qquad 3.4$$

here I – the integrated FL intensity, *OD* – optical density (absorption) of the sample and n is the refractive index of the respective medium. The label '*R*' refers to a reference material with known quantum yield. Essentially, this method is based on comparison of PL intensities emerging from two environments (samples).

A slight variation of the comparative method can be applied to the UC samples. As such, in the UC system, where sensitizer PdPc is used as NIR light absorber and triplet exciton generator, after excitation there is always a residual fluorescence arising from PdPc molecules. The latter statement is true since some excited singlet states do not undergo ISC and rather decay radiatively with small and constant Φ_{FL}. Moreover, this residual Φ_{FL} is not affected by the presence of the emitter and does not overlap with UC. Thus, the known PdPc fluorescence can be used as inner-reference, already existing in the UC sample. Consequently, by knowing the Φ_{FL} of PdPc and considering that both signals (UC and FL) emerge from the same environment ($n = n_{\mathrm{R}}$) and both processes are initiated by NIR absorption of PdPc ($OD = OD_R$) the eqn 3.4 can be simplified to:

$$\Phi_{\mathrm{UC}} = \Phi_{\mathrm{FL}} \frac{N_{UC}}{N_{FL}} \qquad 3.5$$

Here N_{UC} and N_{FL} are the number of photos evaluated by integrating the respective regions of UC and FL in the measured spectra. More broadly, the inner-reference method can be used for any other sensitizer exhibiting detectable and stable emission. The reliability of this method heavily relies on the precision to which the reference Φ_{FL} can be measured (see Fig. 3.3a). The Φ_{FL} of the reference can be determined by utilizing other methods such as integrating sphere or relative to standard chromophore (e.g. in our case Nile Blue).

The example of Φ_{UC} determined using internal reference from the UC spectra is illustrated in Fig. 3.3b. The Φ_{UC} determined in this way agrees with the previous definition presented in section 3, being the ratio of registered UC photons to absorbed ones with the maximal Φ_{UC} ideally reaching 50%, since at least two NIR photons are required to produce one visible photon.

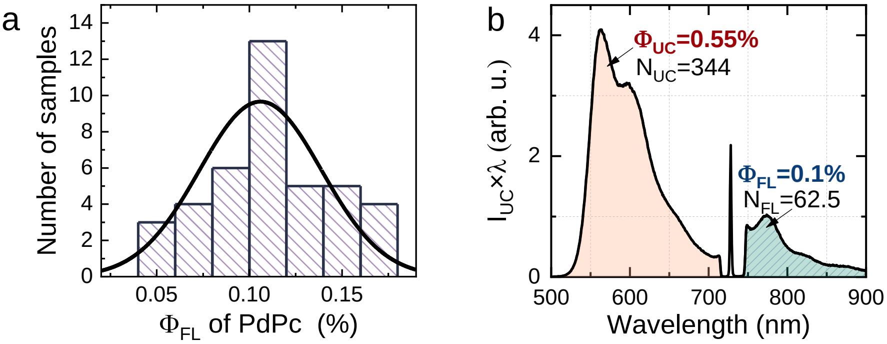

Fig. 3.3 a - Distribution of absolute Φ_{FL} of PdPc-doped polystyrene films at the concentration of 0.1 – 1 wt%. The samples included in the histogram represent various preparation conditions (thickness, concentration etc.) as well as different sample excitation geometries in the integrating sphere. The average Φ_{FL} of PdPc was found to be 0.1% with the standard deviation of 0.03%. b – UC spectra of neat Rub film doped with 0.1 wt% PdPc. This provides an example of the inner-reference method to determine Φ_{UC}.

3.6. Upconversion intensity dependence on excitation power

The UC signal in the sensitizer-emitter system emerges due to TTA occurring between triplet excitations located at the emitter (annihilator) molecules. Namely, for TTA to occur, two triplet excitons must encounter each other to form a fluorescent singlet state. The probability of this encounter is sensitive to the average distance between the generated triplet excitons and increases quadratically with triplet exciton concentration [T]. A simple example of this phenomenon can be illustrated by assuming a random walk of two particles/triplet excitons (Fig. 3.4). We consider that each triplet exciton can move one square at a time with equal probability. In the case of relatively high excitation conditions (Fig. 3.4a) the triplet excitons are nearby and only one hop is sufficient for TTA to occur. In detail, after one hop each particle can take 4 separate paths, while the TTA event can occur only at 2 nodes indicated in red. The final TTA probability (P_{TTA}) is calculated by taking a product of each particle probability to take a path leading to TTA. However, at lower excitation conditions (Fig. 3.4b), we get proportionally lower [T].

Now, exhibiting larger separation triplet excitons require at least two hops to meet and undergo TTA. Notably, only 4 separate paths (noted in green) lead to 3 nodes where TTA is possible. Overall, 2 hops produce 16 different paths for each particle, composing 256 different outcomes in total. If we compare the two scenarios, although the excitation is two times lower, we end up with 4 times reduced P_{TTA}, and conclude that $P_{TTA} \propto I_{exc} \propto [T]^2$.

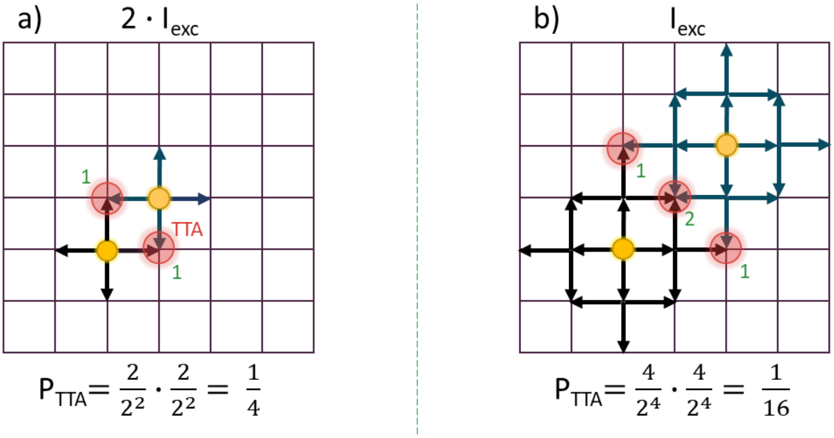

Fig. 3.4 Simplified illustration of the probability tree showing paths of a two particles random walk (moving in 2D) at two excitation conditions. Each particle/triplet exciton (yellow circle) can move (black arrow) one adjacent square (left, right, up, down) at a time with equal probability. a) a case where two particles are nearby requiring only 1 hop for them to meet (red circle; TTA event); b) a case when excitation or triplet density is two times lower, requiring at least 2 hops to meet. In both cases green numbers indicate the number of paths the particle can take to arrive at the indicated node. P_{TTA} is the probability for TTA event and I_{exc} is the excitation intensity.

Experimentally, we observe this by measuring the UC intensity (I_{UC}) dependence on excitation power density (I_{exc}) which is depicted in log-log scale in Fig. 3.5a. First, at low excitation power the I_{UC} increases quadratically (slope of 2). At this regime due to modest [T] the P_{TTA} is low, nevertheless P_{TTA} increases quadratically as explained above. However, at high pump intensity, the immensely increased [T] assures that each triplet exciton find its counterpart within its lifetime and as a result P_{TTA} approaches unity. Now, I_{UC} follows a linear dependence on I_{exc}. The intersection point of these two regimes i.e. square to linear (in double logarithmic scale) is often noted to be the upconversion threshold intensity (I_{th}).[68,71,72] The formal definition of I_{th} is the excitation conditions when the half of the triplets decay through TTA process (Φ_{TTA} = 0.5). The TTA yield can be described by:

$$\Phi_{\mathrm{TTA}} = \frac{k_{\mathrm{TTA}}}{k_{\mathrm{Tot}}} = \frac{\gamma_{\mathrm{TTA}}[T]}{k_{\mathrm{T}} + \gamma_{\mathrm{TTA}}[T]} \qquad 3.6$$

here, γ_{TTA} - second order decay rate for TTA, k_{TTA} – rate of TTA, k_{Tot} – sum of total triplet decay rates, k_{T} – first order triplet decay rate. It follows that I_{th} can also be defined as excitation conditions when the Φ_{UC} reaches half of the maximal theoretical value or Φ_{UC} = ½ × $\Phi_{\mathrm{UC}}^{\infty}$. Correspondingly, the equation for I_{th} can be derived[72]:

$$\mathrm{I}_{\mathrm{th}} = \frac{2(k_{\mathrm{T}})^2}{\gamma_{\mathrm{TTA}}\alpha(E)\Phi_{\mathrm{TET}}} \qquad 3.7$$

here, $\alpha(E)$ – absorption coefficient of the sensitizer at the excitation wavelength, Φ_{TET} – quantum yield of triplet energy transfer from the sensitizer to the emitter. From eqn 3.7 it is evident that for a given system the emitter and sensitizer concentrations should be as high as possible to increase absorption ($\alpha(E)$) and thus to minimize the I_{th}. However, high sensitizer concentrations could be detrimental to the Φ_{UC} due to the back-FRET of UC emission to the sensitizer. Thus, careful optimization needs to be performed to get low I_{th} without compromising the Φ_{UC}.

The Fig. 3.5b displays the Φ_{UC} dependence on pump intensity. The Φ_{UC} increases together with increasing I_{exc} and asymptotically approaches plateau representing maximal $\Phi_{\mathrm{UC}}^{\infty}$. The behaviour of Φ_{UC} can be described by:

$$\Phi_{\mathrm{UC}}^{fit} = \Phi_{\mathrm{UC}}^{\infty}\left(1 + \frac{1 - \sqrt{1 + 2\mathrm{b}\cdot \mathrm{I}_{exc}}}{\mathrm{b}\cdot \mathrm{I}_{exc}}\right) \qquad 3.8$$

here, b = $2/I_{th(38.2\%)}$ = $4/I_{th(50\%)}$. In the parentheses of I_{th} the subscript depicts the percentage value of $\Phi_{UC}/\Phi_{UC}^{\infty}$. This is important since, as pointed out by Murakami et. al. and noted in Fig. 3.5, the conventional intersection of two excitation regimes (slope 2 and slope 1), represents $\Phi_{\mathrm{UC}}/\Phi_{\mathrm{UC}}^{\infty}$ = 38.2%.[68,71] Here, in this dissertation the latter definition of I_{th} is used.

To surely reach TTA domination regime ($I_{exc} >> I_{th}$) amounting to high Φ_{UC} it is convenient to use a system with as low I_{th} as possible. We can see this from Table 3.1, which is based on eqn 3.8. For example, if the I_{exc} is 10 times lower than I_{th} the system operates only at 8.4% of its capacity (Φ_{UC}^{∞}). Evidently, when I_{exc} is 50 times greater than the $I_{th(38.2\%)}$ the Φ_{UC} reaches 86.8% of Φ_{UC}^{∞}. The further increase of I_{exc} leads to a relatively small improvement.

Experimentally, high I_{exc} can cause a deviation from linear I_{UC} dependence, leading to reduced Φ_{UC} and never reaching the potential limit of Φ_{UC}^{∞} (see Fig. 5). This overwhelming excitation can be detrimental for various reasons. For example, typically utilized small concentrations of the sensitizer could lead to conditions where most of the sensitizer molecules are in the excited state, thus causing an absorption bleaching. Additionally, at high excitations exciton-exciton interactions such as singlet-triplet annihilation could occur and thus reduce the I_{UC}.[25]

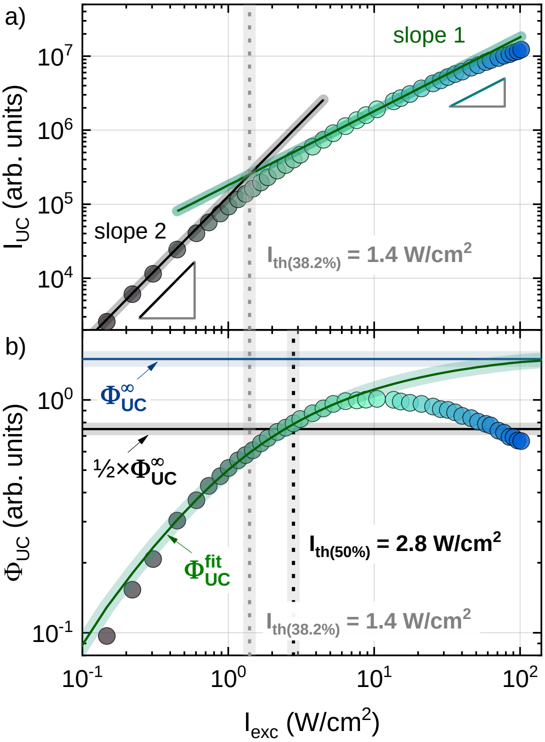

Fig. 3.5 a) UC intensity (I_{UC}) and b) UC yield (Φ_{UC}) *vs.* excitation power density (I_{exc}) of the same UC film. In the top graph a) I_{UC} exhibits typical qudratic (slope = 2) to linear (slope = 1) dependence where the intersection point corresponds to UC threshold ($I_{th(38.2\%)}$). In the bottom part (b) Φ_{UC} or I_{UC}/I_{exc} is fitted (Φ_{UC}^{fit}) with eqn 3.8 and shows how Φ_{UC} asymptotically approaches the theoretical maximal UC yield (Φ_{UC}^{∞}) of the system.

Table 3.1 Φ_{UC} in relation to theoretical limit of $\Phi_{\mathrm{UC}}^{\infty}$ at different excitation conditions based on eqn 3.8. The I_{exc} is the excitation power while $I_{th(38.2\%)}$ and $I_{th(50\%)}$ are UC thresholds defined as 38.2% and 50% of $\Phi_{\mathrm{UC}}^{\infty}$ correspondingly.

I_{exc} / $I_{th(38.2\%)}$	Φ_{UC} / Φ_{UC}^{∞} [%]	I_{exc} / $I_{th(50\%)}$	Φ_{UC} / Φ_{UC}^{∞} [%]
0.1	8.4	0.1	14.6
0.5	26.8	0.5	38.2
1	38.2	1	50.0
2	50.0	2	61.0
5	64.2	5	73.0
10	73.0	10	80.0
20	80.0	20	85.4
50	86.8	50	90.5
100	90.5	100	93.2
200	93.2	200	95.1
500	95.6	500	96.9
1000	96.9	1000	97.8

The measurement of I_{th} was carried out using perpendicular geometry, by exciting a UC sample (either solution in 1 cm thick cuvette or UC film) and collecting the UC emission 90° to the excitation. This allowed to minimize the influence of scattered NIR excitation. For excitation continuous wave laser diode (*PicoQuant*) was utilized exhibiting λ_{exc} = 730nm with a beam diameter of 120 µm. Additionally, to block NIR excitation before the detection, a notch filter was utilized and thus diminished the signal at λ = 730nm by three orders of magnitude. The I_{UC} was collected with CCD spectrometer (*Hamamatsu, PMA-12*), while I_{exc} was determined with power meter (*Ophir photonics, PD-300*).

3.7. Time-resolved spectroscopy

The emitter triplet exciton population, after excitation pulse can decay radiatively, non-radiatively or through TTA. The corresponding rate equation describing triplet exciton concentration [T] is:

$$\frac{d[\mathrm{T}]}{dt} = \mathrm{G_T} - k_{\mathrm{T}}[\mathrm{T}] - \gamma_{\mathrm{TTA}}[\mathrm{T}]^2 \qquad 3.9$$

where $\mathrm{G_T}$ describes the triplet generation (i.e. through TET from the sensitizer), while k_{T} is first order triplet decay rate and γ_{TTA} is the bimolecular annihilation constant. The latter parameter can be further expanded[25]:

$$\gamma_{\mathrm{TTA}} = 8\pi f R D \qquad 3.10$$

where f is the probability for TTA event to result in spin 0 (singlet) state, R is the reaction distance, while D is the triplet diffusion coefficient.

At longer times the $G_T = 0$ and for low excitation conditions when TTA is improbable and k_T is the main deactivation pathway ($k_T\,[\mathrm{T}] >> \gamma_{\mathrm{TTA}}\,[\mathrm{T}]^2$) the solution for eqn 3.9 is:

$$[\mathrm{T}](t) = [\mathrm{T}_0]e^{-k_T t} \qquad 3.11$$

here $[\mathrm{T}_0]$ is the initial triplet concentration. By considering that $I_{UC} \propto [\mathrm{T}]^2$, we can obtain UC signal dependence over time:

$$\mathrm{I}_{\mathrm{UC}}(t) \propto e^{-2k_{\mathrm{T}}t} \qquad 3.12$$

From eqn 3.12 it is evident that I_{UC} decays two times faster than the triplet exciton of the emitter ($\tau_{UC} = ½ \times \tau_T$).

The experimentally measured I_{UC} time dynamics are presented in Fig. 3.6. Evidently there is a region when I_{UC} rises ($t < 10$ µs) and then decays ($t > 10$ µs). At initial times the term G_T is responsible for rise of I_{UC}. Namely, the [T] increases over time due to TET from the sensitizer to the emitter. We can consider the G_T to be time-dependent:

$$\mathrm{G}_{\mathrm{T}}(t) \propto e^{-k_1 t} \qquad 3.13$$

here k_1 is the decay rate of the sensitizer triplets. Now, if we take term G_T from eqn 3.13, under low excitation conditions ($k_T\,[\mathrm{T}] >> \gamma_{\mathrm{TTA}}\,[\mathrm{T}]^2$), the solution to eqn 3.9 describes the whole I_{UC} time dependence:

$$I_{\mathrm{UC}}(t) \propto [\mathrm{T}]^2 \propto (\exp\left(-\frac{t}{\tau_{\mathrm{T}}}\right) - \exp\left(-\frac{t}{\tau_{\mathrm{r}}}\right))^2 \qquad 3.14$$

here, τ_{r} triplet concentration rise time due to TET from the sensitizer and τ_{T} is the time constant of the triplet decay. Since, $\tau_{\mathrm{r}} < \tau_{\mathrm{T}}$, at longer times, we get the eqn. 3.12.

By returning to experimental results (Fig. 3.6), we observe that the sensitizer triplet excitons decay exponentially and at $t = 10$ µs are depleted. At this point emitter [T] reaches a maximum. After this, the I_{UC} decays exponentially (eqn 3.12).

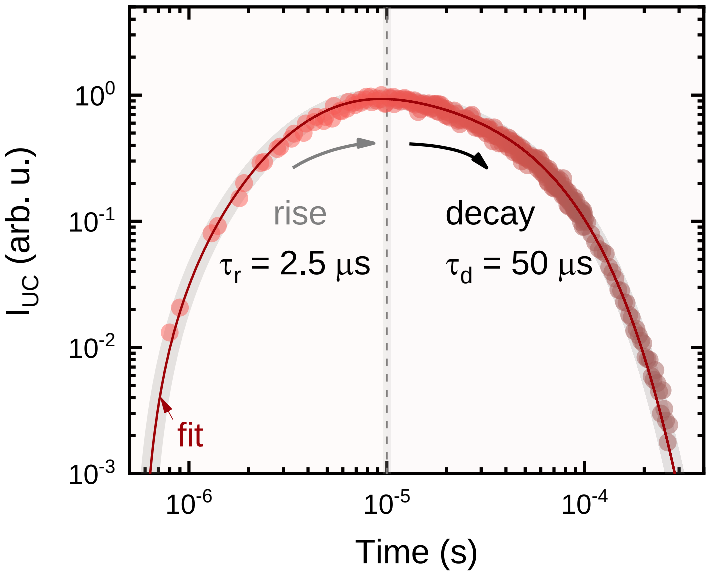

Fig. 3.6 Experimental data of $I_{UC}(t)$. Two distinct regions are visible: rise of UC signal (τ_r) followed by and exponential decay (τ_d). The data points are fitted with eqn 3.14.

The measurement of $I_{UC}(t)$ is carried out with time-gated iCCD camera New iStar DH340T (*Andor*) after exciting the UC samples with emission of tunable-wavelength optical amplifier (*Ekspla*) pumped by a nanosecond Nd^{3+}:YAG laser (λ = 730 nm, pulse duration – 5 ns, repetition rate – 1 kHz). By changing iCCD gate width, delay and exposure the measured UC transients span over three orders of magnitude in intensity and three orders of magnitude in time. The obtained UC spectra are normalized to same measurement conditions (gate and exposure), then integrated and fitted using eqn **Error! Reference source not found.** to obtain τ_r, τ_d, τ_T .

3.8. Determination of the exciton diffusion parameters

In disordered rigid films, molecules are chaotically distributed with fixed positions. Excitation of these molecules leads to locally excited states (Frenkel excitons) that are bound to one molecule. However, excitons can migrate through the molecular manifold, in simplified terms, by means of hoping, from one molecule to another. Generally, the net movement of excitons during their lifetime can be well described by diffusion. In the materials with high triplet diffusivity, the TTA is more probable since TTA event requires two triplet excitons in proximity to each other. This is especially true at low excitation conditions (low [T]). Thus, the characterization of the triplet diffusion in the emitter films is useful to understand when designing the UC systems.

The triplet exciton diffusion in the spin-coated UC films was evaluated by using the time-resolved photoluminescence bulk-quenching technique followed by Stern-Volmer analysis, which was previously demonstrated to be the accurate tool for the determination of exciton diffusion parameters.[73,74] A series of emitter films with varying amounts of randomly distributed exciton quenchers were fabricated. Chloranil, exhibiting strong electron accepting properties and causing instant exciton dissociation in contact with excited Rub species, was chosen as a triplet exciton quencher.[75] In the prepared films with the dispersed quenchers, the excitons are free to diffuse during their lifetime through the Rub network and decay non-radiatively if the quenching site is reached. By measuring UC transients, the quenching efficiency can be evaluated and used to determine Stern-Volmer constant (K_{SV}), and subsequently, the diffusion coefficient (D_T).

The I_{UC} proportional to [T] which is described by eqn 3.9. Thus, by measuring UC transients, generally non-emissive triplet excitons in Rub can be probed indirectly. Special care must be taken to ensure that the transients are dominated by spontaneous triplet decay and not TTA (low excitation conditions), as this will allow to probe triplet exciton lifetime, which in turn is affected by the quenchers. Measuring UC transients at low triplet concentrations also eliminates other unwanted possible deactivation channels, such as singlet-triplet annihilation (STA).

Relative quenching efficiency of the triplets (Q) at a certain quencher concentration ($[\mathrm{Q_c}]$) was evaluated by using the following equation:

$$Q = 1 - \frac{\int \sqrt{\mathrm{I}_{\mathrm{UC(q)}}(t)}\mathrm{d}t}{\int \sqrt{\mathrm{I}_{\mathrm{UC}}(t)}\mathrm{d}t} = 1 - \frac{\tau_{\mathrm{T(q)}}}{\tau_{\mathrm{T}}} = 1 - \frac{\tau_{\mathrm{UC(q)}}}{\tau_{\mathrm{UC}}} \qquad 3.15$$

here $\mathrm{I}_{\mathrm{UC(q)}}$(t) and I_{UC}(t) stand for UC transients of the films with chloranil quenchers present and absent, respectively. τ_{T}(q) and τ_{UC}(q) are corresponding lifetimes with quenchers present.

K_{SV} was estimated by fitting experimental Q data utilizing “hindered access model”[74], by which only a fraction (f_{a}) of the quenchers were accessible to the excitons in emitter molecules due to the possible quencher aggregation.

$$Q = f_{\mathrm{a}} - \frac{f_{\mathrm{a}}}{1 + K_{\mathrm{SV}}[Q_{\mathrm{c}}]} \qquad 3.16$$

Exciton diffusion coefficient (D) for a given K_{SV} can be calculated from the following expression:

$$D = \frac{K_{\mathrm{SV}}}{4\pi r P \tau N_{\mathrm{A}}} \qquad 3.17$$

where r is reactive radius, which in this case is assumed to be a sum of the radiuses of the spheres (volumes) occupied by emitter and quencher molecules in the solid-state, P_{q} is the quenching probability of the exciton upon reaching the quencher (assumed to be =1), N_A is Avogadro's number. Dimensions of the molecules were estimated by taking the cube root of the volume occupied by one mole of that material:

$$d = \sqrt[3]{\frac{M}{\rho N_{\mathrm{A}}}} \qquad 3.18$$

here M is a molar mass and ρ is a density of material.

All things considered the exciton diffusion length (L_{D}) calculated from:

$$L_D = \sqrt{\tau D} \qquad 3.19$$

4. NIR-TO-VIS UPCONVERSION IN SOLUTION: LIMITING FACTORS OF RUBRENE-BASED SYSTEMS

In this chapter, the key aspects of the first publication **PI** are outlined. After introduction to modern NIR-to-Vis UC systems it becomes evident that even the best performing systems lack appropriate efficiency required for practical applications. To address the issue and provide more clarity, we focus on rubrene, by far the most used emitter in the field. To complement Rub in UC scheme, two novel metallophthalocyanines were synthesized, and by absorbing NIR light, served as triplet sensitizers. Moreover, aiming to improve and introduce an alternative TTA emitter, we modified rubrene with solubility increasing *tert*-butyl groups (tBRub). Essentially, by utilizing different combinations of sensitizer and emitter pairs as well as carrying out delicate optimization steps toward best UC efficiency reaching record high Φ_{UC} = 5.6%, we deduce that utmost $\Phi_{\mathrm{UC}}^{\mathrm{max}}$ = 8% can be obtained using Rub as an emitter. The cause of the upper limit is attributed to low statistical probability to obtain a singlet state under TTA event. This encourages to actively seek for alternative TTA emitters to surpass the current efficiency barrier.

Photophysical properties of metallophthalocyanines

At first, two metallophthalocyanines (MPc) were synthesized to serve as NIR photon absorbers and triplet sensitizers. To ensure rapid ISC, the heavy metal atom, either palladium (Pd) or platinum (Pt) were positioned in the MPc core. The chemical structures of these MPc were already presented in the introductory part of the dissertation (see Fig. 2.2). The MPc investigated in **PI** were assessed independently and their main photophysical properties are summarized in Table 4.1. Notably, the lowest triplet state energy (T_1) of PdPc and PtPc were found to be 1.12 eV and 1.18 eV, respectively, as determined from the phosphorescence (Ph) peak. Importantly, T_1 of MPc is similar to T_1 of Rub (1.04 – 1.14 eV)[75,76] proving to be suitable to sensitize Rub. Furthermore, Rub PL emission (see Fig. 4.1) peaking at ~560 nm is positioned in the transparency window of MPc. The same is also valid for tBRub, since added non-conjugated *t*-butyl moieties make an insignificant impact on the absorption and FL properties of the unsubstituted Rub emitter.

Table 4.1. Photophysical properties of PdPc and PtPc sensitizers in toluene solution (c = 1.0 × 10^{-5} M).

	ε^{a}	$\lambda_{abs}{}^{b}$	$\lambda_{FL}{}^{c}$	$\lambda_{PH}{}^{d}$	$\Phi_{FL}^{S}{}^{e}$	$\tau_0{}^{f}$
	×10^5 M^{-1} cm^{-1}	nm, (eV)	nm, (eV)	nm, (eV)	%	μs
PdPc	2.46	720, (1.72)	750, (1.65)	1110, (1.12)	0.3	3.3-4.3
PtPc	1.87	709, (1.75)	785, (1.58)	1055, (1.18)	0.6	0.7

[a] Molar extinction coefficient. [b] Absorption maximum of Q band. [c] Peak fluorescence and [d] phosphorescence emission. [e] FL quantum yield measured in integrating sphere. [f] Triplet lifetime of sensitizers.

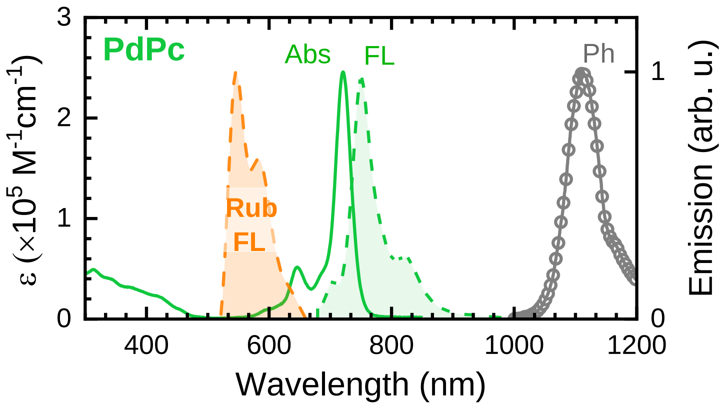

Fig. 4.1. Absorption (solid lines), fluorescence (filled dashed lines) and phosphorescence (circles) spectra of PdPc sensitizer in toluene (c = 1.0 × 10^{-5} M). FL spectra of Rub in toluene (c = 1.0 × 10^{-5} M) is shown for reference. Spectra of PtPc can be found in **PI.**

Seeking for the optimal upconverting solution

Since the UC process requires two components (sensitizer and emitter), the right ratio of the constituents is needed for the effective TTA to occur. Therefore, it is useful to assess the UC using different sensitizer/emitter mixtures (see Fig. 4.2a). Systematically, it is easier to carry out the optimization by fixing the sensitizer concentration and gradually increasing the emitter concentration. From TTA-UC energy scheme it is rational to assume that sensitizer concentration needs to be as low as possible for back-FRET to be minimized, however triplet concentration needs to be high enough for TTA to occur efficiently. The 15 µM of PdPc was selected to be optimal since it ensured strong 730 nm NIR absorption with OD ~ 3.7. In Fig. 4.2a we can see experimental results of emitters concentration optimization. Under conditions, when emitter is absent the 730 nm excitation does not lead to any signal in the visible range. However, noticeable UC emission emerged when 10^{-4} M of Rub was added. The further increase of emitter concentration to 18mM lead to continuous increase of UC intensity. The accompanied FL of PdPc remained constant and indicated persistently improving Φ_{UC} up to the highest possible emitter concentrations. The same tendency was observed by changing the emitter to tBRub. This observation can be rationalized by considering that increase of emitter concentration decreases the average distance between sensitizer and the emitter. This, in turn, leads to more efficient dexter-type triplet energy transfer. Additionally, the average distance between emitters is reduced leading to more probable triplet encounter and thus TTA. At 18mM of Rub we reach the solubility limit. Further concentration increase would lead to detrimental emitter aggregation.

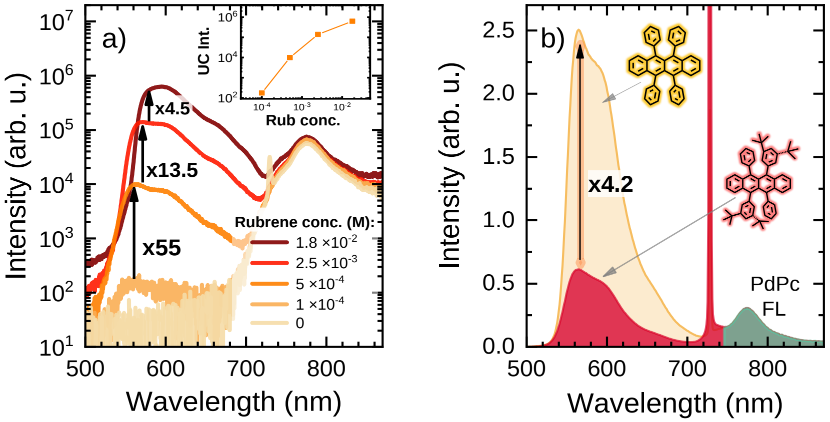

Fig. 4.2 a) UC emission spectra of Rub:PdPc solution at different Rub concentrations (indicated) and fixed PdPc (15 µM) concentration. Inset depicts UC peak intensity *vs.* Rub concentration. b) Comparing UC emission of Rub and tBRub under identical conditions, using 18mM of emitter and 15 µM of PdPc sensitizer. All experiments were carried out under 730 nm CW excitation.

The emerging UC from concentrated Rub was compared to tBRub at otherwise identical conditions (see Fig. 4.2b). This allowed us to assess the differences between the emitters, since observed UC intensity is proportional to Φ_{UC}. Interestingly, the Rub outperformed the tBRub and demonstrated more than 4 times brighter UC emission. By taking the advantage of solubility improving *t*-butyl groups, the tBRub concentration was increased to 40mM, however, the measured UC still demonstrated lower performance. The further analysis aims to investigate the discrepancies between these two emitters and find the processes that hamper UC efficiency.

Evaluating triplet energy transfer in UC solutions

From eqn 3.1 it is evident that ideally Φ_{UC} could reach 50%. In detail, the intermediate energy transfer steps, such ISC, TET, TTA followed by FL could supress the Φ_{UC}. When optimizing UC samples, it is useful to deconstruct each energy transfer step and identify the weakest link in the scheme. Firstly, as discussed in this section, we aim to evaluate the yield of triplets that reaches the emitter (Φ_{TET}).

The Φ_{TET} can be evaluated by performing triplet quenching experiments (see Fig. 4.3). It is considered that sensitizer triplets are quenched by the presence of the emitter.[40,77,78] In turn, the Φ_{TET} can be estimated from the ratio of quenched (τ_1) and non-quenched (τ_0) triplet lifetimes of the sensitizer according to:

$$\Phi_{\mathrm{TET}} = 1 - \frac{\tau_1}{\tau_0} \qquad 4.1$$

Since triplet states are dark, their concentration over time can be evaluated by using UC signal as a probe. Given the dominant triplet relaxation pathway is spontaneous decay, the temporal dynamics of UC intensity, which is proportional to the square of the triplet concentration of Rub, $[T_1^{Rub}]^2$, can be described by eqn 3.14 (see experimental section on time-resolved spectroscopy).

The UC transients along with their fits are depicted in Fig. 4.3a with an emphasis on initial rise of UC intensity. The rise is steeper for concentrated solutions indicating faster TET. After reaching peak intensity the UC transients decay mono-exponentially (inset of Fig. 2.2a) with a lifetime τ_{UC} = 50μs. This corresponds to Rub triplet lifetime of $\tau_T = 2 \times \tau_{\mathrm{UC}}$ = 100 μs.

Extrapolating the τ_1 to zero emitter concentration provides information on unquenched triplet lifetime (τ_0) of PdPc (see Fig. 4.3b). Therefore, the Φ_{TET} can be calculated at any emitter concentration. Namely, the τ_0 of PdPc was determined to be 3.3 μs, which is similar to PdPc reported elsewhere[66] (Fig. 4.3b). By changing the Rub concentration from 1mM to 18mM the Φ_{TET}

increased from ~24% to ~82%. The additional Φ_{TET} measurements for tBRub as an emitter or using the PtPc as a sensitizer can be found in **PI**.

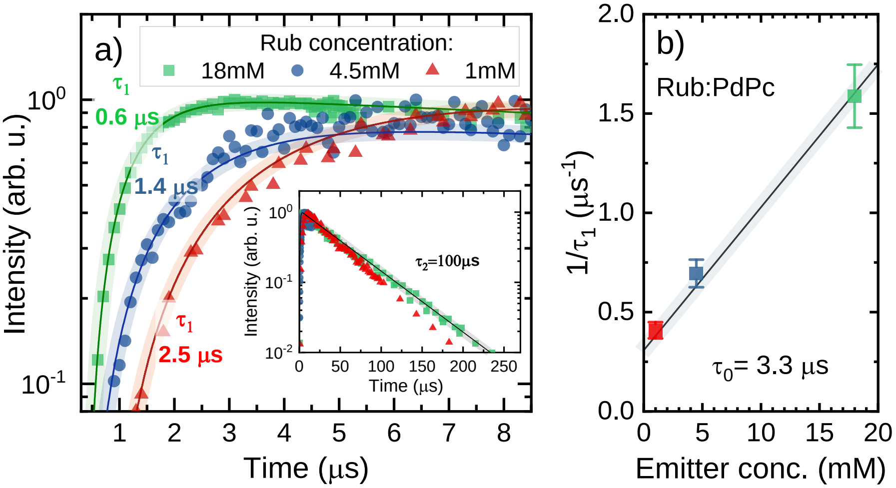

Fig. 4.3 a) UC transients of Rub:PdPc at fixed sensitizer concentration (15 μM) and different emitter concentrations (indicated) obtained using nanosecond laser excitation at 730 nm. Insets depict the transients on a longer time-frame. b) The inverse of UC transient rise time as function of emitter concentration. Concentration of sensitizers PdPc was fixed at 15 μM. Triplet lifetime of sensitizers (τ_0) is indicated wich estimated as the inverse of the intercept.

Upconversion yield and probability factor in rubrene-based systems

All intermediate energy transfer steps in UC scheme were evaluated independently and are summarized in Table 4.2. Although used MPc exhibit Φ_{isc} close to unity, the measured Φ_{TET} and Φ_{FL} are relatively high whereas Φ_{TTA} approaches unity at high excitation regime, the overall Φ_{UC} is low for all studied UC samples (1.3 – 5.7 %). The remaining parameter having a direct impact on Φ_{UC} is statistical probability factor (f). The factor describes probability for the triplet pair in an emitter to form one singlet via TTA. Relying purely on spin statistics and taking into account that triplet encounter complex can be of singlet, triplet or quintet multiplicity with corresponding statistically weighted formation probability of 1:3:5, f should not exceed 1/9 (or 11.1%).[38] However, there are many reports surpassing this limit. This can be rationalized by considering that triplet and quintet complexes may not necessarily quench to the ground state, but instead, depending on the relative position of energy levels, relax back into triplets.

Table 4.2 Obtained quantities determining the performance of the investigated UC systems under CW excitation at 730nm.

UC system	Emitter (18 mM):Sensitizer (15 µM) in Toluene Solution				
	Φ_{TET}[a] %	f[b] %	Φ_{FL}[c] %	Φ_{UC}[d] %	I_{th}[e] W/cm^2
Rub:PdPc	82	15.6	90	5.7	1.9
Rub:PtPc	71	15.4	90	4.9	11.0
tBRub:PdPc	56	5.3	90	1.3	3.6

[a] Triplet energy transfer yield. [b] Statistical probability factor to obtain a singlet from two emitter triplets via TTA. [c] FL and [d] UC quantum yields. [e] UC threshold.

A product $[f \times \Phi_{\mathrm{TTA}}]$ in the studied UC systems was estimated by directly comparing delayed (I_{UC}) and prompt (I_{FL}) FL intensities and considering that both emissions emerge from the same emitter species in the same environment (see Fig. 4.4).[36,37] From eqn. 3.1 we can derive that:

$$[f \cdot \Phi_{\mathrm{TTA}}] = 2\frac{\Phi_{\mathrm{UC}}}{\Phi_{\mathrm{FL}}} \cdot \frac{1}{\Phi_{\mathrm{TET}}\Phi_{\mathrm{ISC}}} \qquad 4.2$$

$$[f \cdot \Phi_{\mathrm{TTA}}] = 2\frac{I_{\mathrm{UC}} I_{\mathrm{exc}}^{485} \lambda_{485}}{I_{\mathrm{FL}} I_{\mathrm{exc}}^{730} \lambda_{730}} \cdot \frac{1}{\Phi_{\mathrm{TET}}\Phi_{\mathrm{ISC}}} \qquad 4.3$$

Importantly, Φ_{TTA} depends on triplet concentration and thus on excitation power. In Rub:PdPc system when the condition $I_{\mathrm{exc}} > I_{\mathrm{th}}$ is met, the I_{UC} increases linearly (see Fig. 4.4a). This correspond to TTA saturation which is reached when TTA outcompetes spontaneous triplet decay and becomes the dominant triplet decay channel. As a result, Φ_{TTA} approaches unity permitting to determine f from the saturated value (see Fig. 4.4b). In case, of Rub:PdPc the f value of 15.6% was obtained. Additionally, the same result was obtained using PtPc as a sensitizer, confirming that f is independent of the sensitizer and is an intrinsic property of the emitter. The determined f imposes maximum limit of $\frac{1}{2} \times f \approx 8\%$ on Φ_{UC} of Rub UC systems provided all the energy transfer/conversion steps are 100% efficient. This results partly explains why out of numerous reports on rubrene-based UC systems, there was not a single demonstration of Φ_{UC} exceeding this limit.[3,19,29,37,48,78–80]

By applying same investigation for tBRub it was revealed that the *t*-butyl moieties produce a negative impact on the UC performance, namely by reducing *f* almost 3 times compared to Rub. Additionally, Φ_{UC} value was confirmed by independent measurement with integrating sphere, providing confidence in the obtained result. It is worth pointing out that the maximal Φ_{UC} (5.7%) obtained by optimizing emitter and sensitizer concentrations in Rub:PdPc is among the largest reported for NIR-to-Vis UC system's absorbing at > 730 nm.[19,48,52,78,79,81] On the other hand for the next breakthrough towards efficiencies reaching close to 50 % the search for novel emitters are required.

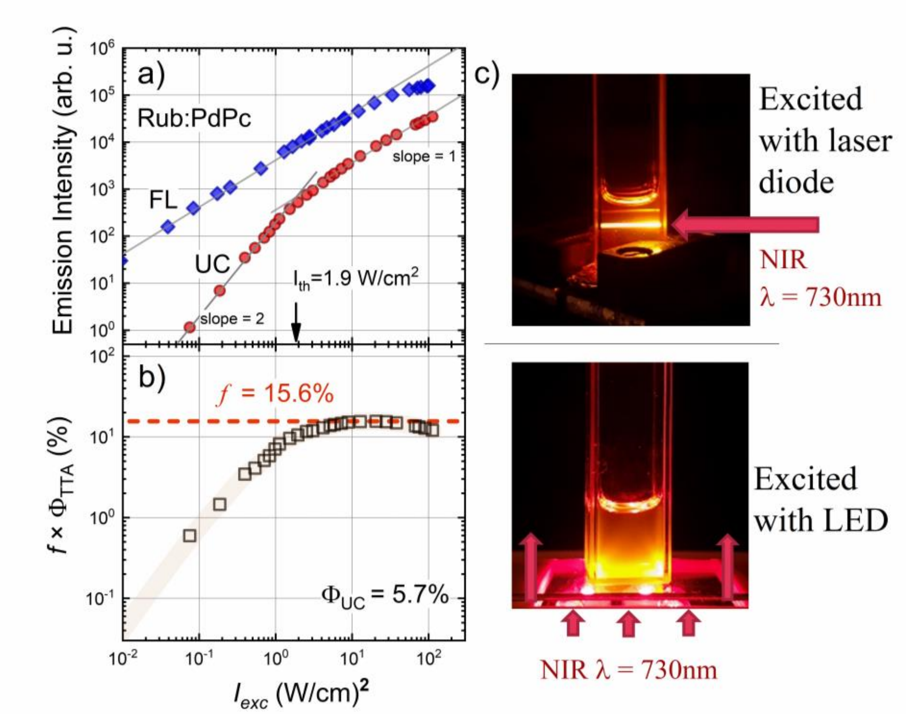

Fig. 4.4 a) FL and UC intensities under CW excitation at 485 nm and 730 nm, respectively, as a function of excitation power density for Rub (18 mM):PdPc (15 µM) system. b) Excitation dependences of the product [$f \times \Phi_{TET}$] of the same systems calculated according to eqn 4.3. *f* value is indicated. c – Pictures of UC emission in Rub:PdPc solution under NIR excitation (no filter used).

5. ACHIEVING SOLID-STATE UPCONVERSION BY MEANS OF MOLECULAR ENGINEERING AND SINGLET EXCITON SINK APPROACH

The previous chapter discussed the main limitations of TTA-UC in solution. However, there are many applications (e.g. photovoltaics) that require TTA-UC to be efficient in the solid-state. The rigid systems with fixed molecule positions are far more complex and introduce additional hurdles that inhibit UC efficiency. **PII** is written in attempt to tackle this problem and here, in this chapter, the main insights are provided with a summary of the results. Specifically, here investigated UC films were prepared by means of spin coating using rubrene and PdPc as active molecules. It was identified that poor TTA-UC performance is related to drastically reduced rubrene fluorescence quantum yield in the solid-state. To improve UC efficiency rubrene was modified with non-conjugated *tert*-butyl moieties (tBRub). Although modification was anticipated to act as spacing groups and supress the undesirable concentration quenching of emission, it could potentially induce adverse effects, i.e. reduce triplet diffusion and diffusion assisted TTA, hence hamper UC efficiency. Additionally, to improve emission yield tetraphenyldibenzoperiflanthene (DBP) was mixed with UC components to collect the UC singlets from the emitter and diminish any non-radiative pathways. Moreover, polystyrene binder was utilized to control the average distance between molecules thus further minimize the extent of aggregation. The UC performance optimization against emitter concentration revealed 4-fold higher Φ_{UC} (0.3%) in tBRub films as compared to that in rubrene films (0.07%) at the optimal emitter doping of 80 wt%.

Introducing singlet exciton sink in UC scheme

Aiming to achieve NIR-to-Vis UC in the solid-state as well as improve Φ_{UC}, we used a TTA-UC scheme composed of a singlet exciton sink Fig. 5.1a. Specifically, the structures of the materials used in **PII** are illustrated in Fig. 5.1b. As a foundation for TTA-UC PdPc triplet sensitizer and Rub or tBRub emitter was used, while DBP served as singlet exciton sink. The later component is used to improve poor Φ_{FL} of the Rub in the solid-state, serving as emissive dopant that via FRET (Fig. 5.1a) collects after TTA generated singlet states that would otherwise decay non-radiatively. This approach, firstly adapted for efficient red OLEDs[82], is also demonstrated to work in solid-state UC. Namely, forming 80 nm thick film by the co-evaporation of 80 nm of Rub and 0.5 vol% of DBP was demonstrated to improve emission intensity by 19-fold in respect to Rub only films.[54] Similar result is also reported for Rub nano particles were the Φ_{FL} is increased from ~3% in neat Rub to ~60% doped with 0.5 mol% of DBP Although, in the literature the exact cause for the efficiency increase is under the debate.[83] Furthermore, there are suggestions that DBP can be altogether omitted. In the works on perovskite sensitized UC films, DBP unnecessarily complicated the UC scheme with a cost of red-shift of the UC emission of 0.15 eV.[84] Nevertheless, we decided to investigate the influence of DBP in our UC films.

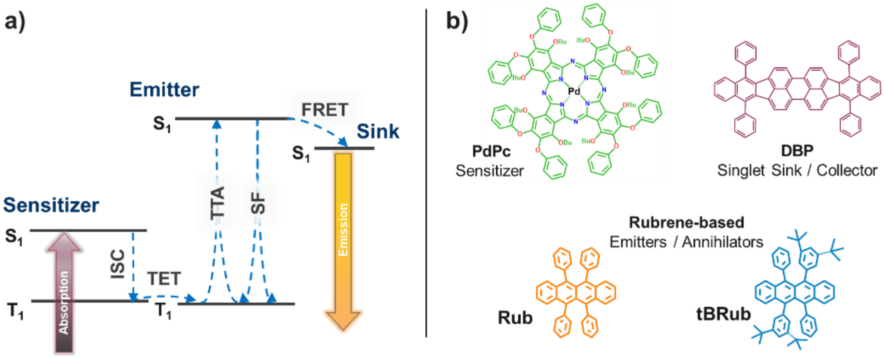

Fig. 5.1 a) TTA-UC energy scheme for PdPc-sensitized rubrene (or tBRub) systems with DBP as singlet sink (collector). Here, ISC – intersystem crossing, TET – triplet energy transfer, TTA – triplet-triplet annihilation, SF – singlet fission, FRET – Förster resonant energy transfer. B) Chemical structures of PdPc sensitizer, singlet exciton sink DBP and rubrene-based emitters (rub and tBRub).

Photophysical properties of UC active components

Firstly, the photophysical properties of UC components were investigated separately. For isolated molecules the main results are displayed in Fig. 5.2. From absorption and FL spectra (Fig. 5.2a) of Rub and *t*-butyl-functionalized rubrene (tBRub) emitters were found to be similar. This indicates negligible impact of *t*-butyl moieties on electronic structure of Rub core. Thus, unaltered energetics allows to presume that TTA process for tBRub emitter is similarly feasible as that for Rub. Additionally, in Fig. 5.2b emission spectrum of DBP dispersed in PS film at 0.01 wt% concentration is displayed. Here, we can expect FRET between emitter and exciton sink, due to overlap of Rub emission and DBP absorption spectra. DBP is also suitable to serve as exciton sink due to high Φ_{FL} (Φ_{FL} ~ 84%). Importantly, although emission of DBP is redshifted by about 60 nm as compared to FL of rubrene (or tBRub) it is still within the transparency region of the sensitizer absorption (Fig. 5.2a). Considering that the lowest triplet state of DBP is ~0.2 eV higher than that of rubrene,[82] DBP is expected not to affect TTA process in the emitter.

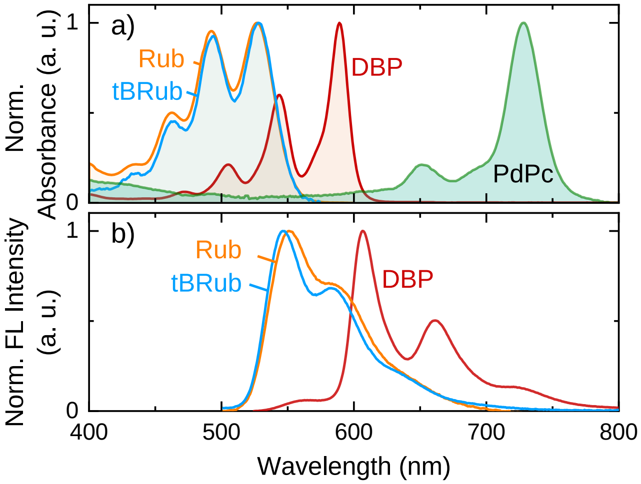

Fig. 5.2 a) Absorption spectra of rubrene, TBR emitters and singlet exciton sink DBP in toluene ($1\cdot10^{-5}$M). The absorption spectrum of PdPc sensitizer is displayed for reference. b) PL emission spectra of rubrene, tBRub and DBP in polystyrene (PS) films at 0.01 wt% concentration.

Concentration quenching of rubrene emitters

Typically, in most organic semiconductors, reduced molecular distance between emissive species results in fluorescence quenching. Often, this can be related to quenching site formation related to impurities or molecular aggregates.[25,69] For Rub there is rapid non-radiative deactivation channel related to excited state energy level alignment. In Rub singlet energy (S_1) is two times higher the triplet energy (T_1), i.e. $S_1 \sim 2\times T_1$. This opens a possibility for singlet splitting into two triplets, the so-called singlet fission (SF). This Dexter-type process requires decent electron wavefunction overlap between the neighbouring molecules making it sensitive to emitter concentration. Since SF occurs at ~ps scale[85] it is the dominant non-radiative singlet decay channel. The *t*-butyl moieties were expected to increase the average distance between emitters and thus minimize the impact of SF.

We prepared a series of spin-coated films with various emitter concentrations in polymer matrix (PS) that represents a gradually changing distance between emitter molecules. The measurements of corresponding spectra and Φ_{FL}

(Fig. 5.3) together with FL lifetime measurements (see **PII**) were assessed to investigate role of *t*-butyl groups in suppression of FL quenching.

In contrast to Rub, tBRub exhibits notably less FL spectral changes with increasing emitter concentration (Fig. 5.3a-b) indicating that emission from amorphous tBRub phase prevails almost up to 100 wt%. Moreover, the extent of spectral change neatly correlates with the change of Φ_{FL} as well as FL lifetimes of the same samples. Namely, the Φ_{FL} of the films were estimated using an integrating sphere and are compared in Fig. 5.3c. At low emitter concentrations (up to 1 wt%) in PS, both emitters expressed Φ_{FL} close to 100%, indicating negligible intermolecular interaction and FL quenching. However, further increase in concentration resulted in rather different Φ_{FL} behaviors. Rub already suffered a steep Φ_{FL} drop at concentrations above 1 wt%, whereas tBRub showed persistently high Φ_{FL} up to 30 wt% and experienced only slight decrease above this concentration. Eventually, in the neat Rub film (at 100 wt% of emitter) Φ_{FL} drastically decreased down to 1.5%, which is ascribed to the formation of crystalline aggregates facilitating already mentioned SF. [76,85–87] On the other hand, Φ_{FL} of the neat tBRub films was found to be a factor of ~20 higher (Φ_{FL} = 35%), thus confirming the preventive role of *t*-butyl moieties in reducing SF promoted FL quenching.

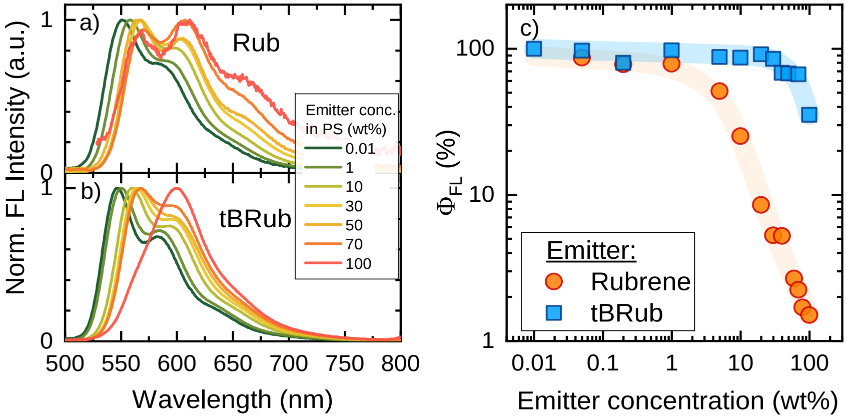

Fig. 5.3 Fluorescence spectra of emitter-doped PS films as a function of emitter concentration, where emitter is a) rubrene and b) tBRub. c) Fluorescence quantum yield of emitter-doped PS films as a function of emitter concentration. Measurements were carried out in the integrating sphere. Lines serve as guidelines to the eye.

The next optimization step was related to the DBP singlet exciton sink and its ability to enhance the emission of spin-coated Rub films. The Fig. 5.4 shows FL spectra and Φ_{FL} of DBP-doped Rub films as a function of doping concentration in the range of 0 – 1 wt%. The FL spectrum change with increasing DBP concentration clearly demonstrates that even a small amount of DBP noticeably changes the emission properties. At 0.5 wt% of DBP, the emission spectrum resembled that of the pure DBP spectrum (see Fig. 5.2) indicating efficient FRET from Rub to DBP. Moreover, DBP doped films showed improved Φ_{FL}. In the in sink-free Rub films the Φ_{FL} = 1.5%, whereas in DBP doped films, the yield has increased 10-fold, up to Φ_{FL} = 15%. Still the latter value is found to be roughly 7 times lower than that of Rub in isolated form ($\Phi_{FL} \sim 100\%$). Evidently, the FL quenching is not completely suppressed by addition of 0.5 wt% DBP, and unfortunately cannot be further minimized due to DBP aggregation at higher concentrations. The optimal 0.5 wt% DBP concentration was further utilized in the fabrication of PdPc-sensitized UC films, with Rub and tBRub emitters.

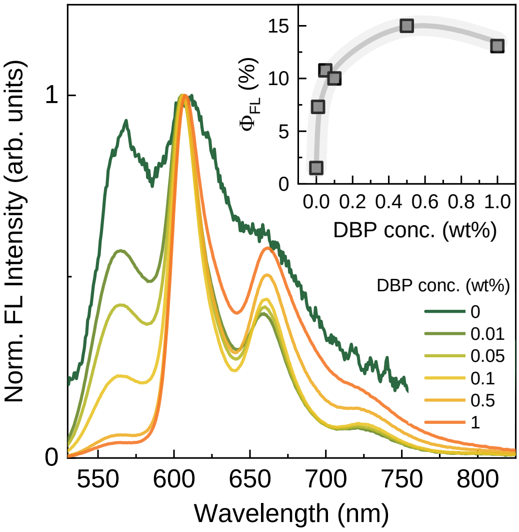

Fig. 5.4 FL spectra of DBP-doped Rub films at various doping concentrations. The inset shows the Φ_{FL} of the films as a function of sink concentration. Excitation wavelength – 450 nm.

Motivated to find the optimal emitter concentration and realize the most efficient TTA-UC, we manufactured PdPc-sensitized UC films with different Rub and tBRub concentrations. During the fabrication, concentrations of the sensitizer PdPc and singlet exciton sink DBP were kept constant, at their optimal values of 0.1 wt% and 0.5 wt%, respectively. The UC and FL performance were evaluated using integrating sphere. The Φ_{FL} of the manufactured films was obtained by directly exciting emitter species (λ_{exc} = 450 nm) (Fig. 5.5a), while Φ_{UC} was obtained by exciting sensitizer species with NIR light (λ_{exc} = 730 nm) in the same sample. The results of such comparison are displayed alongside in Fig. 5.5a-b, for both Rub and tBRub. Notably, investigated UC films exhibited bright Vis emission under NIR excitation, observable by the naked eye (Fig. 5.5c).

We observed monotonous decrease of Φ_{FL} for rubrene UC films, when emitter content changed from 30 to 100 wt% (Fig. 5.5a). We rationalize this result by considering the adverse back-FRET to PdPc as well as increasing influence of SF in emitter as discussed above. Although doped with DBP, at the highest Rub emitter concentration, the UC films containing PdPc exhibited low Φ_{FL} = 2.5%, whereas the same films without sensitizer expressed Φ_{FL} = 15% (see Fig. 5.5a). This implies a factor of 6 lower Φ_{FL} due to back-FRET to sensitizer. The decrease of Φ_{FL} with increasing emitter concentration was also obtained for tBRub, although at a considerably smaller extent.

Contrary to the Φ_{FL} dynamics, the Φ_{UC} of the UC films showed non-monotonous behaviour with increasing emitter contents (Fig. 5.5b). Initially, Φ_{UC} increased with increasing Rub and tBRub concentration up to 80 wt%, where maximum Φ_{UC} were reached, and then began slightly declining above this concentration. The maximum Φ_{UC} attained in these films was 0.07% and 0.3% for Rub and tBRub emitters, respectively. It was determined that the observed initial increase of Φ_{UC} could only be justified by the enhanced Φ_{TET} since Φ_{TET} should exhibit exponential growth with decreasing the distance between emitter and sensitizer. Eventually, the growth of TET will saturate at some Φ_{TET} value (not necessarily at 100%), which in the studied UC films occurs at the emitter concentration of about 80 wt%. Further behaviour of Φ_{UC} with increasing emitter concentration should follow that of Φ_{FL} as all the other intermediate energy transfer steps have already reached maximum efficiency. Indeed, 4-fold higher maximum Φ_{UC} obtained for tBRub film as compared to that of Rub at 80 wt% concentration well corresponds to 4-fold higher Φ_{FL} in tBRub film *vs.* Rub film at the same concentration. This infers similar Φ_{TET} in both emitter-type UC films and additionally clarifies the cause of improved Φ_{UC} in tBRub films mainly due to the suppressed SF.

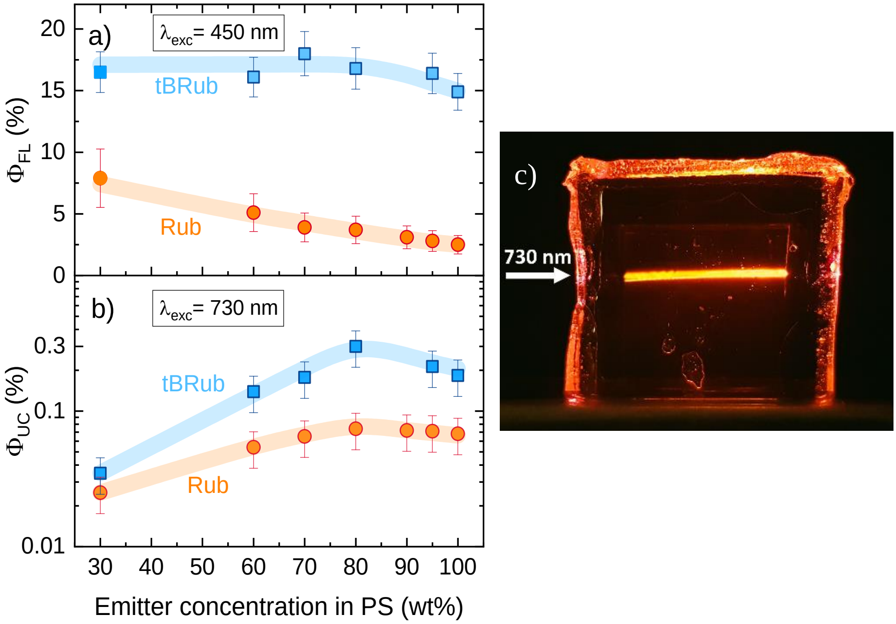

Fig. 5.5 a) FL and b) UC quantum yields of PdPc-sensitized UC films doped with singlet sink DBP as a function emitter Rub or tBRub concentration. All samples contained 0.1 wt% of PdPc and 0.5 wt% DBP. FL and UC excitation wavelengths were 450 nm and 730 nm, respectively. Excitation density at 730 nm – 100 W/cm^2. c) Picture of NIR-to-Vis upconversion in the polymer film with tBRub emitter excited at the edge of the film with 730 nm light.

6. EMITTER OPTIMIZATION: INFLUENCE OF SIDE GROUPS ON RUBRENE EMISSIVE PROPERTIES AND IMPLICATIONS FOR TTA

As discussed in the previous chapter in the solid films Rub emission is strongly hampered by singlet fission. This, in turn, negatively affects the efficiency of UC. The extent of SF in Rub is reduced by adding *t*-butyl moieties and therefore increasing the UC efficiency. Based on the later result obtained in **PII**, we extend the main insight further in the publication **PIII**. In **PIII** we modified Rub emitter with larger and more sterically demanding 3,5-di-*tert*-butylphenyl side-moieties at the periphery (peri-tBRub) and the core (core-tBRub) and achieved 40-fold enhancement of the emission quantum yield in the solid films. Here, the main results of investigating and applying these novel emitters for UC are briefly summarized. Unfortunately, highly emissive emitters did not outperform Rub and tBRub in terms of UC yield due to strongly inhibited triplet energy transfer. Nevertheless, we deduce from an analysis of the prompt and delayed emission, that bulky side-moieties do not necessarily impede TTA. Specifically, for the emitter with bulky groups linked in the periphery, the TTA was as efficient as that of unsubstituted rubrene, whereas these moieties linked directly to the core suppress TTA dramatically. The **PII** unveils the advantage of the peripheral linking *vs.* core linking pattern of rubrene emitters, thereby providing valuable insights for their rational modification towards improved NIR-to-Vis UC efficiency in the solid state.

Photophysical properties of sterically crowded rubrenes

At first, we decided to investigate the fluorescence properties of newly synthesized rubrene-based emitters, aiming to understand what changes were inflicted by introduced modification. This is reflected by comparison of photophysical properties of modified rubrenes with conventional Rub emitter (see Fig. 2.2). The strong similarity of the absorption and FL spectra of the peri-tBRub with those of Rub and tBRub in the dilute solution pointed out that the peripheral bulky groups have a negligible impact on the conjugation. However, the spectra of core-tBRub were redshifted by more than 20 nm, signifying extension of the conjugation attributed to the core-linked side-moieties.

Since the rubrene structure was altered through chemical engineering, we examined whether the emissive properties of the produced molecules were not perturbed. This was assessed by taking measurements of Φ_{FL} and PL lifetime.

More details are provided in **PIII**. Briefly, we note that Φ_{FL} of all the rubrenes was estimated to be close to 100% in isolated from, both for diluted solutions and in diluted polymer films.

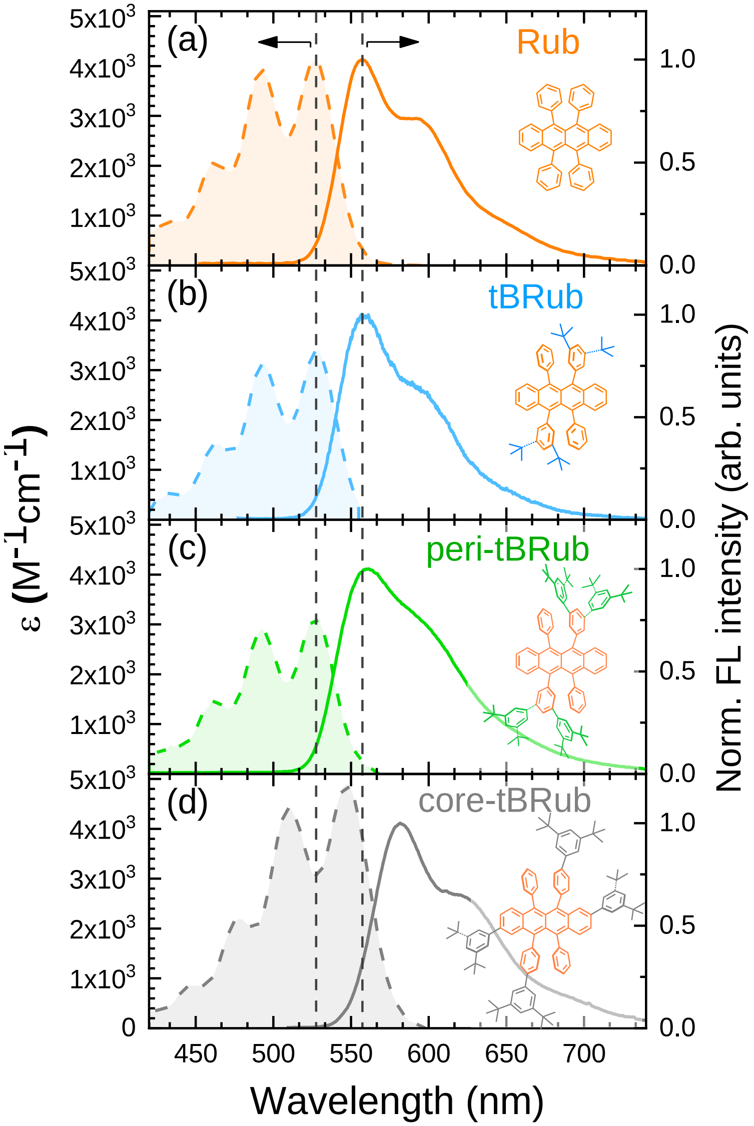

Fig. 6.1 Absorption (dashed lines) and fluorescence spectra (solid lines) of (a) Rub, (b) tBRub, (c) peri-tBRub and (d) core-tBRub in dilute toluene solution (10^{-5}M). Vertical dashed lines serve as guidelines for the eye. The inset contains the molecular structure of corresponding emitter.

The next essential step was to show that newly synthesized rubrenes exhibit suitable characteristics to serve as TTA emitters. Importantly, they should fulfil energetic requirements, to exhibit $2 \times T_1 > S_1$. Since it is not straightforward to measure T_1 of highly emissive materials, we used theoretical DFT calculations as a guideline to estimate the triplet energy levels of rubrenes. As follows, the potential for peri-tBRub and core-tBRub to undergo TTA is supported from the results of DFT calculations (see Table 6.1). The DFT allowed us to draw additional insights. The DFT predicted the overall trend of the excited state energies. For example, in agreement with the experimental results, the S_1 energy estimated for the core-tBRub is the lowest among the rest rubrene emitters. Apart from inhibited SF from the anticipated separation effect induced by sterical moieties, the downshifted S_1 energy in core-tBRub also implies less favourable conditions for the SF in the solid film. Namely, in this molecule the singlet energy could be insufficient to produce two triplet states ($S_1 < 2 \times T_1$). The calculations also revealed that the triplet energies (T_1) of the peri-tBRub and core-tBRub are similar or slightly lower as those of Rub and tBRub. By considering our previous studies (**PI** and **PII**), this implied unmitigated potential for TTA in all studied rubrenes, and viable triplet sensitization using PdPc sensitizer.

Table 6.1 First singlet (S_1) and triplet (T_1) energies of rubrene-based emitters obtained from DFT calculations using B3LYP/6-31G(d) in vacuum.

	S_1 [eV]	T_1 [eV]	$2T_1$*-S_1* [eV]
Rub	2.41	1.26	0.11
tBRub	2.38	1.25	0.12
peri-tBRub	2.39	1.25	0.11
core-tBRub	2.28	1.22	0.16

Fluorescence properties in the solid-state

The impact of the bulky 3,5-di-*tert*-butylphenyl moieties on the singlet fission was assessed by measuring Φ_{FL} of the films with varying the emitter concentration in the PS polymer (Fig. 6.2a). The presented data indicates the central role of the introduced side-moieties in the suppression of concentration quenching. The bulky 3,5-di-*tert*-butylphenyl moieties in peri-tBRub and core-tBRub allowed to retain more than 60 % of the initial Φ_{FL} in the neat films as compared to the substantial quenching observed in the neat films of Rub (Φ_{FL} = 1.5 %) or tBRub (Φ_{FL} = 35 %). The 40 times higher Φ_{FL} obtained in the neat films of structurally more complex rubrenes in respect to that of conventional Rub is promising for TTA-UC applications, since UC efficiency directly depends on Φ_{FL} (see eqn 3.1).

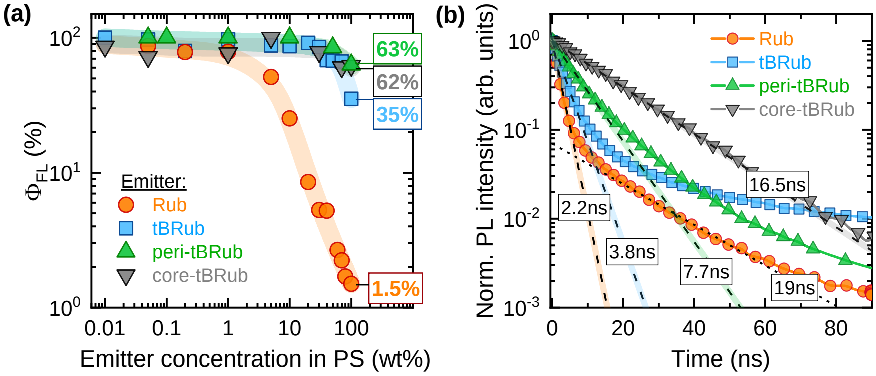

Fig. 6.2 (a) FL quantum yield of the emitter-doped PS films as a function of emitter concentration. Lines serve as guidelines to the eye. (b) Transients of the neat films (or 100 wt% doping) of rubrene-based emitters. Dashed lines show single-exponential fits with the decay time constants indicated. All experiments were carried out with excitation wavelength 485 nm.

The degree of concentration quenching, and correspondingly, the extent of SF could also be determined from the shortening of τ_{PL}, taking the single-exponential decay of the isolated rubrenes with $\tau \approx$ 19 ns as a reference. This approach takes into account that SF rate in Rub films is > $2.5 \cdot 10^{12} s^{-1}$ and is by far the dominant singlet decay channel.[76,85] For neat films the PL transients consist of the initial fast and later slower components (see Fig. 5.5b), associated with the rapid singlet fission in the aggregated domains and intrinsic decay of isolated rubrene species, respectively. Note that core-tBRub of the highest structural complexity features only the slow decay with $\tau =$ 16.5 ns, indicating the negligible aggregation in the neat film. Such decay is one of the key criteria qualifying rubrene films as amorphous.[85] The reduced structural complexity of the rubrenes causes shortening of the initial decay component down to 2.2 ns (in Rub) implying accelerated SF due to the enhanced aggregation. The slow decay component had a similar τ for all the rubrenes except tBRub**,** which exhibited an enlarged contribution from TTA at a later decay stage. The extent of SF in neat films for all rubrenes, is also complemented by utilizing pump-probe technique. The latter results are presented and analysed more deeply in **PIII**.

Employing rubrenes for photon upconversion in solution

The high Φ_{FL} observed in the solid films of peri-tBRub and core-tBRub motivated us to utilize these new emitters for TTA-UC. As a first step, their potential for UC was tested in solutions (see Fig. 6.3). For comparison, the concentrations of the new emitters and PdPc sensitizer were set to 18 mM and

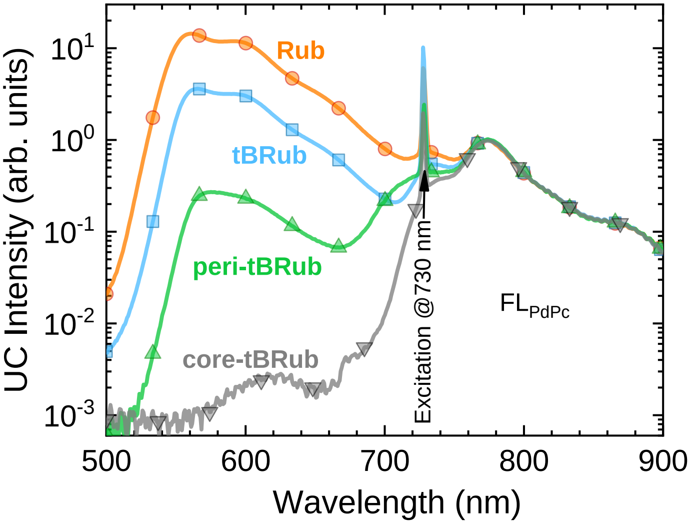

Fig. 6.3 UC emission spectra of the studied emitter:sensitzer (Rub:PdPc, tBRub:PdPc, peri-tBRub:PdPc and core-tBRub:PdPc) solutions in toluene under CW excitation at 730 nm. Emitter and sensitizer concentrations were 18 mM and 15 µM, respectively. Spectra are normalized to FL of the sensitizer.

15 µM, respectively. The concentrations were identical to those utilized previously in **PI**. The UC measurements were carried out by exciting the PdPc sensitizer at the Q band with NIR excitation (λ_{exc}). The recorded UC emission spectra were normalized to FL of the sensitizer ($FL_{\mathbf{PdPc}}$) for the correct comparison of UC efficiencies. In this case the UC intensity at Vis range is directly proportional to UC efficiency (see **PI**). Disappointingly, UC efficiencies of the structurally complex rubrene emitters were found to be inferior to those of conventional emitters Rub and tBRub. Peri-tBRub expressed more than one order of magnitude lower ($\Phi_{UC} = 0.08\%$) as compared to those of Rub ($\Phi_{FL} = 5.7\%$) and tBRub ($\Phi_{UC} = 1.3\%$), whereas UC signal of core-tBRub was barely detectable and too weak to be quantified. We determined Φ_{FL} to be unchanged for all UC samples. Thus, we assume that low Φ_{UC} obtained for the new rubrenes is most likely caused by the bulky side-moieties impeding TET and/or TTA processes.

Hampered TET in core-tBRub and peri-tBRub was confirmed from UC signal transients and from UC threshold measurements (more details in **PIII**). Although efficient in the solid-state (see Fig. 6.2a) these emitters showed barely noticeable UC, indicating that supressed TET was the determining factor of low UC. From these results, we could assume that peri-tBRub and core-tBRub are unsuitable for TTA-UC. However, this view would be too simplistic. The inability to efficiently sensitize new emitters could also be related to sensitizer used (PdPc). Perhaps sensitizer with longer triplet lifetime, or more suitable structure would facilitate more efficient Φ_{TET}. Thus, we further aimed to evaluate the emitters ability to undergo TTA separately from TET.

Evaluating TTA performance in emitter-only rubrene films

To assess the efficiency of TTA in the new rubrenes, we made use of a rather distinct attribute of the rubrenes to exhibit simultaneously both singlet fission and TTA in the aggregated state. By generating triplets in the rubrene films directly through SF without a sensitizer, TTA could be discerned from TET.

The neat films of rubrenes were investigated with a gated ICCD camera to measure FL transients spanning over seven orders of magnitude in intensity and five orders of magnitude in time (see Fig. 6.4). This allowed us to detect extremely low delayed FL signals at tens of microseconds emerging from TTA. Thereby integral of the delayed signal provides useful information about the TTA efficiency.

The extent of SF (initial triplet population) was determined by comparing the obtained signal with mono-exponential decay registered for dilute solutions, where SF is absent. The explicit formula for the calculation of TTA efficiency:

$$\text{TTA eff.} = \frac{\mathrm{N}_S^{TTA}}{\mathrm{N}_T^{SF} \cdot \Phi_{FL}^{prompt}} \qquad 6.1$$

where, N_S^{TTA} – number singlets created via TTA, N_T^{SF} – number of triplets generated due to SF, Φ_{FL}^{prompt} – fluorescence quantum yield of the initial part of the decay. More details are provided in the **PIII.**

The main results are depicted in Table 4.1. We can see that tBRub demonstrates the highest TTA efficiency in agreement with the largest delayed FL integral (Fig. 6.4), even though triplet concentration generated through SF is 5 times lower compared to that of Rub, as deduced previously from the transient absorption measurements. The result is also consistent with our previous finding, inferring higher Φ_{UC} for tBRub-based solid UC films *vs.* Rub films (**PII**). Meanwhile, the most complex core-tBRub exhibits the lowest

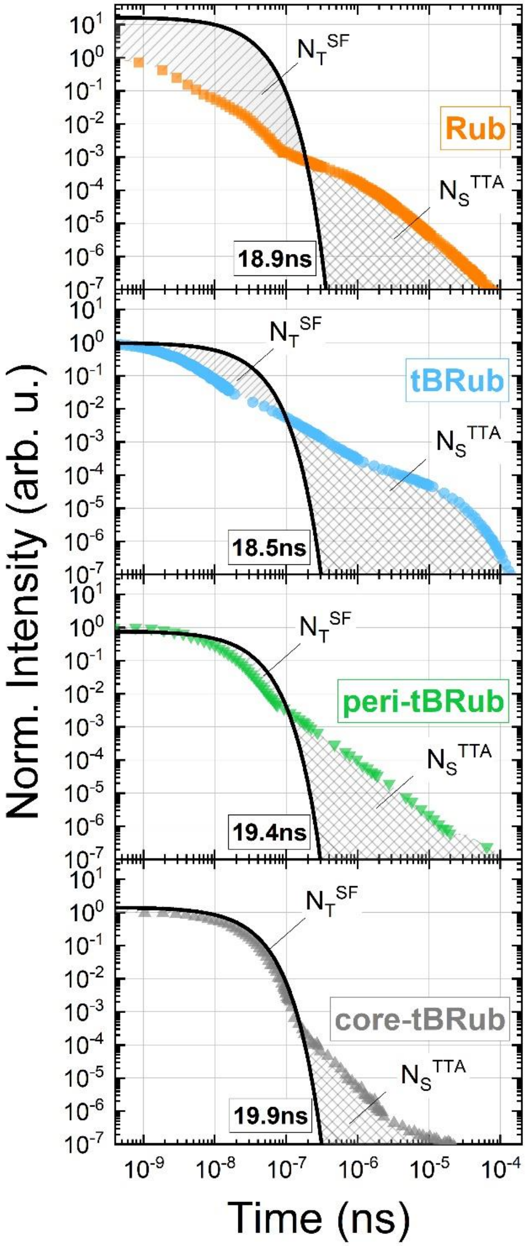

Fig. 6.4 FL transients of each rubrene film scaled so that their integrals correspond to their Φ_{FL}. Prompt-only reference transients are shown by solid line. The integrals representing N_T^{SF} and N_S^{TTA} for each rubrene film, indicated.

TTA efficiency, which is more than two orders of magnitude lower than that of tBRub. Interestingly, peri-tBRub is found to feature comparable TTA efficiency with that of Rub, thus suggesting that bulky 3,5-di-*tert*-butylphenyl moieties in the periphery do not impede TTA significantly. This is in sharp contrast to core-tBRub, possessing the bulky moieties linked directly to the tetracene core and expressing severely suppressed TTA. Regretfully, suppressed SF and enhanced Φ_{FL} in core-tBRub films cannot counterbalance considerably restricted TET and TTA efficiencies, thus making the core-linking of rubrenes unfavourable for TTA-UC.

Table 6.2 The main parameters (related to Fig. 6.4) necessary for the evaluation of TTA efficiency of the neat films of rubrenes. Here, N_T^{SF} represents the number of triplets created via SF; N_S^{TTA} – singlets created via TTA; Φ_{FL}^{prompt} – FL quantum yield obtained from the corresponding integral in the FL transient; TTA eff. – TTA efficiency calculated according to the eqn 6.1.

Rubrene emitter	N_T^{SF}	N_S^{TTA}	Φ_{FL}^{prompt} (%)	TTA eff. (%)
Rub	18.8	0.03	1.0	18.5
tBRub	14.2	2.5	22.4	77.3
peri-tBRub	7.4	0.7	59.5	15.4
core-tBRub	7.0	0.02	62.0	0.6

7. ENHANCING SOLID-STATE PHOTON UPCONVERSION BY SIMPLYFIED THERMAL EVAPORATION

We already established that many practical TTA-UC applications demand high NIR-to-Vis UC efficiency, preferably in a solid state. In the literature related to solid-state NIR-to-Vis UC, most demonstrations involve rubrene as emitter. However, even the very best UC systems operating in the NIR range (>700 nm) usually express very low UC quantum yield, typically <1%.

In the previous chapters we showed that to improve solid-state UC efficiency, it is important to combat the non-radiative decay of rubrene singlets governed by singlet fission (SF). Generally, SF related losses can be mitigated by using two approaches, i.e. i) molecular engineering, which relies on modification of existing emitters or introduction of alternative ones; ii) physical engineering based on altering UC film composition or morphology. While the first approach is studied in **PI-III**, here are summarized the results of publication **PIV** which emphasize the second approach. Name, in **PIV** we investigate the potential of altering UC film morphology by employing different preparation techniques to address the issue of low UC performance. Hot-plate evaporation of rubrene under nitrogen ambient on Peltier-cooled substrate pre-coated with sensitizer layer is demonstrated to significantly improve FL quantum yield (> 10-fold). The subsequent film annealing is demonstrated to improve triplet energy transfer. Overall physical engineering approach increased the UC quantum yield up to (1.2 ± 0.15)%. This is at least twice as high as in any other binary NIR-UC films reported so far. Moreover, in **PIV** we find that the statistical probability (*f* factor) to produce a singlet from two triplets via TTA in amorphous rubrene films ($f = 19.5\%$) is close to that estimated previously for rubrene in a solution (see **PI**).

Fabrication of UC films under various physical conditions

In the study **PIV**, diverse deposition conditions of emitter Rub are investigated to assess the impact of the emitter morphology on Φ_{FL}, and correspondingly to Φ_{UC} in the solid films. Fig. 7.1 a and b illustrate how we performed the step-by-step fabrication of UC films. In the first step, the sensitizer layer composed of an optically inert polymer matrix doped with low concentration (0.1 wt%) of PdPc was formed by spin-coating (Fig. 7.1). Then, Rub was deposited on top by using one of the four distinct thermal evaporation modes to result in the UC film (Fig. 7.1b). In the '*vacuum deposition'* mode, controlled thermal evaporation in high vacuum (~10^{-7} Torr) was used. This mode was previously reported to produce amorphous rubrene films and therefore served as a reference deposition mode.[85] The rest three modes were based on a simplified thermal evaporation of Rub (using the hot-plate) in a nitrogen ambient. In the *cold deposition* mode, Rub molecules were deposited on Peltier cooled (-10 °C) substrate (Fig. 7.1b). This mode is expected to instantly freeze emitter molecules on the substrate, thus producing amorphous films. Aiming to quantify the effect of substrate cooling, cold-deposited films were annealed at 100 °C defining *post-annealing* mode. Lastly, Rub evaporation on uncooled substrate (naturally heated due to the close proximity of the evaporation source) was named *hot deposition* mode.

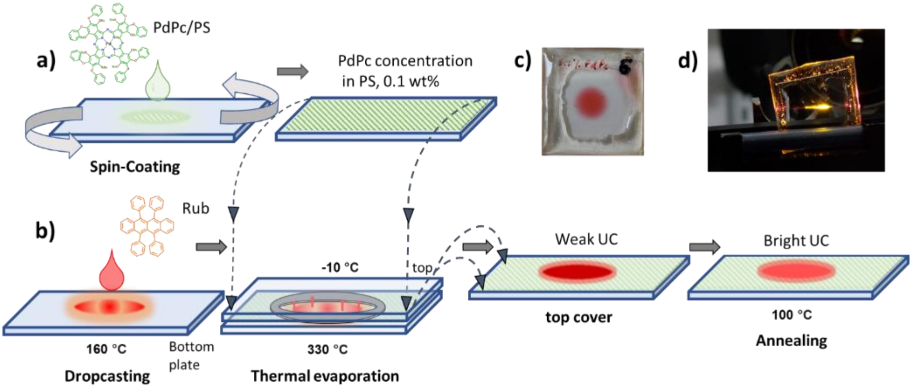

Fig. 7.1 Preparation of UC films. a) formation of sensitizer (PdPc)-doped PS layer by spin-coating; b) deposition of emitter (Rub) by drop-casting stock solution (1mg/ml) on glass substrate followed by thermal evaporation of Rub on actively cooled (previously prepared) sensitizer layer (depicted as top glass). The final UC film is obtained by thermal annealing; c) photo of the final UC film with the encapsulating epoxy visible on the edges; d) the UC film excited with 730nm CW laser.

Photoluminescence lifetime as probe to determine the film morphology

To minimize SF, we must produce amorphous Rub films which exhibit chaotic molecular orientation and large average intermolecular distance. Biaggio et. al. successfully exploited molecular beam deposition in high vacuum to obtain amorphous Rub films.[85] The films were virtually-free from SF and showed mono-exponential fluorescence decay ($\tau = 16.4$ ns) close to that of Rub in solution. In contrast, crystalline films suffer from rapid SF and thus exhibit significantly reduced PL lifetime. Evidently, the fluorescence dynamics could be used as a tool to determine the morphology of the produced Rub films.

Here, the measured FL transients and Φ_{FL} of UC films prepared at different conditions are shown in Fig. 7.2. The FL transients consisted of the dominant prompt decay (fractional contribution of 70 – 90% to an overall decay) affected by SF and the minor slower decay component resembling natural decay of isolated Rub species. The varying fluorescence dynamics are clearly sensitive to Rub deposition mode. The shorter FL lifetime suggested an enhanced SF, and hence, a reduced Φ_{FL}. In the case of vacuum-deposited films, rapid decay with $\tau = 2$ ns and low Φ_{FL} (1.6%) were obtained. Interestingly, the prolonged decay (τ=3.8 ns) as well as increased Φ_{FL} up to 8.5% were obtained for the films fabricated using the *cold deposition* mode, indicating more random molecular orientation, and suppressed SF. Post-annealing of the UC films further extended FL lifetime to 8.5 ns and improved Φ_{FL} almost 2-fold. Finally, the highest Φ_{FL} of 20.5% along with the longest FL lifetime (τ=12 ns) was determined for the films prepared in the *hot deposition* mode.

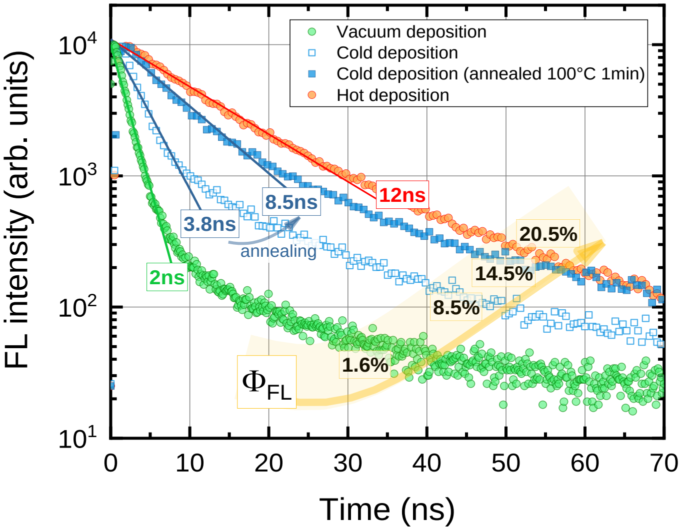

Fig. 7.2 FL transients of Rub films deposited on top of sensitizer layer using different thermal evaporation modes (specified). Lines represent single-exponential fits of the dominant prompt decay components. FL lifetimes and quantum yields indicated.

At a first glance, the role of the heat treatment introduced during the film annealing or *hot deposition* is counterintuitive, since this is anticipated to facilitate Rub crystallization.[88] However, we show that hot Rub molecules can diffuse into polymer layer forming a more amorphous diluted Rub film (see below). Next, we tested the UC properties of manufactured films to investigate whether an increase in Φ_{FL} translates to an improvement of UC performance.

NIR-to-Vis upconversion in manufactured films

Further investigation involved studying UC properties of the films via NIR excitation (730nm) of the sensitizer. The improvement of UC efficiency was expected to be in correspondence with that of Φ_{FL}. Indeed, the films of the lowest Φ_{FL} fabricated using *vacuum deposition* and *cold deposition* modes exhibited barely detectable UC. On the other hand, *annealed* and *hot-deposited* films displayed bright UC. This result can be rationalized by considering the differences in the triplet energy transfer efficiency Φ_{TET} (see eqn 3.1). The temperature difference during the *cold deposition* leads to formation of bilayer UC film featuring a distinct boundary between sensitizer and emitter. As a result, most of the sensitizer triplets are generated far from the emitter species implying that short-range Dexter-type TET can only occur in a narrow interface region. Meanwhile, the promoted molecular diffusion during the film annealing causes mixing of the sensitizer and the emitter, thus reducing intermolecular separation and enhancing TET{PdPc → Rub}. This is supported with Scanning electron microscopy (SEM) cross section images (see Fig. 7.3). The sensitizer-only (left-most, reference) image clearly shows that the sensitizer is spin-coated uniformly. In the middle column, we can see films produced by *cold deposition* where the sensitizer layer is also visible and can be well distinguished from the cold-deposited rubrene, which takes a spherical nano-droplet shape (300 – 1200 nm in size). Moreover, a clear boundary between Rub and sensitizer layer confirms that these layers are not intermixed. However, after the annealing, the symmetrical shape of rubrene particles is lost and rubrene diffuses into the sensitizer layer. Subsequently, the boundary between these two layers disappears. Additionally, the mixing of Rub and sensitizer layer was also verified by evaluating Φ_{TET}. This was done by comparing phosphorescence intensity from the sensitizer PdPc of the cold-deposited UC films with the same films after annealing (for more details see **PIV**).

Although the highest Φ_{FL} of Rub films was achieved using *hot deposition* mode, the UC films prepared in this way had poor reproducibility. In contrast, *cold deposition* followed by *annealing* allowed to manufacture films with high repeatability due to more controllable, stable growth and lack of crystallization centres.

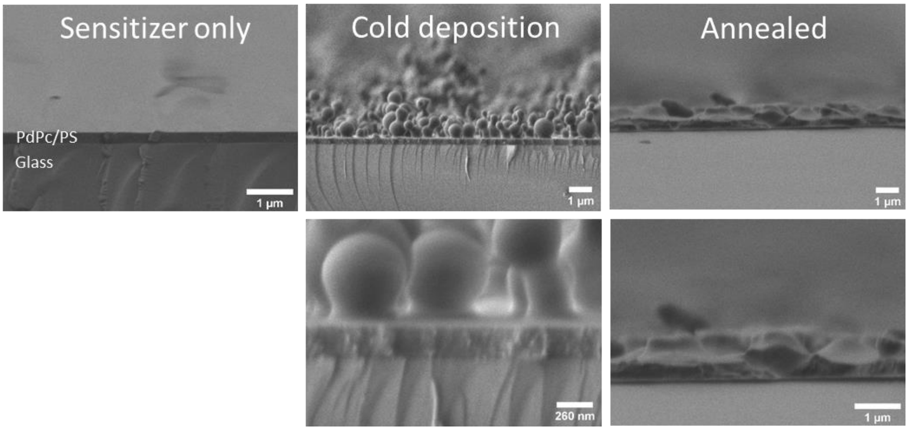

Fig. 7.3 Cross section SEM images of the sensitizer layer as a reference film (left column), cold deposited (middle column) and annealed (right column) UC films. The measurements were performed using 1 kV acceleration voltage and no additional coating. The sensitizer layer thickness, 260nm.

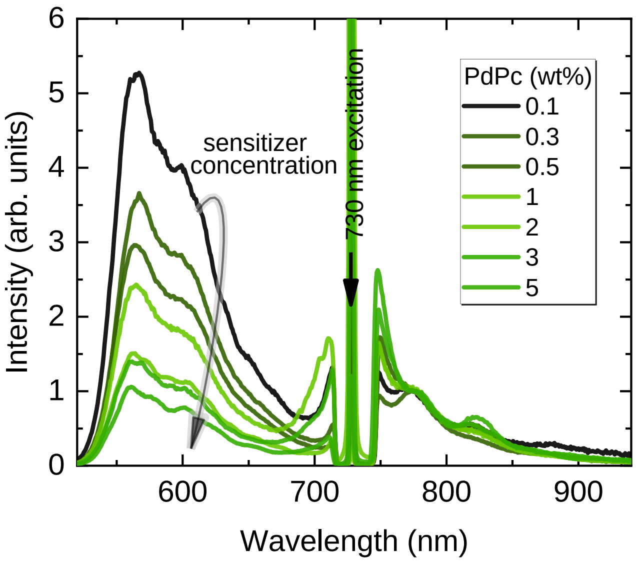

Fig. 7.4 UC emission spectra of PdPc/PS/Rub films with different PdPc concentration. The spectra are normalized to PdPc fluorescence maximum at 774 nm. Rub deposition conditions and PdPc-doped PS layer thickness (260nm) were maintained. Excitation, 730nm CW laser. Notch filter was used to suppress scattered excitation.

Sensitizer concentration for optimal UC performance

By selecting one, the most convenient Rub deposition technique (*cold deposition* followed by *annealing*) we carried out UC optimization by utilizing different sensitizer concentrations. The resulting UC emission from different UC samples is depicted in Fig. 7.4. It is evident that the increasing sensitizer concentration (from 0.1 wt% to 5 wt%) resulted in reduced UC signal by 5-fold. Although higher sensitizer concentration is supposed to improve NIR absorption and reduce UC threshold, densely packed sensitizer molecules facilitate energy back-transfer diminishing overall Φ_{UC}. Aiming to maximize UC efficiency, the lowest PdPc concentration (0.1 wt%) was selected for further optimization. We note that lower PdPc concentration is not utilized since it would result in an unreachable UC threshold, followed by reliably undetectable UC signal.

Optimizing sensitizer layer thickness

Spectra of UC films with varying sensitizer layer thickness, prepared under otherwise the same conditions, are shown in Fig. 7.5. The UC spectra were normalized to PdPc FL peak intensity so that UC intensity would correspond to Φ_{UC} (see experimental section 3.5). Using this value as an internal reference, we could roughly deduce Φ_{UC} to increase from 0.4% to 1% with decreasing the sensitizer layer thickness from 500 to 110 nm (Fig. 7.5). The obtained Φ_{UC} were confirmed by the measurements in the integrating sphere, where the most efficient UC film exhibited $\Phi_{UC} = (1.2 \pm 0.15)\%$. The attained high Φ_{UC} represents 17-fold improvement over our previous spin-coated DBP-doped Rub films[89] and at least 2-fold improvement in respect to the most efficient binary rubrene-based solid-state systems ($\Phi_{UC} \approx 0.3\text{-}0.5\%$)[22,57,90] at the time of the publication **PIV.** We also note that the obtained Φ_{UC} of the binary film approaches the highest efficiency value ($\Phi_{UC} = 2\%$) achieved for the ternary UC film, additionally containing DBP exciton sink.[57] This reduces the gap in the performance of binary and ternary systems, minimizing the demand for the third component (singlet exciton sink) and stressing the importance of UC film morphology rather than energetics of individual molecules.

Statistical probability in UC solid-state rubrene films

Since most of the energy transfer/conversion processes contributing to Φ_{UC} were determined (see eqn 3.1), the probability factor (f) for rubrene in the solid-state can be estimated. If we take the highest measured results for

Φ_{FL} = 20.5% (Fig. 7.2), Φ_{TET} = 60%, Φ_{ISC} = 100%[21,79,91], Φ_{TTA} = 100% and Φ_{UC} = 1.2% the resulting statistical probability *f* to generate a singlet from two triplets via TTA is 19.5 %. Interestingly, the obtained *f* factor is close to that estimated for rubrene in a solution (15.5%)[21]. This can be justified by the similar energy level alignment of rubrene in the different environment (solution or amorphous-like film). The obtained *f* value implies a maximum Φ_{UC} of ½ × *f* ≈ 10% for rubrene UC systems, which is reasonable, since no higher Φ_{UC} was demonstrated so far.[22,53–59,90]

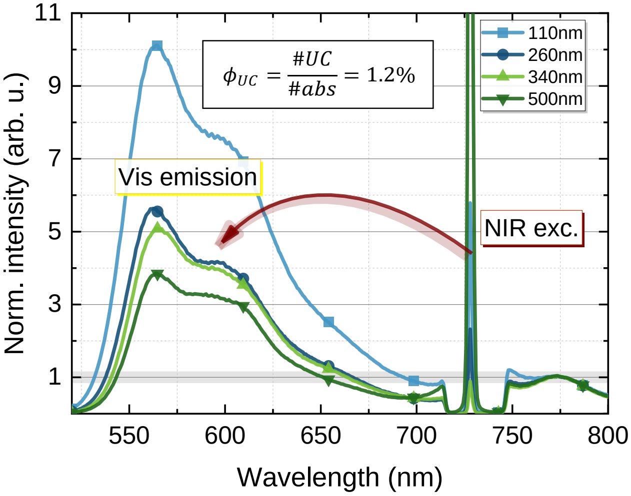

Fig. 7.5 UC spectra of the optimized PS:PdPc/Rub films with different sensitizer layer thickness (indicated). The spectra are normalized to PdPc FL peak intensity (at 774 nm) so that UC intensity would correspond to Φ_{UC}. Excitation wavelength and density, 730 nm and 100 W/cm^2, respectively.

8. EVALUATING THE SINGLET AND TRIPLET EXCITON DIFFUSION IN UPCONVERTING DISORDERED RUBRENE FILMS

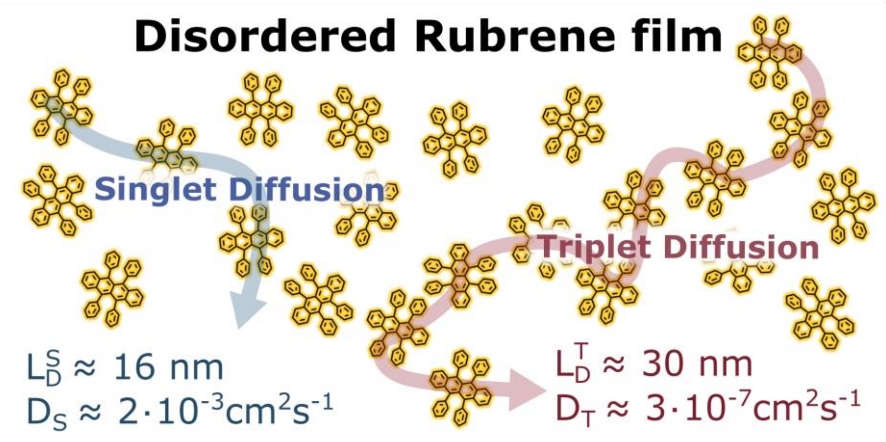

Fig. 8.1 Graphical overview of the **PV** together with the key parameters describing singlet and triplet exciton diffusion in disorder Rub films. Diffusion coefficient (*D*) and diffusion length (L_D) for singlet (left) and triplet excitons (right).

In the solid-state where emitter molecules are fixed, triplet and singlet exciton diffusion plays a decisive role both in triplet-triplet annihilation (TTA) and singlet fission (SF) processes. In this way exciton diffusion has an important consequence for TTA-mediated photon upconversion (UC). For instance, high triplet exciton diffusion is required for TTA to occur efficiently at low excitation power (~mW/cm^2), while low diffusivity of singlets is advantageous to prevent them from reaching SF-favored sites as well as to suppress detrimental back-FRET to sensitizer.

Although triplet diffusion in crystalline Rub was studied before, there is no quantitative data on the diffusion in disordered Rub films most widely employed for NIR-to-Vis UC. The lack of this data hinders the progress of TTA-UC applications relying on Rub annihilator (emitter). Here, a summary of the **PV** is provided, where the disordered spin-coated Rub films are investigated to determine exciton diffusion properties. The visual summary of the main findings of **PV** is depicted in Fig. 8.1. Namely, PL bulk-quenching technique followed by Stern-Volmer analysis was employed to estimate exciton diffusion coefficient (*D*) and diffusion length (L_D). The procedure is carried out both for singlet and triplet excitons. The influence of the singlet sink (DBP) to exciton diffusion is also investigated due to common usage of

DBP in tandem with Rub. From quenching experiments, we estimate the key parameters describing exciton diffusivity (see below or in detail in **PV**).

Importantly in **PV** we conclude that triplet diffusion length (L_D^T) in disordered Rub films can be improved only moderately (up to ~55 nm) considering that the maximum possible triplet lifetime (τ_T) as that for isolated Rub species ($\tau_\mathrm{T} \approx 100$ μs) is achieved. Hence, striving to prolong L_D^T even further for enhanced NIR-to-Vis TTA-UC performance, novel emitters with similar or lower triplet energy as compared to Rub, yet longer triplet lifetime in the solid state are required.

Utilizing NIR-to-Vis upconversion to determine triplet exciton diffusion

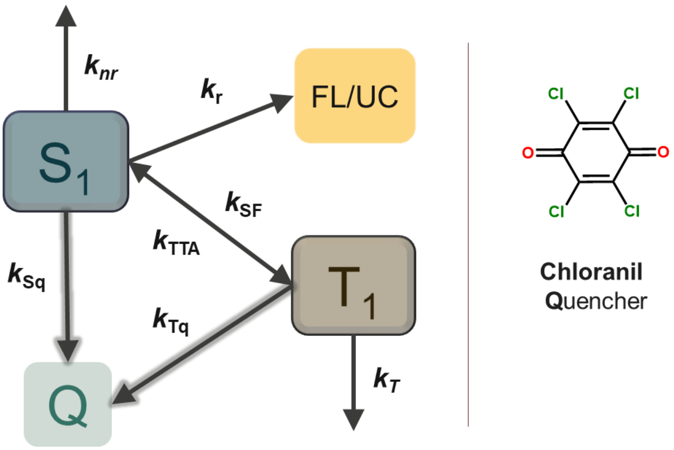

Fig. 8.2 Left - scheme for PL bulk-quenching technique to determine exciton diffusion properties. S_1 and T_1 represents singlet and triplet population. FL/UC is the registered signal (fluorescence or upconversion) in the quenching experiments, while Q is the presence of the quencher (Right). k is the transition rate of the respective process indicated as the subscript: TTA – triplet-triplet annihilation; SF – singlet fission; T – triplet decay (radiative and nonradiative); S_q and T_q singlet and triplet quenching, nr/ r is the singlet nonradiative/ radiative decay respectively.

To quantify triplet exciton diffusion in disordered Rub films, two sets of films with the fixed amount of sensitizer PdPc (0.1wt%) and increasing quencher concentration [Q_c] were investigated. The first set contained 80 wt% of Rub dispersed in PS matrix, whereas the second one was based on the neat Rub films. Additionally, each set contained a series of films doped with exciton sink DBP at 0.5 wt% concentration. PS served as an inert matrix for

Rub, thereby increasing intermolecular distance between the emitter species. Already mentioned 80wt% of Rub emitter was shown to be the optimal in **PII**. On the other hand, knowledge on exciton diffusion in the undiluted (neat) Rub films is also important, as these are often utilized in various optoelectronic devices. Thus, in total 2 sets of samples each containing 2 series of UC films with increasing quencher (chloranil) concentration were investigated by measuring UC transients. Simplified scheme to illustrate the effect of the presence of the quencher on the exciton dynamics is shown in Fig. 8.2. Evidently, the UC is used as a probe to monitor the lifetime of triplet population (T_1). Specifically, the 730nm excitation generates triplet states in the emitter (T_1). The T_1 can be depleted by dominating competing pathways: natural triplet decay or quenched by the presence of chloranil. Due to low excitation conditions ($I_{exc} \ll I_{th}$) the TTA route (k_{TTA}) is minute, however is responsible for detectable signal. Thus, UC signal generated by means of TTA provides unique opportunity to probe otherwise non-emissive triplet states and evaluate their diffusion.

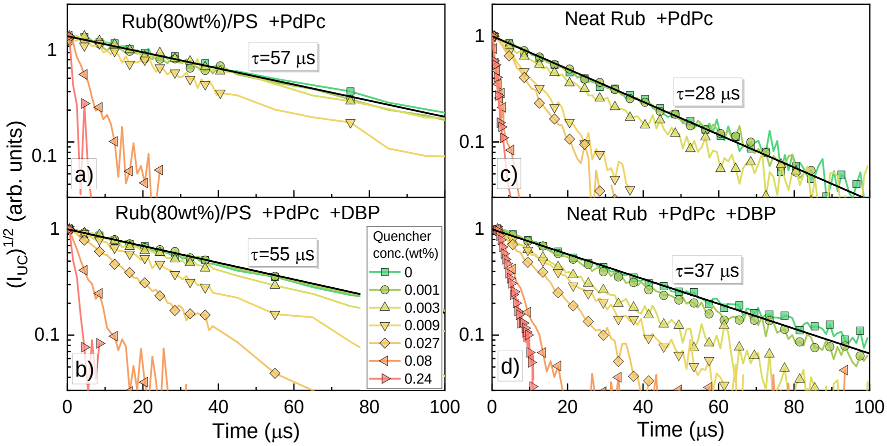

Fig. 8.3 UC transients of the Rub(80 wt%)/PS and neat Rub films with a) and c) 0.1 wt% PdPc; b) and d) 0.1 wt% PdPc and 0.5 wt% DBP, at different triplet quencher concentrations from 0 to 0.24 wt%. Excitation wavelength – 730 nm.

The square root of UC intensity, which is proportional to the triplet concentration, is depicted on Y axis of Fig. 8.3. The transients spanning over μs-time-scale were easily fitted using a single exponential decay profile indicating that spontaneous triplet decay dominates over the TTA channel and the Stern-Volmer model is applicable (see experimental details in page 38). In all the film series, an increase of [Q_c] resulted in the prominent reduction of triplet lifetime from ca. 57 μs (in Rub(80 wt%)/PS series) and ca. 37 μs (in neat Rub series), down to less than one microsecond at the highest [Q_c]. Quencher concentration as low as 0.24 wt% was sufficient to quench triplets with nearly 100% efficiency, indicating that chloranil is indeed a suitable quencher for Rub triplets.

The dependence of the calculated relative quenching efficiency on [Q_c] (Fig. 8.4) was fitted using the Stern-Volmer relationship (eqn 3.16) thereby permitting to estimate the triplet exciton diffusion coefficient (D_T). D_T as well as the other main fitting parameters are summarized in Table 8.1. It was found that DBP has no substantial impact neither on the diffusion coefficient or the triplet lifetime. We note that the difference in τ_T obtained for the neat Rub films with and without DBP can be attributed to DBP related changes in the film morphology (see microscopy images in ESI of **PV**).

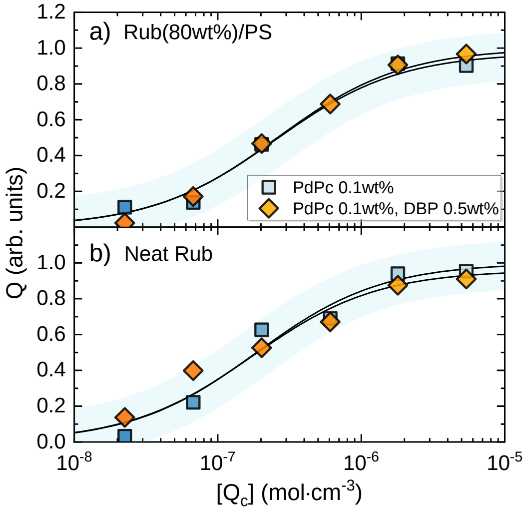

Fig. 8.4 Relative quenching efficiency as a function of quencher concentration for a) Rub(80 wt%)/PS films and b) neat Rub films with 0.1wt% PdPc only and with additional 0.5wt% DBP. Solid lines show Stern-Volmer fits.

Table 8.1 Main results obtained from Stern-Volmer analysis for triplet excitons: D_T – triplet exciton diffusion coefficient; τ_T – triplet exciton lifetime, L_D^T– triplet exciton diffusion length.

	PdPc wt%	DBP wt%	D_T cm^2·s^{-1}	τ_T μs	L_D^T nm
Rub(80 wt%)/PS	0.1	0	$1.13 \cdot 10^{-7}$	57	25.4
Rub(80 wt%)/PS	0.1	0.5	$1.21 \cdot 10^{-7}$	55	25.8
Neat Rub	0.1	0	$3.38 \cdot 10^{-7}$	28	30.7
Neat Rub	0.1	0.5	$2.73 \cdot 10^{-7}$	37	31.8

To evaluate singlet exciton diffusion, we used the same series of films (as for the triplet diffusion measurements) and an additional one with neither triplet sensitizer PdPc nor singlet sink DBP present. Conversely to triplet diffusion measurements, 485 nm excitation wavelength was employed to probe the singlet state of Rub. The transient curves for singlets are depicted in **PV**. From the later PL transient results, the quenching efficiency curves were derived and are depicted in Fig. 8.5. Only the main parameters extracted from the Stern-Volmer analysis are summarized in Table 8.2, additional information can be found in **PV**.

The singlet exciton diffusion length of the Rub(80 wt%)/PS and neat Rub films was found to be 13.7 and 16.4 nm, respectively. The addition of PdPc sensitizer noticeably shortened $L_{\mathrm{D}}^{\mathrm{S}}$ by ca. 20-30%, meanwhile the incorporation of singlet sink DBP reduced it even further down to 7.1 and 5.9 nm for Rub(80 wt%)/PS and neat Rub, respectively. Although short $L_{\mathrm{D}}^{\mathrm{S}}$ is common for disordered films, much longer diffusion lengths of 180-390 nm can be obtained in highly ordered crystalline Rub.[92] In the spin-coated neat Rub films studied in this work, comparatively short τ_{S} of ~1.2 ns was obtained implying the presence of SF sites due to the emerged crystalline domains. Since the long $L_{\mathrm{D}}^{\mathrm{S}}$ is known to foster FRET of the upconverted singlets from annihilator back to a sensitizer, it is detrimental for TTA-UC efficiency and must be avoided.

The proof for the back-FRET occurring in the studied Rub UC films is the apparent shortening of $L_{\mathrm{D}}^{\mathrm{S}}$ in both neat Rub ($L_{\mathrm{D}}^{\mathrm{S}}$ =11.3 nm) and Rub(80 wt%)/PS films ($L_{\mathrm{D}}^{\mathrm{S}}$ =8.6 nm) obtained upon introduction of 0.1 wt% PdPc sensitizer (Table 8.2). The back-FRET is feasible because PdPc has non-zero absorption in the spectral region of Rub emission[93] and $L_{\mathrm{D}}^{\mathrm{S}}$ exceeds half the distance between the sensitizer species (~7 nm) at the given concentration. Moreover, the widely used emissive singlet sink (or trap) DBP introduced into Rub to evade SF further reduces $L_{\mathrm{D}}^{\mathrm{S}}$ in the UC films. It is reduced down to 8.5 and 7.6 nm for Rub(80 wt%)/PS and neat Rub films, respectively (Table 2).

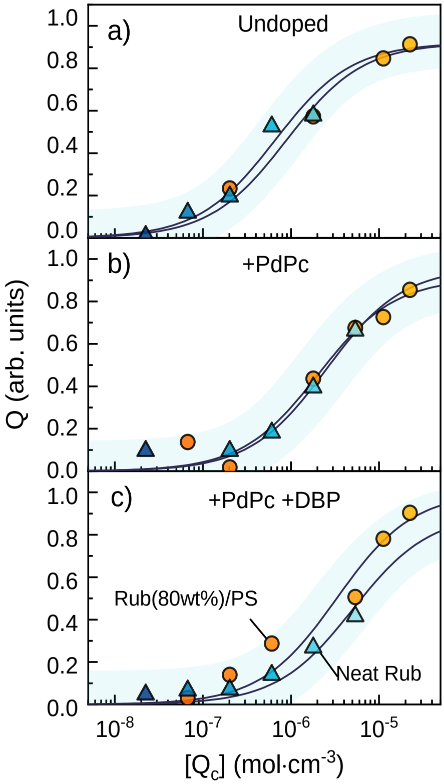

Fig. 8.5 Relative singlet quenching efficiency as a function of chloranil quencher concentration for Rub(80 wt%)/PS and neat Rub films a) without PdPc and DBP; b) with 0.1wt% PdPc; and c) with 0.1wt% PdPc and 0.5wt% DBP. Solid lines show Stern-Volmer fits. The highest molar concentration of the quencher ($2.25 \cdot 10^{-5}$ mol·cm^{-3}) corresponds to 1 wt%.

Table 8.2 Main results obtained from Stern-Volmer analysis for singlet excitons: D_S – triplet exciton diffusion coefficient; $<\tau_S>$ – average singlet exciton lifetime, excluding long decay component, L_D^S– singlet exciton diffusion length.

	PdPc wt%	DBP wt%	D_S cm^2·s^{-1}	τ_S ns	L_D^S nm
Rub(80 wt%)/PS	0	0	$1.26 \cdot 10^{-3}$	1.50	13.7
Rub(80 wt%)/PS	0.1	0	$7.05 \cdot 10^{-4}$	1.17	9.1
Rub(80 wt%)/PS	0.1	0.5	$2.13 \cdot 10^{-4}$	2.37	7.1
Neat Rub	0	0	$2.27 \cdot 10^{-3}$	1.18	16.4
Neat Rub	0.1	0	$5.51 \cdot 10^{-4}$	1.27	8.4
Neat Rub	0.1	0.5	$1.60 \cdot 10^{-4}$	2.17	5.9

Brief comparison of diffusion parameters in various systems

The obtained diffusion parameters can be compared to those of other UC systems or different Rub morphologies. For example, the Rub single crystals can exhibit one of the longest L_D^T (2-8 μm[94,95]). Here in Rub films obtained by spin-coating L_D^T was estimated to be a couple orders of magnitude shorter, i.e. 25 nm and 30 nm for Rub(80 wt%)/PS and neat Rub films, respectively (Table 4.1). However, efficient SF in Rub crystals completely quenches Φ_{FL} rendering them unsuitable for UC applications.

Interestingly, similar L_D^T were previously reported for disordered PMMA/DPA/PtOEP films at the optimal DPA concentration of 25 – 30 wt% corresponding to the maximal UC quantum yield.[13] Comparable L_D^T of a few tens of nanometers were also obtained for amorphous bisfluorene-anthracene/PtOEP films.[96] Even though the triplet diffusion constants in the spin-coated Rub films (D_T ~10^{-7} $cm^2 \cdot s^{-1}$, see Table 8.1) were found to be 1-2 orders of magnitude larger in respect to those based on the anthracene films,[13,93,96] significantly shorter triplet lifetimes of Rub films (τ_T ~30-60 μs) restricted their L_D^T to a nanometer range. Yet, low L_D^T is still >4-fold longer compared to the half the distance between sensitizer molecules at the PdPc concentration of 0.1 wt% implying unrestricted encounter of the triplets from the neighboring sensitizer molecules. This ensured that the TTA domination regime (linear UC dependence *vs.* excitation power) can be easily reached granting the optimal Φ_{UC} for disordered Rub films. It is worth mentioning that still, inherently higher L_D^T would permit using even lower sensitizer concentrations, thus further suppressing singlet losses caused by the back-FRET to the sensitizer. Likewise, lower Rub concentrations could be utilized in UC films reducing the aggregation, and subsequently, the formation of SF centres responsible for low Φ_{FL} and TTA-UC efficiency.[89]

CONCLUSIONS

1. The benefit of doubling the emitter rubrene (Rub) concentration by decorating it with solubility increasing *t*-butyl groups in anticipation of enhanced triplet energy transfer, cannot outcompete the severely reduced statistical probability factor (*f*) from 15.6% (in Rub) to 5.3% (*t*-butyl-Rub).

2. 4-fold higher UC quantum yield (Φ_{UC}) achieved in the spin-coated *t*-butyl-Rub UC films ($\Phi_{UC} = 0.3\%$) compared to that based on unsubstituted Rub ($\Phi_{UC} = 0.07\%$) is caused by the reduced fluorescence concentration quenching mainly due to the suppressed singlet fission.

3. Even though fluorescence quantum yield (Φ_{FL}) of the neat films of sterically crowded Rub is enhanced up to 40 times in respect to unsubstituted Rub films, they are found to exhibit no UC emission, which is attributed to a hampered triplet energy transfer from a Pd-phthalocyanine (PdPc) sensitizer.

4. Simplified hot-plate evaporation of Rub onto sensitizer-doped polystyrene film in nitrogen ambient (as compared to conventional spin-coating or vacuum evaporation) significantly improves Φ_{FL} and triplet energy transfer, allowing to boost Φ_{UC} by a factor of ~20 (from 0.07% to 1.2 %).

5. Triplet exciton diffusion length (L_D^T) in disordered Rub films obtained by spin-coating is estimated to be 25-30 nm. It cannot be significantly enlarged due to inherently short triplet lifetime (100 μs) of Rub emitter. To improve L_D^T governing the UC performance of the current NIR-to-Vis UC films, novel emitters with longer triplet lifetimes are required.

SANTRAUKA LIETUVIŲ KALBA

Įvadas

Technologinis progresas ir nuolat didėjantys globalūs energijos poreikiai konkurencingai žengia koja kojon. Šiose lenktynėse aiškaus lyderio nėra. Cikliškai kintančioje situacijoje naujos technologijos siekia išsiveržti, taigi bando būti pigesnės, efektyvesnės, universalesnės ir labiau suderinamos su aplinka. Technologinis progresas sužadina naujus rinkos poreikius, o šie - naujas technologijas. Šioje besisukančioje karuselėje dalis technologijų galiausiai pasiekia brandą, o tolimesnė pažanga reikalauja išmanių ir sudėtingų inovacijų. Saulės celių (SC) technologija nėra išimtis. Ar tai būtų šiuo metu rinkoje dominuojančios SC paremtos konservatyviuoju siliciu, ar entuziastingu ir daug žadančiu perovskitu, abu SC technologiniai sprendimai turi aiškią efektyvumo ribą. Dar 1961 m. aprašyta Shockley−Queisser (SQ) riba diktuoja, kad SC turinčios tik vieną *pn* sandūrą atitinkančią 1,1 eV draustinį juostos tarpą, idealiu atveju gali pasiekti ~30% efektyvumą. Akivaizdu, jog minėtas vienos *pn* sandūros SC dizainas turi trūkumų: aukštos energijos fotonai švaistomi šiluminiu būdu, o žemesnės energijos fotonai su SC nesąveikauja. Visgi, aprašyta SQ riba nėra neįveikiama kliūtis. Išradingam ir sumaniam mokslininkui tai - įmantrus galvosūkis. Literatūroje galime sutikti keletą SQ ribos įveikimo būdų: i) panaudoti didesnį *pn* sandūrų kiekį ir aprėpti platesnę saulės spektro dalį arba ii) paderinti saulės spektrą, atlikti jo konversiją taip, kad jis būtų labiau tinkamas turimai SC. Visgi, toliau pirmojo būdo neaptarinėsiu, nes jis šiuo metu yra brangus ir technologiškai sudėtingas. Antrasis būdas yra potencialiai pigus, palyginti paprastas, tinkamas dabartinei SC technologijai. Šis metodas gali būti realizuojamas pasitelkiant organinius puslaidininkius. Jau minėta SC efektyvumo problema dėl aukštos energijos fotonų gali būti sprendžiama naudojant singletinių eksitonų skilimo (angl. k. *singlet fission* - SF) procesą. SF proceso metu sužadinimas padalinamas į du eksitonus, kurie abu yra „darbingi“ ir panaudojami SC. Būtent taip gali būti mažinami šiluminiai nuostoliai SC ir didinamas jos efektyvumas. Fotonai, turintys žemesnę energiją, gali būti įdarbinami pasitelkiant fotonų konversiją iš žemesnių energijų į didesnes (angl. k. *photon upconversio* - UC). Šio proceso metu du mažos energijos sužadinimai gali virsti vienu, dvigubai didesnės energijos sužadinimu. Organiniuose junginiuose UC realizuojama pasitelkiant tripletinių eksitonų anihiliaciją (angl. k. *triplet-triplet annihilation* - TTA). Taigi, galime sukurti organinių junginių sistemą galinčią panaudoti nematomą artimąją infraraudonųjų spindulių šviesą (angl. k. near infrared -

NIR) ir pakeisti ją į didesnės energijos regimąją šviesą (angl. k. visible - Vis). Būtent NIR-Vis TTA-UC tyrimui yra paskirta ši disertacija.

Verta paminėti, kad TTA-UC taikymai neapsiriboja tik SC.[1,3] Organinių TTA-UC sistemų panaudojimai gali būti siejami su: 3D spausdinimu,[4] fotokatalize,[5,6] bio-vaizdinimu,[7] mechaniniais jutikliais,[8] naktinio matymo prietaisais,[9] atminties lustais[10] ir kt.[12] Taip pat NIR spinduliuotė yra ypatingai skvarbi biologinėse terpėse.[5] Tai motyvuoja NIR-Vis TTA-UC sistemas panaudoti biomedicinoje[11].

Įprastai TTA-UC sistemos sudarytos iš dviejų komponenčių. Pirmoji komponentė vadinama sensibilizatoriumi ir yra atsakinga už šviesos sugertį ir tripletinių sužadinimų gamybą. Vėliau tripletiniai sužadinimai yra perduodami antrajai komponentei, dar vadinamai emiteriu, spinduoliu arba anihiliatoriumi. Emiteris kaupia ilgai gyvuojančias tripletines būsenas ir esant pakankamai jų koncentracijai, vykdo TTA, po kurios stebima uždelstoji UC emisija. Įdomu tai, kad stebima emisijos energija yra didesnė nei pirminės spinduliuotės, kurią sensibilizatorius sugėrė.

Nors yra ir kitų fizikinių mechanizmų, kuriuose galimas fotonų dažnio (energijos) didinimas, TTA-UC turi akivaizdžių privalumų. Priešingai nei dviejų fotonų sugertis (TPA), kuriai reikalingas didelis sužadinimo tankis (~GW/cm^2) arba antros harmonikos generacija (SHG) vykstanti netiesiniuose kristaluose, kuriai reikalingas koherentinis šviesos šaltinis, TTA-UC gali veikti esant nekoherentiniam mažos energijos sužadinimui. Taigi, efektyvi TTA-UC gali būti pasiekiama naudojant mažo galios tankio (~mW/cm^2) saulės šviesą.[1,3] Tiesa, panašiomis sąlygomis UC gali vykti ir lantaniduose (Er, Eu, Yb), tačiau esminis retųjų žemės elementų trūkumas yra tai, kad jie pasižymi gan prasta šviesos sugertimi.

Dabartinės NIR-Vis TTA-UC sistemos toli gražu nėra tobulos. Tiek tirpaluose, tiek sluoksniuose minėtos sistemos yra neefektyvios. Nors jau yra pademonstruotos Vis-Vis (iš žalios spektro dalies į mėlyną) UC sistemos, kurių kvantinė išeiga (Φ_{UC}) siekia ~30%,[13–18], vos kelios NIR-Vis UC sistemos pasiekia Φ_{UC} viršijantį 4%[19–21]. Akivaizdu, kad papildomi iššūkiai kyla plečiant UC sistemų veikimą į ilgų bangų spektrinį ruožą. Šie iššūkiai gali būti sprendžiami tiek atliekant tinkamų medžiagų paiešką, tiek gilinantis į fizikinius procesus ir našumą ribojančius veiksnius.

Siekiant optimalaus UC veikimo, svarbu naudoti tinkamą emiterį, kurio žema tripletinės būsenos energija būtų suderinta su NIR sensibilizatoriumi. Verta pastebėti, kad gautos našiausios NIR-vis UC sistemos tiek tirpale, tiek kietoje būsenoje naudoja rubreno (Rub) emiterį.[14] Žvelgiant į NIR-vis UC sistemas bendrai, pastebima, kad Rub emiteris dominuoja, o kietuose sluoksniuose yra bene vienintelis pasirinkimas. Kaip jau minėta, NIR-vis UC sistemų našumas netenkina praktiniams taikymams keliamų lūkesčių, todėl jų efektyvumui pagerinti reikalingi sistemingi tyrimai ir pažangūs sprendimai.

Darbo tikslas ir naujumas

Šios disertacijos tikslas buvo ištirti UC sistemas, kurių vienas iš komponentų yra dažnai naudojamas, Rub spinduolis ar jo modifikacija. UC sistemas siekiama charakterizuoti tirpaluose ir sluoksniuose bei nustatyti jų efektyvumą ribojančius veiksnius. Tikimasi, kad pateikti išsamūs tyrimai atskleis naujus metodus, galinčius pagerinti NIR-Vis TTA-UC efektyvumą. Remiantis literatūriniais šaltiniais pastebima, kad UC ribojantys veiksniai nėra iki galo išaiškinti ir suprantami, trūksta aiškios ir vieningos duomenų ir identifikuotų problemų interpretacijos. Tyrimo metu įgytos žinios leistų patobulinti NIR-Vis TTA-UC sistemas, pritaikomas tokiose srityse kaip SC, biomedicinoje, 3D spausdinime ir daugelyje kitų. Tikslui pasiekti buvo suformuotos užduotys:

1) Panaudoti skirtingas sensibilizatoriaus (PdPc) ir emiterio (Rub/tBRub) poras bei atlikti UC sistemos optimizaciją, siekiant gauti aukščiausią UC našumą tirpale.
2) Paruošti ir nuodugniai ištirti UC sluoksnius, kurių sudėtyje būtų Rub ar tBRub emiteriai. Įvertinti FL ir UC kvantines išeigas, nustatyti optimalią sluoksnių sudėtį (emiterio koncentraciją polimere), įvertinti UC slenkstinį sužadinimo galios tankį, tripletinių eksitonų ir UC gyvavimo trukmes.
3) Ištirti naujus didelėmis šoninėmis grupėmis modifikuotus Rub emiterius ir panaudoti juos skystoje ir kietoje UC sistemoje. Atskleisti modifikacijų įtaką pavienių molekulių spindulinėms savybėms, įvertinti gautų junginių pritaikomumą UC.
4) Įvertinti kaip skirtingos Rub sluoksnio paruošimo (nusodinimo) sąlygos keičia Rub PL ir UC savybes.
5) Naudojant laikinį PL gesinimo metodą išmatuoti ir kiekybiškai nustatyti singletinių ir tripletinių eksitonų difuziją aprašančius parametrus netvarkiuose Rub sluoksniuose.

Ginamieji teiginiai

I Rubreno (Rub) emiteriu paremtų ir metaloftalocianinu sensibilizuotų NIR-Vis UC sistemų našumą riboja maža statistinė tikimybė (f) apibūdinanti TTA proceso metu gauti singletinę būseną iš dviejų tripletinių būsenų.

II Rubreno modifikavimas *t*-butilo grupėmis slopina agregacijos sukeltą fluorescencijos (FL) gesinimą daugiausia nulemtą nespindulinio singleto skilimo ir leidžia pasiekti didesnį UC efektyvumą.

III Rubreno modifikacija stambiomis šoninėmis grupėmis jungiant Rub periferijoje arba prie Rub kamieno, leidžia sumažinti singletų skilimo įtaką ir padidinti fluorescencijos kvantinę išeigą. Visgi, periferinis jungimas yra pranašesnis UC proceso atžvilgiu, kadangi netrukdo vykti TTA.

IV Rub sluoksnių FL savybės priklauso nuo bandinio paruošimo sąlygų, kurias keičiant, galime gauti sluoksnį, kurio savybės (didžiausias FL kvantinis išeiga ir FL gyvavimo trukmė) labiausiai atitiktų amorfinio Rub savybes, pageidautinas siekiant pagerinti UC efektyvumą.

V Našų TTA-UC veikimą netvarkiuose Rub sluoksniuose riboja tripletinių eksitonų difuzijos nuotolis, apspręstas sąlyginai trumpa Rub tripletinių eksitonų gyvavimo trukme.

Autoriaus indėlis

Autorius atlikto didžiąją dalį disertacijoje pateikiamų eksperimentų. Ruošė tyrimams skirtus bandinius, atliko jų spektroskopinę ir mikroskopinę analizę, atliko riekiamus skaičiavimus ir analizavo bei apdorojo duomenis. Autorius taip pat ženkliai prisidėjo prie disertacijoje aprašomų publikacijų rengimo, dalyvavo pirminiame eksperimentų konceptualizavime, diskusijose, rengė rankraščius ir buvo įsitraukęs į recenzavimo procesą.

Svarbu paminėti, kad dideli ir svarbūs darbai nuveikiami tik su puikia ir kvalifikuota komanda. Naujų junginių sintezę atliko organinių chemikų grupė, vadovaujama prof. Edvino Orento organinės chemijos katedroje (Vilniaus universitetas). Medžiagų sublimaciją atliko dr. Gediminas Kreiza. Sužadintos būsenos sugerties matavimus atliko dr. Paulius Baronas. Rub sluoksnių terminį vakuuminį nusodinimą atliko dr. Dovydas Banevičius. Eksitonų difuziją charakterizavo Manvydas Dapkevičius ir dr. Steponas Raišys. Lukas Naimovičius gelbėjo ir prisidėjo įvairiuose UC charakterizavimo eksperimentuose. Autorius labai vertina šių kolegų svarų indėlį ir yra labai dėkingas už suteiktą galimybę dirbti su jais komandoje.

Publikacijų santraukos

PI NIR fotonų konversija į regimąją sritį organiniuose tirpaluose: procesą ribojantys veiksniai sistemose su Rubreno spinduoliu

Nors literatūroje galime sutikti jau pademonstruotų našių fotonų konversijos sistemų veikiančių regimojoje spektro dalyje (Vis-Vis UC), tačiau NIR fotonus sugeriančių ir jų dažnį didinančių (NIR-Vis UC) organinių mišinių pasirinkimas yra itin mažas. Be to, minėtų sistemų efektyvumas yra nepakankamas praktiniams taikymams. Priežastys, lemiančios mažėjantį TTA-UC sistemų našumą keliaujant į NIR sritį, nėra iki galo suprastos. Publikacija **PI** parengta siekiant suprasti dabartinių NIR-Vis UC sistemų problematiką. Šioje dalyje trumpai pateikiamos pirmosios publikacijos **PI** esminės įžvalgos.

Vienas pagrindinių **PI** tyrimo objektų yra Rubrenas (Rub), bene dažniausiai naudojamas emiteris našiausiose NIR-Vis UC sistemose. Tyrimo metu susintetinti du nauji metaloftalocianinai (MPc) galintys sugerti NIR spinduliuotę. MPc UC schemoje panaudoti kaip sensibilizatoriai. Papildomai susintetintas naujas emiteris, modifikuotas Rub tirpumą gerinančiomis *tert*-butil grupėmis (tBRub). Paruošti skirtingi sensibilizatoriaus ir emiterio porų deriniai tirpale, atlikta mišinių koncentracijos optimizacija su tikslu pasiekti aukščiausią UC efektyvumą. Atlikta optimizuotų UC tirpalų eksperimentinė analizė ir nustatyti pagrindiniai nuostoliai vykstantys UC sistemoje.

Visų pirma tirti nauji sunkiųjų metalų (Pd, Pt) ftalocianinai (PdPc ir PtPc). Nustatyta, kad abiejų junginių žemiausia tripletinė būsena (T_1 = 1,12 - 1,18 eV) dera su Rub spinduliu (T_1 = 1,04-1,14 eV). Nustatyti sensibilizatorių sugerties, fluorescencijos ir fosforescencijos spektrai, bei tripletų gyvavimo trukmės (τ_T =0,7 - 4,3 µs). Taip pat tirti emiteriai Rub ir tBRub. Remiantis fotofizikiniais tyrimais nustatyta, kad *t*-butil modifikacijos nesutrikdė molekulės konjugacijos. Abu spinduoliai rodė beveik identiškus sugerties ir fluorescencijos spektrus ir pasižymėjo efektyvia spinduline emisija (Φ_{FL} ~ 100%).

Toliau sekė UC tirpalų tyrimai. Pirmiausia panaudota optimali sensibilizatoriaus PdPc koncentracija (15 µM), o šis tirpalas maišytas su Rub spinduoliu. Pastebėta, kad didėjanti Rub koncentracija lemia laipsnišką UC signalo augimą. Pasirinkta Rub koncentracija buvo 18mM, kuri atitinka Rub tirpumo ribą tolueno tirpiklyje. UC našumo augimas, didėjant emiterio koncentracijai, paaiškintas gerėjančia ir efektyvesne tripletinių eksitonų pernaša (TET) iš sensibilizatoriaus į emiterį. Eksperimentiškai TET įvertinta matuojant uždelstosios fluorescencijos gesimo kreives. Našiausiame bandinyje nustatytas TET efektyvumas siekė Φ_{TET} = 82%. TET tyrimai atlikti ir kitiems sensibilizatorių ir emiterių mišiniams. Nustatyta, kad tBRub atveju tomis pačiomis sąlygomis TET yra ribojama *t*-butil skyriklių (Φ_{TET} = 56%). Norint pasiekti efektyvesnę TET, reikalinga aukštesnė emiterio koncentracija.

Atlikti UC tirpalų fluorescencijos (FL) ir UC intensyvumo priklausomybės nuo sužadinimo galios tyrimai. UC atveju prie mažų sužadinimų stebėta įprasta kvadratinė UC priklausomybė. Viršijus tam tikrą sužadinimo galios slenkstinę vertę (I_{th}), UC priklausomybė buvo tiesinė. Žemiausia slenkstinė vertė gauta Rub:PdPc sistemoje (I_{th} = 1,9 W/cm^2), tuo tarpu tBRub atveju, dėl prastesnės TET, slenkstis 2 kart didesnis (I_{th} = 3,6 W/cm^2).

Galiausiai įvertinti mišinių UC našumai. Optimizuota Rub:PdPc sistema demonstravo aukščiausią našumą Φ_{UC} = 5.6%. Šiame UC tirpale įvertinti visi tarpiniai UC energijos perdavimo procesai. Nustatyta, kad svarbiausias veiksnys ribojantis UC procesą yra mažas Rub statistinis faktorius (f = 15,5 ± 3%). Šis faktorius nusako tikimybę TTA proceso metu suformuoti singletinę būseną. Deja, toks mažas Rub f faktorius riboja UC sistemų efektyvumą. Nustatyta, kad maksimalus nagrinėtos UC sistemos Φ_{UC} gali siekti tik ~8% ($\approx 1/2\times f$), neįskaitant galimų papildomų nuostolių. Taigi, siekiant pasiekti Φ_{UC} > 8%, reikalinga naujų emiterių paieška.

PII UC realizavimas sluoksniuose pasitelkiant molekulių inžineriją ir singletinių eksitonų gaudykles

Ankstesniame skyriuje aptarti pagrindiniai UC ribojantys veiksniai skystoje terpėje (tirpale). Tačiau praktiniams taikymams (pvz.: saulės celių našumo didinimui), reikalingas aukštas UC efektyvumas kietojoje būsenoje. Lyginant su tirpalu, kietakūnės UC sistemos, kuriose molekulių padėtys yra fiksuotos, yra daug sudėtingesnės, jose atsiranda papildomų kliūčių, kurios slopina UC efektyvumą. Publikacijoje **PII** tiriami UC sluoksniai ir identifikuojami bei sprendžiami UC našumą ribojantys veiksniai juose. Šiame skyrelyje, pateikiamos tik pagrindinės **PII** įžvalgos ir rezultatų santrauka.

Pirmiausia atliktas koncentracinio gesimo eksperimentas. Pastebėta, kad nekonjuguotos *t*-butil grupės veiksmingai apsaugo emiterio molekules nuo jų agregacijos ir sumažina koncentracinį fluorescencijos gesinimą daugiau kaip 20 kartų. Tiksliau, tBRub atveju fluorescencijos kvantinis našumas (Φ_{FL}) išlieka artimas 100 % padidinus emiterio koncentraciją polimere (PS) net iki 30 %, tuo tarpu rubreno sluoksniuose Φ_{FL} pradeda mažėti jau viršijus 1 % koncentraciją. Galiausiai gryname sluoksnyje Rub Φ_{FL} nukrenta iki 1,5%, o tBRub atveju Φ_{FL} išsilaiko aukštesnis, net 35%. Staigus našumo mažėjimas Rub sluoksniuose yra priskiriamas nespinduliniam singletinių eksitonų skylimui (SF). tBRub atveju, erdvinės *t*-butil grupės mažina SF dėl vidutiniškai didesnio vidutinio atstumo tarp emiterio molekulių.

Tyrimuose taip pat panaudotas kitas būdas pagerinti Rub sluoksnių našumą. Prieš liejant sluoksnius, Rub legiruotas gerai fluorescuojančiu junginiu DBP (singletinių eksitonu gaudykle). Įmaišytos DBP molekulės, pasiskirsčiusios Rub sluoksnyje, konkuruoja su nespinduliniu SF reiškiniu. Gaudyklių dėka Φ_{FL} buvo padidintas 10 kartų ir siekė 15%, esant optimaliai jų koncentracijai (0,5%).

Siekiant suprasti UC našumą ribojančius veiksnius, buvo atlikti nuodugnūs UC sluoksnių tyrimai. UC sluoksniai paruošti legiruojant Rub ir tBRub su PdPc sensibilizatoriumi ir DBP eksitonų gaudykle. Rub UC sluoksniai, nors ir su DBP, demonstravo žemą Φ_{FL} = 2,5%. Šis 6-ių kartų Φ_{FL} sumažėjimas priskirtas žalingai atgalinei FRET pernašai į PdPc. Emiterio koncentracijos polimeriniuose sluoksniuose optimizavimo eksperimentai parodė, kad didžiausias UC našumas buvo pasiektas esant 80% emiterio, 0,1% sensibilizatoriaus ir 0,5% DBP koncentracijoms. tBRub emiterio sluoksniuose pasiektas Φ_{UC} = 0,3%, kuris yra daugiau kaip 4 kartus didesnis, nei Rub atveju (Φ_{UC} = 0,07%). Šio tyrimo rezultatai atskleidė, kad nors nekonjunguoti *t*-butil pakaitai potencialai sumažina tripletinių eksitonų difuziją kietuose sluoksniuose, difuzija yra pakankama vykti TTA procesui, o gautas aukštesnis fluorescencijos našumas leidžia pasiekti efektyvesnę UC.

PIII Šoninių pakaitų įtaka Rubreno junginių spindulinėms savybėms ir taikymams NIR fotonų konversijoje į regimąją sritį

Praėjusiame skyriuje aptarti publikacijos **PII** rezultatai parodė, kad modifikavus Rub mažomis nekonjuguotomis *t*-butil grupėmis, gaunamas junginys tBRub yra pranašesnis už Rub kietame sluoksnyje. Sluoksniuose gautas aukštesnis fluorescencijos našumas (Φ_{FL}) ir, atitinkamai, aukštesnis UC našumas (Φ_{UC}) dėl sumažėjusio žalingo singletų skilimo (SF) efekto. Šiame skyriuje yra aptariami publikacijos **PIII**, kurioje toliau plėtota idėja mažinti SF efektą, rezultatai. Tai buvo daroma jungiant didesnius šoninius pakaitus prie Rub kamieno. Susintetinti du nauji Rub dariniai: pirmu atveju jungtos 3,5-di-*tert*-butilphenil grupės periferijoje (peri-tBRub), o antru - tiesiogiai prie tetraceno kamieno (core-tBRub). Tyrimo metu gauti junginiai lyginami su anksčiau tirtais Rub ir tBRub, atliekant FL ir UC eksperimentus.

Pirmiausia atlikta sugerties ir fluorescencijos spektrų analizė parodė, kad modifikacijos daro silpną įtaką molekulės konjugacijai. Tik core-tBRub atveju, tiek sugerties, tiek emisijos spektrai kitų junginių atžvilgiu pasislinko 20 nm į ilgųjų bangų pusę. Modifikacijos taip pat nepakeitė pavienių molekulių spindulinių savybių, visi Rub dariniai demonstravo artima ~100% Φ_{FL}. Silpną modifikacijų įtaką pavienių molekulių sužadintos būsenos energijoms patvirtino ir teoriniai DFT skaičiavimai. Pastebėta, kad tirti Rub dariniai rodo panašų T_1 lygmenį, išlaiko sąlygą $2\times T_1 > S_1$, todėl gali vykdyti TTA. Taigi, patvirtinta, kad kaip ir Rub, ir tBRub praėjusiuose tyrimuose (**PI** ir **PII**), peri-tBRub ir core-tBRub gali būti panaudoti UC sistemoje kartu su PdPc sensibilizatoriumi.

Vėliau tirti pagaminti Rub darinių sluoksniai. Fluorescencijos kvantinio našumo ir fluorescencijos gyvavimo trukmių matavimai parodė stipriai sumažintą SF įtaką peri-tBRub ir core-tBRub junginiuose. Nustatyta, kad 3,5-di-*tert*-butilphenil modifikacijos gryname sluoksnyje leido išlaikyti daugiau nei 60 % pradinio Φ_{FL}, lyginant su nesąveikaujančiomis molekulėmis. Tai yra net 40 kartų našesnė fluorescencija, nei įprasto Rub atveju, kur Φ_{FL} siekia vos 1.5 %.

Toliau atlikti UC tyrimai, kuriuose Rub dariniai panaudoti kaip emiteriai kartu su PdPc sensibilizatoriumi. Pirmiausia atlikti tyrimai panaudojant medžiagas tirpale. Pagaminti identiškų koncentracijų bandiniai (18mM emiterio ir 15µM PdPc) ir palyginti tarpusavyje. Buvo nustatyta, kad struktūriškai sudėtingų Rub emiterių UC našumas tirpale yra daugiau nei 10 kartų mažesnis Rub ar tBRub atžvilgiu. Vėliau atlikti UC sluoknių tyrimai atskleidė, kad, nors sluoksniuose peri-tBRub ir core-tBRub rodė ypač aukštą Φ_{FL}, UC signalas juose buvo silpnas (vos registruojamas). Atlikta prielaida, kad skurdų Φ_{UC} lėmė stambūs šoniniai pakaitai, trukdantys tripletų energijos pernašai (TET) ir (arba) TTA procesams. Teoriškai, TET procesas galėtų būti pagerintas naudojant peri-tBRub ar core-tBRub su kitu sensibilizatoriumi, pasižyminčiu ilgesne tripletų gyvavimo trukme. Taigi, iš gautų rezultatų vienareikšmiškai nustatyti, UC ribojantį veiksnį (TET ar TTA) nėra lengva.

Siekiant ištirti tik TTA procesą Rub dariniuose, tyrimuose panaudoti grynų medžiagų sluoksniai (be sensibilizatoriaus), matuojant ilgų laikų uždelstosios fluorescencijos signalą. Šis matavimas išskirtinai tinkamas Rub darinių sluoksniams, nes juose, dėl palankaus energinių lygmenų išsidėstymo ($2T_1 \sim S_1$), vyksta tiek SF, tiek TTA. Tokiu būdu, sluoksniuose sukuriami tripletiniai sužadinimai papildomai nenaudojant sensibilizatoriaus, o ilguose laikuose po sužadinimo (>µs), registruojamas signalas dėl TTA. Kiekvienam Rub dariniui buvo įvertinta skilusių singletų dalis (t. y. per SF sugeneruotų tripletų skaičius), bei grįžusių per TTA ir išsišvietusių singletų dalis. Pastarųjų dydžių santykis nusako TTA proceso efektyvumą. Gauti TTA efektyvumo rezultatai parodė, kad našiausias junginys buvo tBRub (77,3 %), o Rub (18,5 %) gauta vertė buvo ~ 4 kartus mažesnė. Pastebėta, kad peri-tBRub pasižymėjo panašia į Rub TTA efektyvumo vertę – 15,4 %. Priešingai core-tBRub junginio atveju, TTA efektyvumas smuko iki 0,6 %. **PIII** atskleidė, kad Rub modifikacijos periferijoje mažina SF įtaką ir nepablogina junginio TTA savybių.

PIV Rubreno UC sluoksnių našumo didinimas panaudojant supaprastintą terminį garinimą

Siekiant išnaudoti NIR fotonų konversijos ypatumus taikymuose, reikalingas aukštas UC našumas, ypač kietame būvyje. Didžioji dalis literatūroje pateikiamų kietos būsenos NIR-vis UC sistemų, kaip spinduolį, naudoja rubreną (Rub). Tačiau, net ir pačios našiausios sistemos, sugeriančios NIR spinduliuotę (>700 nm), pasižymi žemu UC našumu, dažniausiai < 1 %.

Norint Rub sluoksniuose pasiekti didesnį UC našumą, svarbu kovoti su nespinduliniu singletų skilimu (SF), kuris lemia itin žemą Rub fluorescencijos našumą. Efektyviam SF reikalingos dvi, greta esančios, emiterio molekulės. Taigi SF procesas yra jautrus vidutiniam atstumui tarp molekulių. Siekiant sumažinti SF įtaką, galima: modifikuoti emiterį nekonjuguotomis grupėmis, siekiant padidinti vidutinį tarpmolekulinį atstumą; keisti sluoksnio paruošimo sąlygas, kurios lemia atsitiktinį molekulių išsidėstymą. **PIV** darbe tirti skirtingais būdais paruošti Rub sluoksniai, atlikta šių sluoksnių spindulinių savybių analizė ir įvertinta sluoksnių morfologijos įtaka UC našumui.

Visi sluoksniai buvo suformuoti ant iš anksto paruošto padėklo su plonu sensibilizatoriaus PdPc (0,1 wt%) sluoksniu. Darbe tirtos 4 skirtingos Rub sluoksnio nusodinimo sąlygos. Pirmiausia Rub buvo kontroliuojamai užgarintas aukšto *vakuumo* sąlygomis (~10^{-7} Torr). Pastarasis metodas literatūroje pristatomas kaip būdas gauti netvarkų (amorfinį) Rub sluoksnį. Šiuo būdu paruošti sluoksniai naudoti kaip atskaitos taškas. Likę trys nusodinimo būdai, buvo technologiškai žymiai paprastesni. Vietoj sudėtingos garinimo aparatūros, panaudotas paprastas kaitinimo elementas. Garinimai atlikti azoto atmosferoje. *Šalto nusodinimo* sąlygomis Rub buvo garinimas ant šaldomo padėklo (-10 °C). Išskirtas trečiasis paruošimo būdas, atkaitinus *šalto nusodinimo* būdu paruoštus sluoksnius (100 °C). Ketvirtuoju būdu Rub buvo garinamas ant padėklo nenaudojant šaldymo, padėklas natūraliai įkaisdavo, o metodas pavadintas *karštu nusodinimu*.

Yra žinoma, kad Rub sluoksniai, neturintys SF centrų, rodo mono-eksponentines fluorescencijos (FL) gesimo kinetikas (τ = 16.4 ns). Priešingai, trumpas gyvavimo laikas yra stebimas kristaliniuose sluoksniuose, kur SF dominuoja. Todėl FL gesimo kreivės suteikia informacijos apie sluoksnio amorfiškumą. Palyginus visais 4 būdais paruoštus sluoksnius, pastebėta, kad *vakuuminio* nusodinimo būdu pagaminti sluoksniai pasižymėjo trumpiausiu

τ = 2 ns, stipriausiu SF ir, atitinkamai, mažiausiu fluorescencijos kvantiniu našumu Φ_{FL} (1.6 %). Kitais būdais paruošti sluoksniai demonstravo ilgesnę FL gyvavimo trukmę ir aukštesnį fluorescencijos našumą. *Karšto nusodinimo* būdu paruoštas sluoksnis rodė 6 kartus ilgesnę gyvavimo trukmę ir daugiau nei 10 kartų aukštesnį našumą (τ = 12 ns, Φ_{FL} = 20.5 %).

Toliau tirtos paruoštų sluoksnių UC savybės. Pastebėta, kad *šalto nusodinimo* būdu paruoštas sluoksnis demonstruoja pakankamai aukštą Φ_{FL}, tačiau pasižymi prasta UC. Nustatyta, kad to priežastis yra skurdi tripletų pernaša iš sensibilizatoriaus į emiterį, kuri gali vykti tik siaurame prietaiso tūryje (sensibilizatoriaus ir emiterio sluoksniai yra griežtai atskirti). Priešingai, atkaitinus tą patį sluoksnį, emiteris ir sensibilizatoriaus persimaišo, gaunama efektyvi tripletinių eksitonų pernaša, stebimas stiprus UC išaugimas.

Tyrimo metu taip pat atlikta sensibilizatoriaus koncentracijos bei sensibilizatoriaus sluoksnio storio optimizacija. Po sistemingos optimizacijos gautas našiausias sluoksnis, kuris pasižymėjo Φ_{UC} = (1.2 ± 0.15)%. Tai yra 17 kartų geresnis rezultatas, nei mūsų grupės demonstruoti sluoksniai paruošti liejimo būdu. Taip pat, gautas rekordinis Φ_{UC} yra bent 2 kartus aukštesnis už kitų, literatūroje publikuojamų UC sistemų, kurios sudarytos tik iš dviejų komponenčių (sensibilizatoriaus ir emiterio). Gauta našumo vertė yra artima rekordinei Φ_{UC} = 2 % trijų komponenčių sistemai, kurioje naudotas trečias junginys DBP, kaip singletinių eksitonų gaudyklė. Toks rezultatas parodo, kad paruošto sluoksnio morfologija yra itin svarbi, o aukštą našumą įmanoma pasiekti ir nenaudojant trečio junginio UC sistemoje.

Kadangi darbe nuosekliai įvertinti Rub sluoksniuose vykstantys tarpiniai energijos pernašos procesai, kurių visuma susideda į Φ_{UC}, galime įvertinti TTA tikimybės faktorių (f). Žinant, kad maksimaliai gauti Φ_{FL} = 20.5%, Φ_{TET} = 60%, Φ_{ISC} = 100%, Φ_{TTA} = 100% ir Φ_{UC} = 1.2%, apskaičiuojamas f (sugeneruoti singletinę būseną per TTA vyksmą) yra 19.5 %. Artima f vertė yra gauta Rub tirpale (f = 15.5%). Tai gali būti paaiškinta panašiu sužadintų būsenų energijos lygmenų išsidėstymu tiek tirpale, tiek netvarkiame sluoksnyje. Svarbu tai, kad gauta f vertė prognozuoja maksimalią Φ_{UC} ribą, UC sistemoms, naudojančioms Rub emiterį. Nustatyta riba atitinka $\Phi_{UC} \approx ½ \times f \approx 10\%$.

PV Singletinių ir tripletinių eksitonų difuzija netvarkiuose rubreno sluoksniuose

Praktiniams taikymams reikšminga infraraudonosios (IR) šviesos konversija į regimąją sritį yra apribota žemo UC našumo. Ypatingai žemas UC našumas gaunamas sluoksniuose. Kietoje būsenoje, kai emiterio molekulės yra fiksuotos, tripletiniai ir singletiniai eksitonai gali migruoti dėl difuzijos. Būtent difuzija lemia tiek tripletines-tripletines anihiliacijos (TTA), tiek singletų skilimo (SF) procesus, kurie daro reikšmingą įtaką TTA sukeltos fotonų konversijos (UC) našumui. Pavyzdžiui, medžiagose, pasižyminčiose didele tripletinių eksitonų difuzija, TTA gali efektyviai vykti esant mažai sužadinimo galiai (~ mW/cm^2). Priešingai, maža singletų difuzija yra naudinga, ji dažnu atveju lemia aukštesnį spindulinį našumą. Taip yra dėl to, kad singletiniai eksitonai nepasiekia nespindulinių SF centrų arba yra neprarandami, nuostolingai energiją perduodant atgal į sensibilizatorių.

Šiame skyriuje pateikiami **PV** rezultatai. Publikacijoje tiriamos netvarkios Rubreno (Rub) plevelės, siekiant įvertinti tripletų ir singletų difuziją jose. Nors literatūroje galima rasti tripletų difuzijos tyrimų Rub kristaluose, difuzija netvarkiuose Rub sluoksniuose iki šiol nėra tyrinėta. Priešingai nei kristalai, netvarkūs Rub sluoksniai yra naudojami daugumoje UC sistemų. Sužadinimo difuzijos parametrų nežinojimas stipriai riboja šių sistemų progresą.

Siekiant ištirti difuzijos parametrus, pasirinktas eksitonų gesinimo metodas bei panaudota Sterno-Volmerio analizė. Tokiu būdu nustatytas eksitonų difuzijos koeficientas (D) ir eksitonų difuzijos nuotolis (L_D) tiek singletiniams, tiek tripletiniams eksitonams. Kadangi daugumoje UC tiriamųjų darbų Rub yra naudojamas kartu su DBP (singletinių eksitonų sugėriklis), siekta ištirti šio priedo įtaka sužadinimo difuzijai.

Singletų difuzijos nustatymo eksperimentas parodė, kad netvarkiose Rub plėvelėse singletų difuzijos nuotolis (L_D^S) yra ~13,7 - 16,4 nm. Papildomai pridėjus PdPc sensibilizatoriaus (0,1 wt%), stebėtas ~35-50% trumpesnis L_D^S. Tai parodo, kad sužadinti singletai grįžta į PdPc sensibilizatorių ir tokiu būdu yra prarandami. Papildomai maža koncentracija (0,5wt%) DBP taip pat sutrumpina L_D^S, tačiau šiuo atveju singletai yra gesinami spinduliniu būdu. Pastebėta, kad Rub kristaluose L_D^S yra bent ~10 ilgesnis, todėl kristaluose singletai gali pasiekti nespindulinius SF centrus.

Tripletinių eksitonų difuzijos parametrai buvo nustatyti tiriant netvarkius, UC pasižyminčius Rub sluoksnius. Nustatyta, kad Rub tripletų difuzijos konstanta ($D_\mathrm{T} \sim 3\cdot10^{-7}$ cm$^2\cdot$s^{-1}) yra daugiau nei 10 kartų didesnė, nei gerai žinomose antraceno sluoksniuose, kurie demonstruoja žymiai didesnį UC našumą, tačiau regimojoje srityje. Vis dėlto nustatyta, kad netvarkūs Rub sluoksniai pasižymi palyginti trumpu tripletinių eksitonų difuzijos nuotoliu (L_D^T), kurį nulemia trumpas tripletinių eksitonų gyvavimo laikas (τ_T ~30 - 60 μs). Palyginimui, yra žinoma, kad Rub kristaluose šis nuotolis gali siekti 2-8 μm, tačiau darbe liejimo būdu paruoštose Rub UC sluoksniuose nustatytas L_D^T yra ~100 kartų trumpesnis (25 - 30 nm). Verta paminėti, jog kristalai UC procesui nėra tinkami, dėl didelio SF centrų tankio ir žemo spindulinio našumo. Tyrimo metu įvertinta, kad Rub sluoksniuose $L_{\mathrm{D}}^{\mathrm{T}}$ maksimaliai galėtų būti prailgintas ~2 kartus (iki 55 nm). Tai įmanoma pasiekti tuo atveju, jeigu Rub tripletų gyvavimo laikas ($\tau_{\mathrm{T}} \approx 100$ μs) atitiktų pavienių, nesąveikaujančių Rub molekulių laiką. Pastebima, kad $L_{\mathrm{D}}^{\mathrm{T}}$ pagerinimui reikalingi nauji emiteriai, kurie pasižymėtų žemos energijos tripletine būsena ir ilgesne gyvavimo trukme nei Rub.

IŠVADOS

1. Tirpumą gerinančių alkilo grupių (*t*-butil) jungimas prie rubreno (Rub) emiterio leido padvigubinti emiterio koncentraciją UC tirpale ir pagerinti tripletinių sužadinimų pernašą (Φ_{TET}). Visgi, modifikacija neigiamai paveikė UC efektyvumą (Φ_{UC}) dėl sumažėjusios statistinės tikimybės (f), nuo 15.6% (Rub) iki 5.3% (*t*-butil-Rub) TTA proceso metu suformuoti singletinę būseną.

2. Pasiektas 4 kartus aukštesnis Φ_{UC} naudojant *t*-butil grupėmis modifikuotą Rub emiterį (Φ_{UC} = 0,3%) lyginant su nemodifikuotu Rub (Φ_{UC} = 0,07%). Išaugimą lėmė sumažėjęs fluorescencijos koncentracinis gesinimas, kurį didžiąją dalimi apsprendė susilpnėjusi singletų skilimo įtaka.

3. Didelių sterinių grupių jungimas prie Rub emiterio ženkliai pagerina (iki 40 kartų) sluoksnio fluorescencijos kvantinį našumą (Φ_{FL}), tačiau UC sistemoje kartu su Pd-ftalocianino (PdPc) sensibilizatoriumi, lemia prastas UC savybes, kadangi sterinės grupės trukdo vykti efektyviai tripletinių sužadinimų pernašai iš PdPc.

4. Pademonstruotas paprastas Rub terminio nusodinimo metodas, kuomet termiškai nusodinamas Rub emiteris ant sensibilizatoriumi legiruoto polimero sluoksnio. Palyginus su kitais paruošimo metodais (vakuuminio garinimo, liejimo ant besisukančios padėklo) paprastas terminis nusodinimas inertinėje aplinkoje leido pasiekti aukštesnį Φ_{FL} ir efektyvią Φ_{TET} ir dėl to ~ 20 kartų pagerinti Φ_{UC} (nuo 0,07% iki 1.2%).

5. Tripletinių eksitonų difuzijos nuotolis ($L_{\mathrm{D}}^{\mathrm{T}}$) netvarkiuose Rub UC sluoksniuose yra 25-30 nm. Nustatyta, kad galimas tik nežymus $L_{\mathrm{D}}^{\mathrm{T}}$ pagerinimas (iki 55 nm), kurį riboja trumpa Rub tripletinių sužadinimų gyvavimo trukmė (100 μs). Siekiant padidinti $L_{\mathrm{D}}^{\mathrm{T}}$ ir taip pagerinti UC procesą sluoksniuose, reikalingi nauji emiteriai, kurie pasižymėtų ilgesne tripletinių sužadinimų gyvavimo trukme.

BIBLIOGRAPHY

(1) F. Schulze, T.; W. Schmidt, T. Photochemical Upconversion: Present Status and Prospects for Its Application to Solar Energy Conversion. *Energy Environ. Sci.* **2015**, *8* (1), 103–125. https://doi.org/10.1039/C4EE02481H.

(2) Goldschmidt, J. C.; Fischer, S. Upconversion for Photovoltaics – a Review of Materials, Devices and Concepts for Performance Enhancement. *Adv. Optical Mater.* **2015**, *3* (4), 510–535. https://doi.org/10.1002/adom.201500024.

(3) Pedrini, J.; Monguzzi, A. Recent Advances in the Application Triplet–Triplet Annihilation-Based Photon Upconversion Systems to Solar Technologies. *J. Photonics Energy* **2017**, *8* (2), 022005. https://doi.org/10.1117/1.JPE.8.022005.

(4) Limberg, D. K.; Kang, J.-H.; Hayward, R. C. Triplet–Triplet Annihilation Photopolymerization for High-Resolution 3D Printing. *J. Am. Chem. Soc.* **2022**. https://doi.org/10.1021/jacs.1c11022.

(5) Ravetz, B. D.; Pun, A. B.; Churchill, E. M.; Congreve, D. N.; Rovis, T.; Campos, L. M. Photoredox Catalysis Using Infrared Light via Triplet Fusion Upconversion. *Nature* **2019**, *565* (7739), 343–346. https://doi.org/10.1038/s41586-018-0835-2.

(6) Khnayzer, R. S.; Blumhoff, J.; Harrington, J. A.; Haefele, A.; Deng, F.; Castellano, F. N. Upconversion-Powered Photoelectrochemistry. *Chem. Commun.* **2011**, *48* (2), 209–211. https://doi.org/10.1039/C1CC16015J.

(7) Park, Y. I.; Lee, K. T.; Suh, Y. D.; Hyeon, T. Upconverting Nanoparticles: A Versatile Platform for Wide-Field Two-Photon Microscopy and Multi-Modal in Vivo Imaging. *Chem. Soc. Rev.* **2015**, *44* (6), 1302–1317. https://doi.org/10.1039/C4CS00173G.

(8) Yildiz, D.; Baumann, C.; Mikosch, A.; Kuehne, A. J. C.; Herrmann, A.; Göstl, R. Anti-Stokes Stress Sensing: Mechanochemical Activation of Triplet–Triplet Annihilation Photon Upconversion. *Angew. Chem. Int. Ed.* **2019**, *58* (37), 12919–12923. https://doi.org/10.1002/anie.201907436.

(9) Liu, S.-W.; Lee, C.-C.; Yuan, C.-H.; Su, W.-C.; Lin, S.-Y.; Chang, W.-C.; Huang, B.-Y.; Lin, C.-F.; Lee, Y.-Z.; Su, T.-H.; Chen, K.-T. Transparent Organic Upconversion Devices for Near-Infrared Sensing. *Adv. Mater.* **2015**, *27* (7), 1217–1222. https://doi.org/10.1002/adma.201404355.

(10) Zhou, Y.; Han, S.-T.; Chen, X.; Wang, F.; Tang, Y.-B.; Roy, V. a. L. An Upconverted Photonic Nonvolatile Memory. *Nat. Commun.* **2014**, *5*, 4720. https://doi.org/10.1038/ncomms5720.

(11) Askes, S. H. C.; Meijer, M. S.; Bouwens, T.; Landman, I.; Bonnet, S. Red Light Activation of Ru(II) Polypyridyl Prodrugs via Triplet-Triplet Annihilation Upconversion: Feasibility in Air and through Meat.

Molecules **2016**, *21* (11), 1460. https://doi.org/10.3390/molecules21111460.

(12) Zhou, J.; Liu, Q.; Feng, W.; Sun, Y.; Li, F. Upconversion Luminescent Materials: Advances and Applications. *Chem. Rev.* **2015**, *115* (1), 395–465. https://doi.org/10.1021/cr400478f.

(13) Raišys, S.; Kazlauskas, K.; Juršėnas, S.; Simon, Y. C. The Role of Triplet Exciton Diffusion in Light-Upconverting Polymer Glasses. *ACS Appl. Mater. Interfaces* **2016**, *8* (24), 15732–15740. https://doi.org/10.1021/acsami.6b03888.

(14) Mahammed, A.; Chen, K.; Vestfrid, J.; Zhao, J.; Gross, Z. Phosphorus Corrole Complexes: From Property Tuning to Applications in Photocatalysis and Triplet–Triplet Annihilation Upconversion. *Chem. Sci.* **2019**, *10* (29), 7091–7103. https://doi.org/10.1039/C9SC01463B.

(15) Hoseinkhani, S.; Tubino, R.; Meinardi, F.; Monguzzi, A. Achieving the Photon Up-Conversion Thermodynamic Yield Upper Limit by Sensitized Triplet–Triplet Annihilation. *Phys. Chem. Chem. Phys.* **2015**, *17* (6), 4020–4024. https://doi.org/10.1039/C4CP03936J.

(16) Fan, C.; Wei, L.; Niu, T.; Rao, M.; Cheng, G.; Chruma, J. J.; Wu, W.; Yang, C. Efficient Triplet–Triplet Annihilation Upconversion with an Anti-Stokes Shift of 1.08 EV Achieved by Chemically Tuning Sensitizers. *J. Am. Chem. Soc.* **2019**, *141* (38), 15070–15077. https://doi.org/10.1021/jacs.9b05824.

(17) Deng, F.; Blumhoff, J.; Castellano, F. N. Annihilation Limit of a Visible-to-UV Photon Upconversion Composition Ascertained from Transient Absorption Kinetics. *J. Phys. Chem. A* **2013**, *117* (21), 4412–4419. https://doi.org/10.1021/jp4022618.

(18) Duan, P.; Yanai, N.; Kimizuka, N. Photon Upconverting Liquids: Matrix-Free Molecular Upconversion Systems Functioning in Air. *J. Am. Chem. Soc.* **2013**, *135* (51), 19056–19059. https://doi.org/10.1021/ja411316s.

(19) Huang, Z.; Xu, Z.; Mahboub, M.; Liang, Z.; Jaimes, P.; Xia, P.; Graham, K. R.; Tang, M. L.; Lian, T. Enhanced Near-Infrared-to-Visible Upconversion by Synthetic Control of PbS Nanocrystal Triplet Photosensitizers. *J. Am. Chem. Soc.* **2019**, *141* (25), 9769–9772. https://doi.org/10.1021/jacs.9b03385.

(20) Huang, L.; Wu, W.; Li, Y.; Huang, K.; Zeng, L.; Lin, W.; Han, G. Highly Effective Near-Infrared Activating Triplet–Triplet Annihilation Upconversion for Photoredox Catalysis. *J. Am. Chem. Soc.* **2020**, *142* (43), 18460–18470. https://doi.org/10.1021/jacs.0c06976.

(21) Radiunas, E.; Raišys, S.; Juršėnas, S.; Jozeliūnaitė, A.; Javorskis, T.; Šinkevičiūtė, U.; Orentas, E.; Kazlauskas, K. Understanding the Limitations of NIR-to-Visible Photon Upconversion in Phthalocyanine-Sensitized Rubrene Systems. *J. Mater. Chem. C* **2019**, *8* (16), 5525–5534. https://doi.org/10.1039/C9TC06031F.

(22) Bharmoria, P.; Bildirir, H.; Moth-Poulsen, K. Triplet–Triplet Annihilation Based near Infrared to Visible Molecular Photon Upconversion. *Chem. Soc. Rev.* **2020**, *49*, 6529–6554. https://doi.org/10.1039/D0CS00257G.

(23) Weiss, R.; VanOrman, Z. A.; Sullivan, C. M.; Nienhaus, L. A Sensitizer of Purpose: Generating Triplet Excitons with Semiconductor Nanocrystals. *ACS Mater. Au* **2022**. https://doi.org/10.1021/acsmaterialsau.2c00047.

(24) Torre, G. de la; Claessens, C. G.; Torres, T. Phthalocyanines: Old Dyes, New Materials. Putting Color in Nanotechnology. *Chem. Commun.* **2007**, No. 20, 2000–2015. https://doi.org/10.1039/B614234F.

(25) Köhler, A.; Bässler, H. *Electronic Processes in Organic Semiconductors: An Introduction*; Wiley-VCH Verlag GmbH & Co. KGaA: Weinheim, Germany, 2015. https://doi.org/10.1002/9783527685172.

(26) Chen, W.; Song, F.; Tang, S.; Hong, G.; Wu, Y.; Peng, X. Red-to-Blue Photon up-Conversion with High Efficiency Based on a TADF Fluorescein Derivative. *Chem. Commun.* **2019**. https://doi.org/10.1039/C9CC01868A.

(27) Zhang, Y.; Wang, Y.; Song, J.; Qu, J.; Li, B.; Zhu, W.; Wong, W.-Y. Near-Infrared Emitting Materials via Harvesting Triplet Excitons: Molecular Design, Properties, and Application in Organic Light Emitting Diodes. *Advanced Optical Materials* **2018**, *6* (18), 1800466. https://doi.org/10.1002/adom.201800466.

(28) Wieghold, S.; Bieber, A. S.; VanOrman, Z. A.; Nienhaus, L. Influence of Triplet Diffusion on Lead Halide Perovskite-Sensitized Solid-State Upconversion. *J. Phys. Chem. Lett.* **2019**, *10* (13), 3806–3811. https://doi.org/10.1021/acs.jpclett.9b01526.

(29) Nienhaus, L.; Wu, M.; Bulović, V.; Baldo, M. A.; Bawendi, M. G. Using Lead Chalcogenide Nanocrystals as Spin Mixers: A Perspective on near-Infrared-to-Visible Upconversion. *Dalton Trans.* **2018**, *47* (26), 8509–8516. https://doi.org/10.1039/C8DT00419F.

(30) Wu, M.; Lin, T.-A.; Tiepelt, J. O.; Bulović, V.; Baldo, M. A. Nanocrystal-Sensitized Infrared-to-Visible Upconversion in a Microcavity under Subsolar Flux. *Nano Lett.* **2021**, *21* (2), 1011–1016. https://doi.org/10.1021/acs.nanolett.0c04060.

(31) Beery, D.; Wheeler, J. P.; Arcidiacono, A.; Hanson, K. CdSe Quantum Dot Sensitized Molecular Photon Upconversion Solar Cells. *ACS Appl. Energy Mater.* **2019**. https://doi.org/10.1021/acsaem.9b01765.

(32) Haruki, R.; Sasaki, Y.; Masutani, K.; Yanai, N.; Kimizuka, N. Leaping across the Visible Range: Near-Infrared-to-Violet Photon Upconversion Employing a Silyl-Substituted Anthracene. *Chem. Commun.* **2020**. https://doi.org/10.1039/D0CC02240C.

(33) Kimizuka, N.; Yanai, N.; Morikawa, M. Photon Upconversion and Molecular Solar Energy Storage by Maximizing the Potential of

Molecular Self-Assembly. *Langmuir* **2016**, *32* (47), 12304–12322. https://doi.org/10.1021/acs.langmuir.6b03363.

(34) Dexter, D. L. A Theory of Sensitized Luminescence in Solids. *J. Chem. Phys.* **1953**, *21* (5), 836–850. https://doi.org/10.1063/1.1699044.

(35) Fagnoni, M. Modern Molecular Photochemistry of Organic Molecules. By Nicholas J. Turro, V. Ramamurthy and Juan C. Scaiano. *Angewandte Chemie International Edition* **2010**, *49* (38), 6709–6710. https://doi.org/10.1002/anie.201003826.

(36) Bachilo, S. M.; Weisman, R. B. Determination of Triplet Quantum Yields from Triplet−Triplet Annihilation Fluorescence. *J. Phys. Chem. A* **2000**, *104* (33), 7711–7714. https://doi.org/10.1021/jp001877n.

(37) Cheng, Y. Y.; Khoury, T.; Clady, R. G. C. R.; Tayebjee, M. J. Y.; Ekins-Daukes, N. J.; Crossley, M. J.; Schmidt, T. W. On the Efficiency Limit of Triplet-Triplet Annihilation for Photochemical Upconversion. *Phys Chem Chem Phys* **2010**, *12* (1), 66–71. https://doi.org/10.1039/b913243k.

(38) Gray, V.; Dzebo, D.; Abrahamsson, M.; Albinsson, B.; Moth-Poulsen, K. Triplet–Triplet Annihilation Photon-Upconversion: Towards Solar Energy Applications. *Phys. Chem. Chem. Phys.* **2014**, *16* (22), 10345–10352. https://doi.org/10.1039/C4CP00744A.

(39) Ieuji, R.; Goushi, K.; Adachi, C. Triplet–Triplet Upconversion Enhanced by Spin–Orbit Coupling in Organic Light-Emitting Diodes. *Nature Communications* **2019**, *10* (1), 1–10. https://doi.org/10.1038/s41467-019-13044-1.

(40) Schmidt, T. W.; Castellano, F. N. Photochemical Upconversion: The Primacy of Kinetics. *J. Phys. Chem. Lett.* **2014**, *5* (22), 4062–4072. https://doi.org/10.1021/jz501799m.

(41) Bossanyi, D. G.; Sasaki, Y.; Wang, S.; Chekulaev, D.; Kimizuka, N.; Yanai, N.; Clark, J. Spin Statistics for Triplet–Triplet Annihilation Upconversion: Exchange Coupling, Intermolecular Orientation, and Reverse Intersystem Crossing. *JACS Au* **2021**, *1* (12), 2188–2201. https://doi.org/10.1021/jacsau.1c00322.

(42) Yanai, N.; Suzuki, K.; Ogawa, T.; Sasaki, Y.; Harada, N.; Kimizuka, N. Absolute Method to Certify Quantum Yields of Photon Upconversion via Triplet-Triplet Annihilation. *J. Phys. Chem. A* **2019**. https://doi.org/10.1021/acs.jpca.9b08636.

(43) Smith, A. M.; Mancini, M. C.; Nie, S. Second Window for in Vivo Imaging. *Nature Nanotech* **2009**, *4* (11), 710–711. https://doi.org/10.1038/nnano.2009.326.

(44) Loo, J. F.-C.; Chien, Y.-H.; Yin, F.; Kong, S.-K.; Ho, H.-P.; Yong, K.-T. Upconversion and Downconversion Nanoparticles for Biophotonics and Nanomedicine. *Coordination Chemistry Reviews* **2019**, *400*, 213042. https://doi.org/10.1016/j.ccr.2019.213042.

(45) Sasaki, Y.; Oshikawa, M.; Bharmoria, P.; Kouno, H.; Hayashi-Takagi, A.; Sato, M.; Ajioka, I.; Yanai, N.; Kimizuka, N. Near-Infrared

Optogenetic Genome Engineering Based on Photon-Upconversion Hydrogels. *Angew. Chem. Int. Ed.* **2019**, *58* (49), 17827–17833. https://doi.org/10.1002/anie.201911025.

(46) Huang, Z.; Li, X.; Mahboub, M.; Hanson, K. M.; Nichols, V. M.; Le, H.; Tang, M. L.; Bardeen, C. J. Hybrid Molecule–Nanocrystal Photon Upconversion Across the Visible and Near-Infrared. *Nano Lett.* **2015**, *15* (8), 5552–5557. https://doi.org/10.1021/acs.nanolett.5b02130.

(47) Huang, Z.; Simpson, D. E.; Mahboub, M.; Li, X.; Tang, M. L. Ligand Enhanced Upconversion of Near-Infrared Photons with Nanocrystal Light Absorbers. *Chem. Sci.* **2016**, *7* (7), 4101–4104. https://doi.org/10.1039/C6SC00257A.

(48) Mahboub, M.; Huang, Z.; Tang, M. L. Efficient Infrared-to-Visible Upconversion with Subsolar Irradiance. *Nano Lett.* **2016**, *16* (11), 7169–7175. https://doi.org/10.1021/acs.nanolett.6b03503.

(49) Mahboub, M.; Xia, P.; Van Baren, J.; Li, X.; Lui, C. H.; Tang, M. L. Midgap States in PbS Quantum Dots Induced by Cd and Zn Enhance Photon Upconversion. *ACS Energy Lett.* **2018**, *3* (4), 767–772. https://doi.org/10.1021/acsenergylett.8b00122.

(50) Tripathi, N.; Ando, M.; Akai, T.; Kamada, K. Efficient NIR-to-Visible Upconversion of Surface-Modified PbS Quantum Dots for Photovoltaic Devices. *ACS Appl. Nano Mater.* **2021**. https://doi.org/10.1021/acsanm.1c02059.

(51) Pun, A. B.; Sanders, S. N.; Sfeir, M. Y.; Campos, L. M.; Congreve, D. N. Annihilator Dimers Enhance Triplet Fusion Upconversion. *Chem. Sci.* **2019**, *10* (14), 3969–3975. https://doi.org/10.1039/C8SC03725F.

(52) Deng, F.; Sommer, J. R.; Myahkostupov, M.; Schanze, K. S.; Castellano, F. N. Near-IR Phosphorescent Metalloporphyrin as a Photochemical Upconversion Sensitizer. *Chem. Commun.* **2013**, *49* (67), 7406–7408. https://doi.org/10.1039/C3CC44479A.

(53) Wu, M.; Jean, J.; Bulović, V.; Baldo, M. A. Interference-Enhanced Infrared-to-Visible Upconversion in Solid-State Thin Films Sensitized by Colloidal Nanocrystals. *Appl. Phys. Lett.* **2017**, *110* (21), 211101. https://doi.org/10.1063/1.4984136.

(54) Wu, M.; Congreve, D. N.; Wilson, M. W. B.; Jean, J.; Geva, N.; Welborn, M.; Van Voorhis, T.; Bulović, V.; Bawendi, M. G.; Baldo, M. A. Solid-State Infrared-to-Visible Upconversion Sensitized by Colloidal Nanocrystals. *Nat. Photonics* **2016**, *10* (1), 31–34. https://doi.org/10.1038/nphoton.2015.226.

(55) Nienhaus, L.; Wu, M.; Geva, N.; Shepherd, J. J.; Wilson, M. W. B.; Bulović, V.; Van Voorhis, T.; Baldo, M. A.; Bawendi, M. G. Speed Limit for Triplet-Exciton Transfer in Solid-State PbS Nanocrystal-Sensitized Photon Upconversion. *ACS Nano* **2017**, *11* (8), 7848–7857. https://doi.org/10.1021/acsnano.7b02024.

(56) Wang, L.; Yoo, J. J.; Lin, T.-A.; Perkinson, C. F.; Lu, Y.; Baldo, M. A.; Bawendi, M. G. Interfacial Trap-Assisted Triplet Generation in Lead

Halide Perovskite Sensitized Solid-State Upconversion. *Adv Mater* **2021**, e2100854. https://doi.org/10.1002/adma.202100854.

(57) Kinoshita, M.; Sasaki, Y.; Amemori, S.; Harada, N.; Hu, Z.; Liu, Z.; Ono, L. K.; Qi, Y.; Yanai, N.; Kimizuka, N. Photon Upconverting Solid Films with Improved Efficiency for Endowing Perovskite Solar Cells with Near-Infrared Sensitivity. *ChemPhotoChem* **2020**, *4* (11), 5271–5278. https://doi.org/10.1002/cptc.202000143.

(58) Abulikemu, A.; Sakagami, Y.; Heck, C.; Kamada, K.; Sotome, H.; Miyasaka, H.; Kuzuhara, D.; Yamada, H. Solid-State, Near-Infrared to Visible Photon Upconversion via Triplet–Triplet Annihilation of a Binary System Fabricated by Solution Casting. *ACS Appl. Mater. Interfaces* **2019**, *11* (23), 20812–20819. https://doi.org/10.1021/acsami.9b04148.

(59) Nienhaus, L.; Correa-Baena, J.-P.; Wieghold, S.; Einzinger, M.; Lin, T.-A.; Shulenberger, K. E.; Klein, N. D.; Wu, M.; Bulović, V.; Buonassisi, T.; Baldo, M. A.; Bawendi, M. G. Triplet-Sensitization by Lead Halide Perovskite Thin Films for Near-Infrared-to-Visible Upconversion. *ACS Energy Lett.* **2019**, *4* (4), 888–895. https://doi.org/10.1021/acsenergylett.9b00283.

(60) Tripathi, N.; Ando, M.; Akai, T.; Kamada, K. Near-Infrared-to-Visible Upconversion from 980 Nm Excitation Band by Binary Solid of PbS Quantum Dot with Directly Attached Emitter. *J. Mater. Chem. C* **2022**, *10* (12), 4563–4567. https://doi.org/10.1039/D1TC05058C.

(61) Wang, X.; Tom, R.; Liu, X.; Congreve, D. N.; Marom, N. An Energetics Perspective on Why There Are so Few Triplet–Triplet Annihilation Emitters. *J. Mater. Chem. C* **2020**, *8* (31), 10816–10824. https://doi.org/10.1039/D0TC00044B.

(62) Radiunas, E.; Naimovičius, L.; Raišys, S.; Jozeliūnaitė, A.; Orentas, E.; Kazlauskas, K. Efficient NIR-to-Vis Photon Upconversion in Binary Rubrene Films Deposited by Simplified Thermal Evaporation. *J. Mater. Chem. C* **2022**, *10* (16), 6314–6322. https://doi.org/10.1039/D1TC05332A.

(63) Halgren, T. A. Merck Molecular Force Field. I. Basis, Form, Scope, Parameterization, and Performance of MMFF94. *Journal of Computational Chemistry* **1996**, *17* (5–6), 490–519. https://doi.org/10.1002/(SICI)1096-987X(199604)17:5/6<490::AID-JCC1>3.0.CO;2-P.

(64) Hanwell, M. D.; Curtis, D. E.; Lonie, D. C.; Vandermeersch, T.; Zurek, E.; Hutchison, G. R. Avogadro: An Advanced Semantic Chemical Editor, Visualization, and Analysis Platform. *Journal of Cheminformatics* **2012**, *4* (1), 17. https://doi.org/10.1186/1758-2946-4-17.

(65) Neese, F. The ORCA Program System. *WIREs Computational Molecular Science* **2012**, *2* (1), 73–78. https://doi.org/10.1002/wcms.81.

(66) Singh-Rachford, T. N.; Castellano, F. N. Pd(II) Phthalocyanine-Sensitized Triplet−Triplet Annihilation from Rubrene. *J. Phys. Chem. A* **2008**, *112* (16), 3550–3556. https://doi.org/10.1021/jp7111878.

(67) Zhou, Y.; Castellano, F. N.; Schmidt, T. W.; Hanson, K. On the Quantum Yield of Photon Upconversion via Triplet–Triplet Annihilation. *ACS Energy Lett.* **2020**, 2322–2326. https://doi.org/10.1021/acsenergylett.0c01150.

(68) Edhborg, F.; Olesund, A.; Albinsson, B. Best Practice in Determining Key Photophysical Parameters in Triplet–Triplet Annihilation Photon Upconversion. *Photochem Photobiol Sci* **2022**. https://doi.org/10.1007/s43630-022-00219-x.

(69) Lakowicz, J. R.; Masters, B. R. Principles of Fluorescence Spectroscopy, Third Edition. *J. Biomed. Opt.* **2008**, *13* (2), 029901. https://doi.org/10.1117/1.2904580.

(70) Mello, J. C. de; Wittmann, H. F.; Friend, R. H. An Improved Experimental Determination of External Photoluminescence Quantum Efficiency. *Adv. Mater.* **1997**, *9* (3), 230–232. https://doi.org/10.1002/adma.19970090308.

(71) Murakami, Y.; Kamada, K. Kinetics of Photon Upconversion by Triplet-Triplet Annihilation: A Comprehensive Tutorial. *Phys. Chem. Chem. Phys.* **2021**. https://doi.org/10.1039/D1CP02654B.

(72) Monguzzi, A.; Tubino, R.; Hoseinkhani, S.; Campione, M.; Meinardi, F. Low Power, Non-Coherent Sensitized Photon up-Conversion: Modelling and Perspectives. *Phys. Chem. Chem. Phys.* **2012**, *14* (13), 4322–4332. https://doi.org/10.1039/C2CP23900K.

(73) Lin, J. D. A.; Mikhnenko, O. V.; Chen, J.; Masri, Z.; Ruseckas, A.; Mikhailovsky, A.; Raab, R. P.; Liu, J.; Blom, P. W. M.; Loi, M. A.; García-Cervera, C. J.; Samuel, I. D. W.; Nguyen, T.-Q. Systematic Study of Exciton Diffusion Length in Organic Semiconductors by Six Experimental Methods. *Mater. Horiz.* **2014**, *1* (2), 280–285. https://doi.org/10.1039/C3MH00089C.

(74) Hsu, H.-Y.; Vella, J. H.; Myers, J. D.; Xue, J.; Schanze, K. S. Triplet Exciton Diffusion in Platinum Polyyne Films. *J. Phys. Chem. C* **2014**, *118* (42), 24282–24289. https://doi.org/10.1021/jp507403m.

(75) Liu, D. K. K.; Faulkner, L. R. P-Type Delayed Fluorescence from Rubrene. *J. Am. Chem. Soc.* **1977**, *99* (14), 4594–4599. https://doi.org/10.1021/ja00456a011.

(76) Jankus, V.; Snedden, E. W.; Bright, D. W.; Arac, E.; Dai, D.; Monkman, A. P. Competition between Polaron Pair Formation and Singlet Fission Observed in Amorphous Rubrene Films. *Phys. Rev. B* **2013**, *87* (22), 224202. https://doi.org/10.1103/PhysRevB.87.224202.

(77) Gholizadeh, E. M.; Prasad, S. K. K.; Teh, Z. L.; Ishwara, T.; Norman, S.; Petty, A. J.; Cole, J. H.; Cheong, S.; Tilley, R. D.; Anthony, J. E.; Huang, S.; Schmidt, T. W. Photochemical Upconversion of Near-

Infrared Light from below the Silicon Bandgap. *Nature Photonics* **2020**, 1–6. https://doi.org/10.1038/s41566-020-0664-3.

(78) Deng, F.; Sun, W.; Castellano, F. N. Texaphyrin Sensitized Near-IR-to-Visible Photon Upconversion. *Photochem. Photobiol. Sci.* **2014**, *13* (5), 813–819. https://doi.org/10.1039/C4PP00037D.

(79) Han, J.; Zhang, F.; You, J.; Hiroaki, Y.; Yamada, S.; Morifuji, T.; Wang, S.; Li, X. The First Transition Metal Phthalocyanines: Sensitizing Rubrene Emission Based on Triplet–Triplet Annihilation. *Photochem. Photobiol. Sci.* **2017**, *16* (9), 1384–1390. https://doi.org/10.1039/C6PP00464D.

(80) Cheng, Y. Y.; Fückel, B.; Khoury, T.; Clady, R. G. C. R.; Tayebjee, M. J. Y.; Ekins-Daukes, N. J.; Crossley, M. J.; Schmidt, T. W. Kinetic Analysis of Photochemical Upconversion by Triplet−Triplet Annihilation: Beyond Any Spin Statistical Limit. *J. Phys. Chem. Lett.* **2010**, *1* (12), 1795–1799. https://doi.org/10.1021/jz100566u.

(81) Olivier, J.-H.; Bai, Y.; Uh, H.; Yoo, H.; Therien, M. J.; Castellano, F. N. Near-Infrared-to-Visible Photon Upconversion Enabled by Conjugated Porphyrinic Sensitizers under Low-Power Noncoherent Illumination. *J. Phys. Chem. A* **2015**, *119* (22), 5642–5649. https://doi.org/10.1021/acs.jpca.5b03199.

(82) Kondakov, D. Y.; Pawlik, T. D.; Hatwar, T. K.; Spindler, J. P. Triplet Annihilation Exceeding Spin Statistical Limit in Highly Efficient Fluorescent Organic Light-Emitting Diodes. *Journal of Applied Physics* **2009**, *106* (12), 124510. https://doi.org/10.1063/1.3273407.

(83) Bossanyi, D. G.; Sasaki, Y.; Wang, S.; Chekulaev, D.; Kimizuka, N.; Yanai, N.; Clark, J. In Optimized Rubrene-Based Nanoparticle Blends for Photon Upconversion, Singlet Energy Collection Outcompetes Triplet-Pair Separation, Not Singlet Fission. *J. Mater. Chem. C* **2022**, *10* (12), 4684–4696. https://doi.org/10.1039/D1TC02955J.

(84) Wieghold, S.; Bieber, A. S.; VanOrman, Z. A.; Rodriguez, A.; Nienhaus, L. Is Disorder Beneficial in Perovskite-Sensitized Solid-State Upconversion? The Role of DBP Doping in Rubrene. *J. Phys. Chem. C* **2020**, *124* (33), 18132–18140. https://doi.org/10.1021/acs.jpcc.0c05290.

(85) Finton, D. M.; Wolf, E. A.; Zoutenbier, V. S.; Ward, K. A.; Biaggio, I. Routes to Singlet Exciton Fission in Rubrene Crystals and Amorphous Films. *AIP Advances* **2019**, *9* (9), 095027. https://doi.org/10.1063/1.5118942.

(86) Wang, X.; Garcia, T.; Monaco, S.; Schatschneider, B.; Marom, N. Effect of Crystal Packing on the Excitonic Properties of Rubrene Polymorphs. *CrystEngComm* **2016**, *18* (38), 7353–7362. https://doi.org/10.1039/C6CE00873A.

(87) Roberts, S. T.; McAnally, R. E.; Mastron, J. N.; Webber, D. H.; Whited, M. T.; Brutchey, R. L.; Thompson, M. E.; Bradforth, S. E. Efficient

Singlet Fission Discovered in a Disordered Acene Film. *J. Am. Chem. Soc.* **2012**, *134* (14), 6388–6400. https://doi.org/10.1021/ja300504t.

(88) Park, S.-W.; Choi, J.-M.; Lee, K. H.; Yeom, H. W.; Im, S.; Lee, Y. K. Amorphous-to-Crystalline Phase Transformation of Thin Film Rubrene. *J. Phys. Chem. B* **2010**, *114* (17), 5661–5665. https://doi.org/10.1021/jp910459p.

(89) Radiunas, E.; Dapkevičius, M.; Raišys, S.; Juršėnas, S.; Jozeliūnaitė, A.; Javorskis, T.; Šinkevičiūtė, U.; Orentas, E.; Kazlauskas, K. Impact of T-Butyl Substitution in a Rubrene Emitter for Solid State NIR-to-Visible Photon Upconversion. *Phys. Chem. Chem. Phys.* **2020**, *22* (14), 7392–7403. https://doi.org/10.1039/D0CP00144A.

(90) Amemori, S.; Sasaki, Y.; Yanai, N.; Kimizuka, N. Correction to “Near-Infrared-to-Visible Photon Upconversion Sensitized by a Metal Complex with Spin-Forbidden yet Strong S0–T1 Absorption.” *J. Am. Chem. Soc.* **2020**, *142* (17), 8057–8058. https://doi.org/10.1021/jacs.0c03910.

(91) Che, Y.; Yang, W.; Tang, G.; Dumoulin, F.; Zhao, J.; Liu, L.; İşci, Ü. Photophysical Properties of Palladium/Platinum Tetrasulfonyl Phthalocyanines and Their Application in Triplet–Triplet Annihilation Upconversion. *J. Mater. Chem. C* **2018**, *6* (21), 5785–5793. https://doi.org/10.1039/C8TC00513C.

(92) Tamura, H.; Azumaya, K.; Ishikita, H. Long-Range Exciton Diffusion via Singlet Revival Mechanism. *J. Phys. Chem. Lett.* **2019**, *10* (24), 7623–7628. https://doi.org/10.1021/acs.jpclett.9b03029.

(93) Raišys, S.; Juršėnas, S.; Simon, Y. C.; Weder, C.; Kazlauskas, K. Enhancement of Triplet-Sensitized Upconversion in Rigid Polymers via Singlet Exciton Sink Approach. *Chem. Sci.* **2018**, *9* (33), 6796–6802. https://doi.org/10.1039/C8SC02151A.

(94) Irkhin, P.; Biaggio, I. Direct Imaging of Anisotropic Exciton Diffusion and Triplet Diffusion Length in Rubrene Single Crystals. *Phys. Rev. Lett.* **2011**, *107* (1), 017402. https://doi.org/10.1103/PhysRevLett.107.017402.

(95) Najafov, H.; Lee, B.; Zhou, Q.; Feldman, L. C.; Podzorov, V. Observation of Long-Range Exciton Diffusion in Highly Ordered Organic Semiconductors. *Nature Mater* **2010**, *9* (11), 938–943. https://doi.org/10.1038/nmat2872.

(96) Raišys, S.; Adomėnienė, O.; Adomėnas, P.; Rudnick, A.; Köhler, A.; Kazlauskas, K. Triplet Exciton Diffusion and Quenching in Matrix-Free Solid Photon Upconversion Films. *J. Phys. Chem. C* **2021**, *125* (7), 3764–3775. https://doi.org/10.1021/acs.jpcc.0c11048.

CURRICULUM VITAE

Name:	Edvinas Radiunas
Contacts	edvinas.radiunas@ff.vu.lt; eradiunas@gmail.com
Education	2018-2022 Vilnius University, PhD, Physics. 2016-2018 Vilnius University, MSc, Optoelectronics. Thesis: “*Phenanthroimidazole Derivatives as Energy Transfer Hosts for Applications in the Third Generation Organic Light Emitting Diodes*”. 2012-2016 Vilnius University, BSc, Energy Physics. Thesis: “*Influence of Extended Conjugation to Emission Amplification in Bifluorene Compounds*”
Scientific career	2018-2022 *lecturer, junior researcher, project specialist* at Vilnius University Institute of Photonics and Nanotechnology. 2014-2018 *laboratory assistant, engineer, technician* at Vilnius University Institute of Photonics and Nanotechnology
Awards	2021 Award for the best poster in XXIV International Krutyn Summer School 2019. 2019 III place award for the best oral presentation of 44th LNFK conference 2021.

COPIES OF PUBLICATIONS

PI

Understanding the limitations of NIR-to-visible photon upconversion in phthalocyanine-sensitized rubrene systems

Edvinas Radiunas, Steponas Raišys, Saulius Juršėnas, Augustina Jozeliūnaitė, Tomas Javorskis, Ugnė Šinkevičiūtė, Edvinas Orentas, Karolis Kazlauskas.

Journal of Materials Chemistry C, **8**(16), 5525–5534, (2019)

DOI: 10.1039/C9TC06031F

Journal of
Materials Chemistry C

ROYAL SOCIETY
OF CHEMISTRY

PAPER

View Article Online
View Journal | View Issue

Check for updates

Cite this: *J. Mater. Chem. C*, 2020, **8**, 5525

Understanding the limitations of NIR-to-visible photon upconversion in phthalocyanine-sensitized rubrene systems†

Edvinas Radiunas,[a] Steponas Raišys,[a] Saulius Juršėnas,[a] Augustina Jozeliūnaitė,[b] Tomas Javorskis,[b] Ugnė Šinkevičiūtė,[b] Edvinas Orentas[b] and Karolis Kazlauskas*[a]

Received 4th November 2019,
Accepted 4th March 2020

DOI: 10.1039/c9tc06031f

rsc.li/materials-c

Low-power near-infrared (NIR)-to-visible (vis) photon upconversion (UC) systems are in demand for biomedical, photovoltaic and photocatalytic applications; however, the practical utilization is still hampered by low UC efficiency. Aiming to identify efficiency-limiting factors, particularly in metallophthalocyanine-sensitized rubrene systems operational in the NIR-vis range, we thoroughly assessed subsequent energy transfer steps in the TTA-mediated UC scheme. A key limiting factor in the optimized UC systems was found to be rubrene's low statistical probability (f = 15.5 ± 3%) to obtain a singlet from two triplets *via* TTA. The f estimated under the dominance of TTA attained by continuous-wave excitation, *i.e.* the regime frequently encountered (or desired) in practical applications, was determined to be 4 times lower as compared to that obtained under femtosecond pulsed-laser excitation conditions. The results also demonstrate that the benefit of achieving larger emitter concentrations by introducing solubility increasing alkyl groups into the emitter in anticipation of enhanced triplet energy transfer cannot outcompete the severely reduced statistical probability factor (f = 5.3 ± 1%) of *t*-butyl-substituted rubrene. The maximum UC quantum yield (Φ_{UC} = 5.6 ± 1.2%) estimated and verified by two independent methods in the optimized Pd-phthalocyanine–rubrene system is among the largest reported for NIR-to-vis UC systems absorbing at >730 nm. Φ_{UC} is defined here as the number of UC photons emitted per number of absorbed ones, implying a theoretical limit of 50% for TTA-mediated UC.

Introduction

Increasing demand for organic systems capable of incoherent photon upconversion (UC), *i.e.* conversion from lower to higher energies at low excitation intensities, is stimulated by a growing variety of applications such as photocatalysis,[1,2] bioimaging,[3] stress sensing,[4] night vision,[5] memory devices,[6] photovoltaics,[7,8] targeted drug delivery[9] and others.[10] In these typically bicomponent systems, composed of sensitizer and emitter species, long-lived triplet-states of emitters are utilized to produce delayed UC emission from the singlet state that is blue-shifted as compared to the absorbed light. The higher energy UC emission from an emitter emerges through a process called triplet–triplet annihilation (TTA), also referred to as triplet fusion. In the TTA-UC process sensitizer species serve as light absorbers, which subsequently generate triplets *via* intersystem crossing (ISC) and finally transfer triplet energy (TET) to an emitter species. Importantly, TTA-UC can be accomplished at low light conditions close to those of sunlight (~mW cm^{-2}).[7,8]

While a great number of efficient UC systems with a quantum yield (Φ_{UC}) of up to ~30% have been demonstrated in the visible (vis) spectral region,[11–16] only several molecular systems have been shown to produce near-infrared-(NIR)-to-vis UC with Φ_{UC} above 2%.[17–21] It seems that finding proper materials capable of operating with high UC efficiencies under NIR excitation is a big challenge. The surge of interest for NIR-to-vis UC is highly motivated by applications in biomedicine, photocatalysis and solar cells. While the first two applications benefit from profound penetration of IR light,[1] utilization of the TTA-UC phenomenon in solar cells offers the potential to overcome the Shockley–Queisser limit for solar conversion efficiency.[8,22] Since most photovoltaic devices suffer from low efficiencies at NIR-IR wavelengths, conversion of NIR-IR to the vis wavelengths that are well utilized by devices is foreseen to enhance their performance.

Various classes of materials capable of NIR light absorption and triplet sensitization were reported, among which perovskites,[23]

---

[a] *Institute of Photonics and Nanotechnology, Vilnius University, Saulėtekio av. 3, LT-10257 Vilnius, Lithuania. E-mail: karolis.kazlauskas@ff.vu.lt*

[b] *Department of Organic Chemistry, Vilnius University, Naugarduko 24, LT-03225 Vilnius, Lithuania*

† Electronic supplementary information (ESI) available. See DOI: 10.1039/c9tc06031f

supermolecular chromophores,[24] BODIPY derivatives[25] or inorganic semiconductor quantum dots[19,26] are of fundamental interest. However, the lack of a transparency region for UC emission and the consequent huge reabsorption losses in these sensitizers are usually ignored. This severely limits the UC efficiency of such systems and thus hampers their practical applications.[27] To minimize these losses, sensitizers bearing large conjugated macrocycles such as porphyrins[28,29] or phthalocyanines[30–32] providing a decent transparency window between the Soret and Q absorption bands are frequently utilized. Moreover, metallophthalocyanines have an advantage that their Q band expresses a large molar extinction coefficient ($\varepsilon \sim 10^5$ M^{-1} cm^{-1}), which can be tuned in the region of 650–800 nm for efficient harvesting of NIR photons.[30]

No less important is the correct choice of emitter with the triplet state sufficiently low in energy to accept triplet excitons from a NIR sensitizer. In this regard, one of the most widely used emitters for NIR-to-vis upconversion is rubrene[7,19,21,28–30,32–37] featuring a low triplet energy (1.04–1.14 eV) and close to unity fluorescence quantum yield (Φ_{FL}) at yellow wavelengths.[38,39] Regrettably, the majority of porphyrin- or phthalocyanine-sensitized rubrene UC systems reported in the literature so far are limited to $\Phi_{\mathrm{UC}} < 4\%$,[28–30,32,35,36,40,41] although generally regardless of the emitter chosen the maximum limit of Φ_{UC} is 50%.[13]

Another crucial parameter affecting the choice of an emitter and having a direct impact on Φ_{UC} is the statistical probability factor (f).[41] The factor describes the probability for the triplet pair in an emitter to form one singlet *via* TTA. Relying purely on spin statistics and taking into account that the triplet encounter complex can be of singlet, triplet or quintet multiplicity with a corresponding statistically weighted formation probability of 1 : 3 : 5, f should not exceed 1/9 (or 11.1%) as there will be only one complex dissociating to the S_1 state.[42] However, many reports proved this limit to be incorrect considering that triplet and quintet complexes may not necessarily quench to the ground state, but instead, depending on the relative position of energy levels, relax back into triplets. Thus, f values exceeding 11.1%, *e.g.* 50% for diphenylanthracene[43] or even 100% for perylene,[44] were demonstrated. Rubrene was also reported to exhibit a rather large f (= 33%),[40] although much smaller than the previous two emitters, thereby implying greater efficiency losses associated with the statistical probability factor.

Hence, aiming to complement this area of research with more understanding of the performance limitations of NIR-to-vis UC systems, particularly metallophthalocyanine–rubrene systems, we thoroughly investigated the losses for each subsequent energy transfer/conversion step in the TTA-mediated UC scheme. To assess losses associated with the statistical probability to generate a singlet *via* TTA, we utilized a continuous-wave (CW) NIR excitation regime, which is particularly relevant for applications such as photocatalysis or photovoltaics. Although similar studies on rubrene-based UC systems have been previously conducted by the Schmidt group,[40,41] the different excitation regime (femtosecond pulses) employed therein could have some influence on the TTA-UC properties evaluated. The UC systems studied in this work consisted of structurally-modified Pd- and Pt-phthalocyanine sensitizers (**PdPc** and **PtPc**) and rubrene-based emitters designed to express efficient NIR-to-vis (730 nm to 560 nm) upconversion. Taking into account that most of the phthalocyanines are rigid, planar, poorly soluble and therefore susceptible to aggregation,[45] phenoxy and butoxy groups were intentionally introduced to compensate for these shortcomings. Likewise, the investigated rubrene emitter was modified with *t*-butyl side moieties to alleviate solubility problems at high concentrations. Various combinations of sensitizer–emitter pairs as a function of their concentrations were explored to achieve optimized UC performance and to determine the limiting factors. Two independent methods were employed for evaluation of the UC quantum yield (Φ_{UC}) of the studied systems to ensure the reliability of the obtained results. The obtained difference in the statistical factor of obtaining a singlet *via* a TTA event of the unaltered and the *t*-butyl-modified rubrene emitter was found to play a decisive role in the performance of the studied NIR-to-vis UC systems.

Results and discussion

Photophysical properties

The structures of the studied metallophthalocyanine-based NIR sensitizers and rubrene-based emitters are displayed in Chart 1. Their synthesis and identification are provided in the ESI.† Aside from the different metal atom, the palladium(II) 1,4,8,11,15,18,22,25-octabutoxy-2,3,9,10,16,17,23,24-octaphenoxyphthalocyanine (**PdPc**) and platinum(II) 1,4,8,11,15,18,22,25-octabutoxy-2,3,9,10,16,17,23,24-octaphenoxyphthalocyanine (**PtPc**) sensitizers have an identical structure, thus enabling the determination of the influence of the central heavy metal on the photosensitization ability of the compounds. The introduced butoxy and phenoxy

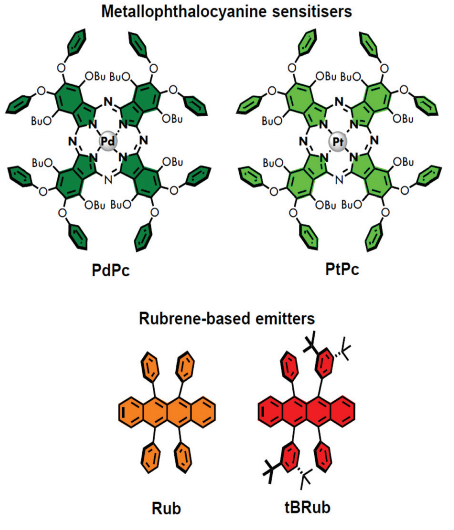

Chart 1 Chemical structures of the Pd- and Pt-phthalocyanine sensitizers (**PdPc** and **PtPc**) and the rubrene-based emitters (**Rub** and **tBRub**) investigated in this work.

twisted peripheral groups mainly served as solubility increasing and steric hindrance groups for suppressing detrimental concentration effects. Similarly, to prevent aggregation of the rubrene emitter (**Rub**) at the highest concentrations, it was functionalized with *t*-butyl moieties to result in the **tBRub** compound. The **Rub** and **tBRub** emitters, possessing otherwise identical structures, were compared in terms of energy transfer efficiencies and probabilities of singlet generation *via* TTA.

Fig. 1 shows absorption, fluorescence and phosphorescence spectra of the sensitizers **PdPc** and **PtPc** in dilute toluene solutions. Their main photophysical properties are listed in Table 1. As expected both sensitizers exhibited strong absorption in the NIR range with a molar extinction coefficient $\varepsilon \approx (1.9\text{–}2.5) \times 10^5\ \mathrm{M^{-1}\ cm^{-1}}$ of the Q bands at 720 nm and 709 nm for **PdPc** and **PtPc**, respectively. Due to the smaller Stokes shift of **PdPc**, its FL band was centered at 750 nm as compared to the more redshifted FL of **PtPc** peaking at 785 nm. The metallophthalocyanine-based sensitizers exhibited very low fluorescence quantum yields ($\Phi_{\mathrm{FL}}^{\mathrm{S}}$) <1% (Table 1). Taking into account Φ_{FL}^{0} = 88% measured by us for the metal-free but otherwise identical phthalocyanine, the drastic quenching of Φ_{FL} obtained with the introduction of Pd and Pt was attributed to the rapid ISC to the triplet manifold induced by the enhanced spin–orbit coupling due to the heavy metal atom. Thus, the ISC yield deduced for our sensitizers **PdPc** and **PtPc** as $\Phi_{\mathrm{ISC}} = 1 - \Phi_{\mathrm{FL}}^{\mathrm{S}}/\Phi_{\mathrm{FL}}^{0}$ was found to exceed 99% in agreement with other reports on metallophthalocyanines.[32,35] The triplet energies (T_1) of **PdPc** and **PtPc** were found to be 1.12 eV and 1.18 eV, respectively, as determined from the phosphorescence (Ph) maxima (Fig. 1 and Table 1). The lower or at least similar T_1 of rubrene (1.04–1.14 eV)[38,39] thereby ensured proper energy level alignment with respect to **PdPc** and **PtPc** for the triplet sensitization of the **Rub** and **tBRub** emitters. Relying on the singlet and triplet energies determined, a TTA-mediated UC scheme with the relevant energy transfer/conversion processes for the Pd- and Pt-phthalocyanine-sensitized rubrene systems was drawn (Scheme 1).

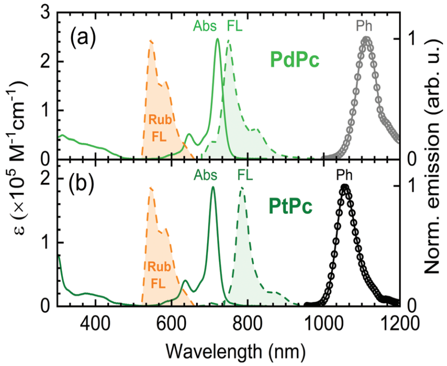

Fig. 1 Absorption (solid lines), fluorescence (filled dashed lines) and phosphorescence (circles) spectra of sensitizers (a) **PdPc** and (b) **PtPc** in toluene (c = 1.0 × 10^{-5} M). The FL spectrum of emitter **Rub** in toluene (c = 1.0 × 10^{-5} M) is shown for reference.

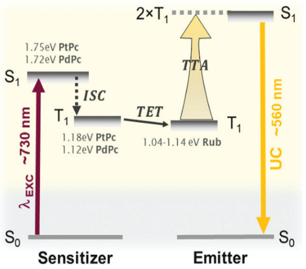

Scheme 1 TTA-UC energy scheme for the PdPc- and PtPc-sensitized **Rub** (or **tBRub**) systems. λ_{EXC} – excitation wavelength, ISC – intersystem crossing, TET – triplet energy transfer, TTA – triplet–triplet annihilation, UC – upconversion.

Importantly, the **Rub** fluorescence centered at ~560 nm, as shown in Fig. 1, resides in the absorption window of both phthalocyanine sensitizers, implying low reabsorption losses for UC emission in the **Rub:PdPc** or **Rub:PtPc** systems. The same is also valid for **tBRub**, since the added non-conjugated *t*-butyl moieties have an insignificant impact on the absorption and FL properties of the unsubstituted **Rub** emitter (ESI,† Fig. S18). Additionally, both emitters were determined to have nearly 100% Φ_{FL} in dilute solution.

t-Butyl-substituted rubrene **tBRub** was designed to increase the solubility of the conventional **Rub** emitter for employing higher emitter concentrations in the UC solution. Since TTA is a bimolecular process, which requires an encounter of two emitter triplets, a higher emitter concentration is anticipated to facilitate TTA, thereby also improving the TTA-UC performance. However, one must be aware of the self-absorption effect in the concentrated emitter solutions as a result of the relatively small Stokes shift (~120 meV) observed for the rubrene-based emitters (ESI,† Fig. S18).

UC efficiency measurements

To optimize the UC performance of the investigated phthalocyanine–rubrene systems, their UC properties were assessed by

Table 1 Photophysical properties of **PdPc** and **PtPc** sensitizers in toluene solution (c = 1.0 × 10^{-5} M)

	$\varepsilon^a \times 10^5$ ($\mathrm{M^{-1}\ cm^{-1}}$)	$\lambda_{\mathrm{abs}}{}^b$ nm, (eV)	$\lambda_{\mathrm{FL}}{}^c$ nm, (eV)	$\lambda_{\mathrm{PH}}{}^d$ nm, (eV)	$\Phi_{\mathrm{FL}}^{\mathrm{S}}{}^e$ (%)	$\tau_0{}^f$ (μs)
PdPc	2.46	720, (1.72)	750, (1.65)	1110, (1.12)	0.3	3.3–4.3
PtPc	1.87	709, (1.75)	785, (1.58)	1055, (1.18)	0.6	0.7

[a] Molar extinction coefficient. [b] Absorption maximum of the Q band. [c] Peak fluorescence emission. [d] Peak phosphorescence emission. [e] FL quantum yield measured using an integrating sphere. [f] Triplet lifetime of the sensitizers.

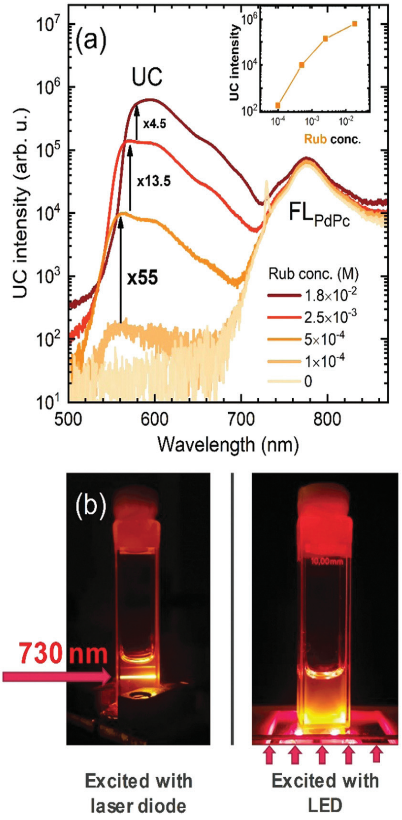

Fig. 2 (a) UC emission spectra of **Rub**:**PdPc** solution in toluene at different **Rub** concentrations (indicated) and fixed **PdPc** (15 μM) concentration under CW excitation at 730 nm. The inset depicts UC peak intensity *vs.* **Rub** concentration. (b) Pictures of UC emission in **Rub**:**PdPc** solution under NIR excitation (no filter used).

varying the concentrations of the constituting species. Fig. 2a shows UC emission spectra of one of the studied couples, **Rub:PdPc**, on a semi-log scale measured at different **Rub** concentrations and a fixed **PdPc** concentration. The measurements were accomplished by selectively exciting the **PdPc** sensitizer at the Q band. Bright yellow UC emission occurring in the **Rub:PdPc** solution under CW excitation with a NIR laser diode (730 nm) was nicely seen by the naked eye (Fig. 2b). Similar vivid UC emission was also observed under NIR LED excitation. The emitter concentration was varied over two orders of magnitude from the lowest 0.1 mM up to the highest 18 mM, which corresponded to the solubility limit of **Rub** at room temperature. The UC emission peaking at ~560 nm corresponded to the FL spectrum of **Rub** (ESI,† Fig. S18), whereas the fluorescence at ~760 nm emanated from **PdPc**. Note that the reference spectrum obtained at 0 mM of **Rub** evidences no UC while only **PdPc** associated fluorescence, proving that both species, *i.e.* the sensitizer and the emitter, are necessary for observation of UC. The constant intensity of the **PdPc** band despite the significantly changing UC signal can be explained by the fixed concentration of sensitizer used in the **Rub:PdPc** solutions and also by the fact that **Rub** has no absorption in the NIR range.

Although a wide range of employed concentrations of phthalocyanine-based sensitizers (10–800 μM) was reported to produce UC,[30,34,35,40] in the current systems it was fixed in the low concentration range at 15 μM. Such a low concentration was found to result in reduced energy back-transfer from the emitter to the sensitizer and deliver optimal UC performance (ESI,† Fig. S19). Note that because of the detrimental energy back-transfer, a low sensitizer concentration was also favoured in solid UC systems.[27]

As it is evident from Fig. 2a and the inset, increasing the **Rub** concentration from 0.1 mM to 18 mM boosted the UC emission by more than three orders of magnitude. The continuously increasing UC intensity accompanied by the unchanged FL of the sensitizer indicated a persistently improving UC yield up to the highest possible emitter concentrations. The similar behavior also observed for the other of the two UC systems studied, **Rub:PtPc** and **tBRub:PdPc**, can be rationalized in terms of enhanced TET as well as increased probability for the triplet encounter and TTA. On the other hand, the increasing **Rub** concentration also caused an undesirable redshift of the UC band due to the self-absorption effect (discussed below), which could in turn adversely affect the UC efficiency.

To highlight the importance of emitter self-absorption in the concentrated UC solution we employed an excitation–detection configuration in which the excitation region was moved away from the detector so as to continuously increase the optical path length, Δx, for the escaping photons (the inset of Fig. 3). Obviously, the short-wavelength slope of the UC spectra experienced enhanced distortion with increasing Δx as compared to the spectra at $\Delta x = 0$, resulting in reduced UC intensity (Fig. 3). Meanwhile, the spectrum at $\Delta x = 0$ resembled that of the non-reabsorbed FL spectrum of isolated **Rub** (ESI,† Fig. S18). The demonstrated issue of the self-absorption clearly indicated that special care must be taken in quantifying Φ_{UC} of the concentrated emitter solutions.

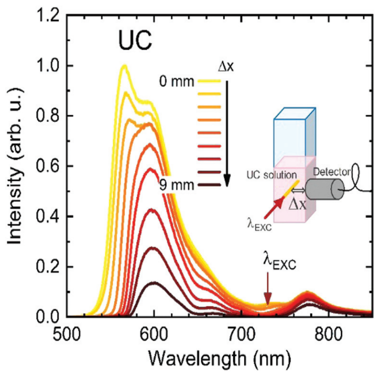

Fig. 3 UC emission spectra of **Rub** (18 mM):**PdPc** (15 μM) in toluene solution measured at different distances (Δx) between the excitation region and detector under CW excitation at 730 nm. The excitation–detection configuration is shown in the inset.

Since generally Φ_{UC} of a particular emitter–sensitizer system is described by the yields of the intermediate energy transfer/conversion steps, namely the ISC yield of the sensitizer, the TET yield from the sensitizer to the emitter, and the TTA and FL yields of the emitter, it thus can be expressed as

$$\Phi_{UC} = \frac{1}{2} f \Phi_{ISC} \Phi_{TET} \Phi_{TTA} \Phi_{FL} \quad (1)$$

where f is a statistical factor representing the probability to obtain a singlet in an emitter from two emitter triplets *via* TTA. f depends on the relative alignment of S_1, T_1, and T_2 as well as other energy levels lying in the vicinity of $2T_1$ and thus accessible through TTA.[13,40] In this representation Φ_{TTA} is determined by the competition of the second- and first-order decay rates, *i.e.* the TTA rate and the spontaneous or impurity related decay rate, respectively. As the TTA process starts prevailing, Φ_{TTA} approaches unity. We note that in this work Φ_{UC} is defined as the number of photons emitted per number absorbed, and since in TTA at most one UC photon can be produced per two absorbed ones, it cannot exceed 50%. Therefore, the factor $\frac{1}{2}$ here imposes a theoretical limit of 50% for Φ_{UC} in the case that all other quantities in eqn (1) are equal to unity. To determine Φ_{UC} of the studied UC systems **Rub:PdPc**, **Rub:PtPc** and **tBRub:PdPc**, the efficiency of each subsequent step has been assessed. Considering $\Phi_{ISC} > 99\%$ previously deduced for our sensitizers **PdPc** and **PtPc**, and $\Phi_{FL} \approx 90\%$ estimated for the **Rub** and **tBRub** emitters at high concentrations (18 mM), determination of Φ_{UC} inferred finding the rest of the quantities, namely, Φ_{TET} and Φ_{TTA} from eqn (1). Φ_{TET} from the phthalocyanine sensitizer to rubrene emitter was elucidated from the triplet quenching experiments, where the change in the triplet lifetime of the sensitizer due to the TET induced quenching was assessed.[21,46,47] Φ_{TET} was estimated from the ratio of the quenched (τ_1) and non-quenched (τ_0) triplet lifetimes of the sensitizer according to

$$\Phi_{TET} = 1 - \frac{\tau_1}{\tau_0} \quad (2)$$

Obtaining τ_0 implied measuring the triplet decay dynamics as a function of emitter concentration and linearly extrapolating the inverse of the quenched lifetime $1/\tau_1$ to zero emitter concentration. Since triplet states are dark, their concentration was monitored by using the UC signal as a probe. Given that the dominant triplet relaxation pathway is spontaneous decay, the temporal dynamics of the UC intensity, which is proportional to the square of the triplet concentration of **Rub**, $[T_1^{Rub}]^2$, can be described by

$$I_{UC}(t) \propto \left[T_1^{Rub}\right]^2 \propto \left(a_1 \exp\left(-\frac{t}{\tau_2}\right) - a_2 \exp\left(-\frac{t}{\tau_1}\right)\right)^2 \quad (3)$$

where τ_1 represents the rise time of I_{UC} due to the TET from the sensitizer to the emitter, while τ_2 corresponds to the triplet lifetime of the emitter; a_1 and a_2 are freely adjustable parameters. UC transients along with their fits (eqn (3)) for the **Rub:PdPc** and for **Rub:PtPc** and **tBRub:PdPc** systems at different emitter concentrations are presented in Fig. 4. Clearly τ_1 estimated from the fits exhibits shortening with increasing emitter concentration for all the studied UC systems, which occurs because of the facilitated TET. Conversely, τ_2 remains roughly similar (~100 μs) at different concentrations of **Rub** or **tBRub**, indicating the same spontaneous triplet lifetime in the rubrene-based emitters (the insets of Fig. 4). The obtained triplet lifetime of rubrene due to first-order decay was in agreement with other reports.[38]

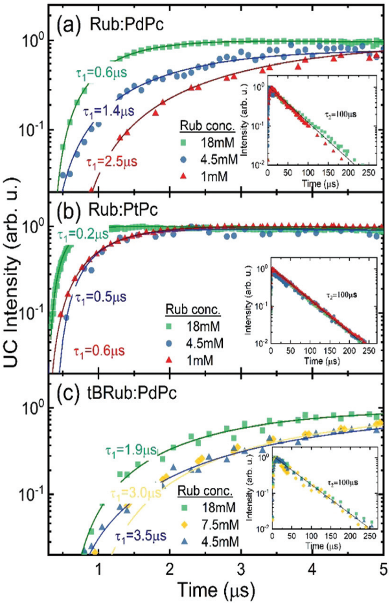

Fig. 4 UC transients of the (a) **Rub**:**PdPc**, (b) **Rub**:**PtPc** and (c) **tBRub**:**PdPc** systems at a fixed sensitizer concentration (15 μM) and different emitter concentrations (indicated) obtained using nanosecond laser excitation at 730 nm. The insets depict the transients in a longer time-frame.

The triplet exciton lifetimes (τ_0) of the phthalocyanine sensitizers were estimated by linearly extrapolating the inverse of the rise time $1/\tau_1$ to zero emitter concentration as shown in Fig. 5. τ_0 was found to be on the order of several microseconds (3.3–4.3 μs) for **PdPc**, while on the sub-microsecond scale (0.7 μs) for **PtPc** (Table 1). The calculated Φ_{TET} (from eqn (2)) at the largest emitter concentration yielded 82%, 71% and 56% for the **Rub:PdPc**, **Rub:PtPc** and **tBRub:PdPc** systems, respectively. Although a rather high TET efficiency was achieved for **Rub:PdPc**, the somewhat reduced Φ_{TET} obtained for the similar system with only the palladium in the sensitizer replaced by platinum could be explained by the shorter triplet lifetime of **PtPc**. The fast intrinsic decay of triplets in **PtPc** implies an alternative deactivation channel hence competing with TET to the **Rub** emitter and reducing Φ_{TET}. This makes **PdPc** more favourable as a sensitizer with respect to **PtPc** for UC systems. The least efficient TET from **PdPc** to **tBRub** is attributed to *t*-butyl moieties in rubrene, which evidently act as spacers, hindering short-range Dexter energy transfer. A similar reduction of TET with introduction of alkyl groups was also reported for perylene derivatives.[48]

The product of the statistical probability and TTA quantum yield [$f \cdot \Phi_{TTA}$] in the studied UC systems was estimated by

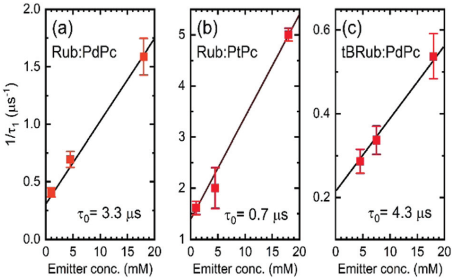

Fig. 5 The inverse rise time of the (a) **Rub**:**PdPc**, (b) **Rub**:**PtPc** and (c) **tBRub**:**PdPc** systems as a function of emitter concentration. The concentration of sensitizers **PdPc** and **PtPc** was fixed at 15 μM. The triplet lifetime of the sensitizers (τ_0) was estimated as the inverse of the intercept as indicated.

directly comparing the delayed (I_{UC}) and prompt (I_{FL}) FL intensities and considering that both emissions originate from the same emitter species in the same environment.[40,49] For this experiment we used a perpendicular excitation–detection configuration like that shown in the inset of Fig. 3 with $\Delta x = 0$, except that the detector was moved by 2 cm away from the cell to make the photon collection efficiency less sensitive to the excitation penetration depth (see the ESI† for details). The comparison of I_{UC} and I_{FL} cancelled any possible FL quenching including that due to emitter self-absorption, thus enabling us to obtain $[f{\cdot}\Phi_{\mathrm{TTA}}]$ from eqn (4) and (5) where the ratio of the UC and FL quantum yields, each representing the number of photons emitted per absorbed ones, is simply expressed through the ratio of I_{UC} and I_{FL}

$$[f\cdot\Phi_{\mathrm{TTA}}] = 2\frac{\Phi_{\mathrm{UC}}}{\Phi_{\mathrm{FL}}}\cdot\frac{1}{\Phi_{\mathrm{TET}}\Phi_{\mathrm{ISC}}} \tag{4}$$

$$[f\cdot\Phi_{\mathrm{TTA}}] = 2\frac{I_{\mathrm{UC}}I_{\mathrm{exc}}^{485}\lambda_{485}}{I_{\mathrm{FL}}I_{\mathrm{exc}}^{730}\lambda_{730}}\cdot\frac{1}{\Phi_{\mathrm{TET}}\Phi_{\mathrm{ISC}}} \tag{5}$$

To warrant the validity of the expression, the number of absorbed photons was substituted by the excitation intensity (I_{exc}), ensuring that all incident excitation (at 485 nm and 730 nm) is absorbed during the experiment, giving rise to the corresponding I_{UC} and I_{FL} values irrespective of the excitation penetration depth in the UC solution (see the ESI† for details). λ_{485} and λ_{730}, the excitation wavelengths for I_{FL} and I_{UC}, respectively, were introduced into the formula to correct the excitation intensities for the photon number. Since Φ_{TET} and Φ_{ISC} have been already determined for the **Rub:PdPc**, **Rub:PtPc** and **tBRub:PdPc** systems, evaluation of their $[f{\cdot}\Phi_{\mathrm{TTA}}]$ essentially implied measuring their I_{UC} and I_{FL}. These quantities as a function of I_{exc} for the three systems are displayed in Fig. 6a–c. While I_{FL} exhibited typical linear behavior in the whole range of pump densities, I_{UC} expressed quadratic behaviour at lower I_{exc}, which changed to linear at a threshold UC intensity (I_{th}) with increasing I_{exc}. The deviation of I_{FL} from linear behavior at the highest CW excitation (>20 W cm^{-2}) was caused by emitter degradation. The obtained I_{th} was found to vary from the lowest in **Rub:PdPc** (I_{th} = 1.9 W cm^{-2}) to the highest in **Rub:PtPc** (I_{th} = 11 W cm^{-2}). Taking into account that I_{th} is expressed as[50]

$$I_{\mathrm{th}} = \frac{2(k_{\mathrm{T}})^2}{\gamma_{\mathrm{TTA}}\alpha(E)\Phi_{\mathrm{TET}}} \tag{6}$$

where k_T and γ_{TTA} are the spontaneous triplet decay and TTA rate, respectively, both depending on the emitter properties only, whereas $\alpha(E)$ is the absorption coefficient of the sensitizer, the obtained differences in I_{th} could be explained as follows. The five times higher UC threshold in the **Rub:PtPc** system containing a different sensitizer yet the same emitter as in

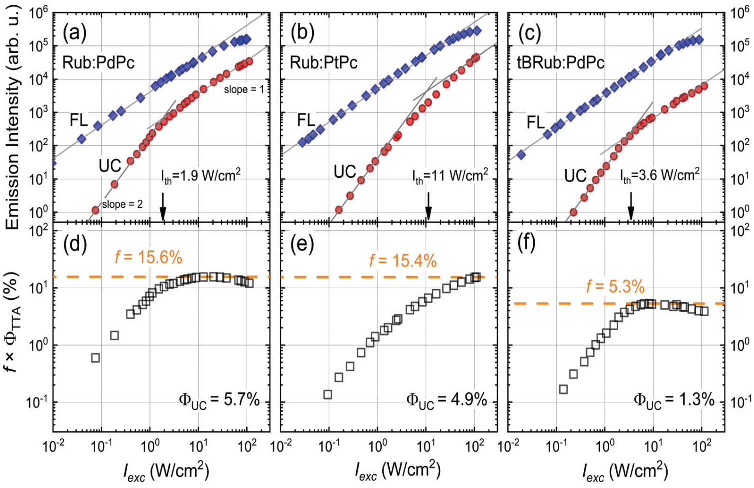

Fig. 6 FL and UC intensities under CW excitation at 485 nm and 730 nm, respectively, as a function of excitation power density for the (a) **Rub** (18 mM):**PdPc** (15 μM), (b) **Rub** (18 mM):**PtPc** (15 μM) and (c) **tBRub** (18 mM):**PdPc** (15 μM) systems. UC threshold values (I_{th}) are indicated. (d–f) Excitation dependences of the product $[f{\cdot}\Phi_{\mathrm{TTA}}]$ of the same systems calculated according to eqn (4). f values are indicated.

Rub:PdPc could be understood by taking into account the 4-fold smaller absorbance of the **PtPc** sensitizer as compared to that of **PdPc** at the UC excitation wavelength (Fig. 1) and by the 10% lower Φ_{TET}. Meanwhile the roughly twice as high I_{th} in the **tBRub:PdPc** system (I_{th} = 3.6 W cm^{-2}) as compared to that in **Rub:PdPc** could be explained by both Φ_{TET} and γ_{TTA} being reduced (to be discussed below). In fact, I_{th} can be reduced significantly for all the studied systems by increasing the sensitizer concentration and thereby improving $\alpha(E)$ and Φ_{TET},[50] however, at the cost of diminished Φ_{UC} due to the enhanced energy back-transfer from the emitter to the sensitizer (ESI,† Fig. S19).

The product $[f{\cdot}\Phi_{\mathrm{TTA}}]$ estimated in accordance with eqn (5) for the investigated UC systems is plotted in Fig. 6d–f as a function of the excitation intensity. To avoid artefacts in this estimation at the highest CW excitations due to the emitter degradation, the I_{FL} data were assumed to behave linearly at >20 W cm^{-2}, similarly to the I_{FL} behavior below this excitation. $[f{\cdot}\Phi_{\mathrm{TTA}}]$ was found to increase with increasing I_{exc} up to the I_{th} point of the corresponding UC system and then saturate beyond this point. According to the definition of Φ_{TTA}

$$[f \cdot \Phi_{\mathrm{TTA}}] = f \cdot \frac{\gamma_{\mathrm{TTA}}[\mathrm{T}_1]}{\gamma_{\mathrm{TTA}}[\mathrm{T}_1] + k_{\mathrm{T}}} \tag{7}$$

saturation is reached when TTA outcompetes spontaneous triplet decay with increasing triplet concentration $[\mathrm{T}_1]$. In the saturation regime Φ_{TTA}= 1, permitting the determination of f from the saturated value. So, an f value of 15.6% was obtained for the **Rub:PdPc** system. Although the different sensitizer employed in the **Rub:PtPc** system shifted the saturation of Φ_{TTA} to much higher excitation intensities, the statistical factor determined at saturation yielded f = 15.4%. As expected the attained value was very similar to that of the **Rub:PdPc** system, possessing an identical emitter species. A similar value ($\sim$13%) for the rubrene emitter in the TTA saturation regime was also reported in texaphyrin-sensitized photon UC.[21] In stark contrast, a 3-fold smaller f value (5.3%) was estimated in the **tBRub:PdPc** system featuring additional *t*-butyl moieties in the rubrene emitter. Given the negligibly small differences in the singlet and triplet state energies of both emitters, the reason for the reduced f factor in **tBRub** is unclear and still under investigation.

The statistical probability factor obtained for **Rub** exceeded the 11.1% statistical limit, which assumes involvement of both the triplet and quintet states as well as complete quenching of encounter complexes in these states to the singlet ground state.[49] On the other hand, the deduced f was below the 20% limit, which is reached in the case that the triplet and quintet encounter complexes decay back into the triplet state.[13,40] Thus, most likely the f of 15.6% (as complying with 11.1% $< f <$ 20%) can be explained by a portion of the triplet and quintet encounter complexes decaying to the ground state while the rest relax back to the triplet manifold.

Interestingly, the statistical probability factor obtained for the unmodified **Rub** emitter in UC solution was found to be 4 times lower as compared to that estimated in ref. 41. However, we need to emphasize that the difference in the estimation of f could arise due to the very different excitation regimes used in these experiments. As detailed in ref. 40 and 41, the femtosecond pulsed-laser excitation employed was likely causing saturation of sensitizer excitation and absorption bleaching, resulting in a larger excitation penetration depth without increasing the local triplet concentration. This caused saturation of Φ_{TTA} even when TTA was not dominant. Therefore, to estimate f, additional kinetic analysis of decaying triplets was performed to separate the proportion decaying *via* a first-order process and *via* TTA. Meanwhile, in our CW excitation experiments no sensitizer saturation and consequently bleaching were observed except probably at the highest I_{exc} ($\sim$100 W cm^{-2}) used. This enabled us to attain saturation of Φ_{TTA} explicitly due to the governance of TTA and thus deduce f in a straightforward manner from eqn (7) (Fig. 6d–f). The slight decrease of $[f{\cdot}\Phi_{\mathrm{TTA}}]$ from the saturated value at the highest I_{exc} in **Rub:PdPc** and **tBRub:PdPc** was caused by analogous deviation of I_{UC} from the linear relationship. Taking into account that an I_{exc} of 100 W cm^{-2} excites $\sim$4 μM of **PdPc** (given $\tau_1^{\mathrm{PdPc}} \approx 1$ μs and excitation penetration depth $d_{\mathbf{PdPc}}$ = 0.15 cm), which is on the same order as that used in our experiments (15 μM), the I_{UC} deviation at the highest I_{exc} could indeed be affected by the sensitizer saturation. To verify that the significantly lower f found in this work as compared to that estimated in ref. 41 is not due to the different excitation–detection configuration employed, we additionally evaluated the ratio of I_{UC} and I_{FL} (in accordance with eqn (5)) in a front-face geometry. The evaluation under the TTA saturation conditions yielded the same statistical probability $f = 15 \pm 3$% for rubrene as in the case of the previously exploited perpendicular excitation–detection geometry (ESI,† Fig. S20). This f imposes a maximum limit of $1/2{\cdot}f \approx 8$% on the Φ_{UC} of rubrene UC systems provided all the energy transfer/conversion steps in TTA-UC are 100% efficient. Since out of numerous reports on rubrene-based UC systems there was not a single demonstration of Φ_{UC} exceeding this limit,[7,19,21,32,33,37,40,41] we strongly believe that the obtained statistical probability value is reasonable.

The determined efficiencies for all intermediate energy transfer steps (ISC, TET, TTA and FL) and the statistical probability factor f of the studied UC systems (see Table 2) allowed us to calculate their Φ_{UC} by using eqn (1). The highest Φ_{UC} values of 5.7% and 4.9% were achieved in the **Rub:PdPc** and **Rub:PtPc** systems, respectively, whereas the lowest one (1.3%) in **tBRub:PdPc**. This remarkable factor-of-5 difference in f in **Rub** and **tBRub** was much less affected by the variance in the TET yields of the UC systems. The result revealed the negative impact of the

Table 2 Obtained quantities determining the performance of the investigated UC systems under CW excitation at 730 nm

	Emitter (18 mM):sensitizer (15 μM) in toluene solution				
UC system	Φ_{TET}[a] (%)	f[b] (%)	Φ_{FL}[c] (%)	Φ_{UC}[d] (%)	I_{th}[e] (W cm^{-2})
Rub:PdPc	82	15.6	90	5.7	1.9
Rub:PtPc	71	15.4	90	4.9	11.0
tBRub:PdPc	56	5.3	90	1.3	3.6

[a] Triplet energy transfer yield. [b] Statistical probability factor to obtain a singlet from two emitter triplets *via* TTA. [c] FL and [d] UC quantum yields. [e] UC threshold.

t-butyl moieties in the emitter on the UC performance, which mainly resulted from the significantly reduced probability for a pair of triplet *t*-butyl-rubrene molecules to yield one singlet emitter state.

To confirm the Φ_{UC} obtained above, we carried out an independent evaluation by utilizing the integrating sphere method. However, as discussed previously, the strong self-absorption in the highly concentrated emitter solution induced a self-quenching effect, which resulted in severely underestimated Φ_{UC} in the UC systems. As an example, the reabsorbed UC spectrum obtained in the sphere for the **Rub** (18 mM):**PdPc** (15 μM) system is displayed in Fig. 7 on a semi-log scale as the dashed line.

The spectrum peak position was found to be similar to that obtained at the largest Δx as shown in Fig. 3 and hence the deduced Φ_{UC} value from this reabsorbed UC spectrum integral has barely reached 1.2%. To be able to compare Φ_{UC} obtained by the integrating sphere with that estimated previously with self-quenching effects canceled out, a correction for the emitter self-absorption needed to be carried out. For this we employed the non-reabsorbed FL of the sensitizer **PdPc** ($\mathbf{FL_{PdPc}}$) as an internal reference. Recently, a similar method to correct for the UC reabsorption utilizing the undistorted phosphorescence signal of a sensitizer was reported.[51] Taking into account that the $\mathbf{FL_{PdPc}}$ intensity remains constant irrespective of the **Rub** concentration (Fig. 2a), the reabsorbed FL spectrum of **Rub** could be restored by taking the reabsorption-free UC spectrum obtained at $\Delta x = 0$ (Fig. 3) and matching its sensitizer FL part ($\mathbf{FL_{PdPc}}$) with the analogous part in the distorted spectrum (Fig. 7). The corrected UC spectrum denoted by the solid line exhibited a 4.6 times larger integral than the uncorrected one, resulting in corrected Φ_{UC} = 5.5% for the **Rub** (18 mM):**PdPc** (15 μM) system. Alternatively, Φ_{UC} could be also deduced by comparing the integral of $\mathbf{FL_{PdPc}}$ corresponding to the previously estimated Φ_{FL} value of 0.3% (Table 1) with that of the corrected UC spectrum. The corrected Φ_{UC} values found in an analogous manner for the other two systems **Rub** (18 mM):**PtPc** (15 μM) and **tBRub** (18 mM):**PdPc** (15 μM) were 5.4% and 1.3%, respectively. Importantly, the corrected for emitter self-absorption Φ_{UC} values estimated by the two independent methods, *i.e.* by the integrating sphere and by evaluating the efficiencies of each subsequent energy transfer step according to eqn (1), yielded very similar values for all three UC systems, proving the reliability of our results, including *f* estimates.

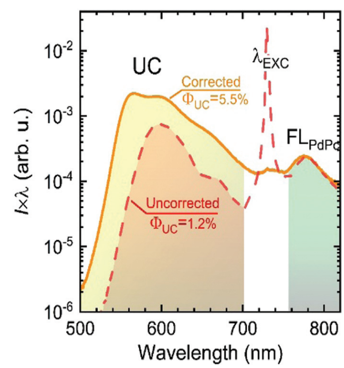

Fig. 7 Uncorrected (dashed line) and corrected for reabsorption (solid line) UC emission spectrum of **Rub** (18 mM):**PdPc** (15 μM) in toluene solution under CW excitation at 730 nm. The area under the curves is proportional to the number of photons registered.

Taking advantage of the solubility improving *t*-butyl moieties in **tBRub**, we further increased the concentration of the emitter from 18 mM, which is the solubility limit of **Rub**, to 40 mM (the solubility limit of **tBRub**). Even though this enhanced Φ_{UC} of **tBRub** (40 mM):**PdPc** (15 μM) from 1.3% to 2.2%, the attained value was still significantly lower as compared to that obtained in the unsubstituted rubrene system **Rub** (18 mM):**PdPc** (15 μM). This result clearly demonstrates that the benefit of attaining larger **tBRub** emitter concentrations by introducing alkyl groups to rubrene in anticipation of enhanced Dexter energy transfer cannot outcompete the big disadvantage related to the severely reduced statistical probability to obtain a singlet from two triplets in the emitter *via* TTA. It is worth pointing out that the maximal Φ_{UC} (5.7%) obtained by optimizing the emitter and sensitizer concentrations in **Rub**:**PdPc** is among the largest reported for NIR-to-vis UC systems absorbing at >730 nm.[19–21,29,32,33] We stress that differently from us the vast majority of reports use a multiplication factor of 2 in the evaluation of Φ_{UC} so as to normalize the UC yield to 100%. Such normalization in our case will translate to a maximum Φ_{UC} of 11.2%.

Conclusions

In summary, we studied phthalocyanine-sensitized NIR-to-vis photon upconversion in rubrene in an effort to determine the factors limiting the UC efficiency. This study is of crucial importance from the application point of view, since typical Φ_{UC} values achieved in UC systems under NIR excitation (>730 nm) are below 4%. By thoroughly assessing subsequent energy transfer/conversion steps in the TTA-mediated UC scheme, we determined rubrene's statistical probability (f = 15.5 ± 3%) to obtain a singlet from two triplets *via* TTA to be the prime efficiency-limiting factor in the optimized UC systems. We emphasize that unlike previous reports exploiting femtosecond pulsed-laser excitation, in this work a 4-fold lower value of the *f* factor was estimated in the TTA saturation regime achieved under CW excitation, *i.e.* the expected working conditions of UC systems utilized for practical applications. The obtained low *f* sets a maximum limit of ~8% ($\approx 1/2 \cdot f$) for Φ_{UC} in rubrene UC systems provided there are no losses in the ISC, TET, TTA and FL quantum yields.

The optimized **Rub** (18 mM):**PdPc** (15 μM) system in toluene solution was shown to express a maximum Φ_{UC} of 5.6 ± 1.2%, which was verified by two independent methods including an integrating sphere, for which the non-reabsorbed FL of the sensitizer was used as an internal reference to correct the UC for emitter self-absorption. The attained maximum Φ_{UC} is among the largest reported for NIR-to-vis UC systems capable of operating under excitation >730 nm. The further increase of the emitter concentration from 18 mM to 40 mM achieved *via* introduction of solubility improving *t*-butyl groups in an attempt to enhance Dexter energy transfer failed to surpass the Φ_{UC} of the **Rub** (18 mM):**PdPc** (15 μM) system mainly because of the significantly reduced statistical probability factor (f = 5.3 ± 1%) of *t*-butyl-substituted rubrene. Regrettably, on one hand, the obtained low statistical probability is expected to demotivate researchers and engineers, thereby preventing them from utilizing rubrene-based UC systems in applications. However, on the other hand, this should encourage the community to search for alternative emitters operational in the NIR-vis range.

Experimental section

Materials and synthesis

All reagents and starting materials were obtained from commercial sources and used as received. Rubrene (**Rub**) was purchased in sublimed grade, whereas the synthesized *t*-butyl-rubrene (**tBRub**) was purified by vacuum sublimation prior to experiments. The synthesis and identification of the new Pd- and Pt-phthalocyanine (**PdPc** and **PtPc**) sensitizers and new **tBRub** emitter are provided in the ESI.†

Preparation of the upconverting solutions

The upconverting solutions composed of a mixture of sensitizer and emitter as well as the solutions of each constituent including metal-free phthalocyanine were prepared in a nitrogen-filled glovebox with O_2 and H_2O concentrations below 0.1 ppm. The toluene solutions of each sensitizer **PdPc** and **PtPc** and emitter **Rub** used in the mixtures were prepared at an initial concentration of 10 mg mL^{-1}, whereas a concentration of 30 mg mL^{-1} was used for the **tBRub** emitter. The UC solutions (**Rub**:**PdPc**, **Rub**:**PtPc** and **tBRub**:**PdPc**) were prepared by mixing the emitters and sensitizers at appropriate ratios to result in final concentrations of **Rub** (0 mM, 0.1 mM, 0.5 mM, 2.5 mM, 18 mM):**PdPc** (15 μM), **Rub** (0 mM, 1 mM, 4.5 mM, 18 mM):**PtPc** (15 μM, 56 μM) and **tBRub** (0 mM, 4.5 mM, 7.5 mM, 18 mM, 40 mM):**PdPc** (15 μM). Prior to mixing the emitters and sensitizers, each solution was stirred overnight at 50 °C. Quartz cells having inner dimensions of 10 × 10 mm with UC solutions were carefully sealed before removing from the glovebox for measurements. The sealing was essential to protect them from triplet quenching by oxygen as well as to avoid photoinduced degradation of the rubrene emitters.[34]

Optical techniques

The absorption spectra of the dilute solutions of the compounds were recorded using a UV-vis-NIR spectrophotometer Lambda 950 (PerkinElmer). Direct fluorescence (FL) excitation of the rubrene-based emitters was accomplished by using a continuous-wave (CW) 485 nm-wavelength semiconductor laser diode (Picoquant). UC emission was induced by exciting at the Q band of the **PdPc** and **PtPc** sensitizers by using a CW 730 nm-wavelength semiconductor laser diode (Picoquant). FL and UC emission were measured utilizing an excitation–detection geometry where the emission signal was detected in a direction perpendicular to the excitation beam. Phosphorescence and UC transients were measured by employing a tunable-wavelength optical amplifier (Ekspla) pumped by a nanosecond Nd^{3+}:YAG laser (wavelength – 730 nm, pulse duration – 5 ns, repetition rate – 1 kHz). Steady state FL and UC emission spectra were measured using a back-thinned CCD spectrometer PMA-12 (Hamamatsu). The phosphorescence of the sensitizers was recorded with an infrared CCD iDus (Andor), whereas UC transients were measured with a time-gated iCCD camera New iStar DH340T (Andor). FL and UC emission quantum yields (Φ_{FL} and Φ_{UC}) were estimated by utilizing an integrating sphere (Sphere Optics) coupled to the CCD PMA-12 spectrometer *via* an optical fiber. The estimations were carried out according to the method described in ref. 52. No filter was used in these measurements, since the UC samples absorbed >95% of the incident light, allowing us to measure both excitation and sample emission signals during the same acquisition. Prior to the measurements the spectral sensitivity of the system was calibrated using halogen and deuterium calibration lamps (Bentham). Some of the Φ_{FL} estimations were also conducted by using a relative method, where Φ_{FL} was determined by comparing its spectrally integrated emission with that of a standard with known Φ_{FL}. A dilute solution of fluorescein (10 μM) in 0.1 M NaOH with Φ_{FL} = 92% was used a Φ_{FL} standard in these measurements.[53] To minimize self-absorption in these measurements a specific excitation–detection geometry was employed, where the exciting beam was directed near the very edge of the cell, while the emission signal was detected in a perpendicular direction. All the experiments were performed at room temperature.

Conflicts of interest

There are no conflicts to declare.

Acknowledgements

The research was funded by the European Social Fund (project No. 09.3.3-LMT-K-712-01-0084) under a grant agreement with the Research Council of Lithuania (LMTLT).

References

1 B. D. Ravetz, A. B. Pun, E. M. Churchill, D. N. Congreve, T. Rovis and L. M. Campos, *Nature*, 2019, **565**, 343–346.
2 R. S. Khnayzer, J. Blumhoff, J. A. Harrington, A. Haefele, F. Deng and F. N. Castellano, *Chem. Commun.*, 2011, **48**, 209–211.
3 Y. I. Park, K. T. Lee, Y. D. Suh and T. Hyeon, *Chem. Soc. Rev.*, 2015, **44**, 1302–1317.
4 D. Yildiz, C. Baumann, A. Mikosch, A. J. C. Kuehne, A. Herrmann and R. Göstl, *Angew. Chem., Int. Ed.*, 2019, **58**, 12919–12923.
5 S.-W. Liu, C.-C. Lee, C.-H. Yuan, W.-C. Su, S.-Y. Lin, W.-C. Chang, B.-Y. Huang, C.-F. Lin, Y.-Z. Lee, T.-H. Su and K.-T. Chen, *Adv. Mater.*, 2015, **27**, 1217–1222.

6 Y. Zhou, S.-T. Han, X. Chen, F. Wang, Y.-B. Tang and V. A. L. Roy, *Nat. Commun.*, 2014, **5**, 4720.
7 J. Pedrini and A. Monguzzi, *J. Photonics Energy*, 2017, **8**, 022005.
8 T. F. Schulze and T. W. Schmidt, *Energy Environ. Sci.*, 2015, **8**, 103–125.
9 S. H. C. Askes, M. S. Meijer, T. Bouwens, I. Landman and S. Bonnet, *Molecules*, 2016, **21**, 1460.
10 J. Zhou, Q. Liu, W. Feng, Y. Sun and F. Li, *Chem. Rev.*, 2015, **115**, 395–465.
11 S. Raišys, K. Kazlauskas, S. Juršėnas and Y. C. Simon, *ACS Appl. Mater. Interfaces*, 2016, **8**, 15732–15740.
12 A. Mahammed, K. Chen, J. Vestfrid, J. Zhao and Z. Gross, *Chem. Sci.*, 2019, **10**, 7091–7103.
13 S. Hoseinkhani, R. Tubino, F. Meinardi and A. Monguzzi, *Phys. Chem. Chem. Phys.*, 2015, **17**, 4020–4024.
14 C. Fan, L. Wei, T. Niu, M. Rao, G. Cheng, J. J. Chruma, W. Wu and C. Yang, *J. Am. Chem. Soc.*, 2019, **141**, 15070–15077.
15 F. Deng, J. Blumhoff and F. N. Castellano, *J. Phys. Chem. A*, 2013, **117**, 4412–4419.
16 P. Duan, N. Yanai and N. Kimizuka, *J. Am. Chem. Soc.*, 2013, **135**, 19056–19059.
17 Y. Sasaki, M. Oshikawa, P. Bharmoria, H. Kouno, A. Hayashi-Takagi, M. Sato, I. Ajioka, N. Yanai and N. Kimizuka, *Angew. Chem., Int. Ed.*, 2019, **58**, 17827–17833.
18 Z. Huang, Z. Xu, M. Mahboub, Z. Liang, P. Jaimes, P. Xia, K. R. Graham, M. L. Tang and T. Lian, *J. Am. Chem. Soc.*, 2019, **141**, 9769–9772.
19 M. Mahboub, Z. Huang and M. L. Tang, *Nano Lett.*, 2016, **16**, 7169–7175.
20 J.-H. Olivier, Y. Bai, H. Uh, H. Yoo, M. J. Therien and F. N. Castellano, *J. Phys. Chem. A*, 2015, **119**, 5642–5649.
21 F. Deng, W. Sun and F. N. Castellano, *Photochem. Photobiol. Sci.*, 2014, **13**, 813–819.
22 J. C. Goldschmidt and S. Fischer, *Adv. Opt. Mater.*, 2015, **3**, 510–535.
23 S. Wieghold, A. S. Bieber, Z. A. VanOrman and L. Nienhaus, *J. Phys. Chem. Lett.*, 2019, **10**, 3806–3811.
24 T. N. Singh-Rachford, A. Nayak, M. L. Muro-Small, S. Goeb, M. J. Therien and F. N. Castellano, *J. Am. Chem. Soc.*, 2010, **132**, 14203–14211.
25 W. Wu, H. Guo, W. Wu, S. Ji and J. Zhao, *J. Org. Chem.*, 2011, **76**, 7056–7064.
26 M. Wu, D. N. Congreve, M. W. B. Wilson, J. Jean, N. Geva, M. Welborn, T. Van Voorhis, V. Bulović, M. G. Bawendi and M. A. Baldo, *Nat. Photonics*, 2016, **10**, 31–34.
27 S. Raišys, S. Juršėnas, Y. C. Simon, C. Weder and K. Kazlauskas, *Chem. Sci.*, 2018, **9**, 6796–6802.
28 A. Abulikemu, Y. Sakagami, C. Heck, K. Kamada, H. Sotome, H. Miyasaka, D. Kuzuhara and H. Yamada, *ACS Appl. Mater. Interfaces*, 2019, **11**, 20812–20819.
29 F. Deng, J. R. Sommer, M. Myahkostupov, K. S. Schanze and F. N. Castellano, *Chem. Commun.*, 2013, **49**, 7406–7408.
30 J. L. Han, J. You, H. Yonemura, S. Yamada, S. R. Wang and X. G. Li, *Photochem. Photobiol. Sci.*, 2016, **15**, 1039–1045.
31 A. B. Pun, S. N. Sanders, M. Y. Sfeir, L. M. Campos and D. N. Congreve, *Chem. Sci.*, 2019, **10**, 3969–3975.
32 J. Han, F. Zhang, J. You, Y. Hiroaki, S. Yamada, T. Morifuji, S. Wang and X. Li, *Photochem. Photobiol. Sci.*, 2017, **16**, 1384–1390.
33 Z. Huang, Z. Xu, M. Mahboub, Z. Liang, P. Jaimes, P. Xia, K. R. Graham, M. L. Tang and T. Lian, *J. Am. Chem. Soc.*, 2019, **141**, 9769–9772.
34 T. N. Singh-Rachford and F. N. Castellano, *J. Phys. Chem. A*, 2008, **112**, 3550–3556.
35 Y. Che, W. Yang, G. Tang, F. Dumoulin, J. Zhao, L. Liu and Ü. İşci, *J. Mater. Chem. C*, 2018, **6**, 5785–5793.
36 V. Yakutkin, S. Aleshchenkov, S. Chernov, T. Miteva, G. Nelles, A. Cheprakov and S. Baluschev, *Chem. – Eur. J.*, 2008, **14**, 9846–9850.
37 L. Nienhaus, M. Wu, V. Bulović, M. A. Baldo and M. G. Bawendi, *Dalton Trans.*, 2018, **47**, 8509–8516.
38 D. K. K. Liu and L. R. Faulkner, *J. Am. Chem. Soc.*, 1977, **99**, 4594–4599.
39 V. Jankus, E. W. Snedden, D. W. Bright, E. Arac, D. Dai and A. P. Monkman, *Phys. Rev. B: Condens. Matter Mater. Phys.*, 2013, **87**, 224202.
40 Y. Y. Cheng, T. Khoury, R. G. C. R. Clady, M. J. Y. Tayebjee, N. J. Ekins-Daukes, M. J. Crossley and T. W. Schmidt, *Phys. Chem. Chem. Phys.*, 2010, **12**, 66–71.
41 Y. Y. Cheng, B. Fückel, T. Khoury, R. G. C. R. Clady, M. J. Y. Tayebjee, N. J. Ekins-Daukes, M. J. Crossley and T. W. Schmidt, *J. Phys. Chem. Lett.*, 2010, **1**, 1795–1799.
42 V. Gray, D. Dzebo, M. Abrahamsson, B. Albinsson and K. Moth-Poulsen, *Phys. Chem. Chem. Phys.*, 2014, **16**, 10345–10352.
43 A. Monguzzi, R. Tubino, S. Hoseinkhani, M. Campione and F. Meinardi, *Phys. Chem. Chem. Phys.*, 2012, **14**, 4322–4332.
44 S. Hoseinkhani, R. Tubino, F. Meinardi and A. Monguzzi, *Phys. Chem. Chem. Phys.*, 2015, **17**, 4020–4024.
45 G. de la Torre, C. G. Claessens and T. Torres, *Chem. Commun.*, 2007, 2000–2015.
46 T. Schmidt, E. Gholizadeh, S. Prasad, Z. L. Teh, T. Ishwara, S. Norman, A. J. Petty, J. E. Anthony and S. Huang, *ChemRxiv*, DOI: 10.26434/chemrxiv.7834838.v1.
47 T. W. Schmidt and F. N. Castellano, *J. Phys. Chem. Lett.*, 2014, **5**, 4062–4072.
48 C. Ye, V. Gray, K. Kushwaha, S. K. Singh, P. Erhart and K. Börjesson, *Phys. Chem. Chem. Phys.*, 2020, **22**, 1715–1720.
49 S. M. Bachilo and R. B. Weisman, *J. Phys. Chem. A*, 2000, **104**, 7711–7714.
50 A. Monguzzi, J. Mezyk, F. Scotognella, R. Tubino and F. Meinardi, *Phys. Rev. B: Condens. Matter Mater. Phys.*, 2008, **78**, 195112.
51 N. Yanai, K. Suzuki, T. Ogawa, Y. Sasaki, N. Harada and N. Kimizuka, *J. Phys. Chem. A*, 2019, **123**, 10197–10203.
52 J. C. de Mello, H. F. Wittmann and R. H. Friend, *Adv. Mater.*, 1997, **9**, 230–232.
53 G. Weber and F. W. J. Teale, *Trans. Faraday Soc.*, 1957, **53**, 646–655.

PII

Impact of t-butyl substitution in a rubrene emitter for solid state NIR-to-visible photon upconversion

Edvinas Radiunas, Manvydas Dapkevičius, Steponas Raišys, Saulius Juršėnas, Augustina Jozeliūnaitė, Tomas Javorskis, Ugnė Šinkevičiūtė, Edvinas Orentas, Karolis Kazlauskas.

Physical Chemistry Chemical Physics, **22**(14), 7392-7403, (2020)

10.1039/D0CP00144A

PCCP

ROYAL SOCIETY OF CHEMISTRY

PAPER

View Article Online
View Journal | View Issue

Cite this: *Phys. Chem. Chem. Phys.*, 2020, **22**, 7392

Impact of *t*-butyl substitution in a rubrene emitter for solid state NIR-to-visible photon upconversion

Edvinas Radiunas,[a] Manvydas Dapkevičius,[a] Steponas Raišys,[a] Saulius Juršėnas,[a] Augustina Jozeliūnaitė,[b] Tomas Javorskis,[b] Ugnė Šinkevičiūtė,[b] Edvinas Orentas[b] and Karolis Kazlauskas*[a]

Solid state NIR-to-visible photon upconversion (UC) mediated by triplet–triplet annihilation (TTA) is necessitated by numerous practical applications. Yet, efficient TTA-UC remains a highly challenging task. In this work palladium phthalocyanine-sensitized NIR-to-vis solid UC films based on a popular rubrene emitter are thoroughly studied with the primary focus on revealing the impact of *t*-butyl substitution in rubrene on the TTA-UC performance. The solution-processed UC films were additionally doped with a small amount of emissive singlet sink tetraphenyldibenzoperiflanthene (DBP) for collecting upconverted singlets from rubrene and in this way diminishing detrimental singlet fission. Irrespective of the excitation conditions used, *t*-butyl-substituted rubrene (TBR) was found to exhibit enhanced TTA-UC performance as compared to that of rubrene at an optimal emitter doping of 80 wt% in polystyrene films. Explicitly, in the TTA dominated regime attained at high excitation densities, 4-fold higher UC quantum yield (Φ_{UC}) achieved in TBR-based films was caused by the reduced fluorescence concentration quenching mainly due to suppressed singlet fission. Under low light conditions, *i.e.* in the regime governed by spontaneous triplet decay, even though triplet exciton diffusion was obstructed in TBR films by *t*-butyl moieties, the subsequently reduced TTA rate was counterbalanced by both suppressed singlet fission and non-radiative triplet quenching, still ensuring higher Φ_{UC} of these films as compared to those of unsubstituted rubrene films.

Received 9th January 2020,
Accepted 5th March 2020

DOI: 10.1039/d0cp00144a

rsc.li/pccp

Introduction

Photon energy conversion from lower to higher energies proceeding through triplet–triplet annihilation (TTA), commonly referred to as TTA-mediated upconversion (UC) is appealing for various applications such as photocatalysis,[1] bioimaging,[2] stress sensing,[3] night vision,[4] memory devices,[5] targeted drug delivery[6] and others.[7] Low excitation power density (such as that available from the sun) sufficient to drive the incoherent UC process makes TTA-UC especially attractive in photovoltaics, where the weakly absorbed near-infrared (NIR) portion of solar energy (>700 nm), particularly in organic solar cells, could be converted into visible light hence enabling more efficient photon harvesting.[8,9]

Briefly, in a typical step like TTA-UC process, low energy photons absorbed by the singlet states of sensitizer species are converted into triplet excitons *via* intersystem crossing (ISC), which then undergo energy transfer (TET) to triplet manifold of emitter species. Long-lived triplet-states of emitters are utilized to generate singlets from triplets through incoherent TTA events, which subsequently result in emission of higher energy photons as compared to the absorbed ones. Since during the TTA at most one UC photon can be produced per two absorbed ones, the quantum yield of the net process cannot exceed 50%.

Although the studies on red/green-to-blue (vis-to-vis) photon UC in solution dominates the TTA-UC field,[8,10] there is a high demand for efficient NIR-to-vis UC systems operative in the solid state as best suited for practical applications.[11–13] Regrettably, UC quantum yields (Φ_{UC}) of such solid systems capable of utilizing NIR photons (>700 nm) are still very low (typically <1%)[13–18] and improving Φ_{UC} was found to be a challenging task.

Presently, the majority of the NIR-to-vis UC systems utilize rubrene as an emitter[8,19–29] due to its low lying triplet energy ($T_1 \approx 1.14$ eV) and close to unity fluorescence (FL) quantum yield (Φ_{FL}) in the isolated form.[30,31] However, since singlet energy (S_1) of rubrene is roughly twice that of the triplet manifold, *i.e.* $S_1 = 2 \times T_1$, this also causes a reverse process – singlets splitting into two triplets, the so-called singlet fission (SF), given the two rubrene molecules are in close proximity to each other.[32,33] Taking into account that in the rigid environment

---

[a] *Institute of Photonics and Nanotechnology, Vilnius University, Saulėtekio av. 3, LT-10257 Vilnius, Lithuania. E-mail: karolis.kazlauskas@ff.vu.lt*

[b] *Institute of Chemistry, Faculty of Chemistry and Geosciences, Vilnius University, Naugarduko 24, LT-03225 Vilnius, Lithuania*

molecule positions are fixed, TTA must rely on efficient energy transfer and exciton diffusion, which in the case of triplet excitons are governed by a Dexter-type mechanism.[12,27,34–37] Since Dexter transfer requires electron wavefunction overlap between the neighboring molecules and thus is a short-range process, high emitter concentrations in the solid state are required for TTA-UC to occur. High rubrene content in the solid films is known to cause detrimental concentration quenching mainly due to efficient SF, which lowers Φ_{FL} of rubrene neat films down to a few percent.[13,38] Strongly reduced Φ_{FL} of the neat films was reported to be one of the key-limiting factors in achieving efficient UC in the systems based on rubrene emitter.[21] Therefore, the suppression of concentration quenching and maintenance of high Φ_{FL} at high emitter concentration in the solid films are of crucial importance.

Nagata *et al.* have recently demonstrated that decorating rubrene with *t*-butyl moieties can significantly lower SF in the solid films resulting in the enhancement of Φ_{FL} by a factor of 9 (from 5% to 46%).[38] Diminished SF is obtained as a result of enlarged intermolecular separation and thus effectively reduced interaction between the neighboring rubrene molecules. Note that this is expected to also cause a side effect, namely, a slowdown of triplet diffusion. The observed reduction of charge carrier mobility in *t*-butyl-substituted rubrene as compared to that of unsubstituted rubrene serves as indirect evidence for this.[39] Since the same Dexter mechanism is involved in the transfer of charges and transfer/diffusion of triplet excitons in the films, lowered triplet exciton diffusion in *t*-butyl-substituted rubrene films is indeed highly probable.

The TTA-UC process is known to heavily depend on triplet transfer/diffusion, which can be impeded by the *t*-butyl spacers. Hence, even though the utilization of *t*-butyl moieties can sustain high Φ_{FL} in high-rubrene-content films due to suppressed SF, it may also adversely affect Φ_{UC} because of the reduced triplet migration. Considering that *t*-butyl-substituted rubrene was not investigated as an emitter for TTA-UC before, the net effect of *t*-butyl groups on the UC performance of rubrene solid films needs to be clarified.

To this end, TTA-assisted photon upconversion in solid rubrene and *t*-butyl-rubrene (TBR) films was studied and compared. The studied solution-processed UC films contained a small amount of triplet sensitizer palladium phthalocyanine and singlet sink DBP for reducing undesirable energy back-transfer from emitter to sensitizer and for diminishing SF in rubrene, respectively. TTA-UC performance, and in particular, the importance of *t*-butyl substituents on the performance was revealed by assessing SF, diffusion-facilitated non-radiative triplet quenching and TTA as a function of emitter concentration in UC films. Having virtually no impact on electronic properties of rubrene, *t*-butyl groups were found to significantly affect TTA-UC performance of the films resulting in 4-fold enhanced NIR-to-vis Φ_{UC}. Better UC efficiency in optimized TBR films as compared to optimized rubrene films was attributed to reduced SF of upconverted singlets and diminished non-radiative triplet quenching.

Experimental

Materials

Sublimation grade rubrene was purchased from TCI; meanwhile DBP was purchased from Merck. The synthesis of TBR and palladium phthalocyanine (PdPc) was published elsewhere.[40] TBR was purified by vacuum sublimation prior to use in the experiments.

Preparation of the upconverting films

Materials were dissolved in toluene at concentrations of rubrene (10 mg mL^{-1}), TBR (10 mg mL^{-1}), PdPc (1 mg mL^{-1}), DBP (1 mg mL^{-1}), and PS (50 mg mL^{-1}) and mixed at appropriate ratios to result in the following final concentrations of emitter in PS (in wt%): 0.01, 0.05, 0.2, 1, 5, 10, 20, 30, 40, 50, 60, 70, 80, 90 and 100; DBP in rubrene (in wt%): 0.01, 0.05, 0.1, 0.5, and 1; emitter in PS/PdPc[0.1 wt%]/DBP[0.5 wt%] (in wt%): 30, 60, 70, 80, 90, 95, and 100. Here wt% is defined as a weight percentage relative to the total weight content of the mixture. Films were prepared by spincoating at 4000 rpm for 1 min on 1 mm-thick 25 × 25 mm microscope glass slides. Low concentration PS films ($<$1 wt%) were drop-cast to produce thicker films. The film preparation of all the films and solutions were performed in a nitrogen-filled glovebox with O_2 and H_2O concentrations below 0.1 ppm.

The prepared films were covered with additional microscope slides and encapsulated inside the glovebox by using a 2-component epoxy resin prior to conducting different types of photophysical measurements at ambient conditions. The sealing was essential to protect films from triplet quenching by oxygen and to avoid photoinduced degradation of rubrene emitters.[23]

Optical techniques

Absorption spectra of the dilute solutions of compounds were recorded using a UV-vis-NIR spectrophotometer, Lambda 950 (PerkinElmer). Fluorescence (FL) of the samples was excited at 450 nm by using a xenon arc lamp coupled to a monochromator, whereas photon upconversion (UC) was induced by exciting at 730 nm using a 12 mW power continuous-wave semiconductor laser diode (Picoquant). Steady state FL and UC emission spectra were measured using a back-thinned CCD spectrometer, PMA-12 (Hamamatsu). Fluorescence transients of the samples were measured by using a time-correlated single photon counting system, PicoHarp 300 (Picoquant), which utilized a pulsed semiconductor laser diode (repetition rate – 1 MHz, pulse duration – 70 ps, and emission wavelength – 450 nm) as an excitation source. High excitation FL and UC transients were measured using a time-gated iCCD camera, New iStar DH340T (Andor), after exciting samples with emission of a tunable-wavelength optical amplifier (Ekspla) pumped by a nanosecond Nd^{3+}:YAG laser (wavelength – 450 nm or 730 nm, pulse duration – 5 ns, and repetition rate – 1 kHz). FL and UC emission quantum yields (Φ_{FL} and Φ_{UC}) were estimated by utilizing an integrating sphere (Sphere Optics) coupled to a CCD PMA-12 spectrometer *via* an optical fiber. All the experiments were performed at room temperature.

Results and discussions

Chemical structures of compounds used in the current work, namely, the structures of emitters rubrene and TBR, sensitizer palladium phthalocyanine (PdPc) and singlet exciton sink tetraphenyldibenzoperiflanthene (DBP) are illustrated in Chart 1.

In contrast to a report of Nagata *et al.*[38] where *t*-butyl groups were appended to a rubrene scaffold at the *para*-position, we devised a new bulky rubrene derivative (TBR) with *meta-t*-butyl-disubstituted phenyl rings on the periphery of the tetracene core. Such bifurcated molecular architecture featuring *t*-butyl groups on both sides of the tetracene unit is expected to have a more pronounced steric effect on the packing of TBR in the solid phase as opposed to *t*-butyl groups in the *para*-positions where the effect of the bulkiness of these groups is somewhat offset by the size of the phenyl ring itself.

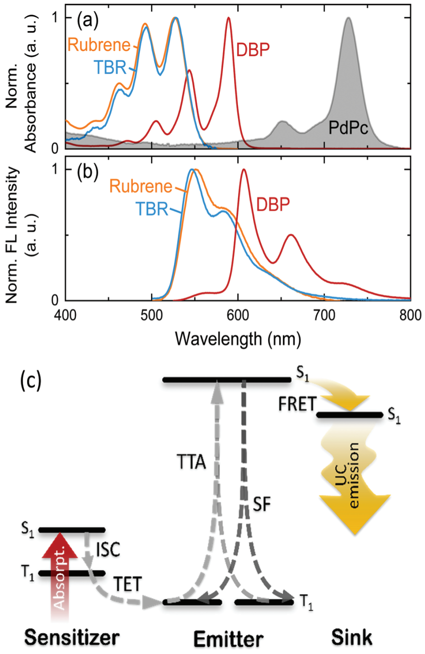

Fig. 1 (a) Absorption spectra of rubrene, and TBR emitters and singlet exciton sink DBP in toluene (1×10^{-5} M). Absorption spectrum of the PdPc sensitizer is displayed for reference. (b) FL spectra of rubrene, TBR and DBP in polystyrene (PS) films at 0.01 wt% concentration. (c) TTA-UC energy scheme for PdPc-sensitized rubrene (or TBR) systems with DBP as a singlet sink. Here, ISC – intersystem crossing, TET – triplet energy transfer, TTA – triplet–triplet annihilation, SF – singlet fission, FRET – Förster resonant energy transfer.

Absorption and FL spectra of rubrene and *t*-butyl-functionalized rubrene (TBR) emitters were found to be very similar indicating negligible impact of *t*-butyl moieties on the electronic structure of rubrene (Fig. 1). This finding suggested that the TTA process for the TBR emitter is similarly feasible as that for rubrene. Molar extinction of TBR at the lowest energy vibronic peak was somewhat smaller as compared to that of rubrene, 3390 M^{-1} cm^{-1} and 4120 M^{-1} cm^{-1}, respectively; nevertheless, the estimated Φ_{FL} of both emitters in the diluted form (either in toluene or PS film) were the same and close to 100%. To reduce SF of the upconverted photons and thereby improve Φ_{UC} of the rubrene-based solid films, DBP as the third component was introduced in small amounts. The emission spectrum of DBP dispersed in PS film at 0.01 wt% concentration is displayed in Fig. 1b. Featuring a large overlap integral with rubrene emission spectrum and high Φ_{FL} (Φ_{FL} = 84% in toluene) DBP served as a singlet exciton sink (emissive trap) for the upconverted singlets in rubrene.[13] Although emission of DBP is redshifted by about 60 nm as compared to FL of rubrene (or TBR) it is still within the transparency region of the sensitizer absorption (Fig. 1a). Taking into account that the lowest triplet state of DBP is ~0.2 eV higher than that of rubrene,[41] DBP is expected to not affect the TTA process in the emitter. Palladium phthalocyanine (PdPc) was used as a sensitizer in this study. Weak absorption of the sensitizer in the UC emission spectral range is essential to ensure reduced energy back-transfer from the emitter to the sensitizer, which

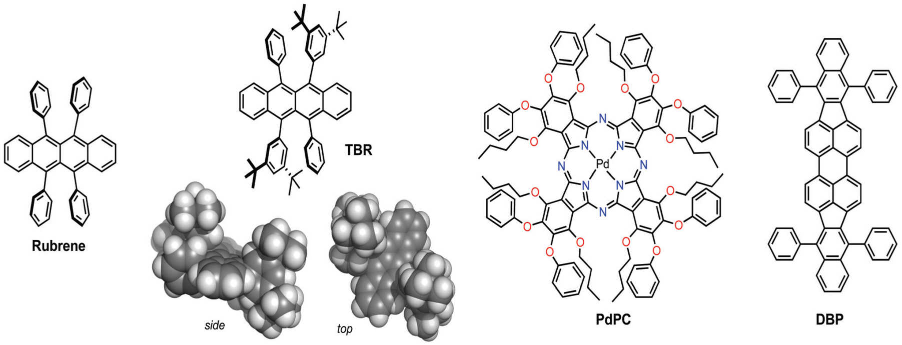

Chart 1 Chemical structures of emitters rubrene and TBR (together with molecular models), sensitizer PdPc and singlet exciton sink DBP.

was demonstrated to cause significant energy losses in UC systems.[42,43]

The role of *t*-butyl groups in the suppression of FL quenching at high emitter concentrations was elucidated by evaluating Φ_{FL} of the PS films with increasing rubrene and TBR concentrations. Φ_{FL} of the rubrene- and TBR-doped PS films estimated using an integrating sphere are compared in Fig. 2. At low emitter concentrations (up to 1 wt%) in PS, both emitters expressed Φ_{FL} close to 100% indicating negligible intermolecular interaction and FL quenching; however, further increasing the concentration resulted in rather different Φ_{FL} behaviors. In the case of rubrene, Φ_{FL} experienced a rapid drop with increasing emitter concentration already above 1 wt%, whereas TBR showed persistently high Φ_{FL} up to 30 wt% and only above this concentration a slight decrease of Φ_{FL} was observed. In the neat rubrene film (at 100 wt% of emitter) Φ_{FL} decreased down to tiny 1.5%, which is ascribed to the formation of crystalline aggregates facilitating SF.[31,44–46] Φ_{FL} of the neat TBR films was found to be a factor of ∼20 higher (Φ_{FL} = 35%) as compared to that of rubrene films, thus in turn confirming the preventive role of *t*-butyl moieties in reducing SF-promoted FL quenching.

The discussed Φ_{FL} behaviors with increasing emitter concentration are well supported by the corresponding dynamics observed in the FL spectra (Fig. 3). With up to 1 wt% of rubrene in the PS films, no changes in FL spectral shape are observed. Above this concentration the relative intensity of vibronic peaks begin to change finally resulting in a domination of the second vibronic replica at 610 nm for an emitter concentration of 70 wt% and above. These changes are also accompanied by the pronounced FL redshift and band broadening, which all together signifies onset of rubrene aggregation with the emission band (at ∼610 nm) corresponding to rubrene in the crystalline enviroment.[47] In contrast, TBR exhibits considerably smaller FL spectral changes with increasing emitter concentration indicating that emission from the amorphous TBR phase prevails almost up to 100 wt% (Fig. 3).

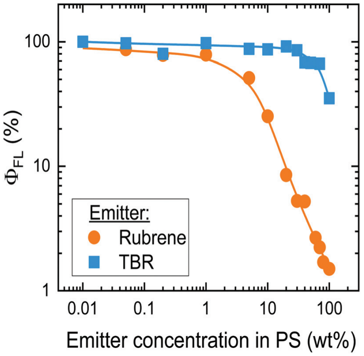

Fig. 2 Fluorescence quantum yield of emitter-doped PS films as a function of emitter concentration. Lines serve as guidelines to the eye. Excitation wavelength – 450 nm.

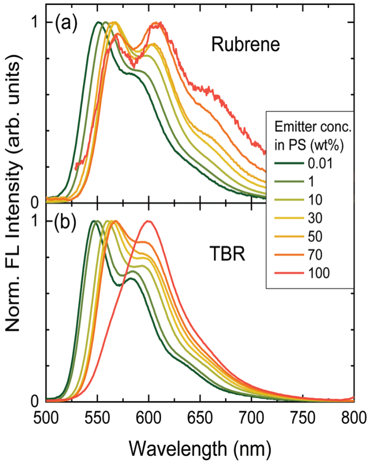

Fig. 3 Fluorescence spectra of emitter-doped PS films as a function of emitter concentration, where the emitter is (a) rubrene and (b) TBR. Excitation wavelength – 450 nm.

More detailed understanding on the role of *t*-butyl groups in suppressing FL concentration quenching can be obtained from the FL transients. FL transients of rubrene- and TBR-doped PS films at different doping concentrations are compared in Fig. 4.

At a low doping concentration (∼1 wt%), both rubrene and TBR transients followed a single exponential decay law with similar FL lifetimes of ∼19 ns indicating the absence of concentration quenching. The increasing rubrene concentration

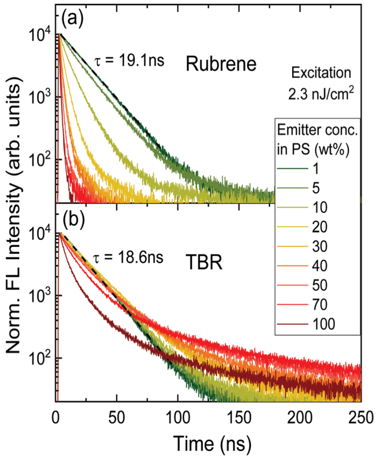

Fig. 4 FL transients of emitter-doped PS films as a function of emitter concentration, where the emitter is (a) rubrene and (b) TBR. Measurements carried out at FL maximum. Excitation energy density per pulse – 2.3 nJ cm^{-2}; excitation wavelength – 450 nm; repetition rate – 1 MHz. FL lifetimes of 1 wt% doped PS films are indicated.

in PS films rapidly accelerated FL decay eventually transforming it to bi-exponential. The average FL lifetime at the 100 wt% doping level (neat film) was shortened dramatically, down to 0.58 ns. Such an abrupt shortening of the FL lifetime nicely correlates with Φ_{FL} quenching dynamics observed with increasing rubrene concentration (Fig. 2).

Compared to rubrene, the TBR emitter also demonstrated shortening of FL lifetime, yet at a much smaller degree (Fig. 4b). This again hints at a decrease of concentration quenching likely due to diminished SF in TBR films. Nevertheless, increase of TBR concentration causes an emergence of a delayed FL component (>100 ns), which was absent in rubrene films. We attribute the delayed component to annihilation of triplet excitons generated *via* the SF process. Surprisingly, the delayed FL is not visible in the rubrene-doped PS film, even though SF is much stronger. The reason for this intricate behavior is discussed below.

The role of SF was further disclosed in FL transients measured at a significantly higher excitation density (300 μJ cm^{-2} per pulse) (Fig. 5). PS films with low emitter concentration (1 wt%) expressed the same mono-exponential FL decay profile independently of the pump level used, whereas an increased doping level (up to 70 wt%) resulted in the appearance of well-pronounced delayed FL components for both emitters, rubrene and TBR. Since no significant FL spectral changes have been observed at several nanosecond and hundreds of nanosecond delays, prompt and delayed FL components were associated with the same emitting species, thereby signifying that the delayed FL originates from TTA. From this, it became obvious that there must be a mechanism responsible for triplet generation, which apparently is SF in agreement with other reports on rubrene.[31,44] Undoubtedly, a large excitation density plays a crucial role here, because TTA is a bimolecular process and large triplet concentration is required for the TTA-caused delayed FL component to be substantial. In contrast, low excitation density conditions imply much lower triplet concentration generated *via* SF, which efficiently spread in the bulk of rubrene films because of the greater triplet diffusion. This concomitantly facilitates triplet quenching and thus justifies the absence of a delayed FL component in rubrene transients at a given registration dynamic range (Fig. 4a).

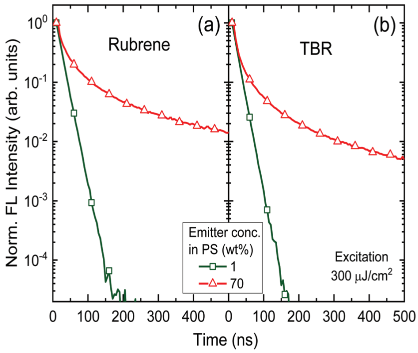

Fig. 5 FL transients of emitter-doped PS films at different emitter concentrations, where the emitter is (a) rubrene and (b) TBR. Excitation energy density per pulse – 300 μJ cm^{-2}, excitation wavelength – 450 nm; repetition rate – 1 kHz.

Having realized from our previous experiments that TTA indeed occurs in TBR-doped PS films, we attempted to use TBR as an emitter in sensitized NIR-to-vis photon upconversion. To reveal the net effect of *t*-butyl groups on the UC performance of rubrene films, a triplet sensitizer, palladium phthalocyanine (see Chart 1), was additionally introduced. The choice of the current sensitizer was based on the rapid intersystem crossing delivered, which enabled virtually perfect conversion of singlet excitations to triplets (Φ_{ISC} = 1), and moreover, featured well-matched triplet and singlet energy levels with those of rubrene.[22,23] Sensitizer concentrations in the UC films was kept low (0.1 wt%) to avoid undesirable aggregation and to lessen detrimental singlet energy back-transfer from emitter to sensitizer.[11,42,48] Yet this concentration was not set too low to have sufficient absorption of excitation light, and consequently, the detectable UC signal for conducting reliable measurements.

To diminish SF of the upconverted singlets in the studied solution-processed rubrene films, singlet exciton sink DBP[13,14,28,42] with high Φ_{FL} was also introduced. By collecting upconverted singlets from rubrene *via* a Förster resonant energy transfer (FRET) mechanism DBP was anticipated to prevent undesirable SF. Indeed, as previously demonstrated it served well for this purpose enabling Φ_{FL} to be improved, and consequently, external quantum efficiency of rubrene-based OLEDs by a few tens of times.[49] To ensure efficient energy transfer from rubrene to DBP, the optimal concentration of DBP has to be found. Although, intuitively, larger amount of DBP should yield larger FRET efficiency, a planar structure possessing DBP will likely aggregate at larger concentrations unavoidably causing emission quenching. Therefore, optimization of DBP concentration in the rubrene film with respect to Φ_{FL} was performed. Fig. 6 shows the FL spectra as well as the Φ_{FL} of the DBP-doped rubrene films as a function of doping concentration in the range of 0–1 wt%. FL spectrum evolution with increasing DBP concentration clearly demonstrates that even a small amount of sink noticeably changes the emission properties. Explicitly, already at 0.5 wt% of DBP, the emission spectrum resembled that of the pure DBP spectrum (see Fig. 1b) indicating efficient FRET from rubrene to DBP. Maximum Φ_{FL} of 15% attained at this doping concentration signifies a factor of 10 enhancement of Φ_{FL} in respect to that obtained in the sink-free rubrene film (Φ_{FL} = 1.5%). Still the achieved maximum Φ_{FL} in the DBP-doped films is found to be roughly 7 times less than that (~100%) attained by pure rubrene in the isolated form. This indicates that FL quenching due to SF is not completely suppressed by addition of 0.5 wt% DBP, and unfortunately cannot be further suppressed because of DBP aggregation at higher concentrations. Nevertheless, the determined optimal DBP concentration (0.5 wt%) in solution-processed rubrene films is found to be very similar to those reported by others for thermally evaporated films.[13,17] This DBP concentration was further utilized in the fabrication of PdPc-sensitized UC films with rubrene and TBR emitters.

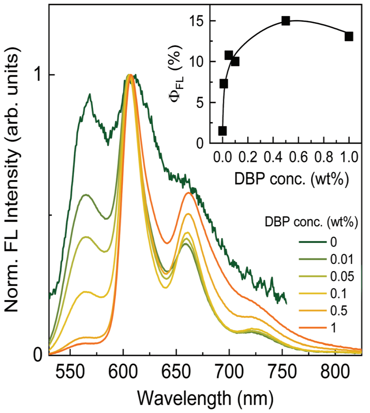

Fig. 6 FL spectra of DBP-doped rubrene films at various doping concentrations. Φ_{FL} of the films as a function of sink concentration is shown in the inset. Excitation wavelength – 450 nm.

Aiming to find the optimal emitter concentration for the most efficient TTA-UC, we fabricated PdPc-sensitized UC films with different rubrene and TBR concentrations. During the fabrication, concentrations of the sensitizer PdPc and singlet sink DBP were kept constant at their optimal values of 0.1 wt% and 0.5 wt%, respectively, as determined previously. Bright yellow UC emission was observed from the upconverting films even by the naked eye under excitation of a NIR laser diode at 730 nm (Fig. 7e). Φ_{UC} evaluated using an integrating sphere and expressed as a ratio of the emitted UC photons to the absorbed ones for the fabricated UC films are shown in Fig. 7b. Note that such a definition of Φ_{UC} implies a maximum theoretical UC yield of 50%. Φ_{FL} of the same films obtained by directly exciting emitter species are displayed in Fig. 7a.

First of all, it is worth noting that even though the rubrene UC films contain singlet sink DBP, their Φ_{FL} is several times lower, particularly at higher emitter concentrations, as compared to a Φ_{FL} of 15% obtained in Fig. 6 at the same optimal DBP doping. This is explained by the presence of a sensitizer in the UC films, which causes detrimental back-FRET from DBP to PdPc. The FRET is feasible due to a small yet existing spectral overlap between DBP emission and PdPc absorption (Fig. 1). In close analogy, the detrimental energy back-transfer induced by the introduction of 0.1 wt% of the sensitizer (platinum octaethylporphyrin) was previously demonstrated to be responsible for ~20-fold reduction in Φ_{FL} of 9,10-diphenylanthracene solid films.[42] Thus, the decrease of Φ_{FL} observed for rubrene UC films with increasing emitter content from 30 to 100 wt% (Fig. 7a) results from the adverse back-FRET to PdPc and persisting SF in the emitter as discussed above. For instance, at the highest rubrene emitter concentration (close to 100 wt%) UC films containing PdPc exhibited Φ_{FL} = 2.5%, whereas the same films without sensitizer expressed Φ_{FL} = 15% (see Fig. 6) implying a factor of 6 lower Φ_{FL} due to back-FRET to sensitizer. On the other hand, similar (a factor of 7) reduction in Φ_{FL} was

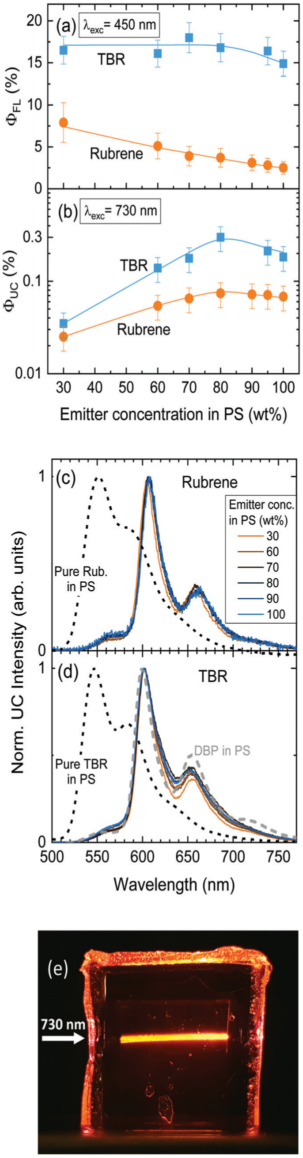

Fig. 7 (a) FL and (b) UC quantum yields of PdPc-sensitized UC films doped with singlet sink DBP as a function emitter rubrene or TBR concentration. UC emission spectra of the same films containing different emitters (c) rubrene and (d) TBR. Emission spectra of pure rubrene, TBR and DBP in PS at low concentrations are presented for reference. PdPc and DBP concentrations in the UC films were fixed at 0.1 wt% and 0.5 wt%, respectively. FL and UC excitation wavelengths are 450 nm and 730 nm, respectively. Excitation density at 730 nm–100 W cm^{-2}. (e) Picture of the NIR-to-visible upconversion in the polymer film with the TBR emitter excited at the edge of the film with 730 nm light.

also experienced by the rubrene films due to SF effects resulting in the net decrease of Φ_{FL} from 100% to 2.5%. The decrease of Φ_{FL} with increasing emitter concentration was also obtained for TBR although at a considerably smaller extent due to suppressed SF.

Contrary to the Φ_{FL} dynamics, Φ_{UC} of the UC films showed non-monotonous behavior with increasing emitter contents (Fig. 7b). Initially, Φ_{UC} increased with increasing rubrene and TBR concentrations up to 80 wt%, where maximum Φ_{UC} values were reached, and then began slightly declining above this concentration. The maximum Φ_{UC} values attained in these films were 0.07% and 0.3% for rubrene and TBR emitters, respectively. Note that for all emitter concentration ranges the studied UC was dominated by the emission from DBP (Fig. 7c and d) signifying the essential role of the singlet sink in alleviating SF. The excitation density chosen for Φ_{UC} measurements was sufficiently high ($\sim$100 W cm^{-2}) for TTA to dominate over spontaneous triplet decay. This is confirmed by the data presented in Fig. 9, where UC intensity dependence on excitation power density is displayed (see discussion below). The chosen excitation regime allowed us to disregard non-radiative triplet quenching (k_{T}) as being negligibly small as compared to the TTA rate ($k_{\mathrm{TTA}} \gg k_{\mathrm{T}}$), hence rendering $\Phi_{\mathrm{TTA}} = k_{\mathrm{TTA}}/(k_{\mathrm{TTA}} + k_{\mathrm{T}}) = 1$. Taking into consideration that Φ_{UC} is determined by the yields of intermediate energy transfer steps (shown in Fig. 1c), explicitly, by ISC yield of a sensitizer, TET yield from a sensitizer to an emitter and TTA and FL yields of an emitter, *i.e.*

$$\Phi_{\mathrm{UC}} = 0.5f\Phi_{\mathrm{ISC}}\Phi_{\mathrm{TET}}\Phi_{\mathrm{TTA}}\Phi_{\mathrm{FL}}, \quad (1)$$

the observed initial increase of Φ_{UC} could only be justified by the enhanced Φ_{TET}. Note that Φ_{FL} here also includes efficiency of FRET from emitter to DBP as depicted in Fig. 7a and f is a constant representing statistical probability to obtain a singlet from two emitter triplets *via* TTA. Since TET is a short-range Dexter-type process necessitating molecular orbital overlap, Φ_{TET} should exhibit exponential growth with decreasing distance between emitter and sensitizer. Eventually, the growth of TET will saturate at some Φ_{TET} value (not necessarily at 100%), which in the studied UC films occurs at the emitter concentration of about 80 wt%. Further behavior of Φ_{UC} with increasing emitter concentration should follow that of Φ_{FL} as all the other intermediate energy transfer steps have already reached maximum efficiency. Indeed, 4-fold higher maximum Φ_{UC} obtained for the TBR film as compared to that of rubrene at 80 wt% concentration well corresponds to 4-fold higher Φ_{FL} in the TBR film *vs* rubrene film at the same concentration. This infers similar Φ_{TET} in both emitter-type UC films at this particular emitter concentration and also clarifies the improvement of Φ_{UC} in TBR films under the TTA domination conditions to be caused by the suppressed SF.

We point out that UC films containing an emitter in excess of 80 wt% are rather inhomogeneous. This can contribute to more substantial reduction of Φ_{UC} with increasing emitter concentration (Fig. 7b) above 80 wt% as that expected from Φ_{FL} dependence. The spatial inhomogeneity in the films infers local fluctuations in composition, which likely cause FL and UC to emerge from different spatial regions. The most intense FL (unlike UC) is expected from the less aggregated regions with smaller emitter concentrations and thus diminished SF; meanwhile stronger UC is anticipated from the regions with larger emitter concentration as this facilitates triplet diffusion and TTA. Yet, the latter regions are more prone to detrimental SF, which adversely affects Φ_{UC}. Additionally, the emitter aggregation may also induce spatial fluctuations, *e.g.* in sensitizer concentration. Obviously, sensitizer-poor regions will contribute most to the overall FL signal due to lowered back-FRET. Conversely, UC will be predominantly observed from sensitizer-rich regions; however these will suffer from enhanced back-FRET and thus reduced Φ_{UC}. The reproducibility of the measurements in the case of spatially inhomogeneous films was ensured by probing large excitation volumes. The sample edge excitation configuration used (Fig. 7e) resulted in a long excitation stripe allowing an ensemble-averaged signal to be collected, which was independent of the excitation spot position.

In practice there might be frequent situations when operational conditions for TTA-assisted photon upconversion in solid UC films are not optimal, *e.g.* due to low sunlight. To find out how TTA-UC performance is affected by the change in the regime, *i.e.* from that governed by TTA (discussed above) to that dominated by spontaneous triplet decay ($k_{\mathrm{T}} \gg k_{\mathrm{TTA}}$), UC properties of the rubrene and TBR films were investigated at low excitation conditions. UC transients of the films in these conditions at different emitter concentrations (60–100 wt%) are depicted in Fig. 8a. Emitter concentrations lower than 60 wt% precluded us from obtaining reliable UC transients because of too weak UC signals in the microsecond-time-domain.

The transients of rubrene and TBR films expressed mainly single-exponential decay confirming the dominance of spontaneous triplet decay against non-linear TTA, and thus enabling easy deduction of triplet exciton lifetime (τ_{T}) from UC lifetime (τ_{UC}) by using the following expression $\tau_{\mathrm{T}} = 2 \times \tau_{\mathrm{UC}}$.[50] Compositional inhomogeneities of UC films at high emitter concentrations ($\geq$80 wt%), particularly in rubrene films, conditioned dispersive triplet diffusion and appearance of multi-exponential UC decay profiles,[51] which nonetheless did not obscure the clear tendencies observed. τ_{UC} and τ_{T} values estimated at different emitter concentrations are summarized in Table 1. The lifetime data evidence that increasing emitter contents from 60 wt% to 100 wt% accelerates UC decay resulting in τ_{T} shortening from 51 μs to $\sim$28 μs and from 91 μs to 63 μs for rubrene and TBR films, respectively. The monotonous shortening of triplet lifetime in the UC films with increasing emitter concentration is a signature of triplet exciton diffusion facilitated triplet quenching at non-radiative decay sites. We emphasize that 2-fold longer τ_{T} obtained in TBR films highlights the essential role of *t*-butyl moieties in effectively reducing triplet exciton diffusion and quenching as compared to those in rubrene films. Note, however, that diffusion in TBR films is still sufficient for TTA-UC to occur. The reduced triplet diffusion and thus prolonged τ_{T} (91 μs) obtained in TBR films at the lowest measured emitter concentration (60 wt%) is close to the intrinsic triplet lifetime

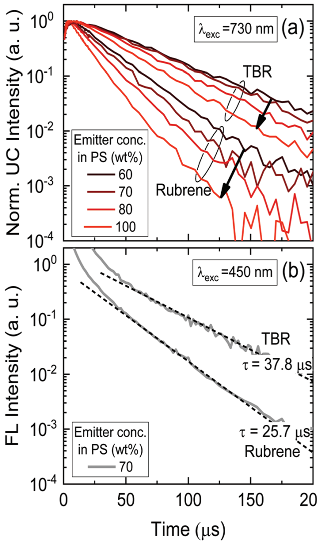

Fig. 8 (a) UC transients of rubrene and TBR films for different emitter concentrations (indicated) excited at 730 nm and measured at UC maxima. PdPc and DBP concentrations in the UC films were fixed at 0.1 wt% and 0.5 wt%, respectively. Excitation energy density per pulse – 7 mJ cm^{-2}. (b) FL transients of the emitter-doped PS films at 70 wt% doping excited at 450 nm and measured at FL maxima. Excitation energy density per pulse – 300 μJ cm^{-2}. Dashed lines indicate exponential fits.

Table 1 UC and triplet exciton lifetimes of PdPc-sensitized UC films doped with singlet sink DBP at various emitter (rubrene or TBR) concentrations

Conc. in PS	60 wt%	70 wt%	80 wt%	100 wt%
Rubrene				
τ_{UC} (μs)	25.6	22.2	16.1 [74%][b] 25.9 [36%]	10.9 [52%][b] 17.7 [48%]
τ_T[a] (μs)	51.2	44.4	⟨37.2⟩[c]	⟨28.4⟩[c]
TBR				
τ_{UC} (μs)	45.5	44.1	38.2	31.5
τ_T[a] (μs)	91.0	88.2	76.4	63.0

[a] $\tau_T = 2 \times \tau_{UC}$ considering that UC decay follows an exponential model. [b] Fractional contribution of each decay component to the overall UC decay is indicated in brackets. [c] Average lifetime estimated by taking into account fractional contributions of each decay component.

of rubrene or TBR emitters measured in dilute solution (τ_T = 100 μs).[40]

Fig. 8b illustrates FL transients of the emitter-doped PS films at 70 wt% doping. They are similar to those shown in Fig. 5 just depicted on a longer (microsecond) time-frame. Delayed FL occurring as a result of subsequent SF and TTA events follows a single-exponential decay profile for the delay of >50 μs as indicated by the linear fits in the semi-log plot. Single-exponential decay designates spontaneous triplet relaxation as a major deactivation pathway with decay lifetimes of ~38 μs and ~26 μs for TBR and rubrene emitter, respectively. These delayed FL lifetimes are found to be similar to τ_{UC} obtained in UC films containing identical emitter species at 70 wt% doping (see Table 1), and therefore serve as an additional proof that the delayed FL in sensitizer-free rubrene and TBR films originates from subsequently occurring SF and TTA processes.

Fig. 9 displays excitation density dependences of UC intensity for rubrene and TBR UC films measured at emitter doping concentrations of 80 wt% (at which maximum Φ_{UC} was obtained) and 30 wt%. At low excitation the UC intensities exhibit quadratic behavior (indicated by slope 2 in Fig. 9), which switches to linear (slope 1) at a certain threshold density (I_{th}) with increasing excitation. The observed quadratic and linear behaviors in the TTA-UC systems are well-known to correspond to two different regimes, *i.e.* the one dominated by spontaneous triplet decay and the second one governed by TTA, respectively.[50] It is worth noting that irrespective of the emitter type used, the UC films featured similar I_{th} (3.7 W cm^{-2}) for an emitter doping concentration of 30 wt%. At higher 80 wt% doping I_{th} was found to be slightly larger for TBR (2.4 W cm^{-2}) as compared to that for rubrene (2.1 W cm^{-2}). The obtained I_{th} values are consistent with those reported by other groups for solid NIR-to-vis UC systems.[13–16,21] Generally, the higher I_{th} observed for lower emitter doping concentrations with respect to that of higher doping can be mainly explained by reduced triplet diffusion because of the larger emitter interspacing, and thus reduced γ_{TTA} and diminished sensitizer-to-emitter TET efficiency. Note that the reduced Φ_{TET} was found to be also responsible for significantly lowered Φ_{UC} at 30 wt% doping as discussed

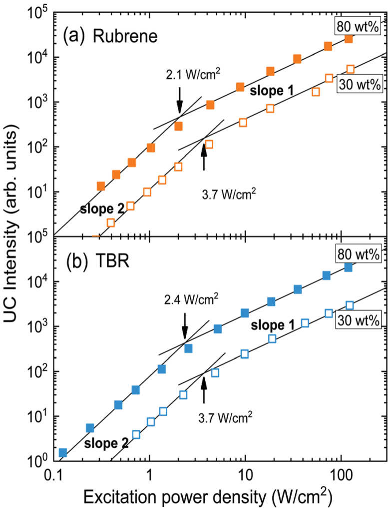

Fig. 9 UC intensity *vs.* excitation power density of (a) rubrene- and (b) TBR-based UC films containing 30 wt% and 80 wt% of emitters. PdPc and DBP concentrations in the UC films were fixed at 0.1 wt% and 0.5 wt%, respectively. Excitation wavelength – 730 nm.

previously (see Fig. 7b). Meanwhile similar I_{th} obtained for rubrene and TBR UC films at 30 wt% doping can be understood by considering threshold expression for TTA[52]

$$I_{\mathrm{th}} = \frac{2(k_{\mathrm{T}})^2}{\gamma_{\mathrm{TTA}}\alpha(E)\Phi_{\mathrm{TET}}}, \tag{2}$$

where γ_{TTA} (=$k_{\mathrm{TTA}}/n_{\mathrm{T}}$) is the second-order TTA rate constant independent of the triplet concentration in the emitter (n_{T}), and $\alpha(E)$ is the absorption coefficient of the sensitizer. Eqn (2) is valid if $\Phi_{\mathrm{ISC}} = 1$, which is exactly the case for the PdPc sensitizer. Since the same sensitizer (PdPc) and its concentration (0.1 wt%) was used in all the studied UC films, $\alpha(E)$ is considered to be the same. Previously we showed that *t*-butyl moieties in TBR reduce triplet diffusion, and consequently, diffusion facilitated triplet quenching resulting in a smaller k_{T} (=$1/\tau_{\mathrm{T}}$) as compared to that in rubrene (see Table 1). Taking into account that TTA and TET are also governed by triplet diffusion described by the same Dexter transfer mechanism, the reduced diffusion is expected to similarly reduce γ_{TTA} and Φ_{TET} in TBR films. Conversely, enhanced triplet diffusion in rubrene UC films will correspondingly enlarge all three quantities k_{T}, γ_{TTA} and Φ_{TET}. In accordance with eqn (2), the obtained similar I_{th} for rubrene and TBR UC films suggest that the enlargement of $(k_{\mathrm{T}})^2$ quantity in rubrene is compensated by the same increase of the product of $[\gamma_{\mathrm{TTA}}\cdot\Phi_{\mathrm{TET}}]$. In other words, reduction of UC threshold, which could be attained through diffusion-enhanced TET and TTA processes in sensitized rubrene films is countervailed by diffusion-facilitated non-radiative triplet quenching, and *vice versa*, reduced triplet quenching and thus remaining larger triplet population in TBR films are counterbalanced by the diminished TET and TTA.

The smaller γ_{TTA} in TBR films can be confirmed by using the following expression

$$\gamma_{\mathrm{TTA}} = \frac{k_{\mathrm{T}}}{n_{\mathrm{T}}} = \frac{2(k_{\mathrm{T}})^2}{G} = \frac{2(k_{\mathrm{T}})^2}{I_{\mathrm{th}}\alpha(E)\Phi_{\mathrm{ISC}}\Phi_{\mathrm{TET}}}, \tag{3}$$

at I_{th} excitation when spontaneous triplet decay rate is equal to that of TTA.[52] Here G is the triplet generation rate in the emitter. Given the identical $\alpha(E)$ and Φ_{ISC} for the same sensitizer used and considering equal Φ_{TET} for TBR and rubrene films at the emitter concentration of 80 wt% as discussed previously, G values evaluated at the threshold density could also be considered to be the same. Owing to 2-fold smaller k_{T} obtained in TBR films, 4 times smaller γ_{TTA} in these films is expected with respect to rubrene films at 80 wt% emitter concentration.

UC quantum yield evaluated at optimal 80 wt% emitter doping as a function of excitation density is shown in Fig. 10. Obviously, at high excitations in TTA dominated regime Φ_{UC} is saturated at 0.07% and 0.3% for rubrene and TBR films, respectively, in agreement with the maximum Φ_{UC} values obtained in Fig. 7b. Decreasing excitation density apparently causes reduction of Φ_{UC} below 10 W cm^{-2} indicating change of the regime from that governed by TTA to that dominated by spontaneous triplet decay. Similar I_{th} values found for rubrene and TBR UC films imply similar excitation density at which Φ_{UC} starts decreasing. This in fact determines that Φ_{UC} of TBR films will remain higher as compared to that of rubrene films even at low light conditions ($k_{\mathrm{T}} \gg k_{\mathrm{TTA}}$) as it is shown in Fig. 10. Taking into account that in such conditions expression for Φ_{TTA} simplifies into the following

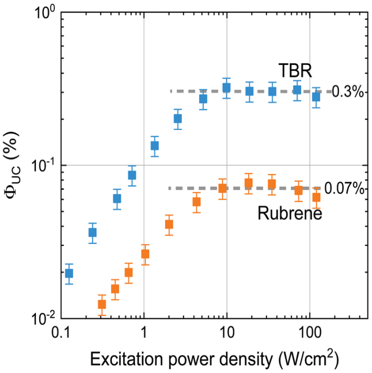

Fig. 10 UC quantum yield of PdPc-sensitized UC films containing 80 wt% of emitter as a function of excitation power density. PdPc and DBP concentrations in the UC films were fixed at 0.1 wt% and 0.5 wt%, respectively. Excitation wavelength – 730 nm. Dashed lines indicate Φ_{UC} saturation values.

$$\begin{aligned}\Phi_{\mathrm{UC}} \propto \Phi_{\mathrm{TTA}} &= \frac{k_{\mathrm{TTA}}}{k_{\mathrm{TTA}} + k_{\mathrm{T}}} = \frac{\gamma_{\mathrm{TTA}}\cdot n_{\mathrm{T}}}{\gamma_{\mathrm{TTA}}\cdot n_{\mathrm{T}} + k_{\mathrm{T}}} \\ &\approx \frac{\gamma_{\mathrm{TTA}}}{k_{\mathrm{T}}}\cdot n_{\mathrm{T}},\end{aligned} \tag{4}$$

the larger Φ_{UC} in TBR films will also be afforded by lowered k_{T} (in addition to larger Φ_{FL} due to reduced SF). The latter result demonstrates that even though triplet exciton diffusion is impeded in TBR films due to the presence of *t*-butyl substituents, the subsequently reduced γ_{TTA} is counterbalanced by suppressed non-radiative triplet quenching k_{T} and SF resulting in better overall TTA-UC performance of these films as compared to the performance of unsubstituted rubrene films. Despite the fact that the unsubstituted rubrene as an emitter performs better in UC solutions,[40] the obtained results indicate that the TBR emitter is more efficient in the optimized solid UC films.

Conclusions

To summarize, we evaluated and compared TTA-UC performance of solution-processed films based on the popular rubrene emitter with those based on a *t*-butyl-substituted rubrene (TBR) emitter. Although *t*-butyl moieties were anticipated to act as spacing groups suppressing undesirable concentration quenching of emission, they could also induce adverse effects, *i.e.* reduced triplet diffusion and diffusion-assisted TTA, hence hampering UC efficiency. A small amount (0.1 wt%) of triplet sensitizer PdPc was used in the studied UC films to diminish detrimental energy transfer of upconverted singlets back to the sensitizer. All the UC films were additionally doped with 0.5 wt% of DBP, which served as an emissive singlet sink collecting upconverted singlet excitons and in this way reducing SF, particularly at high emitter contents. UC performance optimization carried out against emitter concentration revealed 4 times higher maximum Φ_{UC} (0.3%) in TBR films as compared to that in rubrene films (Φ_{UC} = 0.07%) at the optimal emitter doping of 80 wt%. Note that Φ_{UC} defined in this work cannot exceed 50%, since during the TTA at most one UC photon can be produced per two absorbed ones. Importantly, TBR films outperformed rubrene films in terms of Φ_{UC} irrespective of excitation conditions applied. Enhanced UC performance in the case of TBR in the TTA dominated regime was determined by the reduced fluorescence concentration quenching mainly due to suppressed SF. In the regime dominated by spontaneous triplet decay typically attained at low excitation densities, the impeded triplet diffusion and thus TTA in TBR films were counterbalanced by reduced non-radiative triplet quenching and SF rendering higher Φ_{UC} of these films as compared to unsubstituted rubrene films. The obtained results imply peripheral spacing groups (*e.g.* *t*-butyl) in the emitters are beneficial for UC performance of the solid films, which are desired in practical TTA-UC applications.

Conflicts of interest

There are no conflicts to declare.

Acknowledgements

The research was funded by the European Social Fund (project No. 09.3.3-LMT-K-712-01-0084) under grant agreement with the Research Council of Lithuania (LMTLT).

Notes and references

1 B. D. Ravetz, A. B. Pun, E. M. Churchill, D. N. Congreve, T. Rovis and L. M. Campos, Photoredox catalysis using infrared light via triplet fusion upconversion, *Nature*, 2019, **565**, 343.

2 Y. I. Park, K. T. Lee, Y. D. Suh and T. Hyeon, Upconverting nanoparticles: a versatile platform for wide-field two-photon microscopy and multi-modal in vivo imaging, *Chem. Soc. Rev.*, 2015, **44**, 1302–1317.

3 D. Yildiz, C. Baumann, A. Mikosch, A. J. C. Kuehne, A. Herrmann and R. Göstl, Anti-Stokes Stress Sensing: Mechanochemical Activation of Triplet–Triplet Annihilation Photon Upconversion, *Angew. Chem., Int. Ed.*, 2019, **58**, 12919–12923.

4 S.-W. Liu, C.-C. Lee, C.-H. Yuan, W.-C. Su, S.-Y. Lin, W.-C. Chang, B.-Y. Huang, C.-F. Lin, Y.-Z. Lee, T.-H. Su and K.-T. Chen, Transparent Organic Upconversion Devices for Near-Infrared Sensing, *Adv. Mater.*, 2015, **27**, 1217–1222.

5 Y. Zhou, S.-T. Han, X. Chen, F. Wang, Y.-B. Tang and V. A. L. Roy, An upconverted photonic nonvolatile memory, *Nat. Commun.*, 2014, **5**, 4720.

6 S. H. C. Askes, M. S. Meijer, T. Bouwens, I. Landman and S. Bonnet, Red Light Activation of Ru(II) Polypyridyl Prodrugs via Triplet-Triplet Annihilation Upconversion: Feasibility in Air and through Meat, *Molecules*, 2016, **21**, 1460.

7 J. Zhou, Q. Liu, W. Feng, Y. Sun and F. Li, Upconversion Luminescent Materials: Advances and Applications, *Chem. Rev.*, 2015, **115**, 395–465.

8 J. Pedrini and A. Monguzzi, Recent advances in the application triplet–triplet annihilation-based photon upconversion systems to solar technologies, *J. Photonics Energy*, 2017, **8**, 022005.

9 T. F. Schulze and T. W. Schmidt, Photochemical upconversion: present status and prospects for its application to solar energy conversion, *Energy Environ. Sci.*, 2015, **8**, 103–125.

10 T. N. Singh-Rachford and F. N. Castellano, Photon upconversion based on sensitized triplet–triplet annihilation, *Coord. Chem. Rev.*, 2010, **254**, 2560–2573.

11 V. Gray, K. Moth-Poulsen, B. Albinsson and M. Abrahamsson, Towards efficient solid-state triplet–triplet annihilation based photon upconversion: supramolecular, macromolecular and self-assembled systems, *Coord. Chem. Rev.*, 2018, **362**, 54–71.

12 B. Joarder, N. Yanai and N. Kimizuka, Solid-State Photon Upconversion Materials: Structural Integrity and Triplet–Singlet Dual Energy Migration, *J. Phys. Chem. Lett.*, 2018, **9**, 4613–4624.

13 M. Wu, D. N. Congreve, M. W. B. Wilson, J. Jean, N. Geva, M. Welborn, T. Van Voorhis, V. Bulović, M. G. Bawendi and M. A. Baldo, Solid-state infrared-to-visible upconversion sensitized by colloidal nanocrystals, *Nat. Photonics*, 2016, **10**, 31–34.

14 M. Wu, J. Jean, V. Bulović and M. A. Baldo, Interference-enhanced infrared-to-visible upconversion in solid-state thin films sensitized by colloidal nanocrystals, *Appl. Phys. Lett.*, 2017, **110**, 211101.

15 S. Amemori, Y. Sasaki, N. Yanai and N. Kimizuka, Near-Infrared-to-Visible Photon Upconversion Sensitized by a Metal Complex with Spin-Forbidden yet Strong S0–T1 Absorption, *J. Am. Chem. Soc.*, 2016, **138**, 8702–8705.

16 L. Nienhaus, J.-P. Correa-Baena, S. Wieghold, M. Einzinger, T.-A. Lin, K. E. Shulenberger, N. D. Klein, M. Wu, V. Bulović, T. Buonassisi, M. A. Baldo and M. G. Bawendi, Triplet-Sensitization by Lead Halide Perovskite Thin Films for Near-Infrared-to-Visible Upconversion, *ACS Energy Lett.*, 2019, **4**, 888–895.

17 L. Nienhaus, M. Wu, N. Geva, J. J. Shepherd, M. W. B. Wilson, V. Bulović, T. Van Voorhis, M. A. Baldo and M. G. Bawendi, Speed Limit for Triplet-Exciton Transfer in Solid-State PbS Nanocrystal-Sensitized Photon Upconversion, *ACS Nano*, 2017, **11**, 7848–7857.

18 K. M. Felter, M. C. Fravventura, E. Koster, R. D. Abellon, T. J. Savenije and F. C. Grozema, Solid-State Infrared Upconversion in Perylene Diimides Followed by Direct Electron Injection, *ACS Energy Lett.*, 2019, 124–129.

19 Z. Huang, Z. Xu, M. Mahboub, Z. Liang, P. Jaimes, P. Xia, K. R. Graham, M. L. Tang and T. Lian, Enhanced Near-Infrared-to-Visible Upconversion by Synthetic Control of PbS Nanocrystal Triplet Photosensitizers, *J. Am. Chem. Soc.*, 2019, **141**, 9769–9772.

20 F. Deng, W. Sun and F. N. Castellano, Texaphyrin sensitized near-IR-to-visible photon upconversion, *Photochem. Photobiol. Sci.*, 2014, **13**, 813–819.

21 A. Abulikemu, Y. Sakagami, C. Heck, K. Kamada, H. Sotome, H. Miyasaka, D. Kuzuhara and H. Yamada, Solid-State, Near-Infrared to Visible Photon Upconversion via Triplet–Triplet Annihilation of a Binary System Fabricated by Solution Casting, *ACS Appl. Mater. Interfaces*, 2019, **11**, 20812–20819.

22 J. L. Han, J. You, H. Yonemura, S. Yamada, S. R. Wang and X. G. Li, Metallophthalocyanines as triplet sensitizers for highly efficient photon upconversion based on sensitized triplet–triplet annihilation, *Photochem. Photobiol. Sci.*, 2016, **15**, 1039–1045.

23 T. N. Singh-Rachford and F. N. Castellano, Pd(II) Phthalocyanine-Sensitized Triplet–Triplet Annihilation from Rubrene, *J. Phys. Chem. A*, 2008, **112**, 3550–3556.

24 Y. Che, W. Yang, G. Tang, F. Dumoulin, J. Zhao, L. Liu and Ü. İşci, Photophysical properties of palladium/platinum tetrasulfonyl phthalocyanines and their application in triplet–triplet annihilation upconversion, *J. Mater. Chem. C*, 2018, **6**, 5785–5793.

25 V. Yakutkin, S. Aleshchenkov, S. Chernov, T. Miteva, G. Nelles, A. Cheprakov and S. Baluschev, Towards the IR Limit of the Triplet–Triplet Annihilation-Supported Up-Conversion: Tetraanthraporphyrin, *Chem. – Eur. J.*, 2008, **14**, 9846–9850.

26 L. Nienhaus, M. Wu, V. Bulović, M. A. Baldo and M. G. Bawendi, Using lead chalcogenide nanocrystals as spin mixers: a perspective on near-infrared-to-visible upconversion, *Dalton Trans.*, 2018, **47**, 8509–8516.

27 S. Wieghold, A. S. Bieber, Z. A. VanOrman and L. Nienhaus, Influence of Triplet Diffusion on Lead Halide Perovskite-Sensitized Solid-State Upconversion, *J. Phys. Chem. Lett.*, 2019, **10**, 3806–3811.

28 N. Geva, L. Nienhaus, M. Wu, V. Bulović, M. A. Baldo, T. Van Voorhis and M. G. Bawendi, A Heterogeneous Kinetics Model for Triplet Exciton Transfer in Solid-State Upconversion, *J. Phys. Chem. Lett.*, 2019, **10**, 3147–3152.

29 S. N. Sanders, M. K. Gangishetty, M. Y. Sfeir and D. N. Congreve, Photon Upconversion in Aqueous Nanodroplets, *J. Am. Chem. Soc.*, 2019, **141**, 9180–9184.

30 D. K. K. Liu and L. R. Faulkner, P-Type delayed fluorescence from rubrene, *J. Am. Chem. Soc.*, 1977, **99**, 4594–4599.

31 V. Jankus, E. W. Snedden, D. W. Bright, E. Arac, D. Dai and A. P. Monkman, Competition between polaron pair formation and singlet fission observed in amorphous rubrene films, *Phys. Rev. B: Condens. Matter Mater. Phys.*, 2013, **87**, 224202.

32 W. G. Herkstroeter and P. B. Merkel, The triplet state energies of rubrene and diphenylisobenzofuran, *J. Photochem.*, 1981, **16**, 331–341.

33 X. Qiao and D. Ma, Nonlinear optoelectronic processes in organic optoelectronic devices: triplet–triplet annihilation and singlet fission, *Mater. Sci. Eng., R*, 2019, 100519.

34 Y. C. Simon and C. Weder, Low-power photon upconversion through triplet–triplet annihilation in polymers, *J. Mater. Chem.*, 2012, **22**, 20817–20830.

35 S. Raišys, K. Kazlauskas, S. Juršėnas and Y. C. Simon, The Role of Triplet Exciton Diffusion in Light-Upconverting Polymer Glasses, *ACS Appl. Mater. Interfaces*, 2016, **8**, 15732–15740.

36 V. Gray, D. Dzebo, M. Abrahamsson, B. Albinsson and K. Moth-Poulsen, Triplet–triplet annihilation photon-upconversion: towards solar energy applications, *Phys. Chem. Chem. Phys.*, 2014, **16**, 10345–10352.

37 D. L. Dexter, A Theory of Sensitized Luminescence in Solids, *J. Chem. Phys.*, 1953, **21**, 836–850.

38 R. Nagata, H. Nakanotani, W. J. Potscavage and C. Adachi, Exploiting Singlet Fission in Organic Light-Emitting Diodes, *Adv. Mater.*, 2018, **30**, 1801484.

39 H. H. Fong, S. K. So, W. Y. Sham, C. F. Lo, Y. S. Wu and C. H. Chen, Effects of tertiary butyl substitution on the charge transporting properties of rubrene-based films, *Chem. Phys.*, 2004, **298**, 119–123.

40 E. Radiunas, S. Raišys, S. Juršėnas, A. Juzeliūnaitė, T. Javorskis, U. Šinkevičiūtė, E. Orentas and K. Kazlauskas, Understanding the limitations of NIR-to-visible photon upconversion in phthalocyanine-sensitized rubrene systems, *J. Mater. Chem. C*, 2020, DOI: 10.1039/c9tc06031f.

41 D. Y. Kondakov, T. D. Pawlik, T. K. Hatwar and J. P. Spindler, Triplet annihilation exceeding spin statistical limit in highly efficient fluorescent organic light-emitting diodes, *J. Appl. Phys.*, 2009, **106**, 124510.

42 S. Raišys, S. Juršėnas, Y. C. Simon, C. Weder and K. Kazlauskas, Enhancement of triplet-sensitized upconversion in rigid polymers via singlet exciton sink approach, *Chem. Sci.*, 2018, **9**, 6796–6802.

43 T. Ogawa, M. Hosoyamada, B. Yurash, T.-Q. Nguyen, N. Yanai and N. Kimizuka, Donor–Acceptor–Collector Ternary Crystalline Films for Efficient Solid-State Photon Upconversion, *J. Am. Chem. Soc.*, 2018, **140**, 8788–8796.

44 D. M. Finton, E. A. Wolf, V. S. Zoutenbier, K. A. Ward and I. Biaggio, Routes to singlet exciton fission in rubrene crystals and amorphous films, *AIP Adv.*, 2019, **9**, 095027.

45 X. Wang, T. Garcia, S. Monaco, B. Schatschneider and N. Marom, Effect of crystal packing on the excitonic properties of rubrene polymorphs, *CrystEngComm*, 2016, **18**, 7353–7362.

46 S. T. Roberts, R. E. McAnally, J. N. Mastron, D. H. Webber, M. T. Whited, R. L. Brutchey, M. E. Thompson and S. E. Bradforth, Efficient Singlet Fission Discovered in a Disordered Acene Film, *J. Am. Chem. Soc.*, 2012, **134**, 6388–6400.

47 Y. Chen, B. Lee, D. Fu and V. Podzorov, The Origin of a 650 nm Photoluminescence Band in Rubrene, *Adv. Mater.*, 2011, **23**, 5370–5375.

48 Z. A. VanOrman, A. S. Bieber, S. Wieghold and L. Nienhaus, A perspective on triplet fusion upconversion: triplet sensitizers beyond quantum dots, *MRS Commun.*, 2019, 1–12.

49 Y. Zhang and S. R. Forrest, Triplets Contribute to Both an Increase and Loss in Fluorescent Yield in Organic Light Emitting Diodes, *Phys. Rev. Lett.*, 2012, **108**, 267404.

50 A. Köhler and H. Bässler, Triplet states in organic semiconductors, *Mater. Sci. Eng., R*, 2009, **66**, 71–109.

51 M. Scheidler, B. Cleve, H. Bässler and P. Thomas, Monte Carlo simulation of bimolecular exciton annihilation in an energetically random hopping system, *Chem. Phys. Lett.*, 1994, **225**, 431–436.

52 A. Monguzzi, R. Tubino, S. Hoseinkhani, M. Campione and F. Meinardi, Low power, non-coherent sensitized photon up-conversion: modelling and perspectives, *Phys. Chem. Chem. Phys.*, 2012, **14**, 4322–4332.

PIII

NIR-to-vis photon upconversion in rubrenes with increasing structural complexity

Edvinas Radiunas, Manvydas Dapkevičius, Lukas Naimovičius, Paulius Baronas, Steponas Raišys, Saulius Juršėnas, Augustina Jozeliūnaitė, Tomas Javorskis, Ugnė Šinkevičiūtė, Edvinas Orentas, Karolis Kazlauskas.

Journal of Materials Chemistry C, **9**(12), 4359-4366, (2021)

10.1039/D1TC00296A

Journal of
Materials Chemistry C

ROYAL SOCIETY
OF CHEMISTRY

PAPER

View Article Online
View Journal | View Issue

Check for updates

Cite this: *J. Mater. Chem. C*, 2021, 9, 4359

NIR-to-vis photon upconversion in rubrenes with increasing structural complexity†

Edvinas Radiunas,[a] Manvydas Dapkevičius,[a] Lukas Naimovičius,[a]
Paulius Baronas,[a] Steponas Raišys,[a] Saulius Juršėnas,[a]
Augustina Jozeliūnaitė,[b] Tomas Javorskis,[b] Ugnė Šinkevičiūtė,[b]
Edvinas Orentas[b] and Karolis Kazlauskas*[a]

Received 21st January 2021,
Accepted 4th March 2021

DOI: 10.1039/d1tc00296a

rsc.li/materials-c

Rubrene is the most widely used triplet–triplet annihilation (TTA) emitter for NIR-to-vis photon upconversion (UC), however, strong singlet fission (SF) in the solid films quenches its emission and hampers practical TTA-UC applications. Herein, the issue was addressed by decorating the rubrene with sterically demanding 3,5-di-*tert*-butylphenyl side-moieties at the periphery and the core to result in 40-fold enhancement of the emission quantum yield. Nevertheless, the sterically crowded rubrenes were found to exhibit lower sensitized UC performance compared to the conventional rubrene, which was ascribed to inefficient triplet energy transfer from a sensitizer and poor TTA (for the core-modified rubrene only). By exploiting the distinct feature of rubrenes to simultaneously express both SF and TTA in the solid films, their TTA efficiency was assessed independently from TET in the sensitizer-free films. The results implied a trade-off between suppressed SF and enhanced TTA in the rubrene emitters, which could be addressed *via* careful selection of the degree of sterical hindrance and linking position of the side-moieties. Thorough analysis of the prompt and delayed fluorescence revealed that the bulky side-moieties at the periphery do not impede TTA, *i.e.*, it is as efficient as that of unsubstituted rubrene, whereas these moieties linked directly to the core suppress TTA dramatically. The current study unveils an advantage of the peripheral linking *vs.* core linking pattern of rubrene emitters, thereby providing valuable insights for their rational modification towards improved NIR-to-vis UC efficiency in the solid state.

Introduction

Photon energy upconversion (UC) accomplished in organic compounds through triplet–triplet annihilation (TTA) gained significant interest over the past decade due to the important applications in photocatalysis,[1–3] bioimaging,[4] photovoltaics,[5–15] targeted drug delivery,[16–18] *etc.*[19–21] TTA-UC was demonstrated to operate at milliwatt power of incoherent excitation (such as the sunlight),[5,7,22] thus implying the attractive possibility for photovoltaics to harvest weakly absorbed near-infrared (NIR) photons *via* their conversion to visible light.[5,7] General scheme of the energy level alignment along with the corresponding energy transfer processes occurring in the typical UC system composed of a sensitizer and emitter (annihilator) are depicted in Fig. 1. The sensitizer is responsible for low energy photon absorption, triplet generation by way of intersystem crossing (ISC) and triplet energy transfer (TET) to the emitter, whereas the emitter is accountable for TTA process, which mediates energy UC ultimately resulting in high energy photon emission.

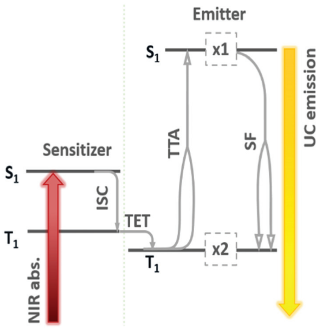

Fig. 1 TTA-UC energy scheme with corresponding energy transfer processes. ISC – intersystem crossing, TET – triplet energy transfer, TTA – triplet–triplet annihilation, SF – singlet fission, UC – upconversion.

---

[a] Institute of Photonics and Nanotechnology, Vilnius University, Saulėtekio av. 3, LT-10257 Vilnius, Lithuania. E-mail: karolis.kazlauskas@ff.vu.lt

[b] Institute of Chemistry, Faculty of Chemistry and Geosciences, Vilnius University, Naugarduko 24, LT-03225 Vilnius, Lithuania

† Electronic supplementary information (ESI) available. See DOI: 10.1039/d1tc00296a

Essentially, practical TTA-UC applications in photovoltaics demand high NIR-to-vis UC efficiency, preferably in a solid state.[8,23] This, however, creates a big challenge, because the vast majority of solid-state UC systems operating in NIR range (>700 nm) usually express very low UC quantum yield (Φ_{UC}), $<1\%$.[15,23–29] We note that the maximum Φ_{UC} is limited to 50%, because during the TTA, at most one UC photon can be produced per two absorbed ones.[30,31]

Among the suitable emitters exploited for NIR spectral range are tetracenes,[32–34] rubrenes,[27,28,35–40] perylenes,[23,41,42] and diketopyrrolopyrroles.[43] Yet, the best-performing NIR-to-vis UC systems demonstrated so far, both in solution and solid state, rely on the rubrene emitter.[15] In fact, currently there is no alternative TTA emitter to rubrene for the solid state UC.[15] Recently, our group showed that even though unsubstituted rubrene (**Rub**) yields the highest Φ_{UC} in solution,[44] *t*-butyl-substituted rubrene (***t*BRub**) exhibits 4-fold higher Φ_{UC} in the solid films.[45] The enhanced UC performance of ***t*BRub** was found to be caused by (i) the reduced concentration quenching due to suppressed singlet fission and (ii) suppressed non-radiative triplet quenching.

Considering that the peripheral spacing groups in the emitter can be beneficial for UC performance of the solid films, we extended the current series of rubrene emitters (**Rub** and ***t*BRub**)[44,45] by designing a couple of new ones (**peri-*t*BRub** and **core-*t*BRub**) decorated with more bulky 3,5-di-*tert*-butylphenyl moieties (see Fig. 2). **peri-*t*BRub** featured the bulky moieties only in the periphery, whereas **core-*t*BRub** additionally had these moieties linked directly to the core. The imposed modifications were anticipated to further suppress singlet fission, thereby improving FL (and UC) emission efficiency. However, it is unclear, whether the bulky side-moieties will not reduce triplet migration to the degree that TTA-UC is no longer possible. Additionally, what is the effect of the linking position, *i.e.*, peripheral- or core-linking, of the side-groups on the singlet fission and TTA. Motivated to clarify the impact of the sterically demanding groups on the processes behind the TTA-UC, including the overall UC performance in the solid state, singlet, and triplet exciton dynamics in rubrene-based solid films was studied. In the study, palladium phthalocyanine (**PdPc**) was employed as a triplet sensitizer.[44] Previously reported **Rub** and ***t*BRub** emitters[44,45] were also investigated under the same conditions as **peri-*t*BRub** and **core-*t*BRub** for comparison.

Principally, both peripheral and core-linked side-moieties were found to alleviate detrimental SF, meanwhile the former ones performed substantially better in terms of TTA efficiency, which was found to be equivalent to that of conventional rubrene emitter. The weak sensitized UC emission of the **peri-*t*BRub** and **core-*t*BRub** emphasized the need to enhance triplet energy transfer, reduced due to the sterically demanding side-moieties.

Results and discussions

Photophysical properties

The chemical structures of the studied rubrene emitters in the order of increasing complexity are displayed in Fig. 2. Firstly, singlet and triplet energies of the rubrene emitters were estimated by quantum chemical calculations to verify their feasibility for TTA and the ability to accept triplets from **PdPc** sensitizer (Table S1 in the ESI†). Note that previously, we confirmed **PdPc** to be a suitable triplet sensitizer for the **Rub** and ***t*BRub**.[45] The calculations revealed T_1 of the **peri-*t*BRub** and **core-*t*BRub** to be close or slightly lower as those of **Rub** and ***t*BRub** implying unmitigated potential for the triplet sensitization using **PdPc**. Furthermore, the energy gap between the reorganized energies $2T_1^*$ and S_1^* was found to be lower for the **peri-*t*BRub** and **core-*t*BRub** compared to that for the **Rub** confirming TTA to be energetically viable (see Table S1, ESI† and the explanation therein).[34,46]

The strong similarity of the absorption and FL spectra of the **peri-*t*BRub** with those of **Rub** and ***t*BRub** in the dilute solution pointed out that the peripheral bulky groups have negligible impact on the conjugation (Fig. S1 in the ESI†). Conversely, the spectra of **core-*t*BRub** were redshifted by more than 20 nm, signifying extension of the conjugation attributed to the core-linked side-moieties. This result was also supported by the DFT calculations indicating S_1 energy in the **core-*t*BRub** to be the lowest among the rest rubrene emitters (see Table S1 in the ESI†). Apart from the anticipated effect of the sterical moieties on SF, the downshifted S_1 energy in **core-*t*BRub** also implies less favorable conditions for the SF in the solid film.

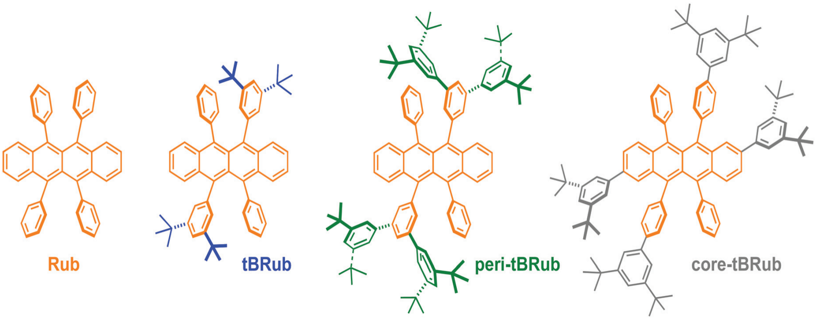

Fig. 2 Chemical structures of the studied rubrene-based emitters in the order of increasing complexity.

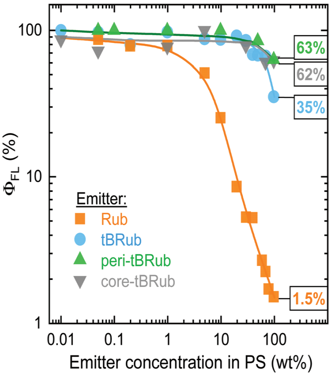

Fig. 3 FL quantum yield of the emitter-doped PS films as a function of emitter concentration. Lines serve as guidelines to the eye. Excitation wavelength, 485 nm. **Rub** and ***t*BRub** data taken from ref. 45.

We note that Φ_{FL} of all the rubrenes was estimated to be close to 100% in both dilute solutions and low-doping-concentration polymer films (Fig. 3). Moreover, polystyrene (PS) films doped with the rubrenes at low concentration (0.01 wt%) exhibited similar single-exponential FL transients with the decay time constant (τ) of ~19 ns (see Fig. S2 in the ESI†), irrespective of the side-moieties attached.

The impact of the bulky 3,5-di-*tert*-butylphenyl moieties on the singlet fission was assessed by measuring Φ_{FL} quenching with increasing the emitter concentration in the PS films (Fig. 3). The presented data evidences the central role of the introduced side-moieties in the suppression of concentration quenching due to SF. The bulky 3,5-di-*tert*-butylphenyl moieties in **peri-*t*BRub** and **core-*t*BRub** allowed to retain more than 60% of the initial Φ_{FL} in the neat films as compared to the substantial quenching observed in the neat films of **Rub** (Φ_{FL} = 1.5%) and even ***t*BRub** (Φ_{FL} = 35%). 40 times higher Φ_{FL} obtained in the neat films of structurally more complex rubrenes in respect to that of conventional **Rub** is promising for TTA-UC applications, because UC efficiency directly depends on Φ_{FL}. In contrast, low solid-state Φ_{FL} is one of the prime causes of poor Φ_{UC}.[29,45]

The reduced concentration quenching in **peri-*t*BRub** and **core-*t*BRub** films is accompanied by the insignificant shift of their PL peak (6–16 nm) compared to the PL peak of the isolated compounds (compare Fig. 4a and Fig. S1 in the ESI†). Meanwhile, in the case of ***t*BRub**, and particularly **Rub** films, the spectral changes are more pronounced resulting in the PL peak redshift of ~50 nm, which is attributed to the enhanced intermolecular interaction. The emergence of an additional PL band above 600 nm due to aggregates is clearly observed for the **Rub** neat film.[47]

The degree of concentration quenching, and correspondingly, the extent of SF could be also determined from the shortening of τ_{PL}, taking the single-exponential decay of the isolated rubrenes with $\tau \approx$ 19 ns as a reference (Fig. S2 in the ESI†). Generally, the PL transients in Fig. 4b consist of the initial fast and later slower components, associated with the rapid singlet fission in the aggregated domains and intrinsic decay of isolated rubrene species, respectively. Note that **core-*t*BRub** of the highest structural complexity features only the slow decay with τ = 16.5 ns, indicating the negligible aggregation in the neat film. Such decay is one of the key criteria qualifying rubrene films as amorphous.[48] The reduced structural complexity of the rubrenes causes shortening of the initial decay component down to 2.2 ns (in **Rub**) implying accelerated SF due to the enhanced aggregation. The slow decay component had a similar τ for all the rubrenes except ***t*BRub**, which exhibited an enlarged contribution from TTA at a later decay stage.[45]

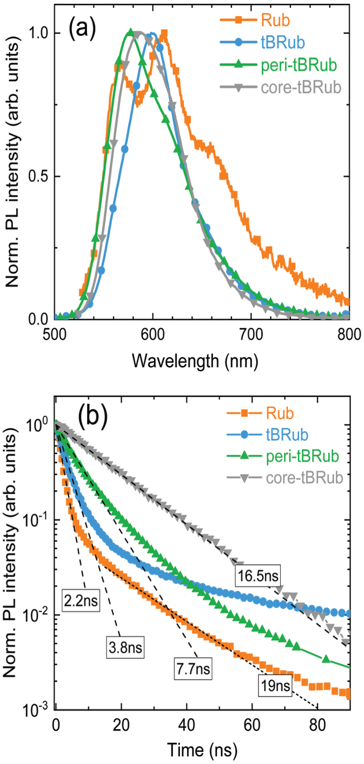

Fig. 4 (a) Photoluminescence spectra and (b) transients of the neat films of rubrene-based emitters (indicated). Dashed lines show single-exponential fits with the decay time constants indicated. Excitation wavelength, 485 nm. **Rub** and ***t*BRub** data taken from ref. 45.

UC efficiency measurements

The high Φ_{FL} observed in the solid films of **peri-*t*BRub** and **core-*t*BRub** motivated us to utilize these new emitters for TTA-UC. At first, their potential for UC was tested in solutions (see Fig. 5). For comparison, the concentrations of the new emitters and **PdPc** sensitizer were set to 18 mM and 15 μM, respectively, identical to those utilized previously for **Rub** and ***t*BRub**.[44] The UC measurements were accomplished by selectively exciting the **PdPc** sensitizer at the Q band. The recorded UC emission spectra were normalized to FL of the sensitizer ($FL_{\mathbf{PdPc}}$) for the correct comparison of UC efficiencies.[44] The latter correspond to the area under UC spectra between 500 and 700 nm. Disappointingly, UC efficiencies of the structurally complex rubrene emitters were found to be inferior to those of conventional emitters **Rub** and ***t*BRub**. **peri-*t*BRub** expressed more than one order of magnitude lower Φ_{UC} (= 0.08%) as compared to those of **Rub** (Φ_{UC} = 5.7%) and ***t*BRub** (Φ_{UC} = 1.3%), whereas UC signal of **core-*t*BRub** was barely detectable and too weak to be quantified. Taking into account that (i) Φ_{FL} of the studied rubrene:**PdPc** based UC systems in the solution was determined to be the same (90%), irrespective of the rubrene emitter employed, and (ii) Φ_{ISC} is identical for the UC systems with the same **PdPc** sensitizer, the low Φ_{UC} obtained for the new rubrenes is most likely caused by the bulky side-moieties impeding TET and/or TTA processes.

The knowledge about TET efficiency (Φ_{TET}) in the liquid UC systems can be gained by analyzing UC transients. While the UC intensity decay (τ_{UC}) reflects a lifetime of the triplet excitons ($\tau_T = 2 \times \tau_{UC}$) in an emitter, the rise of UC intensity immediately upon excitation corresponds to Φ_{TET}.[49] τ_T in **peri-*t*BRub** was found to be similar to that of **Rub** and ***t*BRub** ($\sim$100 μs),[44] whereas the rise time (τ_{rise}) differed significantly (Fig. S4 in the ESI†). Generally, the steeper rise or the shorter τ_{rise} is a signature of the faster TET from a sensitizer to an emitter. In the case of impeded TET, τ_{rise} should approach intrinsic triplet lifetime (τ_0) of a sensitizer, which for **PdPc** is 3.3–4.3 μs.[44] Indeed, τ_{rise} very close to τ_0 was obtained for **peri-*t*BRub**:**PdPc** based UC system (= 4.2 μs), confirming significantly suppressed TET due to the sterically demanding side moieties. Moreover, as an additional confirmation for the diminished Φ_{TET}, we observed increased UC threshold (I_{th}). Note that I_{th} is inversely proportional to Φ_{TET}.[50] A few times higher I_{th} was determined for the **peri-*t*BRub:PdPc** system (11.8 W cm^{-2}, see Fig. S3a in the ESI†), as opposed to that for **Rub:PdPc** (1.9 W cm^{-2}) and ***t*BRub:PdPc** (3.6 W cm^{-2}).[44]

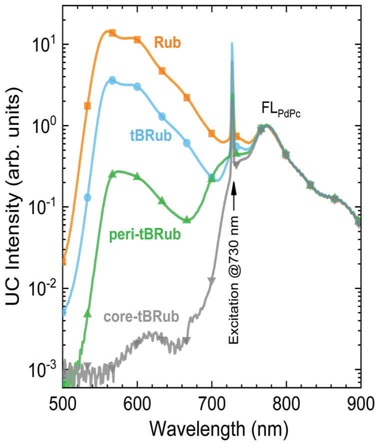

Fig. 5 UC emission spectra of the studied emitter:sensitzer (**Rub**:**PdPc**, ***t*BRub**:**PdPc**, **peri-*t*BRub**:**PdPc** and **core-*t*BRub**:**PdPc**) solutions in toluene under CW excitation at 730 nm. Emitter and sensitizer concentrations were 18 mM and 15 μM, respectively. Spectra are normalized to FL of the sensitizer. **Rub** and ***t*BRub** data taken from ref. 44.

The ineffective TET revealed in the structurally complex rubrenes likely also contributed to their poor TTA-UC performance in the solid state, regardless of their high Φ_{FL} therein (Fig. 3). UC emission measurements of the **peri-*t*BRub:PdPc** and **core-*t*BRub:PdPc** solid films carried out under identical conditions as those previously used for **Rub:PdPc** and ***t*BRub:PdPc** films,[45] (80 wt% and 0.1 wt% of emitter and sensitizer in PS matrix, respectively) resulted in barely noticeable UC for **peri-*t*BRub:PdPc** and no UC signal for **core-*t*BRub:PdPc**. Naturally, poor TET in the **peri-*t*BRub:PdPc** and **core-*t*BRub:PdPc** solid films can be attributed to an increased TET distance, because of the sterically demanding side-groups. However, the molecular orientation factor can be also important, since the certain orientations of sensitizer and emitter may reduce intermolecular distance locally, thus facilitating TET. Unfortunately, it is impossible to discern the orientation factor originating from the different molecular packing, because the studied films are amorphous with random molecular orientation. In addition to the poor TET, the reduced triplet diffusion due to the bulky side-moieties can be critical as well, thereby impeding TTA. The verification of the later hypothesis is of high importance, as this might preclude further utilization of the similar sterically demanding groups in rubrene for TTA-UC. To assess the efficiency of TTA in the new rubrenes, we made use of a rather distinct attribute of the rubrenes to exhibit simultaneously both singlet fission and TTA in the aggregated state. By generating triplets in the rubrene films directly through SF without a sensitizer, TTA could be discerned from TET. To this end, we prepared sensitizer-free neat films and investigated SF as well as delayed FL caused by TTA for each rubrene emitter separately.

Transient absorption spectroscopy

Since TTA depends on the concentration of triplets, created through SF on a picosecond time-scale, this concentration in the different rubrene films was probed using femtosecond transient absorption spectroscopy. The transient absorption spectra of **Rub** neat film (Fig. 6a) showed typical SF dynamics, where a rise of the triplet excited state absorption (ESA) signal at 510 nm corresponding to T1–T3 transition coincided with a rapid decay of singlet ESA signal at 440 nm corresponding to S1–S3 transition.[48,51] In contrast, a significantly weaker triplet ESA signal at 505 nm was observed for ***t*BRub** neat film (Fig. 6b) suggesting significantly suppressed SF. At least 5-fold lower initial triplet density was estimated in ***t*BRub** film compared to **Rub** film from a direct comparison of absolute triplet ESA intensity. Unfortunately, the limited sensitivity of transient absorption setup not permitted to detect weak triplet ESA signal in the neat films of **peri-*t*BRub** and **core-*t*BRub** (see Fig. S5 in the ESI†), which implied strongly suppressed SF. This was confirmed by the different evolution of transient absorption

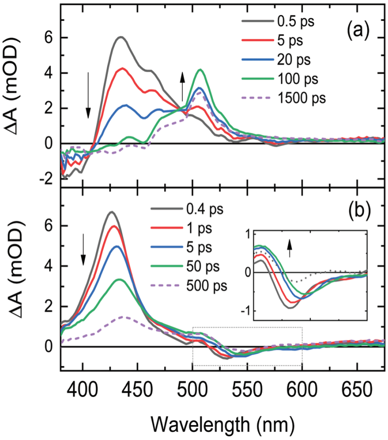

Fig. 6 Transient absorption spectra of (a) **Rub** and (b) ***t*BRub** neat films at different delay times. Signal around excitation region of 485 nm was corrected due to the strong scattering of the samples. Arrows indicate the trend of signal intensity. Inset shows the magnified area of the triplet excited state absorption signal.

signal observed for the studied rubrene films (Fig. 7). Singlet excited state absorption (ESA) decay evidenced more pronounced slowdown of SF rate for the more complex rubrenes.

TTA efficiency measurements

Remarkably, the triplet concentration in the films of sterically crowded rubrenes could be assessed by monitoring UC signal generated *via* TTA. The UC signal in the sensitizer-free films of **peri-*t*BRub** and **core-*t*BRub** was detected by measuring delayed FL on the time-gated iCCD setup (Fig. 8). Gate widths increasing dynamically with the time delay[52–54] enabled us to measure FL transients spanning over seven orders of magnitude in intensity and five orders of magnitude in time. This allowed to detect extremely low delayed FL signals at tens of microseconds, thereby providing useful information about TTA efficiency. ‘To display the high dynamic range FL data in Fig. 8 without losing the information in the prompt and delayed FL time domains, we used log–log scale.

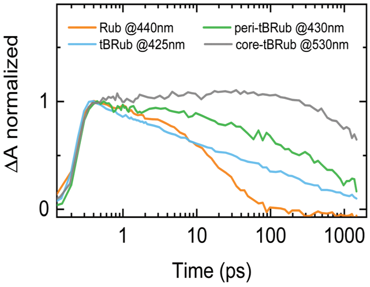

Fig. 7 Evolution of transient absorption signal intensity recorded at the maximum of singlet excited state absorption of the corresponding rubrene emitter in the neat film.

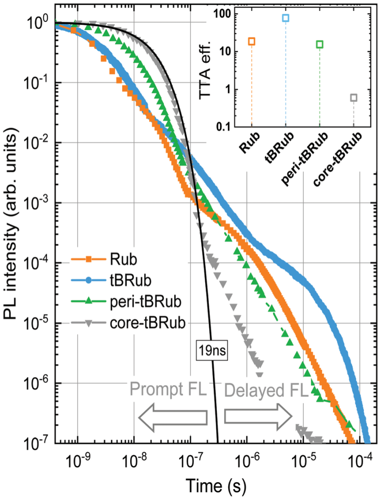

Fig. 8 Normalized FL transients (symbols) of the sensitizer-free neat films of the rubrene emitters measured at 300 μJ cm^{-2} per pulse. Single-exponential decay curve (solid line) with τ = 19 ns serves as a reference for prompt-only SF-free transient. Inset shows TTA efficiency of the different rubrene films.

Essentially, the shown FL transients consist of the prompt and delayed FL parts delineated by single-exponential FL decay curve (solid line) with τ = 19 ns. We remind that such curve is obtained for isolated rubrene molecules with SF absent, and therefore, represent prompt-only FL signal. The acceleration of fast-decaying prompt FL, also shown in Fig. 4b (in log-linear scale), reflects the number of triplets created *via* SF (N_T^{SF}). On the other hand, the amount of slow-declining delayed FL corresponds to the number of singlets created *via* TTA (N_S^{TTA}), otherwise no delayed FL could be observed. Assuming the only non-radiative deactivation pathway for the singlets is SF, we can roughly judge TTA efficiency for each rubrene film from the ratio of N_S^{TTA} to N_T^{SF}. For the estimation of N_T^{SF} and N_S^{TTA}, the FL transients are scaled so that their integrals correspond to their Φ_{FL} estimated previously (Fig. 3). N_T^{SF} is evaluated by subtracting two integrals, *i.e.*, the reference one obtained from the prompt-only SF-free transient (with τ = 19 ns) and the second one obtained from the prompt part of the particular FL transient. Finding N_S^{TTA} implies calculating the integral of the delayed part of the particular FL transient and scaling it by prompt Φ_{FL} (Φ_{FL}^{prompt}) to take into account non-unity emission quantum yield of the created singlets. The explicit formula for the calculation of TTA efficiency is as follows

$$\text{TTA eff.} = \frac{N_S^{TTA}}{N_T^{SF} \cdot \Phi_{FL}^{prompt}} \tag{1}$$

The scaled FL transients along with the integrals representing N_T^{SF} and N_S^{TTA} for each rubrene film are shown in Fig. S6 in the

ESI,† whereas the main parameters necessary for the evaluation of TTA efficiency according to eqn (1) are provided in Table S2 in the ESI.† We note that the obtained number representing TTA efficiency should be considered not as an absolute quantity, describing the particular rubrene film, but rather as a relative parameter intended for comparing TTA probability among the series of rubrene films. This is because of the difficulties in correct estimation of the prompt and delayed FL, which arise from the undefined contribution of geminate triplet pair annihilation.[48,51,55,56] Depending on the triplet diffusivity in each rubrene film, the geminate triplet pair annihilation may add up to UC signal at the early prompt FL stage, distorting the correct integral values. Nevertheless, we believe a comparison of TTA efficiency among the different rubrene films can be made. The data provided in the inset of Fig. 8 and Table S2 in the ESI† evidences the changes in the propensity for TTA with increasing the structural complexity (sterical crowding) of the rubrene emitters. ***t*BRub** demonstrates the highest TTA efficiency in agreement with the largest delayed FL integral, even though triplet concentration generated through SF is 5 times lower compared to that of **Rub**, as deduced from the transient absorption measurements. The result is also consistent with our previous finding, inferring higher Φ_{UC} for ***t*BRub** based solid UC films *vs.* **Rub** films.[45] Meanwhile, the most complex **core-*t*BRub** exhibits the lowest TTA efficiency, which is more than two orders of magnitude lower than that of ***t*BRub**. This is in accordance with the smallest delayed FL and the least efficient SF, evidenced by the prompt FL of the **core-*t*BRub** film being very similar to the SF-free reference decay curve (Fig. 8). Interestingly, **peri-*t*BRub** is found to feature comparable TTA efficiency with that of **Rub**, thus suggesting that bulky 3,5-di-*tert*-butylphenyl moieties in the periphery do not impede TTA significantly. This is in sharp contrast to **core-*t*BRub**, possessing the bulky moieties linked directly to the tetracene core and expressing severely suppressed TTA. Regretfully, suppressed SF and enhanced Φ_{FL} in **core-*t*BRub** films cannot counterbalance considerably restricted TET and TTA efficiencies, thus making the core-linking of rubrenes unfavorable for TTA-UC. Although the TTA efficiency in **peri-*t*BRub** films is almost as good as that of **Rub** films, the poor TET from the **PdPc** sensitizer, and subsequently low Φ_{UC}, leaves room for improvement. Possibly, the improvement in TET could be achieved by combining **peri-*t*BRub** with some another sensitizer featuring a longer triplet lifetime compared to **PdPc**. This should enable TET channel to compete with the triplet ground state relaxation.[57] Another possibility could be substituting butoxy and/or phenoxy peripheral groups in **PdPc** sensitizer with less bulky groups, as this should reduce its steric crowding (and intermolecular distance), thereby also enhancing TET.

Conclusions

In this work, structurally modified rubrene emitters possessing 3,5-di-*tert*-butylphenyl side-moieties were investigated as potential TTA emitters and an alternative to conventional rubrene for sensitized UC. Transient absorption spectroscopy and delayed FL analysis revealed significant differences in the SF-induced triplet production as well as TTA-promoted singlet generation throughout the series of emitters. The sterically demanding side-moieties at the periphery (**peri-*t*BRub**) and the core (**core-*t*BRub**) enabled to suppress detrimental SF and considerably enhance the emission efficiency (by a factor of 40) in the solid films compared to that in conventional rubrene films. The linking position of the bulky side groups was found to be pivotal for the TTA efficiency of these emitters, inferring huge advantage of the peripheral linking *vs.* core linking. Remarkably, the side-moieties at the periphery almost did not impede TTA, which was as efficient as that of unsubstituted rubrene, meanwhile the core-linked side-groups reduced TTA dramatically. The bottleneck for the low UC efficiency in the PdPc-sensitized **peri-*t*BRub** and **core-*t*BRub** systems, both in solution and solid state, was mainly determined to be the poor TET from the sensitizer. The obtained results imply the core-linking of rubrenes with sterically demanding moieties to be unfavorable for TTA-UC, whereas peripheral linking (as in ***t*BRub** and **peri-*t*BRub**) much more promising. The results also suggest a clear trade-off between suppressed SF and enhanced TTA in the rubrene emitters, which needs to be addressed *via* careful selection of the degree of sterical hindrance and linking position of the side-moieties. We believe this study will stimulate further research and design optimization of the rubrene TTA emitters towards improved NIR-to-vis UC performance in the solid state.

Experimental section

Materials

Rubrene (**Rub**) was purchased from TCI. Polystyrene (PS) was purchased from Sigma-Aldrich. The synthesis of ***t*BRub** and palladium phthalocyanine (**PdPc**) was published elsewhere.[44] Synthesis of **peri-*t*BRub** and **core-*t*BRub** can be found in the ESI.†

Preparation of the upconverting films

All samples were prepared using toluene solvent. The rubrenes (**Rub**, ***t*BRub**, **peri-*t*BRub**, **core-*t*BRub**) were dissolved to produce concentrated stock solutions (10 mg mL^{-1}), while in the case of the sensitizer **PdPc** and polystyrene, concentrations of 1 mg mL^{-1} and 50 mg mL^{-1} were used, respectively. The corresponding stock solutions were used to prepare: dilute emitter solutions (10^{-5} M), upconverting **peri-*t*BRub** and **core-*t*BRub** solutions with 18 mM of emitter and 15 μM of **PdPc** sensitizer, PS films doped with **peri-*t*BRub** and **core-*t*BRub** at concentrations ranging from 0.01 wt% to 100 wt% (neat films), upconverting neat films doped with 0.1 wt% of **PdPc** sensitizer. Here, wt% is defined as a weight percentage relative to the total weight content of the mixture. Films were formed by spin-coating at 2500 rpm for 1 min on 1 mm-thick 25 × 25 mm microscope glass slides. PS films containing low emitter concentration ($<$1 wt%) were drop-casted to produce thicker layers. All the samples were prepared in the glovebox under nitrogen atmosphere with O_2 and H_2O concentrations below 0.1 ppm.

The prepared films were encapsulated inside the glovebox using 2-component epoxy resin and an additional glass cover on top. The encapsulation was essential to protect the films from triplet quenching by oxygen as well as to avoid photoinduced degradation of the rubrenes in ambient conditions.[36] The photostability data of the studied rubrene neat films is provided in Fig. S7 in the ESI.†

Optical techniques

Absorption spectra of the dilute solutions of the rubrene compounds were recorded using a UV-vis-NIR spectrophotometer Lambda 950 (PerkinElmer). Fluorescence (FL) of the samples was excited at 485 nm either by using a 150 W xenon arc lamp (Oriel) coupled to a monochromator (Sciencetech), or by utilizing continuous-wave semiconductor laser diode (Picoquant). Photon upconversion (UC) was induced by exciting at 730 nm using a 12 mW power continuous-wave semiconductor laser diode (Picoquant). Steady state FL and UC emission spectra were measured using a back-thinned CCD spectrometer PMA-12 (Hamamatsu). Fluorescence transients of the samples were measured by using a time-correlated single photon counting system PicoHarp 300 (Picoquant), which utilized a pulsed semiconductor laser diode (wavelength – 485 nm, pulse duration – 70 ps, repetition rate – 1 MHz) as an excitation source. Additionally, long-lasting FL and UC transients were measured with time-gated iCCD camera New iStar DH340T (Andor) after exciting the samples with emission of tunable-wavelength optical amplifier (Ekspla) pumped by a nanosecond Nd^{3+}:YAG laser (wavelength – 485 nm or 730 nm, pulse duration – 5 ns, repetition rate – 1 kHz). FL quantum yields (Φ_{FL}) were estimated by utilizing an integrating sphere[58] (Sphere Optics) coupled to the CCD spectrometer PMA-12 *via* an optical fiber; the xenon arc lamp was used as an excitation source. Φ_{UC} was estimated by comparing the integral of UC spectrum (I_{UC}) with that of FL spectrum of PdPc sensitizer (I_{FL}) serving as an internal reference.[44] Since Φ_{FL} of the sensitizer is known, Φ_{UC} was simply obtained from the following relation

$$\Phi_{UC} = \frac{I_{UC}}{I_{FL}}\Phi_{FL}.$$

For strong UC signals both integrating sphere and comparative methods were used to ensure the reliability of the obtained values.

Femtosecond transient absorption measurements were carried out using spectrometer Harpia pumped with a pulsed femtosecond laser Pharos and parametric amplifier system Orpheus (Light Conversion). Excitation wavelength was set to 385 nm. Probe source was white light continuum (WLC) pulses generated by focusing the fundamental harmonic 1030 nm into the water-filled quartz cuvette, which resulted in the broad WLC ranging from 380 nm to 1200 nm. The probe pulses were recorded using the linear CCD sensor (Hamamatsu). All the experiments were performed at room temperature.

Author contributions

Edvinas Radiunas – investigation, formal analysis, writing – original draft. Manvydas Dapkevičius – investigation. Lukas Naimovičius – investigation. Paulius Baronas – investigation. Steponas Raišys – methodology, formal analysis. Saulius Juršėnas – formal analysis, resources. Augustina Jozeliūnaitė – investigation, methodology. Tomas Javorskis – methodology, data curation. Ugnė Šinkevičiūtė – investigation. Edvinas Orentas – validation, supervision, resources. Karolis Kazlauskas – conceptualization, supervision, writing – review & editing, funding acquisition, project administration.

Conflicts of interest

There are no conflicts to declare.

Acknowledgements

The research was funded by a grant (no. S-MIP-17-77) from the Research Council of Lithuania (LMTLT).

Notes and references

1 B. D. Ravetz, A. B. Pun, E. M. Churchill, D. N. Congreve, T. Rovis and L. M. Campos, *Nature*, 2019, **565**, 343–346.

2 R. S. Khnayzer, J. Blumhoff, J. A. Harrington, A. Haefele, F. Deng and F. N. Castellano, *Chem. Commun.*, 2011, **48**, 209–211.

3 A. L. Hagstrom, S. Weon, W. Choi and J.-H. Kim, *ACS Appl. Mater. Interfaces*, 2019, **11**, 13304–13318.

4 Y. I. Park, K. T. Lee, Y. D. Suh and T. Hyeon, *Chem. Soc. Rev.*, 2015, **44**, 1302–1317.

5 J. Pedrini and A. Monguzzi, *J. Photonics Energy*, 2017, **8**, 022005.

6 L. Frazer, J. K. Gallaher and T. W. Schmidt, *ACS Energy Lett.*, 2017, **2**, 1346–1354.

7 T. F. Schulze and T. W. Schmidt, *Energy Environ. Sci.*, 2015, **8**, 103–125.

8 V. Gray, K. Moth-Poulsen, B. Albinsson and M. Abrahamsson, *Coord. Chem. Rev.*, 2018, **362**, 54–71.

9 A. Khare, *J. Alloys Compd.*, 2019, 153214.

10 Y. Y. Cheng, B. Fückel, R. W. MacQueen, T. Khoury, R. G. C. R. Clady, T. F. Schulze, N. J. Ekins-Daukes, M. J. Crossley, B. Stannowski, K. Lips and T. W. Schmidt, *Energy Environ. Sci.*, 2012, **5**, 6953–6959.

11 R. A. S. Ferreira, S. F. H. Correia, A. Monguzzi, X. Liu and F. Meinardi, *Mater. Today*, 2020, **33**, 105–121.

12 J. C. Goldschmidt and S. Fischer, *Adv. Opt. Mater.*, 2015, **3**, 510–535.

13 L. Nienhaus, N. Geva, J.-P. Correa-Baena, M. Wu, S. Wieghold, V. Bulović, T. V. Voorhis, M. A. Baldo, T. Buonassisi and M. G. Bawendi, *7th World Conference on Photovoltaic Energy Conversion (WCPEC)*, 2018, pp. 3698–3702.

14 J. Zhou, Q. Liu, W. Feng, Y. Sun and F. Li, *Chem. Rev.*, 2015, **115**, 395–465.

15 P. Bharmoria, H. Bildirir and K. Moth-Poulsen, *Chem. Soc. Rev.*, 2020, **49**, 6529–6554.

16 L. Huang, Y. Zhao, H. Zhang, K. Huang, J. Yang and G. Han, *Angew. Chem., Int. Ed.*, 2017, **56**, 14400–14404.

17 Q. Liu, W. Wang, C. Zhan, T. Yang and D. S. Kohane, *Nano Lett.*, 2016, **16**, 4516–4520.

18 L. Huang, L. Zeng, Y. Chen, N. Yu, L. Wang, K. Huang, Y. Zhao and G. Han, *Nat. Commun.*, 2021, **12**, 122.

19 D. Yildiz, C. Baumann, A. Mikosch, A. J. C. Kuehne, A. Herrmann and R. Göstl, *Angew. Chem., Int. Ed.*, 2019, **58**, 12919–12923.

20 S.-W. Liu, C.-C. Lee, C.-H. Yuan, W.-C. Su, S.-Y. Lin, W.-C. Chang, B.-Y. Huang, C.-F. Lin, Y.-Z. Lee, T.-H. Su and K.-T. Chen, *Adv. Mater.*, 2015, **27**, 1217–1222.

21 Y. Zhou, S.-T. Han, X. Chen, F. Wang, Y.-B. Tang and V. A. L. Roy, *Nat. Commun.*, 2014, **5**, 4720.

22 T. Jia, Q. Wang, M. Xu, W. Yuan, W. Feng and F. Li, *Chem. Commun.*, 2021, **57**, 1518–1521.

23 K. M. Felter, M. C. Fravventura, E. Koster, R. D. Abellon, T. J. Savenije and F. C. Grozema, *ACS Energy Lett.*, 2019, 124–129.

24 M. Wu, D. N. Congreve, M. W. B. Wilson, J. Jean, N. Geva, M. Welborn, T. Van Voorhis, V. Bulović, M. G. Bawendi and M. A. Baldo, *Ant. Photonics*, 2016, **10**, 31–34.

25 M. Wu, J. Jean, V. Bulović and M. A. Baldo, *Appl. Phys. Lett.*, 2017, **110**, 211101.

26 S. Amemori, Y. Sasaki, N. Yanai and N. Kimizuka, *J. Am. Chem. Soc.*, 2016, **138**, 8702–8705.

27 L. Nienhaus, J.-P. Correa-Baena, S. Wieghold, M. Einzinger, T.-A. Lin, K. E. Shulenberger, N. D. Klein, M. Wu, V. Bulović, T. Buonassisi, M. A. Baldo and M. G. Bawendi, *ACS Energy Lett.*, 2019, **4**, 888–895.

28 L. Nienhaus, M. Wu, N. Geva, J. J. Shepherd, M. W. B. Wilson, V. Bulović, T. Van Voorhis, M. A. Baldo and M. G. Bawendi, *ACS Nano*, 2017, **11**, 7848–7857.

29 A. Abulikemu, Y. Sakagami, C. Heck, K. Kamada, H. Sotome, H. Miyasaka, D. Kuzuhara and H. Yamada, *ACS Appl. Mater. Interfaces*, 2019, **11**, 20812–20819.

30 Y. Zhou, F. N. Castellano, T. W. Schmidt and K. Hanson, *ACS Energy Lett.*, 2020, 2322–2326.

31 S. Hoseinkhani, R. Tubino, F. Meinardi and A. Monguzzi, *Phys. Chem. Chem. Phys.*, 2015, **17**, 4020–4024.

32 C. J. Imperiale, P. B. Green, E. G. Miller, N. H. Damrauer and M. W. B. Wilson, *J. Phys. Chem. Lett.*, 2019, **10**, 7463–7469.

33 S. N. Sanders, M. K. Gangishetty, M. Y. Sfeir and D. N. Congreve, *J. Am. Chem. Soc.*, 2019, 9180–9184.

34 K. J. Fallon, E. M. Churchill, S. N. Sanders, J. Shee, J. L. Weber, R. Meir, S. Jockusch, D. R. Reichman, M. Y. Sfeir, D. N. Congreve and L. M. Campos, *J. Am. Chem. Soc.*, 2020, **142**, 19917–19925.

35 V. Yakutkin, S. Aleshchenkov, S. Chernov, T. Miteva, G. Nelles, A. Cheprakov and S. Baluschev, *Chem. – Eur. J.*, 2008, **14**, 9846–9850.

36 T. N. Singh-Rachford and F. N. Castellano, *J. Phys. Chem. A*, 2008, **112**, 3550–3556.

37 Y. Y. Cheng, T. Khoury, R. G. C. R. Clady, M. J. Y. Tayebjee, N. J. Ekins-Daukes, M. J. Crossley and T. W. Schmidt, *Phys. Chem. Chem. Phys.*, 2009, **12**, 66–71.

38 Y. Y. Cheng, B. Fückel, T. Khoury, R. G. C. R. Clady, M. J. Y. Tayebjee, N. J. Ekins-Daukes, M. J. Crossley and T. W. Schmidt, *J. Phys. Chem. Lett.*, 2010, **1**, 1795–1799.

39 J. Han, F. Zhang, J. You, Y. Hiroaki, S. Yamada, T. Morifuji, S. Wang and X. Li, *Photochem. Photobiol. Sci.*, 2017, **16**, 1384–1390.

40 A. S. Bieber, Z. A. VanOrman, S. Wieghold and L. Nienhaus, *J. Chem. Phys.*, 2020, **153**, 084703.

41 Y. Che, W. Yang, G. Tang, F. Dumoulin, J. Zhao, L. Liu and Ü. İşci, *J. Mater. Chem. C*, 2018, **6**, 5785–5793.

42 L. Huang, W. Wu, Y. Li, K. Huang, L. Zeng, W. Lin and G. Han, *J. Am. Chem. Soc.*, 2020, **142**, 18460–18470.

43 A. B. Pun, L. M. Campos and D. N. Congreve, *J. Am. Chem. Soc.*, 2019, **141**, 3777–3781.

44 E. Radiunas, S. Raišys, S. Juršėnas, A. Jozeliūnaitė, T. Javorskis, U. Šinkevičiūtė, E. Orentas and K. Kazlauskas, *J. Mater. Chem. C*, 2020, **8**, 5525–5534.

45 E. Radiunas, M. Dapkevičius, S. Raišys, S. Juršėnas, A. Jozeliūnaitė, T. Javorskis, U. Šinkevičiūtė, E. Orentas and K. Kazlauskas, *Phys. Chem. Chem. Phys.*, 2020, **22**, 7392–7403.

46 X. Wang, R. Tom, X. Liu, D. N. Congreve and N. Marom, *J. Mater. Chem. C*, 2020, **8**, 10816–10824.

47 Y. Chen, B. Lee, D. Fu and V. Podzorov, *Adv. Mater.*, 2011, **23**, 5370–5375.

48 D. M. Finton, E. A. Wolf, V. S. Zoutenbier, K. A. Ward and I. Biaggio, *AIP Adv.*, 2019, **9**, 095027.

49 E. M. Gholizadeh, S. K. K. Prasad, Z. L. Teh, T. Ishwara, S. Norman, A. J. Petty, J. H. Cole, S. Cheong, R. D. Tilley, J. E. Anthony, S. Huang and T. W. Schmidt, *Nat. Photonics*, 2020, 1–6.

50 A. Monguzzi, R. Tubino, S. Hoseinkhani, M. Campione and F. Meinardi, *Phys. Chem. Chem. Phys.*, 2012, **14**, 4322–4332.

51 L. Ma, K. Zhang, C. Kloc, H. Sun, M. E. Michel-Beyerle and G. G. Gurzadyan, *Phys. Chem. Chem. Phys.*, 2012, **14**, 8307–8312.

52 C. Rothe and A. P. Monkman, *Phys. Rev. B: Condens. Matter Mater. Phys.*, 2003, **68**, 075208.

53 S. Raišys, K. Kazlauskas, S. Juršėnas and Y. C. Simon, *ACS Appl. Mater. Interfaces*, 2016, **8**, 15732–15740.

54 S. Raišys, S. Juršėnas, Y. C. Simon, C. Weder and K. Kazlauskas, *Chem. Sci.*, 2018, **9**, 6796–6802.

55 V. Jankus, E. W. Snedden, D. W. Bright, E. Arac, D. Dai and A. P. Monkman, *Phys. Rev. B: Condens. Matter Mater. Phys.*, 2013, **87**, 224202.

56 A. I. Shushin, *J. Chem. Phys.*, 2019, **151**, 034103.

57 Y. Sasaki, M. Oshikawa, P. Bharmoria, H. Kouno, A. Hayashi-Takagi, M. Sato, I. Ajioka, N. Yanai and N. Kimizuka, *Angew. Chem., Int. Ed.*, 2019, **58**, 17827–17833.

58 J. C. de Mello, H. F. Wittmann and R. H. Friend, *Adv. Mater.*, 1997, **9**, 230–232.

PIV

Efficient NIR-to-vis photon upconversion in binary rubrene films deposited by simplified thermal evaporation

Edvinas Radiunas, Lukas Naimovičius, Steponas Raišys, Augustina Jozeliūnaitė, Edvinas Orentas, Karolis Kazlauskas.

Physical Chemistry Chemical Physics, **10**(16), 6314-6322, (2022)

10.1039/D1TC05332A

Journal of
Materials Chemistry C

ROYAL SOCIETY
OF CHEMISTRY

PAPER

View Article Online
View Journal | View Issue

Check for updates

Cite this: *J. Mater. Chem. C*, 2022, 10, 6314

Efficient NIR-to-vis photon upconversion in binary rubrene films deposited by simplified thermal evaporation†

Edvinas Radiunas,[a] Lukas Naimovičius,[a] Steponas Raišys,[a]
Augustina Jozeliūnaitė,[b] Edvinas Orentas[b] and Karolis Kazlauskas*[a]

Received 4th November 2021,
Accepted 14th March 2022

DOI: 10.1039/d1tc05332a

rsc.li/materials-c

Low-power NIR-to-vis upconversion (UC) of incoherent excitation mediated by triplet–triplet annihilation (TTA) has a variety of promising applications, *e.g.* in photovoltaics; however, these are strongly hampered by low UC efficiency in the solid state. The issue is mainly related to the most efficient rubrene annihilator (emitter) utilized for this spectral range, which experiences severe concentration quenching in films due to singlet fission (SF). Herein, a simplified thermal evaporation technique is introduced to alter the morphology of binary rubrene films without involving a singlet sink aiming to suppress SF and boost UC efficiency. Hot-plate evaporation of rubrene under ambient nitrogen on a Peltier-cooled substrate pre-coated with a sensitizer layer is demonstrated to significantly improve the FL quantum yield and triplet energy transfer after annealing, subsequently ramping UC quantum yield up to (1.2 ± 0.15)% (out of maximum 50%). This is at least twice as high as that found in any other binary NIR-UC film reported so far. Moreover, we find that the statistical probability (*f* factor) of producing a singlet from two triplets *via* TTA in amorphous rubrene films (f = 19.5%) is close to that estimated for rubrene in a solution. This finding infers a maximum UC yield of $1/2 \times f \approx 10\%$ and explains why there are no reports on rubrene UC systems exceeding this value.

Introduction

Growing research interest in photon energy upconversion (UC) attainable in organic materials *via* triplet–triplet annihilation (TTA) is stimulated by promising applications in photocatalysis,[1–3] bioimaging,[4] photovoltaics,[5–14] targeted drug delivery,[15,16] *etc.*[17–19] The inherent ability of TTA-UC to be driven by incoherent irradiation and at low power densities ($\sim$mW cm^{-2})[5,7,20] implies great opportunities for solar energy harvesting, since poorly utilized near-infrared (NIR) photons in solar cells can be readily converted into the visible radiation and reused thereafter for photocurrent generation.[5,7] The general energy scheme depicting energy transfer processes in a typical TTA-UC system is shown in Fig. 1. Usually, TTA-UC is realized in binary systems composed of a sensitizer and an annihilator (emitter). The sensitizer is responsible for low energy photon absorption into the singlet state, conversion of the singlet excitation to triplet *via* intersystem crossing (ISC) and triplet energy transfer (TET) to the emitter. Meanwhile, the emitter ensures triplet migration until the two of them meet, promoting one of the triplets to a higher-energy singlet state *via* TTA. The whole process is finalized by the UC emission from the singlet state. Considering that each intermediate energy transfer step contributes to the UC quantum yield (ϕ_{UC}), it can be expressed as[14,21,22]

$$\phi_{\mathrm{UC}} = \frac{1}{2} f \phi_{\mathrm{ISC}} \phi_{\mathrm{TET}} \phi_{\mathrm{TTA}} \phi_{\mathrm{FL}}. \qquad (1)$$

Here f is a statistical factor representing the probability of obtaining a singlet from two triplets *via* TTA.[14,22–24] ϕ_{FL} is a fluorescence quantum yield of an emitter. We note that the maximum ϕ_{UC} is limited to 50%, because during the TTA, at most one UC photon can be produced per two absorbed ones.[21,25]

Challenging practical TTA-UC applications, such as in photovoltaics, demand high NIR-to-vis UC efficiency, preferably in the solid state.[8,26] A fulfilment of the latter requirement remains an important issue that many research groups aim to overcome. It is evident that the vast majority of demonstrated solid-state UC systems operating in the NIR range (>700 nm) usually express very low ϕ_{UC}, typically <1%.[14,26–32]

---

[a] *Institute of Photonics and Nanotechnology, Vilnius University, Saulėtekio av. 3, LT-10257 Vilnius, Lithuania. E-mail: karolis.kazlauskas@ff.vu.lt*

[b] *Institute of Chemistry, Faculty of Chemistry and Geosciences, Vilnius University, Naugarduko 24, LT-03225 Vilnius, Lithuania*

† Electronic supplementary information (ESI) available. See DOI: 10.1039/d1tc05332a

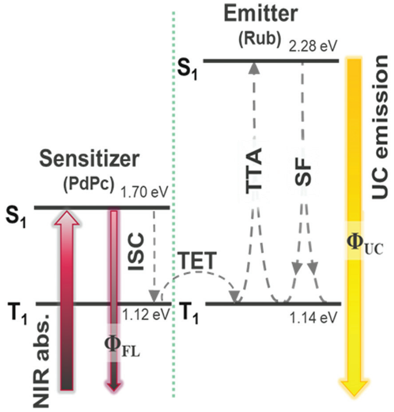

Fig. 1 TTA-UC energy scheme of Rub/PdPc with the corresponding energy transfer processes. ISC – intersystem crossing, TET – triplet energy transfer, TTA – triplet–triplet annihilation, SF – singlet fission, UC – upconversion.

Commonly exploited TTA emitters for the NIR spectral range are tetracenes,[33–35] rubrenes,[24,30,31,36–40] perylenes[26,41] or diketopyrrolopyrroles.[42] Most of these emitters are efficient in the liquid environment. Meanwhile, there is a lack of emitters with a low lying triplet-state that are fluorescent in the solid state.[14] The best-performing NIR-to-vis UC systems demonstrated so far, both in solution and the solid state, rely on the rubrene (**Rub**) emitter.[14]

Previously, we demonstrated that in the **Rub**-based UC solutions ϕ_{UC} is limited to ~7.8% due to the relatively low f factor (~15.6%).[22] In the solid-state, however, **Rub** additionally suffers from severe concentration quenching mainly attributed to singlet fission (SF), which results in a more than 60-fold drop in the fluorescence quantum yield (ϕ_{FL}). Thus, even the most efficient **Rub**-based UC films typically demonstrate one or two orders of magnitude lower ϕ_{UC} compared to those of UC solutions, where ϕ_{FL} of **Rub** is almost unity.

Generally, SF related losses can be mitigated by using two approaches, *i.e.* (i) molecular engineering, which relies on the chemical modification of the existing emitters or the introduction of alternative ones; and (ii) physical engineering based on altering the UC film composition or morphology.

Previously, we utilized a molecular engineering approach to introduce *t*-butyl substituents into **Rub** and improve the NIR-to-vis ϕ_{UC} in the solid films.[43] It was also revealed that **Rub** modifications at the periphery do not inhibit TTA step; however, substituents linked directly to the tetracene core suppress TTA dramatically.[44] The standard physical engineering approach to combat low ϕ_{FL} in **Rub** films and mitigate SF is to introduce the third component, *i.e.* a singlet exciton sink (collector), dibenzotetraphenylperiflanthene (DBP). Doping **Rub** films with a low concentration of DBP was reported to boost ϕ_{FL} by a factor of 20 due to the efficient FRET of upconverted singlets from **Rub** to DBP.[27,45] Yet, the potential for altering the UC film morphology by employing different preparation techniques to address low ϕ_{UC} issues was not exploited to the fullest extent.

In this work, we demonstrate the potential of the physical engineering approach to boost the UC efficiency in the binary emitter/sensitizer films without involving an exciton sink. To prepare UC films, we introduce a simplified thermal evaporation technique (using a hot plate) in an inert atmosphere. The highly concentrated **Rub** films obtained in this way display an order of magnitude higher fluorescence quantum yield (ϕ_{FL}) compared to the films produced by solution-processing or sophisticated thermal deposition in a vacuum. Furthermore, we show that in these films the sensitizer and emitter are well dispersed and intermixed to result in an efficient triplet energy transfer (ϕ_{TET}). The improved ϕ_{FL} along with the efficient ϕ_{TET} results in a record-high ϕ_{UC} of the **Rub**-based binary solid-state systems, which is at least twice as high as that obtained in any other binary NIR-UC film reported so far.[14,32,46]

Experimental

Materials

Rubrene (**Rub**) was purchased from TCI. Polystyrene (PS) was purchased from Sigma-Aldrich. The synthesis of palladium phthalocyanine (**PdPc**) was published elsewhere.[22]

Optical techniques

The absorption spectra of the investigated samples were recorded using a UV-vis-NIR spectrophotometer Lambda 950 (PerkinElmer). Fluorescence (FL) of the samples was excited at 485 nm either by using a 150 W xenon arc lamp (Oriel) coupled to a monochromator (Sciencetech), or by utilizing a continuous-wave semiconductor laser diode (Picoquant). Photon upconversion (UC) was induced by exciting at 730 nm using a 12 mW power continuous-wave semiconductor laser diode (Picoquant). Steady state FL and UC emission spectra were measured using a back-thinned CCD spectrometer PMA-12 (Hamamatsu). Fluorescence transients of the samples were measured by using a time-correlated single photon counting system PicoHarp 300 (Picoquant), which utilized a pulsed semiconductor laser diode (wavelength – 485 nm, pulse duration – 70 ps, repetition rate – 1 MHz) as an excitation source. Phosphorescence spectra in the NIR range were measured using a water-cooled iDus InGaAs 1.7 array detector (Andor). FL quantum yields (ϕ_{FL}) were estimated by utilizing an integrating sphere (Sphere Optics) coupled to the CCD spectrometer PMA-12 *via* an optical fiber; the xenon arc lamp was used as an excitation source. ϕ_{UC} was estimated by comparing the integral of the UC spectrum with that of the FL spectrum of the **PdPc** sensitizer with known quantum yield, as described previously.[22] For strong UC signals both integrating sphere and comparative methods were used to ensure the reliability of the obtained values.

Results and discussion

Due to the low-lying triplet state (T_1) in the NIR region and $2 \times T_1$ close to the singlet energy (S_1) in the visible range, **Rub** became the standard emitter for NIR-to-vis photon upconversion.[14,27,28,31,32,47,48] In fact, by far there are almost no alternative emitters capable of delivering comparable performance in the solid-state.[14] Even though solution-processed **Rub** neat films have low ϕ_{FL} ($\sim$1%), other similar TTA emitters with low triplet energy ($T_1 < 1.2$ eV) are almost non-emissive, because of aggregation-caused quenching. Low ϕ_{FL} is disastrous, as it subsequently reduces ϕ_{UC} (eqn (1)). One of the main causes of low ϕ_{FL} in **Rub** films is singlet fission (SF), which is feasible due to the favorable energetics ($S_1 \approx 2 \times T_1$) of **Rub**. Lasting on a time-scale of picoseconds SF outcompetes radiative decay by opening the alternative deactivation channel for the singlets, *i.e.* splitting into two triplets. Depending on the local molecular environment, the emerged triplet pairs can rapidly undergo geminate triplet fusion or dissociate and either (i) decay non-radiatively, or (ii) diffuse and form encounter complexes at a much slower rate for non-geminate TTA.[23,45,49,50]

It is well known that SF-associated losses are strongly related to the degree of crystallinity of the **Rub** films. The crystallinity can be altered by varying film preparation conditions and probed by monitoring their optical properties.

To minimize SF, amorphous **Rub** films with a chaotic molecular orientation and large average intermolecular distance must be produced. Biaggio *et al.* successfully exploited molecular beam deposition in a high vacuum to obtain amorphous **Rub** films.[50] The films were virtually free from SF and showed mono-exponential fluorescence decay (τ = 16.4 ns) close to that of **Rub** in solution.[50]

In the current study, diverse deposition conditions of emitter **Rub** are investigated to assess the impact of emitter morphology on ϕ_{FL}, and correspondingly ϕ_{UC} in the solid films. Featuring an appropriate energy level alignment, palladium phthalocyanine (**PdPc**) was chosen as a triplet sensitizer for the **Rub.**[43] Fig. 2a and b illustrates the step-by-step fabrication of UC films under investigation. In the first step, the sensitizer layer composed of an optically inert polymer matrix doped with low concentration (0.1 wt%) of **PdPc** was formed by spin-coating (Fig. 2a). Then **Rub** was deposited on top by using one of the four distinct thermal evaporation modes to result in the formation of the UC film (Fig. 2b). In the vacuum deposition mode, controlled thermal evaporation in a high vacuum ($\sim 10^{-7}$ Torr) was used. This mode was previously reported to produce amorphous rubrene films and therefore served as a reference deposition mode.[50] The remaining three modes were based on a simplified thermal evaporation of **Rub** (using the hot-plate) in ambient nitrogen. In the cold deposition mode, rubrene molecules were deposited on a Peltier cooled (−10 °C) substrate (Fig. 2b). This mode is expected to instantly freeze emitter molecules on the substrate, thus producing amorphous films. Aiming to quantify the effect of substrate cooling, cold-deposited films were annealed at 100 °C defining the post-annealing mode. Lastly, **Rub** evaporation on an uncooled substrate (naturally heated due to the close proximity of the evaporation source) was named the hot deposition mode.

The UC films prepared at different conditions were initially evaluated by measuring FL transients and ϕ_{FL} (Fig. 3). The results clearly show high sensitivity to the **Rub** deposition mode. The FL transients consisted of the dominant prompt decay (fractional contribution of 70–90% to an overall decay) affected by SF and the minor slower decay component resembling natural decay of the isolated **Rub** species. The prompt

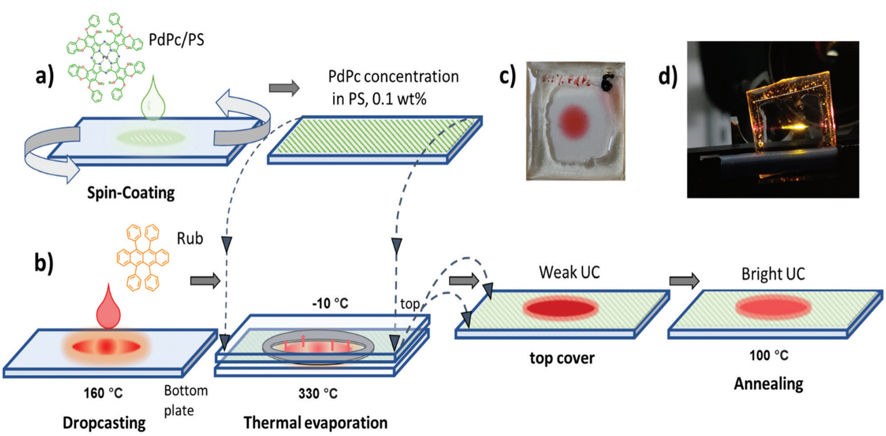

Fig. 2 Preparation of UC films. (a) Formation of sensitizer (**PdPc**)-doped PS layer by spin-coating; (b) deposition of emitter (**Rub**) by drop-casting stock solution (1 mg ml^{-1}) on a glass substrate followed by thermal evaporation of **Rub** on actively cooled (previously prepared) sensitizer layer (depicted as top glass). The final UC film is obtained by thermal annealing; (c) photo of the final UC film with the encapsulating epoxy visible on the edges; and (d) the UC film excited with a 730 nm CW laser.

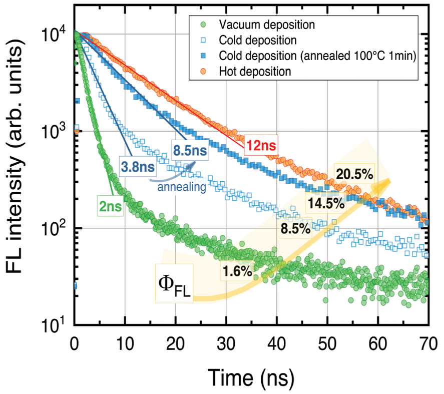

Fig. 3 FL transients of **Rub** films deposited on top of the sensitizer layer using different thermal evaporation modes (specified). Lines represent single-exponential fits of the dominant prompt decay components. FL lifetimes and quantum yields indicated.

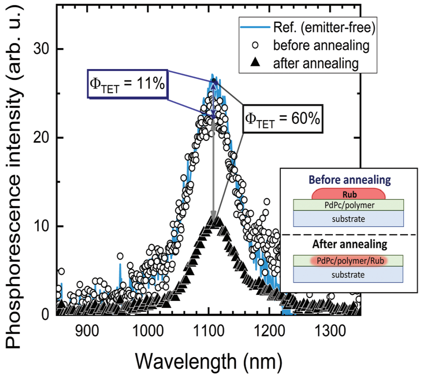

Fig. 4 **PdPc** phosphorescence spectra of the cold-deposited UC film before (circles) and after (triangles) annealing, and of the reference emitter-free film (solid line). TET{**PdPc** → **Rub**} efficiency of the untreated as well as annealed film is indicated. The inset schematically illustrates the UC film before and after annealing.

component was described by a single-exponential decay profile to determine excited state lifetime. The shorter FL lifetime suggested an enhanced SF, and hence, a reduced ϕ_{FL}.

In the case of vacuum-deposited films, rapid decay with τ = 2 ns and low ϕ_{FL} (1.6%) was obtained. This was unexpected, since a vacuum-deposition previously was reported to result in amorphous films[50] free from SF and with the FL lifetime similar to that of Rub in solution (τ = 16.4 ns).

Interestingly, prolonged decay (τ = 3.8 ns) as well as increased ϕ_{FL} up to 8.5% was obtained for the films fabricated using the cold deposition mode, indicating a more random molecular orientation and suppressed SF. Post-annealing of the UC films further extended the FL lifetime to 8.5 ns and improved ϕ_{FL} by almost 2-fold. Finally, the highest ϕ_{FL} of 20.5% along with the longest FL lifetime (τ = 12 ns) was determined for the films prepared in the hot deposition mode.

At first glance, the role of the heat treatment introduced during the film annealing or hot deposition is counterintuitive, since this is anticipated to facilitate **Rub** crystallization.[51] Excess energy supplied in the form of heat may suffice to rearrange and crystallize **Rub** causing the formation of non-radiative SF centers. We note that the annealing temperature was set to correspond to the glass transition temperature (T_g) of the PS polymer employed. However, excess heat during the annealing can also promote **Rub** diffusion into the bottom sensitizer layer thereby diluting it and suppressing aggregation-caused FL quenching (see the inset of Fig. 4). Likewise, the hot deposition mode may result in a deeper **Rub** diffusion and thus stronger dilution more resembling the behavior of isolated **Rub** species or that of the purely amorphous film.

Further investigation in support of molecular diffusion involved studying the UC properties of the films *via* NIR excitation (730 nm) of the sensitizer. The improvement of UC efficiency was expected to be in correspondence with that of ϕ_{FL}. Indeed, the films of the lowest ϕ_{FL} fabricated using vacuum deposition and cold deposition modes exhibited barely detectable UC. On the other hand, annealed and hot-deposited films displayed bright UC. This result can be rationalized by considering the differences in the triplet energy transfer efficiency ϕ_{TET} (eqn (1)). The big temperature contrast during the cold deposition implies the formation of a bilayer UC film featuring a distinct boundary between the sensitizer and the emitter. As a result, most of the sensitizer triplets are generated far from the emitter species implying that short-range Dexter-type TET can only occur in a narrow interface region. Meanwhile, the promoted molecular diffusion during the film annealing causes mixing of the sensitizer and the emitter, thus reducing intermolecular separation and enhancing TET{**PdPc** → **Rub**}. Scanning electron microscopy (SEM) images supporting the mixing of the sensitizer and the emitter after annealing are provided in ESI† (see Fig. S1 and S2 and explanation therein). The mixing was also verified by evaluating ϕ_{TET}, where we compared phosphorescence intensity from the sensitizer **PdPc** of the cold deposited UC films with the same films after annealing (Fig. 4). For reference, we also measured phosphorescence of the emitter-free film containing only the sensitizer layer (polymer doped with **PdPc**). The experimental conditions ensured identical concentrations of **PdPc** and the sensitizer layer thickness of the tested films, thus enabling the intermixing effect of **Rub** and **PdPc** on TET to be addressed explicitly. The most intense **PdPc** phosphorescence peaked at 1106 nm was observed for the emitter-free film, since no TET{**PdPc** → **Rub**} was possible. Cold-deposited films expressed just a slightly reduced phosphorescence intensity due to inefficient ϕ_{TET}, whereas this intensity for the annealed films was severely decreased as a result of enhanced TET{**PdPc** → **Rub**}. Considering that

$$\phi_{TET} = 1 - \frac{I}{I_0}, \qquad (2)$$

where I and I_0 are the phosphorescence intensities of the studied and the reference (emitter-free) films, respectively,[22,32] we estimated that ϕ_{TET} in the cold deposited UC films is up to 11%, whereas it reaches 60% in the annealed films. The obtained ϕ_{TET} in the annealed films was verified by performing phosphorescence measurements in the integrating sphere (see Fig. S3, ESI†). In this way, the light scattering effects of the films impacting the light outcoupling could be taken into account.

Spatial variations of **PdPc** phosphorescence intensity and ϕ_{TET} in the annealed films are presented in the ESI† (see Fig. S4 and explanation therein). Taking into account the simplified thermal evaporation technique employed for the fabrication of the UC films, the reproducible ϕ_{TET} values could be obtained within the central area of ~4 mm in size.

Even though the most efficient ϕ_{FL} was achieved using the hot deposition mode of **Rub**, the UC films prepared in this way had poor reproducibility. Specifically, **Rub** films were determined to be very sensitive to growth time and exhibited rapid crystallization already in the first growth stages (Fig. S5, ESI†). The morphological changes were accompanied by drastic spectral and FL decay time variations, *i.e.*, additional aggregate-related FL band started emerging at 740 nm and τ reduced from 5.3 ns to 0.27 ns indicating increasing domination of SF.

Taking into account the reproducibility issues in the hot-deposition mode, further UC performance optimization was carried out for the films prepared by cold deposition followed by annealing. This deposition mode permitted control of the **Rub** thickness avoiding crystallization and allowed for consistent results (Fig. S6a, ESI†). Unlike neat **Rub** films obtained by the same method and showing increasing crystallization within a few weeks after fabrication, UC films fabricated by depositing **Rub** on top of the sensitizer-doped polymer layer followed by annealing were found to be stable. No signs of crystallization were detected several months after fabrication (see Fig. S7, ESI†) where FL lifetimes of the films are shown to remain constant at least within 240 days after film deposition). We attribute this to the dilution of **Rub** within the polymer layer, and thus suppression of rubrene aggregation.

Rub film thickness of approximately 600 nm, which corresponded to 3 min evaporation time was found to be optimal based on the UC intensity measurements (Fig. S6b, ESI†). Post-annealing of the films performed at 100 °C for ~5 min yielded good film uniformity and bright UC emission, whereas longer annealing durations as well as higher temperatures induced strong crystallization (see Fig. S8, ESI†), and thus, were unacceptable for the UC film fabrication.

In the following UC optimization step, different sensitizer concentrations were tested while maintaining identical **Rub** deposition conditions (Fig. 5). Clearly, the increasing sensitizer concentration from 0.1 wt% to 5 wt% reduced the UC signal by 5 times suggesting enhanced upconverted energy back-transfer from **Rub** to **PdPc**. Although a higher sensitizer concentration is supposed to improve NIR absorption and reduce UC threshold, densely packed sensitizer molecules facilitate energy back-transfer diminishing the overall ϕ_{UC}.[52] Aiming to maximize UC efficiency, the lowest **PdPc** concentration (0.1 wt%) was selected for further optimization. In fact, even lower concentration should potentially lead to a higher ϕ_{UC}; however, the subsequently decreased sensitizer absorption and thereby significantly weakened UC signal would compromise reliability of the results.

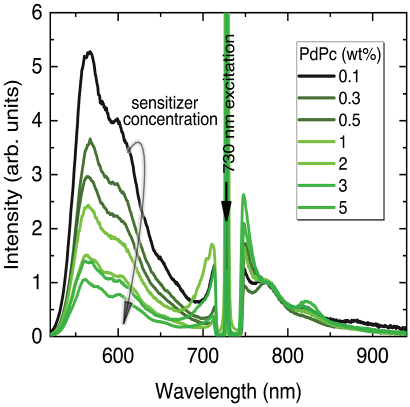

Fig. 5 UC emission spectra of **PdPc**/PS/**Rub** films with different **PdPc** concentrations. The spectra are normalized to the **PdPc** fluorescence maximum at 774 nm. **Rub** deposition conditions and **PdPc**-doped PS layer thickness (260 nm) were maintained the same. Excitation, 730 nm CW laser. A notch filter was used to suppress scattered excitation.

In the next step, the uniformity of the rubrene film deposited on top of **PdPc**-doped PS (sensitizer layer) was investigated. The measurements were carried out for different sensitizer layer thicknesses enabling the optimal one for maximal UC performance to be revealed. As discussed above, well mixed sensitizer and emitter films are required to have efficient ϕ_{TET} as well as high ϕ_{FL} of **Rub**. By assuming limited **Rub** diffusion into the sensitizer layer during the annealing, the too thick sensitizer layers could cause high absorption, yet likely reduced ϕ_{UC} due to lowered ϕ_{TET}. To verify this, we prepared a series of spin-coated sensitizer layers of different thickness, which was varied by altering mixture viscosity and spin coater speed. The film thickness was probed using AFM (see Fig. S9, ESI†). The **Rub** was deposited on top of the sensitizer layer through a circular metal spacer, forming a disk-shaped film (see the inset of Fig. 6). The prepared UC films were investigated by scanning across the surface in the x direction with the focused 730 nm laser beam and collecting the emission spectra as illustrated in Fig. 6.

The detailed scheme of this experiment is presented in Fig. S10 (ESI†). The measured spectra were analysed by discerning UC and $\mathrm{FL}_{\mathrm{PdPc}}$ spectral components peaking at 560 nm and 774 nm, respectively, and examining they relative intensities. Prior to $\mathrm{FL}_{\mathrm{PdPc}}$ analysis, the strong background signal due to the scattered excitation light and UC emission tail was subtracted.

The UC intensity was found to exhibit a steep increase by almost 3 orders of magnitude with the excitation spot moving

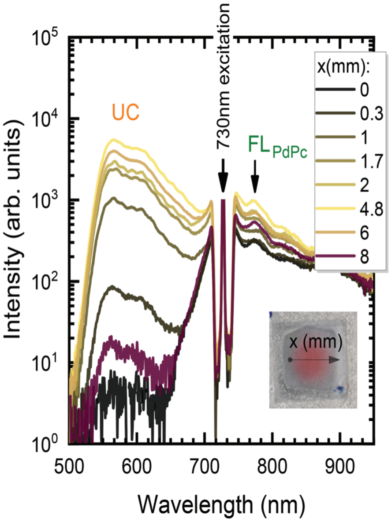

Fig. 6 Semi-log plot of UC emission spectra of PS:**PdPc**/**Rub** film measured at different excitation spots along *x* direction (indicated). Excitation, 730 nm. **PdPc** concentration in PS, 0.1 wt%. Sensitizer layer thickness, 110 nm. A picture of UC film is shown in the inset.

from the film edge to the centre (Fig. 7a). The intensity profile resembled Gaussian-like thickness distribution of the evaporated **Rub** and suggested that some critical thickness of the emitter is required to promote TTA in the **Rub** layer. Additionally, the sensitizer layer thickness of 110 nm was determined to be the optimal as giving rise to the highest UC intensity at these deposition conditions. Spatial distribution of FL intensity emanating from **PdPc** was found to be much more flat (Fig. 7b) in agreement with rather homogeneous sensitizer layers formed by spin-coating. These layers contained roughly the same amount of **PdPc** across the scanned area implying insignificant FL intensity variation *vs* the excitation coordinate. Taking into account that FL$_{\mathbf{PdPc}}$ is not affected by the presence of **Rub** due to the energy level alignment, FL$_{\mathbf{PdPc}}$ intensity should be proportional to the sensitizer layer thickness and **PdPc** concentration. Since the latter was fixed at 0.1 wt%, the thicker sensitizer layers (as more absorbing 730 nm radiation) resulted in the higher FL$_{\mathbf{PdPc}}$ intensity. Importantly, considering that ϕ_{FL} of **PdPc** is constant across the film, this intensity can be used as an internal reference for the UC signal, thereby enabling the judgement of ϕ_{UC} from the UC and FL$_{\mathbf{PdPc}}$ intensity ratio (Fig. 7c). For instance, although 25 nm and 500 nm-thick films showed similar UC intensity, the thicker films exhibited higher FL$_{\mathbf{PdPc}}$ intensity correspondingly implying lower ϕ_{UC}. Unfortunately, the FL$_{\mathbf{PdPc}}$ signal of 25 nm films was too weak to be measured; however, the data presented in Fig. 7c clearly suggest that thin sensitizer layers are more favorable for the realization of high ϕ_{UC}.

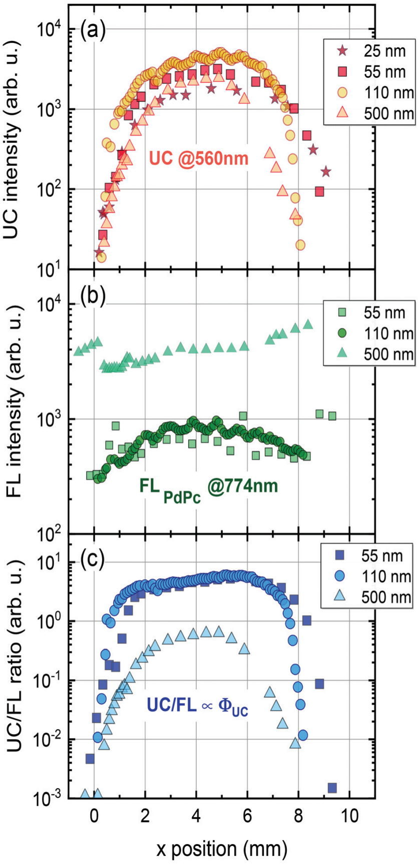

Fig. 7 (a) UC intensity at 560 nm, (b) FL intensity of **PdPc** at 774 nm and (c) UC/FL intensities ratio for different sensitizer layer thickness (indicated). Excitation, 730 nm. **PdPc** concentration in PS, 0.1 wt%. Each measurement was performed under the same conditions.

We note that the UC films with thin sensitizer layers (<100 nm) were difficult to measure as they were highly scattering and featured weak absorption, and hence, a relatively low UC intensity. These layers acted as a buffer for evaporated **Rub** and had a significant influence on the final UC film morphology. During the **Rub** deposition thin buffer experienced partial melting thereby forming a rough surface with enhanced scattering of the incident radiation. Taking this into account, a sensitizer layer thickness of 110 nm delivering one of the highest UC/FL$_{\mathbf{PdPc}}$ ratios was selected to be optimal for UC films. Measurement of UC intensity *vs* excitation power density for these UC films enabled to determine the UC threshold of 1.4 W cm^{-2} (Fig. S11, ESI†), which was found to be similar to those of other rubrene-based solid-state UC systems.[27,28,43,46] The optimized UC films were subjected to further evaluation of

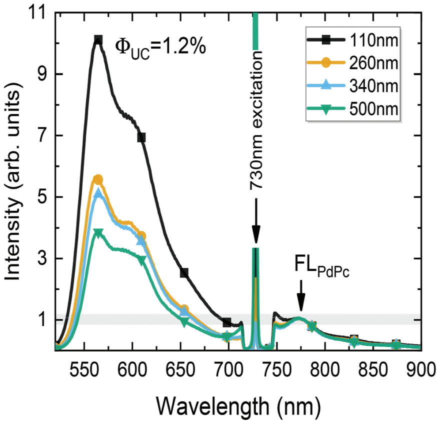

Fig. 8 UC spectra of the optimized PS:**PdPc**/**Rub** films with different sensitizer layer thicknesses (indicated). The spectra are normalized to $FL_{\mathbf{PdPc}}$ peak intensity (at 774 nm) so that UC intensity would correspond to ϕ_{UC}. Excitation wavelength and density, 730 nm and 100 W cm^{-2}, respectively.

ϕ_{UC} by using the $FL_{\mathbf{PdPc}}$ signal as an internal quantum yield reference (Fig. 8) as well as by means of an integrating sphere. The methodological details for the determination of ϕ_{UC} using an internal reference are provided in the ESI.†

Fig. 8 illustrates the UC spectrum of the optimized UC film containing a 110 nm-thick sensitizer layer. Additional spectra of UC films with varying sensitizer layer thickness, prepared under otherwise the same conditions, are also shown for comparison. The UC spectra were normalized to the $FL_{\mathbf{PdPc}}$ peak intensity so that UC intensity would correspond to ϕ_{UC}, as discussed earlier. Based on the independent measurements of UC films with different sensitizer layer thicknesses, yet with a fixed **PdPc** concentration of 0.1 wt%, the FL quantum yield of **PdPc** was determined (ϕ_{FL}^{PdPc} = 0.1%). The reproducibility data of ϕ_{FL}^{PdPc} tested for different films are included in the ESI.† Essentially, the data confirmed the average ϕ_{FL}^{PdPc} to be 0.1% with a standard deviation of 0.03%.

Using this value as an internal reference, we could roughly deduce ϕ_{UC} to increase from 0.4% to 1% with decreasing sensitizer layer thickness from 500 to 110 nm (Fig. 8). The obtained ϕ_{UC} were confirmed by the measurements in the integrating sphere, where the most efficient UC film exhibited ϕ_{UC} = (1.2 ± 0.15)% (out of maximum 50%).

A slight underestimation of ϕ_{UC} by using an internal reference method can be explained by the strong background signal in the spectral region of $FL_{\mathbf{PdPc}}$ due to the intense long-wavelength tail of UC emission. The accurate subtraction of such a strong background is complicated, which results in artificially increased $FL_{\mathbf{PdPc}}$ intensity, and subsequently, somewhat reduced ϕ_{UC}. The calculated relative error for ϕ_{UC} in the case of the internal reference method was 32% (see the ESI†) implying that ϕ_{UC} values obtained by both methods agree well within these errors.

ϕ_{UC} of (1.2 ± 0.15)% attained in this work represents a 17-fold improvement over our previous spin-coated DBP-doped rubrene films[43] and at least a 2-fold improvement in respect to the most efficient binary rubrene-based solid-state systems reported to date ($\phi_{UC} \approx$ 0.3–0.5%).[14,29,46]

We also note that the obtained ϕ_{UC} of the binary film approaches the highest efficiency value (ϕ_{UC} = 2%) achieved for the ternary UC film, additionally containing the DBP exciton sink.[46] This reduces the gap in the performance of binary and ternary systems, minimizing the demand for the third component (singlet exciton sink) and stressing the importance of the UC film morphology rather than energetics of individual molecules.

Inserting the maximum efficiency values of the energy transfer/conversion processes determined for our UC films in eqn (1), the probability factor *f* for rubrene in the solid state can be estimated. Thus, taking into consideration that ϕ_{FL} = 20.5% (Fig. 3), ϕ_{TET} = 60% (Fig. 4), and ϕ_{ISC} = 100% for palladium phthalocyanine-based sensitizers,[22,39,41] $\phi_{TTA} \approx$ 100% in the TTA domination regime and that the maximal ϕ_{UC} = 1.2%, the statistical probability *f* to generate a singlet from two triplets *via* TTA is 19.5%. The confirmation for the deactivation occurring totally through the second-order path ($\phi_{TTA} \approx$ 100%) achieved under excitation density of 100 W cm^{-2}, *i.e.*, well exceeding UC threshold is provided in the ESI.†

Interestingly, the obtained *f* factor is close to that estimated for rubrene in a solution (15.5%).[22] This can be justified by the similar energy level alignment of rubrene in the different environment (solution or amorphous-like film) supporting the finding that the statistical probability of creating a singlet from two triplets *via* TTA should be in the range of 15–20%. We note that *f* estimated by us in the TTA-dominating conditions under continuous-wave excitation is 3–4 times lower as compared to that obtained under femtosecond pulsed-laser excitation conditions.[38] The obtained *f* value implies a maximum ϕ_{UC} of $1/2 \times f \approx$ 10% for rubrene UC systems, which is reasonable, since no higher ϕ_{UC} has been demonstrated so far.[14,27–32,46,53]

Conclusions

In summary, this work addresses the low UC quantum yield issue in binary emitter/sensitizer films with rubrene serving as the annihilator (emitter). The issue is known to be related to detrimental singlet fission (SF) in highly concentrated rubrene films causing dramatic degradation of the FL quantum yield and subsequent reduction of UC efficiency. To cope with this problem, we offer an altering UC film morphology by exploiting different rubrene deposition techniques so as to suppress SF-promoting rubrene crystallization. From a variety of deposition modes explored, the simplified thermal evaporation of rubrene in ambient nitrogen using a hot plate delivered the features (highest FL quantum yield and longest FL lifetime) that most resemble those of an amorphous rubrene film. Explicitly, rubrene evaporation on a Peltier-cooled substrate pre-coated with a sensitizer layer and later annealing resulted in enhanced

FL quantum yield ($\phi_{FL} \approx 15\%$) and triplet energy transfer ($\phi_{TET} = 60\%$), which enabled reaching a record-high NIR-to-vis UC quantum yield of $(1.2 \pm 0.15)\%$ (out of a maximum of 50%). The attained UC yield is at least 2-fold higher than for any other binary UC film reported so far that is capable of upconverting NIR radiation (>700 nm). Furthermore, the f factor describing the probability for a singlet to be created from two triplets *via* TTA in rubrene films ($f = 19.5\%$) was found to be close to that estimated for rubrene in a solution.[22] Assuming all the intermediate energy transfer processes are 100% efficient, the latter result implies a maximum UC quantum yield of $1/2 \times f \approx 10\%$ thereby also explaining why there are no reports on rubrene UC systems exceeding this value.

Conflicts of interest

There are no conflicts to declare.

Acknowledgements

The research was funded by the European Social Fund (Project No. 09.3.3-LMT-K-712-01-0084) under a grant agreement with the Research Council of Lithuania (LMTLT).

Notes and references

1 B. D. Ravetz, A. B. Pun, E. M. Churchill, D. N. Congreve, T. Rovis and L. M. Campos, *Nature*, 2019, **565**, 343–346.
2 R. S. Khnayzer, J. Blumhoff, J. A. Harrington, A. Haefele, F. Deng and F. N. Castellano, *Chem. Commun.*, 2011, **48**, 209–211.
3 A. L. Hagstrom, S. Weon, W. Choi and J.-H. Kim, *ACS Appl. Mater. Interfaces*, 2019, **11**, 13304–13318.
4 Y. I. Park, K. T. Lee, Y. D. Suh and T. Hyeon, *Chem. Soc. Rev.*, 2015, **44**, 1302–1317.
5 J. Pedrini and A. Monguzzi, *J. Photonics Energy*, 2017, **8**, 022005.
6 L. Frazer, J. K. Gallaher and T. W. Schmidt, *ACS Energy Lett.*, 2017, **2**, 1346–1354.
7 T. F. Schulze and T. W. Schmidt, *Energy Environ. Sci.*, 2015, **8**, 103–125.
8 V. Gray, K. Moth-Poulsen, B. Albinsson and M. Abrahamsson, *Coord. Chem. Rev.*, 2018, **362**, 54–71.
9 A. Khare, *J. Alloys Compd.*, 2019, 153214.
10 Y. Y. Cheng, B. Fückel, R. W. MacQueen, T. Khoury, R. G. C. R. Clady, T. F. Schulze, N. J. Ekins-Daukes, M. J. Crossley, B. Stannowski, K. Lips and T. W. Schmidt, *Energy Environ. Sci.*, 2012, **5**, 6953–6959.
11 R. A. S. Ferreira, S. F. H. Correia, A. Monguzzi, X. Liu and F. Meinardi, *Mater. Today*, 2020, **33**, 105–121.
12 J. C. Goldschmidt and S. Fischer, *Adv. Opt. Mater.*, 2015, **3**, 510–535.
13 J. Zhou, Q. Liu, W. Feng, Y. Sun and F. Li, *Chem. Rev.*, 2015, **115**, 395–465.
14 P. Bharmoria, H. Bildirir and K. Moth-Poulsen, *Chem. Soc. Rev.*, 2020, **49**, 6529–6554.
15 L. Huang, Y. Zhao, H. Zhang, K. Huang, J. Yang and G. Han, *Angew. Chem., Int. Ed.*, 2017, **56**, 14400–14404.
16 Q. Liu, W. Wang, C. Zhan, T. Yang and D. S. Kohane, *Nano Lett.*, 2016, **16**, 4516–4520.
17 D. Yildiz, C. Baumann, A. Mikosch, A. J. C. Kuehne, A. Herrmann and R. Göstl, *Angew. Chem., Int. Ed.*, 2019, **58**, 12919–12923.
18 S.-W. Liu, C.-C. Lee, C.-H. Yuan, W.-C. Su, S.-Y. Lin, W.-C. Chang, B.-Y. Huang, C.-F. Lin, Y.-Z. Lee, T.-H. Su and K.-T. Chen, *Adv. Mater.*, 2015, **27**, 1217–1222.
19 Y. Zhou, S.-T. Han, X. Chen, F. Wang, Y.-B. Tang and V. a. L. Roy, *Nat. Commun.*, 2014, **5**, 4720.
20 T. Jia, Q. Wang, M. Xu, W. Yuan, W. Feng and F. Li, *Chem. Commun.*, 2021, **57**, 1518–1521.
21 Y. Zhou, F. N. Castellano, T. W. Schmidt and K. Hanson, *ACS Energy Lett.*, 2020, 2322–2326.
22 E. Radiunas, S. Raišys, S. Juršėnas, A. Jozeliūnaitė, T. Javorskis, U. Šinkevičiūtė, E. Orentas and K. Kazlauskas, *J. Mater. Chem. C*, 2020, **8**, 5525–5534.
23 D. G. Bossanyi, Y. Sasaki, S. Wang, D. Chekulaev, N. Kimizuka, N. Yanai and J. Clark, *JACS Au*, 2021, **1**, 2188–2201.
24 Y. Y. Cheng, T. Khoury, R. G. C. R. Clady, M. J. Y. Tayebjee, N. J. Ekins-Daukes, M. J. Crossley and T. W. Schmidt, *Phys. Chem. Chem. Phys.*, 2009, **12**, 66–71.
25 S. Hoseinkhani, R. Tubino, F. Meinardi and A. Monguzzi, *Phys. Chem. Chem. Phys.*, 2015, **17**, 4020–4024.
26 K. M. Felter, M. C. Fravventura, E. Koster, R. D. Abellon, T. J. Savenije and F. C. Grozema, *ACS Energy Lett.*, 2019, 124–129.
27 M. Wu, D. N. Congreve, M. W. B. Wilson, J. Jean, N. Geva, M. Welborn, T. Van Voorhis, V. Bulović, M. G. Bawendi and M. A. Baldo, *Nat. Photonics*, 2016, **10**, 31–34.
28 M. Wu, J. Jean, V. Bulović and M. A. Baldo, *Appl. Phys. Lett.*, 2017, **110**, 211101.
29 S. Amemori, Y. Sasaki, N. Yanai and N. Kimizuka, *J. Am. Chem. Soc.*, 2020, **142**, 8057–8058.
30 L. Nienhaus, J.-P. Correa-Baena, S. Wieghold, M. Einzinger, T.-A. Lin, K. E. Shulenberger, N. D. Klein, M. Wu, V. Bulović, T. Buonassisi, M. A. Baldo and M. G. Bawendi, *ACS Energy Lett.*, 2019, **4**, 888–895.
31 L. Nienhaus, M. Wu, N. Geva, J. J. Shepherd, M. W. B. Wilson, V. Bulović, T. Van Voorhis, M. A. Baldo and M. G. Bawendi, *ACS Nano*, 2017, **11**, 7848–7857.
32 A. Abulikemu, Y. Sakagami, C. Heck, K. Kamada, H. Sotome, H. Miyasaka, D. Kuzuhara and H. Yamada, *ACS Appl. Mater. Interfaces*, 2019, **11**, 20812–20819.
33 C. J. Imperiale, P. B. Green, E. G. Miller, N. H. Damrauer and M. W. B. Wilson, *J. Phys. Chem. Lett.*, 2019, **10**, 7463–7469.
34 S. N. Sanders, M. K. Gangishetty, M. Y. Sfeir and D. N. Congreve, *J. Am. Chem. Soc.*, 2019, 9180–9184.
35 K. J. Fallon, E. M. Churchill, S. N. Sanders, J. Shee, J. L. Weber, R. Meir, S. Jockusch, D. R. Reichman, M. Y. Sfeir, D. N. Congreve and L. M. Campos, *J. Am. Chem. Soc.*, 2020, **142**, 19917–19925.

36 V. Yakutkin, S. Aleshchenkov, S. Chernov, T. Miteva, G. Nelles, A. Cheprakov and S. Baluschev, *Chem. – Eur. J.*, 2008, **14**, 9846–9850.

37 T. N. Singh-Rachford and F. N. Castellano, *J. Phys. Chem. A*, 2008, **112**, 3550–3556.

38 Y. Y. Cheng, B. Fückel, T. Khoury, R. G. C. R. Clady, M. J. Y. Tayebjee, N. J. Ekins-Daukes, M. J. Crossley and T. W. Schmidt, *J. Phys. Chem. Lett.*, 2010, **1**, 1795–1799.

39 J. Han, F. Zhang, J. You, Y. Hiroaki, S. Yamada, T. Morifuji, S. Wang and X. Li, *Photochem. Photobiol. Sci.*, 2017, **16**, 1384–1390.

40 A. S. Bieber, Z. A. VanOrman, S. Wieghold and L. Nienhaus, *J. Chem. Phys.*, 2020, **153**, 084703.

41 Y. Che, W. Yang, G. Tang, F. Dumoulin, J. Zhao, L. Liu and Ü. İşci, *J. Mater. Chem. C*, 2018, **6**, 5785–5793.

42 A. B. Pun, L. M. Campos and D. N. Congreve, *J. Am. Chem. Soc.*, 2019, **141**, 3777–3781.

43 E. Radiunas, M. Dapkevičius, S. Raišys, S. Juršėnas, A. Jozeliūnaitė, T. Javorskis, U. Šinkevičiūtė, E. Orentas and K. Kazlauskas, *Phys. Chem. Chem. Phys.*, 2020, **22**, 7392–7403.

44 E. Radiunas, M. Dapkevičius, L. Naimovičius, P. Baronas, S. Raišys, S. Juršėnas, A. Jozeliūnaitė, T. Javorskis, U. Šinkevičiūtė, E. Orentas and K. Kazlauskas, *J. Mater. Chem. C*, 2021, **9**, 4359–4366.

45 D. G. Bossanyi, Y. Sasaki, S. Wang, D. Chekulaev, N. Kimizuka, N. Yanai and J. Clark, *J. Mater. Chem. C*, 2022, **10**, 4684–4696.

46 M. Kinoshita, Y. Sasaki, S. Amemori, N. Harada, Z. Hu, Z. Liu, L. K. Ono, Y. Qi, N. Yanai and N. Kimizuka, *ChemPhotoChem*, 2020, **4**, 5271–5278.

47 S. R. Pristash, K. L. Corp, E. J. Rabe and C. W. Schlenker, *ACS Appl. Energy Mater.*, 2020, **3**, 19–28.

48 S. Wieghold, A. S. Bieber, Z. A. VanOrman and L. Nienhaus, *J. Phys. Chem. Lett.*, 2019, **10**, 3806–3811.

49 K. Seki, T. Yoshida, T. Yago, M. Wakasa and R. Katoh, *J. Phys. Chem. C*, 2021, **125**, 3295–3304.

50 D. M. Finton, E. A. Wolf, V. S. Zoutenbier, K. A. Ward and I. Biaggio, *AIP Adv.*, 2019, **9**, 095027.

51 S.-W. Park, J.-M. Choi, K. H. Lee, H. W. Yeom, S. Im and Y. K. Lee, *J. Phys. Chem. B*, 2010, **114**, 5661–5665.

52 N. Geva, L. Nienhaus, M. Wu, V. Bulović, M. A. Baldo, T. Van Voorhis and M. G. Bawendi, *J. Phys. Chem. Lett.*, 2019, **10**, 3147–3152.

53 L. Wang, J. J. Yoo, T.-A. Lin, C. F. Perkinson, Y. Lu, M. A. Baldo and M. G. Bawendi, *Adv. Mater.*, 2021, e2100854.

PV

Triplet and singlet exciton diffusion in disordered rubrene films: implications for photon upconversion

Edvinas Radiunas, Manvydas Dapkevičius, Steponas Raišys, Karolis Kazlauskas.

Journal of Materials Chemistry C, **24**(39), 243
45-24352, (2022)

10.1039/D2CP02798D

PCCP

ROYAL SOCIETY OF CHEMISTRY

PAPER

View Article Online
View Journal | View Issue

Check for updates

Cite this: *Phys. Chem. Chem. Phys.*, 2022, **24**, 24345

Triplet and singlet exciton diffusion in disordered rubrene films: implications for photon upconversion†

Edvinas Radiunas, Manvydas Dapkevičius, Steponas Raišys and Karolis Kazlauskas*

Received 20th June 2022,
Accepted 15th September 2022

DOI: 10.1039/d2cp02798d

rsc.li/pccp

Triplet and singlet exciton diffusion plays a decisive role in triplet–triplet annihilation (TTA) and singlet fission (SF) processes of rubrene (Rub) films at low excitation power, and therefore has an important implication for TTA-mediated photon upconversion (UC). Although triplet diffusion in crystalline Rub was studied before, there is no quantitative data on diffusion in disordered Rub films most widely employed for NIR-to-Vis UC. The lack of these data hinders the progress of TTA-UC applications relying on a Rub annihilator (emitter). Herein, a time-resolved PL bulk-quenching technique was employed to estimate the exciton diffusion coefficient (*D*) and diffusion length (L_D) in the neat Rub films as well as Rub-doped PS films at 80 wt% doping concentration, previously reported to be optimal in terms of UC efficiency. The impact of commonly utilized singlet energy collector (sink) DBP on exciton diffusion was also assessed, highlighting its importance exclusively on the dynamics of singlets in Rub films. Our study revealed that triplet diffusion lengths (L_D^T) of 25–30 nm estimated for the disordered Rub films are sufficient for encountering triplets from the neighboring sensitizer molecules at a low sensitizer PdPc concentration (0.1 wt%), thereby enabling the desired TTA domination regime to be reached. Essentially, the performance of Rub-based UC systems was found to be limited by the modest maximal L_D^T (up to ∼55 nm) in disordered films resulting from a short maximum triplet lifetime τ_T (∼100 μs) inherent to this emitter. Thus, to enhance the NIR-to-Vis TTA-UC performance, new emitters with a longer triplet lifetime in the solid state are required.

Introduction

Rubrene (Rub) has been studied for almost a century now. It gained popularity mainly due to its high emission efficiency (close to 100% in the isolated state) and high carrier mobility (up to 40 $cm^2 V^{-1} s^{-1}$) in single crystals.[1,2] The high fluorescence quantum yield (Φ_{PL}) of Rub was extensively exploited in organic light-emitting devices (OLEDs) for light emission, both in the 1st generation fluorescent[3] and the latest generation hyperfluorescent[4,5] OLEDs. Meanwhile, the high carrier mobility of crystalline Rub facilitated the development of important devices[6] such as organic field-effect transistors,[7] organic diodes[8] and organic solar cells.[9,10] Besides applications in organic electronics, Rub has found niche uses in photoredox catalysis[11] and organic spintronics.[12] Moreover, Rub is frequently utilized as the benchmark material for photon upconversion[13–16] as well as singlet fission,[17–19] demonstrating high efficiencies in both areas.

Rubrene is rather unique in that its triplet state energy (T_1) is roughly half the singlet energy (S_1) implying $S_1 \approx 2 \times T_1$.[20–22] This opens up the possibility for the singlet fission (SF) effect, whereby the singlet exciton splits into two triplets.[17,23] The SF effect leads to doubling of the quantum efficiency in optoelectronic devices such as OLEDs and organic solar cells up to the theoretical limit of 200%, and in this way it allows the Shockley–Quiesser limit of organic photovoltaics to be overcome.[19,24,25] SF typically manifests in the crystalline environment featuring small intermolecular separation and favorable molecular orientation, thereby providing sufficient electronic coupling between the neighboring molecules for SF to occur on the picosecond time scale.[18,26]

The intricate energy level arrangement in Rub also enables the reverse process to SF, *i.e.* the triplet exciton fusion also known as triplet–triplet annihilation (TTA), whereby energy of two triplet excitons is combined to form one singlet. The latter process is utilized for TTA-mediated photon upconversion (TTA-UC), which drew a lot of attention due to various practical

---

Institute of Photonics and Nanotechnology, Vilnius University, Saulėtekio av. 3, LT-10257 Vilnius, Lithuania. E-mail: karolis.kazlauskas@ff.vu.lt

† Electronic supplementary information (ESI) available: Materials, film preparation techniques, experimental details on the determination of singlet and triplet exciton diffusion, microscopy images, *etc.* See DOI: **https://doi.org/10.1039/d2cp02798d**

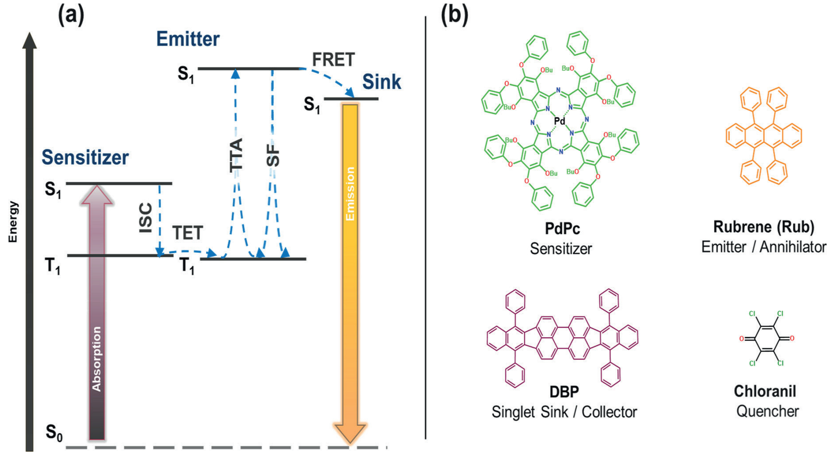

Fig. 1 (a) TTA-UC energy scheme with corresponding energy transfer processes. ISC-intersystem crossing, TET-triplet energy transfer, TTA-triplet–triplet annihilation, SF-singlet fission, and FRET-Förster resonance energy transfer. (b) Molecular structures of the PdPc sensitizer, Rub emitter/annihilator, DBP singlet sink/collector, and chloranil quencher.

applications, *e.g.* in bioimaging and photovoltaics.[27–29] Conventional TTA-UC is realized using a triplet exciton sensitizer and an annihilator (often serving as an emitter). In such systems, the sensitizer ensures absorption of incident light and rapid generation of triplets *via* intersystem crossing, which is then followed by triplet energy transfer from the sensitizer to emitter species (Fig. 1a). These triplets diffuse through the network of emitter species until they encounter each other and annihilate resulting in the formation of a singlet exciton (S_1 state). The final step in the cascade of TTA-UC events is the emission from the S_1 state of an emitter.

Importantly, both the SF event and UC fluorescence can occur simultaneously in Rub films; however, since SF is three orders of magnitude faster ($\sim$10 ps)[15] as compared to fluorescence ($\sim$16 ns),[17] it dominates the deactivation pathway of S_1. This reduces Φ_{PL} down to a few percent[30] and is often regarded as the main factor limiting the TTA-UC yield in Rub-based solid films.[31] Regardless of the low Φ_{PL}, Rub is the most widely used emitter for NIR-to-VIS TTA-UC, demonstrating record-high solid-state UC efficiencies in this spectral range (up to 2%).[9,13,15,32,33] The efficiencies, however, are still far below the theoretical limit of 50% taking into account that two triplets are needed for generation of one singlet *via* TTA. A possible solution to the SF related problem could be the increase of intermolecular separation *via* chemical engineering or the dilution of emitter molecules in an optically inert polymer matrix.[30,34] However, this will inevitably impair the energy transfer rate slowing down triplet diffusion till TTA-UC is no longer feasible. An alternative way for circumventing SF is to additionally introduce a singlet exciton collector (or sink) as an extra radiative decay channel for singlets. Tetraphenyldibenzoperiflanthene (DBP) featuring a high Φ_{PL} and suitable energy level alignment is commonly employed as the singlet sink for Rub. DBP is demonstrated to significantly enhance the emission efficiency of Rub in the solid-state.[14,30,33,35,36] Interestingly, in some reports the role of DBP has been under debate[15] and in the case of a solution-processed perovskite-sensitized system, it was found to have a negligible effect on the UC enhancement.[37] Since this singlet sink is widely used in tandem with Rub, it is essential to investigate its impact on exciton diffusion in Rub films. Considering that triplet generation *via* SF can reach 100% in crystalline Rub,[18] producing disordered (ultimately purely amorphous) films should eliminate the issue;[17] however, fabrication of large area films is technologically extremely challenging. The presence of a small amount of SF-favoring aggregates in amorphous Rub films can nevertheless drastically quench Rub emission due to the efficient singlet diffusion to SF sites.[38] Although singlet diffusion in the neat films of Rub and its derivatives has been studied before,[39] it is in fact greatly affected by the degree of disorder. Thus, assessing the singlet diffusion of the particular film deposited under specific conditions is nonetheless important, especially when aiming for improved TTA-UC performance.

Likewise, the efficiency of the bimolecular TTA process at low excitation power ($\sim$mW cm^{-2}) heavily relies on triplet diffusion. Hence, materials with a long triplet lifetime and high triplet diffusivity are desirable to attain efficient TTA.[35] Micron-range triplet exciton diffusion in Rub crystals has been previously reported;[40–43] however, there are no quantitative data on triplet diffusion in disordered Rub films. Taking into account that singlet and triplet diffusion are crucial for the design of high-performance solid-state TTA-UC systems, the key parameters determining exciton diffusivity, such as exciton lifetime, diffusion coefficient and length, need to be thoroughly assessed.

To this end, herein, both singlet and triplet exciton diffusion in disordered UC films based on a Rub emitter were investigated. Rub films were prepared by spin-coating in the same way as described by us previously[30] to achieve high UC efficiencies in the solid state. The time-resolved photoluminescence bulk-quenching technique was employed to estimate the exciton diffusion coefficient (D) and diffusion length (L_D) in the neat Rub films as well as Rub-doped PS films at 80 wt% doping, previously reported to be the optimal doping for TTA-UC.[30] Palladium phthalocyanine (PdPc) served as a triplet exciton sensitizer[13] in this study; meanwhile chloranil was utilized as an exciton quencher in PL quenching experiments. Exciton diffusion was also assessed in the films additionally doped with singlet exciton sink DBP to diminish SF-induced PL quenching in Rub.

Results and discussion

Triplet exciton diffusion

To quantify triplet exciton diffusion in disordered Rub films, two sets of films with a fixed amount of sensitizer PdPc (0.1 wt%) and increasing quencher concentration [Q_c] were investigated. The first set contained 80 wt% of Rub dispersed in a PS matrix, whereas the second one was based on the neat Rub films.

Additionally, each set contained a series of films doped with exciton sink DBP at 0.5 wt% concentration. DBP doping is frequently used by the community to diminish notorious SF in Rub films and improve Φ_{PL}. The overlap of Rub emission and DBP absorption bands allowing for efficient FRET can be visualized in Fig. S4 in the ESI.† PS served as an inert matrix for Rub, thereby increasing the intermolecular distance between the emitter species. This particular dilution of the Rub emitter previously was shown to be the optimal in terms of TTA-UC efficiency.[30] On the other hand, knowledge on exciton diffusion in the undiluted (neat) Rub films is also important, as these are often utilized in various optoelectronic devices.

Thus, in total 2 sets of samples each containing 2 series of UC films with increasing quencher (chloranil) concentrations were investigated by measuring UC transients. The square root of UC intensity, which is proportional to the triplet concentration, is depicted on the Y axis of Fig. 2. The transients spanning over the μs-time-scale were easily fitted using a single exponential decay profile indicating that spontaneous triplet decay dominates over the TTA channel and the Stern–Volmer model is applicable.

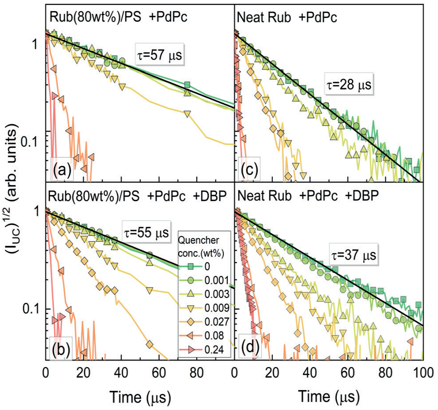

Fig. 2 UC transients of the Rub(80 wt%)/PS and neat Rub films with (a and c) 0.1 wt% PdPc; (b and d) 0.1 wt% PdPc and 0.5 wt% DBP, at different triplet quencher concentrations from 0 to 0.24 wt%. Excitation wavelength – 730 nm.

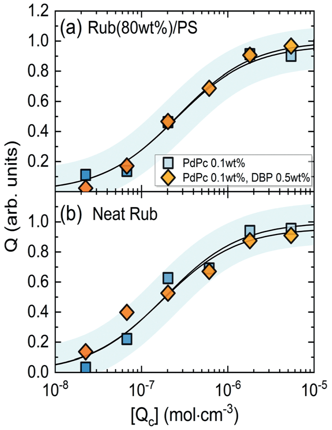

Fig. 3 Relative triplet quenching efficiency as a function of quencher concentration for (a) Rub(80 wt%)/PS films and (b) neat Rub films with 0.1 wt% PdPc only and with additional 0.5 wt% DBP. Solid lines show Stern–Volmer fits.

In all the film series, an increase of [Q_c] resulted in the prominent reduction of the triplet lifetime from *ca.* 57 μs (in Rub(80 wt%)/PS series) and *ca.* 37 μs (in neat Rub series) down to less than one microsecond at the highest [Q_c]. The quencher concentration as low as 0.24 wt% was sufficient to quench triplets with nearly 100% efficiency, indicating that chloranil is indeed a suitable quencher for Rub triplets. The films with a higher chloranil content (> 0.24 wt%) exhibited insufficient UC intensity for reliable lifetime evaluation.

The dependence of the calculated relative quenching efficiency on [Q_c] (Fig. 3) was fitted using the Stern–Volmer relationship (see eqn (S3) in the ESI†) thereby permitting the triplet exciton diffusion coefficient (D_T) to be estimated. D_T and the other main fitting parameters are summarized in Table 1.

The Stern–Volmer analysis revealed D_T of 1.1–1.2 × 10^{-7} cm^2 s^{-1} in Rub(80 wt%)/PS films, which gave rise to L_D^T of 25–26 nm (Table 1). As anticipated, the shorter intermolecular distance in the denser neat Rub films significantly enhanced triplet diffusivity resulting in the tripled D_T (up to 3.4 × 10^{-7} cm^2 s^{-1}) as compared to that of Rub(80 wt%)/PS. However, L_D^T was only slightly increased (up to 31 nm) due to the shortened τ_T (down to 28 μs) in the neat Rub films. DBP was found to have no

Table 1 Stern–Volmer fitting parameters of Rub films

	PdPc (wt%)	DBP (wt%)	K_{SV} (cm^3 mol^{-1})	D_T (cm^2 s^{-1})	f_a	r (nm)	τ_T (μs)	L_D^T (nm)
Rub(80 wt%)/PS	0.1	0	3.84×10^6	1.13×10^{-7}	0.99	0.79	57	25.4
Rub(80 wt%)/PS	0.1	0.5	3.97×10^6	1.21×10^{-7}	0.97	0.79	55	25.8
Neat Rub	0.1	0	5.36×10^6	3.38×10^{-7}	0.99	0.75	28	30.7
Neat Rub	0.1	0.5	5.73×10^6	2.73×10^{-7}	0.96	0.75	37	31.8

K_{SV} – Stern–Volmer constant, D_T – triplet exciton diffusion coefficient, f_a – fraction of quenchers accessible to excitons in the emitter, r – reactive radius, τ_T – triplet exciton lifetime, and L_D^T – triplet exciton diffusion length.

substantial impact neither on the diffusion coefficient nor on the triplet lifetime.

We note that the difference in τ_T obtained for the neat Rub films with and without DBP can be attributed to DBP related changes in the film morphology. This is also supported by the optical microscopy images of the neat Rub films (see Fig. S1 in the ESI†).

Singlet exciton diffusion

Unlike triplets, singlet excitons should preferably exhibit the shortest possible diffusion length. This is to avoid Förster resonant energy transfer (FRET) back to the sensitizer or other exciton quenching sites.[44] To evaluate singlet exciton diffusion we used the same series of films (as for the triplet diffusion measurements) and an additional one with neither triplet sensitizer PdPc nor singlet sink DBP present. Conversely to triplet diffusion measurements, 485 nm excitation wavelength was employed to probe the singlet state of Rub. The obtained D and L_D values for the singlets were compared to the literature values.

Fig. S5 in the ESI† illustrates the full time-range PL transients of the Rub(80 wt%)/PS and neat Rub films measured with the gradually increasing quencher concentration. The transients feature a multi-exponential decay profile, which can be best described using a three-exponent decay function. The first two decay components, which can be well discerned from Fig. 4(a)–(f), expressed lifetimes on the order of a few and tens of nanoseconds, ~2 ns and ~15 ns, respectively, while the lifetime of the third (the longest) component was on the order of several hundreds of nanoseconds (~200 ns). The lifetimes of the first two decay components were found to be sensitive to the introduced quenchers, whereas the lifetime of the third component remained invariant with the quencher concentration. Based on these findings, the first two decay components were associated with the PL from the Rub singlet state, whereas the third one was associated with the delayed emission. The delayed emission emerged from SF followed by rapid TTA from geminate triplet pairs in the Rub.[15] Since the longest PL decay component is of a different origin and does not depend on the introduced singlet quencher concentration, it was disregarded in the exciton diffusion calculations. The 1st decay component, which was the dominant one (fractional intensity >70%) and strongly affected by the quencher, is ascribed to the singlet diffusion in aggregate-rich regions, meanwhile the 2nd weakly quenched component is attributed to exciton migration in amorphous-like regions (see Table S1, ESI†). This is due to the severely suppressed singlet diffusion in amorphous Rub as compared to the faster diffusion in the aggregated areas. Considering that the lifetime of the 2nd decay component was only weakly affected by the quencher up to the highest concentrations (<1 wt%) used, we utilized only the 1st component for the estimation of singlet diffusion.

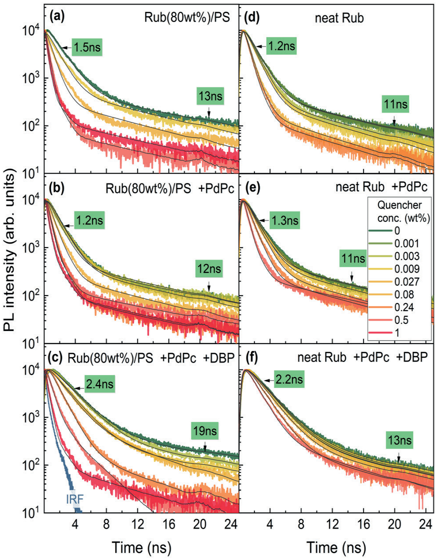

Fig. 4 PL transients of the Rub(80 wt%)/PS and neat Rub films (a and d) undoped; (b and e) doped with 0.1 wt% PdPc; (c and f) doped with 0.1 wt% PdPc and 0.5 wt% DBP, at different singlet quencher concentrations from 0 to 1 wt%. IRF-instrument response function. Excitation wavelength – 485 nm. Black solid lines represent the exponential fits of the first two decay components (lifetimes indicated).

The PL lifetimes of the Rub(80 wt%)/PS as well as neat Rub films without quenchers are summarized in Table 2. The lifetime of the singlet excitons (τ_S) in Rub(80 wt%)/PS films was in the range of 1.5–2.4 ns, whereas it was somewhat shorter (1.2–2.2 ns) in the neat Rub films. The introduction of singlet sink DBP was found to prolong τ_S (Fig. 4(c) and (f)) as well as slightly increase the PL rise-time due to the FRET from Rub to DBP.

Fig. 5 displays the quenching efficiency of each film calculated from the PL transient data provided in Fig. 4. Here the

Table 2 Stern–Volmer fitting parameters for singlet excitons of Rub films

	PdPc (wt%)	DBP (wt%)	K_{SV} (cm^3 mol^{-1})	D_S (cm^2 s^{-1})	f_a	r (nm)	τ_S (ns)	L_D^S (nm)
Rub(80 wt%)/PS	0	0	1.13×10^6	1.26×10^{-3}	0.92	0.79	1.50	13.7
Rub(80 wt%)/PS	0.1	0	4.93×10^5	7.05×10^{-4}	0.91	0.79	1.17	9.1
Rub(80 wt%)/PS	0.1	0.5	3.02×10^5	2.13×10^{-4}	1.00	0.79	2.37	7.1
Neat Rub	0	0	1.52×10^6	2.27×10^{-3}	0.92	0.75	1.18	16.4
Neat Rub	0.1	0	3.97×10^5	5.51×10^{-4}	0.95	0.75	1.27	8.4
Neat Rub	0.1	0.5	1.97×10^5	1.60×10^{-4}	0.90	0.75	2.17	5.9

K_{SV} – Stern–Volmer constant, D_S – singlet exciton diffusion coefficient, f_a – fraction of quenchers accessible to excitons in the emitter, r – reactive radius, τ_S – singlet exciton lifetime (determined from the shortest decay component associated with the singlet diffusion in aggregate-rich regions), and L_D^S – singlet exciton diffusion length.

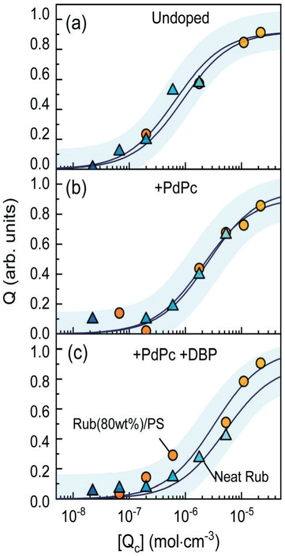

Fig. 5 Relative singlet quenching efficiency as a function of chloranil quencher concentration for Rub(80 wt%)/PS and neat Rub films (a) without PdPc and DBP; (b) with 0.1 wt% PdPc; (c) with 0.1 wt% PdPc and 0.5 wt% DBP. Solid lines show the Stern–Volmer fits.

quencher content in the X axis is expressed in molar concentration. The highest molar concentration of the quencher (2.25×10^{-5} mol cm^{-3}) corresponds to 1 wt%. Solid lines in Fig. 5 represent the Stern–Volmer fits (see eqn (S3) in the ESI†). K_{SV} constants as well as other important parameters extracted from the Stern–Volmer analysis are summarized in Table 2. For the best fits, factor f_a, describing the fraction of quenchers accessible to excitons, was close to 1.0 (within the accuracy of a few percent), thereby inferring almost complete dissolution of the quencher within the film. The determined singlet exciton diffusion coefficient was on the order of 10^{-3}–10^{-4} cm^2 s^{-1} for both Rub(80 wt%)/PS and neat Rub films (Table 2). The singlet exciton diffusion length of the Rub(80 wt%)/PS and neat Rub films was found to be 13.7 and 16.4 nm, respectively. The addition of the PdPc sensitizer noticeably shortened L_D^S by *ca.* 30–50%; meanwhile the incorporation of singlet sink DBP reduced it even further down to 7.1 and 5.9 nm for Rub(80 wt%)/PS and neat Rub, respectively.

Implications for photon upconversion

Crystalline Rub featuring an ordered molecular structure exhibits efficient triplet exciton diffusion with diffusion lengths in the micrometer range.[42,43] This is consistent with the high carrier mobility obtained for Rub single crystals,[2] since both triplet diffusion and carrier transport share the same Dexter energy transfer mechanism due to the electron exchange. However, the UC films desired for practical applications are typically disordered (amorphous-like), hence with radically different energy transport properties compared to those of the crystalline films. We note that there is a lack of data on triplet diffusion in disordered Rub films hampering the understanding of exciton migration in such systems, and therefore, limiting the progress of TTA-UC applications relying on a Rub annihilator. The UC signal generated by means of TTA provides unique opportunity to probe otherwise non-emissive triplet states and evaluate their diffusion.

A few reports investigating triplet generation in solid films by SF suggested that UC quantum yields of 30% or higher are possible in Rub.[15,23] The SF process is feasible in dimerized/aggregated molecular species with the specific orientation, which facilitates the creation of correlated triplet pairs that later may dissociate into free triplets. However, in the case of Rub, the reverse process of triplet fusion (or geminate TTA) is also highly probable, and was reported to attain a similar high rate to that of SF ($\sim$10 ps^{-1}).[15] Thereby, even if the probability of TTA is assumed to be high (60%[23]), repetitive triplet-singlet recycling due to TTA ↔ SF events will drastically deteriorate Φ_{UC}. For instance, 5-fold recycling should limit Φ_{UC} to only 4% ($=1/2 \times 0.6^5$). Note that this estimation does not take into account Φ_{PL} and Φ_{TET}, which can be well below unity in the solid state, thus further reducing Φ_{UC}.

Low Φ_{UC} in SF-dominated crystalline Rub films explains why efficient TTA-UC is mostly observed in amorphous-like or at least partly disordered Rub films.[14,30,37] The improved morphology of such films also benefits the reduced sensitizer segregation, increased triplet sensitization (Φ_{TET}) and enhanced Φ_{PL}. We note that small morphological changes, *e.g.* formation of dimers, trimers, *etc.*, often cannot be distinguished even by atomic force microscopy due to the lack of proper resolution at a molecular level (see Fig. S3, ESI†). In fact, the singlet state lifetime (τ_S) in Rub films can serve as an indicator of the film morphology. Purely amorphous Rub films has the longest τ_S, which is close to that observed in dilute Rub solutions ($\sim$16 ns).[17] Indeed, several groups have succeeded in fabricating amorphous-like films by the thermal evaporation method with a τ_S of 9–12 ns and a singlet diffusion length of 6.4 nm.[16,39] Although such short L_D^S is common for disordered films, much longer diffusion lengths of 180–390 nm can be obtained in highly ordered crystalline Rub films.[40] In the spin-coated neat Rub films studied in this work, a comparatively short τ_S of $\sim$1.2 ns was obtained implying the presence of SF sites due to the emerged crystalline domains. Dispersion of Rub in the PS matrix at 80 wt% concentration led to slight prolongation of τ_S (up to $\sim$1.5 ns) due to the suppressed Rub aggregation. Despite the continuously increasing τ_S along with the degree of amorphicity of Rub films, L_D^S gradually reduced, *i.e.* from 16.4 nm in the spin-coated neat films to 13.7 nm in Rub(80 wt%)/PS films and 6.4 nm in thermally deposited neat films. This evidenced the key role of singlet exciton diffusion D_S whose fast decrease could not be compensated by the increasing τ_S (Table 2). In other words, unlike the singlet exciton lifetime, singlet diffusion was found to be much more sensitive to the variations of intermolecular spacing (induced by morphological changes) and thus it governed the L_D^S behavior (see eqn (S6) in the ESI†). Since long L_D^S is known to foster FRET of the upconverted singlets from annihilator back to a sensitizer, it is detrimental for TTA-UC efficiency and must be avoided. Therefore, as far as it concerns the singlet excitons, the most suitable Rub films for efficient photon upconversion are those with a high degree of amorphicity, and subsequently a short L_D^S, as these suppress both unfavorable back-FRET and SF.

The proof for the occurrence of back-FRET in the studied Rub UC films is the apparent shortening of L_D^S in both neat Rub (L_D^S = 8.4 nm) and Rub(80 wt%)/PS films (L_D^S = 9.1 nm) obtained upon the introduction of the 0.1 wt% PdPc sensitizer (Table 2). The back-FRET is feasible because PdPc has non-zero absorption in the spectral region of Rub emission (see Fig. S4 in the ESI†) and L_D^S exceeds half the distance between the sensitizer species ($\sim$7 nm) at the given concentration. Moreover, the widely used emissive singlet sink (or trap) DBP introduced into Rub to evade SF further reduces L_D^S in the UC films. It is reduced down to 7.1 and 5.9 nm for Rub(80 wt%)/PS and neat Rub films, respectively (Table 2). Note, that due to the fast singlet capture rate by DPB (50 ps^{-1})[15] in the DBP-doped films, diffusion of singlet excitons is associated with DBP rather than Rub itself.

From the viewpoint of triplet exciton diffusion, it is preferred to be large for TTA-assisted UC to be efficient at low excitation power. Rub single crystals exhibit superior triplet diffusion leading to their long L_D^T (2–8 μm[42,43]); however efficient SF in such crystals completely quenches Φ_{PL} rendering them unsuitable for UC applications. In contrast, L_D^T in the disordered Rub films obtained by spin-coating was estimated to be a couple of orders of magnitude shorter, *i.e.* 25 nm and 30 nm for Rub(80 wt%)/PS and neat Rub films, respectively (Table 1). Interestingly, similar L_D^T values were previously reported for disordered PMMA/DPA/PtOEP films at the optimal DPA concentrations of 25–30 wt% corresponding to the maximal UC quantum yield.[45] Comparable L_D^T values of a few tens of nanometers were also obtained for amorphous bisfluorene-anthracene/PtOEP films.[46] Even though the triplet diffusion constants in the spin-coated Rub films (D_T $\sim$10^{-7} cm^2 s^{-1}, see Table 1) were found to be 1–2 orders of magnitude larger with respect to those based on anthracene films,[44–46] significantly shorter triplet lifetimes of Rub films (τ_T $\sim$ 30–60 μs) restricted their L_D^T to a nanometer range. Nonetheless, such L_D^T as being >4-fold longer compared to the half the distance between sensitizer molecules at the PdPc concentration of 0.1 wt% implied unrestricted encounter of the triplets from the neighboring sensitizer molecules. This ensured that the TTA domination regime (linear UC dependence *vs* excitation power) can be easily reached granting the optimal Φ_{UC} for disordered Rub films. It is worth mentioning that still, inherently higher L_D^T would permit using even lower sensitizer concentrations, thus further suppressing singlet losses caused by the back-FRET to the sensitizer. Likewise, lower Rub concentrations could be utilized in UC films reducing the aggregation, and subsequently, the formation of SF centers responsible for low Φ_{PL} and TTA-UC efficiency.[30] Aggregation related issues, on the other hand, can be also addressed *via* chemical engineering of the Rub backbone by steric side-moieties.[30,34] However, despite benefits of the suppressed SF, steric groups were found to adversely affect TET from the sensitizer as well as triplet diffusion-assisted TTA depending on the degree of steric hindrance and linking position of the side-moieties.

Considering that long L_D^T is preferred for TTA-UC and may aid in reducing the excitation threshold of TTA dominating regime, ways to enlarge it must be sought out. Theoretically, this can be accomplished by enlarging either D_T or τ_T (eqn (S6) in the ESI†)). Yet, practically increasing D_T beyond the values estimated for the neat Rub films ($D_T \approx 3 \times 10^{-7}$ cm^2 s^{-1}, see Table 1) is rather complicated, since a further decrease of the intermolecular distances is hardly possible. Meanwhile, τ_T can still be somewhat prolonged, *e.g.* by eliminating triplet exciton traps or increasing the degree of amorphicity of the neat Rub films. By assuming the maximum possible τ_T as that for Rub-based UC systems in dilute solution ($\tau_T \approx$ 100 μs), L_D^T could be improved up to $\sim$55 nm. A further increase of L_D^T demands for the search of novel non-tetracene based emitters with $\tau_T >$ 100 μs in the solid state, which is a very challenging task due to the enhanced nonradiative decay rates in low-triplet-energy emitters (energy bandgap law).

Conclusions

In summary, both singlet and triplet exciton diffusion in disordered Rub films was thoroughly investigated to determine its important implications for the performance of NIR-to-Vis TTA-UC. The time-resolved PL bulk-quenching technique followed by Stern–Volmer analysis was employed to estimate the exciton diffusion coefficient (D) and diffusion length (L_D) in the spin-coated neat Rub films as well as Rub-doped PS films at 80 wt% doping, previously reported to be optimal for UC performance. Although efficient triplet diffusion (easily attainable in crystalline Rub) is highly desired to ensure bimolecular TTA at low excitation powers, low diffusivity inherent to amorphous-like Rub is required by the singlets to prevent them from reaching SF-favored (aggregated Rub) sites as well as to suppress the detrimental back-FRET to the sensitizer. Notably, 25–30 nm triplet diffusion lengths (L_D^T) estimated for the disordered Rub films under study were found to be sufficient for encountering the triplets from the neighboring sensitizer molecules at low PdPc concentration (0.1 wt%), thereby enabling the desired TTA domination regime to be achieved.

Increasing the degree of disorder or intermolecular spacing was found to significantly reduce the singlet exciton diffusion coefficient (D_S), which in turn shortened L_D^S down to 13.7 nm as it could not be compensated by the increased singlet lifetime (τ_S). Introduction of 0.1 wt% sensitizer PdPc and 0.5% singlet sink DBP in Rub films was found to have a similar effect, *i.e.* it further decreased L_D^S by several nm due to FRET.

Our study shows that L_D^T in disordered Rub films can be improved only moderately (up to ~55 nm) considering that the maximum possible τ_T as that for isolated Rub species ($\tau_T \approx$ 100 μs) is achieved. Hence, to prolong L_D^T even further for enhanced NIR-to-Vis TTA-UC performance, novel emitters with similar or lower triplet energy as compared to Rub, yet longer triplet lifetime in the solid state, are required.

Conflicts of interest

There are no conflicts to declare.

Acknowledgements

The research was funded by the European Social Fund (project No. 09.3.3-LMT-K-712-01-0084) under grant agreement with the Research Council of Lithuania (LMTLT).

Notes and references

1 M. L. Clapham, E. C. Murphy and C. J. Douglas, *Synthesis*, 2021, 461–474.
2 J. Takeya, M. Yamagishi, Y. Tominari, R. Hirahara, Y. Nakazawa, T. Nishikawa, T. Kawase, T. Shimoda and S. Ogawa, *Appl. Phys. Lett.*, 2007, **90**, 102120.
3 D. Y. Kondakov, T. D. Pawlik, T. K. Hatwar and J. P. Spindler, *J. Appl. Phys.*, 2009, **106**, 124510.
4 D. Berenis, G. Kreiza, S. Juršėnas, E. Kamarauskas, V. Ruibys, O. Bobrovas, P. Adomėnas and K. Kazlauskas, *Dyes Pigm.*, 2020, **182**, 108579.
5 H. Abroshan, V. Coropceanu and J.-L. Brédas, *ACS Mater. Lett.*, 2020, **2**, 1412–1418.
6 S. Liu, H. Wu, X. Zhang and W. Hu, *Front. Phys.*, 2020, **16**, 13304.
7 J. Nitta, K. Miwa, N. Komiya, E. Annese, J. Fujii, S. Ono and K. Sakamoto, *Sci. Rep.*, 2019, **9**, 9645.
8 M. F. Sawatzki, H. Kleemann, B. K. Boroujeni, S.-J. Wang, J. Vahland, F. Ellinger and K. Leo, *Adv. Sci.*, 2021, **8**, 2003519.
9 M. Kinoshita, Y. Sasaki, S. Amemori, N. Harada, Z. Hu, Z. Liu, L. K. Ono, Y. Qi, N. Yanai and N. Kimizuka, *ChemPhotoChem*, 2020, **4**, 5271–5278.
10 T. Zhang and R. J. Holmes, *Appl. Phys. Lett.*, 2018, **113**, 143302.
11 B. D. Ravetz, A. B. Pun, E. M. Churchill, D. N. Congreve, T. Rovis and L. M. Campos, *Nature*, 2019, **565**, 343.
12 J. H. Shim, K. V. Raman, Y. J. Park, T. S. Santos, G. X. Miao, B. Satpati and J. S. Moodera, *Phys. Rev. Lett.*, 2008, **100**, 226603.
13 E. Radiunas, S. Raišys, S. Juršėnas, A. Jozeliūnaitė, T. Javorskis, U. Šinkevičiūtė, E. Orentas and K. Kazlauskas, *J. Mater. Chem. C*, 2020, **8**, 5525–5534.
14 L. Nienhaus, M. Wu, N. Geva, J. J. Shepherd, M. W. B. Wilson, V. Bulović, T. Van Voorhis, M. A. Baldo and M. G. Bawendi, *ACS Nano*, 2017, **11**, 7848–7857.
15 D. G. Bossanyi, Y. Sasaki, S. Wang, D. Chekulaev, N. Kimizuka, N. Yanai and J. Clark, *J. Mater. Chem. C*, 2022, **10**, 4684–4696.
16 E. Radiunas, L. Naimovičius, S. Raišys, A. Jozeliūnaitė, E. Orentas and K. Kazlauskas, *J. Mater. Chem. C*, 2022, **10**, 6314–6322.
17 D. M. Finton, E. A. Wolf, V. S. Zoutenbier, K. A. Ward and I. Biaggio, *AIP Adv.*, 2019, **9**, 095027.
18 I. Breen, R. Tempelaar, L. A. Bizimana, B. Kloss, D. R. Reichman and D. B. Turner, *J. Am. Chem. Soc.*, 2017, **139**, 11745–11751.
19 L. Ma, K. Zhang, C. Kloc, H. Sun, M. E. Michel-Beyerle and G. G. Gurzadyan, *Phys. Chem. Chem. Phys.*, 2012, **14**, 8307–8312.
20 D. K. K. Liu and L. R. Faulkner, *J. Am. Chem. Soc.*, 1977, **99**, 4594–4599.
21 T. N. Singh-Rachford and F. N. Castellano, *J. Phys. Chem. A*, 2008, **112**, 3550–3556.
22 C. Sutton, N. R. Tummala, D. Beljonne and J.-L. Brédas, *Chem. Mater.*, 2017, **29**, 2777–2787.
23 D. G. Bossanyi, Y. Sasaki, S. Wang, D. Chekulaev, N. Kimizuka, N. Yanai and J. Clark, *JACS Au*, 2021, **1**, 2188–2201.
24 R. Nagata, H. Nakanotani, W. J. Potscavage and C. Adachi, *Adv. Mater.*, 2018, **30**, 1801484.
25 A. Rao and R. H. Friend, *Nat. Rev. Mater.*, 2017, **2**, 1–12.
26 M. B. Smith and J. Michl, *Annu. Rev. Phys. Chem.*, 2013, **64**, 361–386.
27 P. Bharmoria, H. Bildirir and K. Moth-Poulsen, *Chem. Soc. Rev.*, 2020, **49**, 6529–6554.
28 V. Gray, K. Moth-Poulsen, B. Albinsson and M. Abrahamsson, *Coord. Chem. Rev.*, 2018, **362**, 54–71.
29 J. Zhou, Q. Liu, W. Feng, Y. Sun and F. Li, *Chem. Rev.*, 2015, **115**, 395–465.
30 E. Radiunas, M. Dapkevičius, S. Raišys, S. Juršėnas, A. Jozeliūnaitė, T. Javorskis, U. Šinkevičiūtė, E. Orentas and K. Kazlauskas, *Phys. Chem. Chem. Phys.*, 2020, **22**, 7392–7403.

31 A. Abulikemu, Y. Sakagami, C. Heck, K. Kamada, H. Sotome, H. Miyasaka, D. Kuzuhara and H. Yamada, *ACS Appl. Mater. Interfaces*, 2019, **11**, 20812–20819.

32 L. Nienhaus, J.-P. Correa-Baena, S. Wieghold, M. Einzinger, T.-A. Lin, K. E. Shulenberger, N. D. Klein, M. Wu, V. Bulović, T. Buonassisi, M. A. Baldo and M. G. Bawendi, *ACS Energy Lett.*, 2019, **4**, 888–895.

33 M. Wu, D. N. Congreve, M. W. B. Wilson, J. Jean, N. Geva, M. Welborn, T. Van Voorhis, V. Bulović, M. G. Bawendi and M. A. Baldo, *Nat. Photonics*, 2016, **10**, 31–34.

34 E. Radiunas, M. Dapkevičius, L. Naimovičius, P. Baronas, S. Raišys, S. Juršėnas, A. Jozeliūnaitė, T. Javorskis, U. Šinkevičiūtė, E. Orentas and K. Kazlauskas, *J. Mater. Chem. C*, 2021, **9**, 4359–4366.

35 S. Wieghold, A. S. Bieber, Z. A. VanOrman and L. Nienhaus, *J. Phys. Chem. Lett.*, 2019, **10**, 3806–3811.

36 A. S. Bieber, Z. A. VanOrman, S. Wieghold and L. Nienhaus, *J. Chem. Phys.*, 2020, **153**, 084703.

37 S. Wieghold, A. S. Bieber, Z. A. VanOrman, A. Rodriguez and L. Nienhaus, *J. Phys. Chem. C*, 2020, **124**, 18132–18140.

38 V. Jankus, E. W. Snedden, D. W. Bright, E. Arac, D. Dai and A. P. Monkman, *Phys. Rev. B: Condens. Matter Mater. Phys.*, 2013, **87**, 224202.

39 T. K. Mullenbach, K. A. McGarry, W. A. Luhman, C. J. Douglas and R. J. Holmes, *Adv. Mater.*, 2013, **25**, 3689–3693.

40 H. Tamura, K. Azumaya and H. Ishikita, *J. Phys. Chem. Lett.*, 2019, **10**, 7623–7628.

41 P. Irkhin, I. Biaggio, T. Zimmerling, M. Döbeli and B. Batlogg, *Appl. Phys. Lett.*, 2016, **108**, 063302.

42 P. Irkhin and I. Biaggio, *Phys. Rev. Lett.*, 2011, **107**, 017402.

43 H. Najafov, B. Lee, Q. Zhou, L. C. Feldman and V. Podzorov, *Nat. Mater.*, 2010, **9**, 938–943.

44 S. Raišys, S. Juršėnas, Y. C. Simon, C. Weder and K. Kazlauskas, *Chem. Sci.*, 2018, **9**, 6796–6802.

45 S. Raišys, K. Kazlauskas, S. Juršėnas and Y. C. Simon, *ACS Appl. Mater. Interfaces*, 2016, **8**, 15732–15740.

46 S. Raišys, O. Adomėnienė, P. Adomėnas, A. Rudnick, A. Köhler and K. Kazlauskas, *J. Phys. Chem. C*, 2021, **125**, 3764–3775.

NOTES

Vilniaus universiteto leidykla
Saulėtekio al. 9, III rūmai, LT-10222 Vilnius
El. p. info@leidykla.vu.lt, www.leidykla.vu.lt
Tiražas 20 egz.